# Investigating the expression and function of neutrophil elastase in murine monocyte migration in vivo

Leese, Andrew John

# Investigating the expression and function of neutrophil elastase in murine monocyte migration *in vivo*

**Andrew John Leese**

For the degree of:

**Doctor of Philosophy**

Registered at:

**Barts & The London School of Medicine and Dentistry**
**Queen Mary, University of London**

Centre for Microvascular Research
William Harvey Research Institute
John Vane Science Centre
Charterhouse Square,
London EC1M 6BQ

# Acknowledgements

In helping me negotiate the trials and tribulations inherent to a PhD, I would first and foremost like to thank everyone in the Centre of Microvascular Research. Special thanks go to all my primary supervisors, namely James Whiteford, Martina Beyrau and Professor Sussan Nourshargh, who have had to guide and tolerate me more directly and to whom I will always be grateful. I would also like to pay tributes to my fellow PhD students, both past and present, who have provided me not only with moral support but with heaps of joy and laughter. On this front, I would like to specifically mention Chris Schultz, my future business partner, and Emma Kay, my Kentish friend for life. My deepest thanks extend more broadly to all those at QMUL who have helped me over the past three years, as well as my family and friends, in particular my girlfriend Katie who is 'fabulous and has put up with a lot'.

Upon reflection, I feel proud of what I have achieved and endured during my PhD. It has been a once in a lifetime experience – certainly I won't ever embark on another one – which has taught me an awful lot, not just about science, but about work and life more generally. In three words, it's been tough; it's been enlightening; it's been interesting.

# Abstract

Monocytes comprise a key component of the innate immune system. Their excessive and/or prolonged recruitment and/or activation can however be harmful and has been associated with the pathogenesis of numerous inflammatory disorders, most notably atherosclerosis. Consequently there is much interest in deciphering the mechanisms by which monocytes migrate into sites of inflammation. In this context, whilst many studies have investigated the roles of adhesion molecules and chemokine receptors, very little attention has been placed on the potential involvement of proteases. To help address this point, and considering cigarette smoke-induced recruitment of monocytes to the lung is impaired in mice deficient in neutrophil elastase ($NE^{-/-}$), we sought to further investigate the role of NE, a serine protease, in monocyte migration.

To achieve this we successfully crossed $CX_3CR1$-eGFP-knock-in mice, which exhibit fluorescently labelled monocytes, with $NE^{-/-}$ mice. By comparing $NE^{-/-}$ and $NE^{+/+}$ littermates we demonstrated, for the first time, NE expression in murine monocytes. Peritonitis, ear, and cremaster muscle models of inflammation were subsequently employed to assess the involvement of NE in monocyte recruitment. In CCL2-induced peritonitis, a predominantly monocyte-driven inflammatory model, monocyte infiltration was significantly reduced after 16 hours in $NE^{-/-}$ mice compared to $NE^{+/+}$ controls. Monocyte transmigration was also defective in the ears (though interestingly not the cremaster muscles) of $NE^{-/-}$ mice stimulated with CCL2, with the majority of monocytes seemingly unable to penetrate the venular endothelium. Furthermore, immunostaining revealed transmigrating monocytes were depleted of their intracellular NE stores. Taken together, it appears the release of NE by monocytes promotes their transmigration in response to CCL2, identifying NE as a potential therapeutic target for monocyte-driven pathologies.

# Table of contents

# List of figures

# List of tables

# Abbreviations

| | |
|---|---|
| 4',6-diamidino-2-phenylindole | DAPI |
| 7-aminoactinomycin D | 7-AAD |
| Activator protein 1 | AP-1 |
| Acute lung injury | ALI |
| Adult respiratory distress syndrome | ARDS |
| Alpha smooth muscle actin | α-SMA |
| Alpha-1 antitrypsin | $\alpha_1$-AT |
| Ammonium-chloride-potassium | ACK |
| Apolipoprotein E | ApoE |
| Base pairs | bp |
| Beta-mercaptoethanol | β-ME |
| Bone marrow | BM |
| Bovine serum albumin | BSA |
| Cathepsin G | CG |
| C-C chemokine ligand | CCL |
| C-C chemokine receptor | CCR |
| Chronic obstructive pulmonary disease | COPD |
| Common myeloid progenitor | CMP |
| Complement receptor 1 | CR1 |
| Complementary DNA | cDNA |
| Critical threshold | $C_T$ |
| Damage-associated molecular pattern | DAMP |
| Dendritic cell | DC |
| Deoxynucleotide triphosphates | dNTPs |
| Deoxyribonucleic acid | DNA |
| Dipeptidyl peptidase I | DPPI |
| Dulbecco's modified eagle's medium | DMEM |
| Endothelial basement membrane | EBM |
| Endothelial cell | EC |
| Endothelial cell-selective adhesion molecule | ESAM |
| Enhanced green fluorescence protein | eGFP |
| Enzyme-linked immunosorbent assay | ELISA |
| Ethylenediaminetetraacetic acid | EDTA |

| | |
|---|---|
| Extracellular matrix | ECM |
| Foetal bovine serum | FBS |
| Flow cytometry | FC |
| Fluorescence activated cell sorting | FACS |
| Foetal calf serum | FCS |
| Forward scatter | FSC |
| G protein-coupled receptor | GPCR |
| Glyceraldehyde 3-phosphate dehydrogenase | GAPDH |
| Granulocyte/macrophage progenitor | GMP |
| Granulocyte-macrophage colony-stimulating factor | GM-CSF |
| Heat inactivated | HI |
| Haematopoietic stem cell | HSC |
| Horseradish peroxidise | HRP |
| Human umbilical vein endothelial cell | HUVEC |
| Immunofluorescence | IF |
| Interferon gamma | IFNγ |
| Interleukin | IL |
| Intradermal | i.d. |
| Intramuscular | i.m. |
| Intraperitoneal | i.p. |
| Intrascrotal | i.s. |
| Intravenous | i.v. |
| Intravital microscopy | IVM |
| Junctional adhesion molecule | JAM |
| Keratinocyte chemoattractant | KC |
| Kilodalton | kDa |
| Lateral border recycling compartment | LBRC |
| Leukotriene $B_4$ | $LTB_4$ |
| Lipopolysaccharide | LPS |
| Low expression region | LER |
| Low-density lipoprotein | LDL |
| Lymphocyte function-associated antigen-1 | LFA-1 |
| Lysozyme M | lysM |
| Macrophage | MΦ |
| Macrophage colony-stimulating factor | M-CSF |

| | |
|---|---|
| Macrophage disappearance reaction | MDR |
| Macrophage receptor 1 | MAC-1 |
| Macrophage/DC progenitor | MDP |
| Magnetic-activated cell sorting | MACS |
| Matrix metalloproteinase | MMP |
| Median fluorescence intensity | MFI |
| Molecular weight | MW |
| Mononuclear phagocyte system | MPS |
| mRNA | Messenger RNA |
| Mucosal addressin cellular adhesion molecule-1 | MAdCAM-1 |
| Myosin light chain | MLC |
| Natural killer cell | NK cell |
| Neutrophil elastase | NE |
| Neutrophil extracellular trap | NET |
| N-formyl-methionyl-leucyl-phenylalanine | fMLP |
| NOD-like receptor | NLR |
| Normal goat serum | NGS |
| Nuclear factor κb | NF-κB |
| Outer membrane protein A | OmpA |
| Paraformaldehyde | PFA |
| Pathogen-associated molecular pattern | PAMP |
| Pattern recognition receptor | PRR |
| Phorbol 12-myristate 13-acetate | PMA |
| Phosphate buffered saline | PBS |
| Phycoerythrin | PE |
| Platelet endothelial cell adhesion molecule-1 | PECAM-1 |
| Polyacrylamide gel electrophoresis | PAGE |
| Polymerase chain reaction | PCR |
| Polymorphonuclear neutrophil | PMN |
| Polyvinylidene fluoride | PVDF |
| Protease activated receptor | PAR |
| Proteinase 3 | PR3 |
| P-selectin glycoprotein ligand 1 | PSGL1 |
| Quantitative PCR | qPCR |
| Radioimmunoprecipitation assay buffer | RIPA buffer |

| | |
|---|---|
| Reactive oxygen species | ROS |
| Relative centrifugal force | RCF |
| Relative fluorescence intensity | RFI |
| Reverse transendothelial migration | rTEM |
| Ribonucleic acid | RNA |
| Room temperature | RT |
| Roswell Park Memorial Institute medium | RPMI medium |
| Serum free | SF |
| Side scatter | SSC |
| Skin endothelial cell | sEND |
| Sodium dodecyl sulphate | SDS |
| Standard deviation | SD |
| Standard error of the mean | SEM |
| Stromal cell-derived factor 1 | SDF-1 |
| Tetramethylbenzidine | TMB |
| *Thermus aquaticus* | TAQ |
| Tissue inhibitor of metalloproteinase 1 | TIMP-1 |
| TNF/inducible nitric oxide synthase-producing dendritic cell | TIP-DC |
| Toll-like receptor | TLR |
| Transendothelial migration | TEM |
| Tris-acetate-EDTA | TAE |
| Tumor necrosis factor alpha | TNF-α |
| Vascular adhesion protein 1 | VAP1 |
| Vascular cell adhesion molecule-1 | VCAM-1 |
| Vascular endothelial cadherin | VE-cadherin |
| Very late antigen-4 | VLA-4 |
| Vesiculo-vacuolar organelle | VVO |
| Western blot | WB |
| Wild-type | WT |

# Arising publications

Leese, A., Beyrau, M., & Whiteford, J. (2015). **Neutrophil elastase facilitates monocyte transendothelial migration *in vivo*.** Manuscript being prepared for *PLOS ONE*.

## Statement of originality

The approach and experiments presented here are novel. The author has personally undertaken all the work described here, unless stated otherwise.

# CHAPTER 1: General introduction

## *1.1 Inflammation*

All animals possess some form of immune system that serves to maintain good health by eliminating invading pathogens (e.g. viruses and bacteria) and other harmful substances. The immune system of humans and other higher vertebrates can be divided into two interdependent branches: innate and adaptive. The innate immune system provides general protection against all foreign agents, while the adaptive immune system initiates a more potent response, specific to each pathogen. Both systems operate by utilising a cellular component, represented mainly by specialised immune cells called leukocytes, and a humoral component, mediated by soluble macromolecules that reside in extracellular fluids. In addition, the innate immune system features anatomical barriers, including the skin and mucous membranes, which physically and chemically resist pathogens and ultimately represent the first line of defence against infection.

If these barriers are penetrated, or the host incurs some other form of tissue damage (e.g. burn or blunt trauma injuries), inflammation is triggered. Inflammation is a physiological response mediated in large by the innate immune system and is characterised by the accumulation of blood plasma and leukocytes at the site of damage. It functions to contain, if not remove the inciting stimulus as well as any damaged or necrotic cells resulting from the insult, and initiate tissue repair. Furthermore, as innate immune cells are integral to the priming of T and B lymphocytes, the inflammatory response contributes to activating the adaptive immune system, the ultimate weapon against most infections and capable of generating immunological memory. Inflammation is therefore essential to resolving injury and restoring tissue homeostasis and typically promotes a healthy state.

*a) Acute inflammation:*

Inflammation can be classified as acute or chronic. Acute inflammation is triggered immediately at a site of injury by resident cells, predominantly those belonging to the innate immune system, such as macrophages, mast cells, and dendritic cells (DCs) (Newton and Dixit, 2012). These cells express a variety of germline encoded intra- and extracellular pattern recognition receptors (PRRs) that detect pathogen-associated

molecular patterns (PAMPs) during infection and damage-associated molecular patterns (DAMPs) released from injured host cells. Collectively termed inflammatory inducers, the recognition of these molecules by PRRs activates intracellular signalling pathways stimulating the release of chemical molecules that cause and regulate local inflammation (*Figure 1.1*).

Several families of PRRs exist including the cytoplasmic nucleotide-binding oligomerization domain (NOD)-like receptors (NLRs) and the membrane-bound Toll-like receptors (TLRs), which have been most expansively characterised. Having an extensive repertoire of PRRs, many of which can recognise several inducer molecules, ensures a rapid and effective immune response is elicited upon exposure to a variety of stimuli. PAMPs are molecules exclusively expressed by microbial pathogens. They are evolutionarily highly conserved and typically play an essential role in pathogen survival. They include fungal β-glucans and lipopolysaccharide (LPS), the major cell wall component of Gram-negative bacteria and one of the most potent PAMPs known (Mogensen, 2009). Certain pathogens also release toxins and other virulence factors that are not sensed directly by PRRs but rather induce an inflammatory response through their adverse effects on the host tissue (Medzhitov, 2008). This process is mediated in part by DAMPs, endogenous host-derived molecules with defined intracellular functions under basal conditions. During stress however, DAMPs are actively secreted or released from cells and subsequently bound by PRRs. Among the best characterised human DAMPs are the cytoplasmic proteins S100A8 and S100A9 and the nuclear protein HMGB1, all of which can induce inflammation by engaging TLRs (Medzhitov, 2008).

PRRs promote two main functions upon ligand binding: they activate resident macrophages and DCs to remove microbes and host debris by phagocytosis and they initiate intracellular signal transduction cascades. Different inducer molecules activate distinct sets of PRRs, triggering distinct signalling pathways that allow for a more tailored stimulus-dependent immune response (Akira et al., 2006). Common to all PRR signalling however is the activation of transcription factors. Nuclear factor κB (NF-κB) and activator protein 1 (AP-1) are two major, ubiquitously expressed transcription factors that respond to the vast majority of inflammatory stimuli and lie downstream of all TLR signalling (Akira et al., 2006). They work in synergy with other inducible transcription factors to regulate the expression and release of many different

inflammatory mediators. These include antimicrobial peptides capable of killing microorganisms directly, as well as small intercellular signalling proteins called cytokines, which ultimately co-ordinate the development of the inflammatory response.

The release of inflammatory mediators results in three major and interrelated responses that occur locally at the site of tissue damage: vascular dilation, increased vascular permeability, and leukocyte infiltration and activation. This collective effect clinically manifests as redness, heat, swelling, and pain, the cardinal signs of acute inflammation. Vascular dilation is initiated by mediators such as histamine and nitric oxide. Their release relaxes vascular smooth muscle cells, widening the lumen of precapillary arterioles and engorging the tissue with blood. Histamine also increases vascular permeability, along with bradykinin and leukotrienes. These mediators trigger contraction of endothelial cells of postcapillary venules, which separates intercellular junctions forming small pores (Kumar et al., 2010). An increase in blood flow and vascular permeability results in the net movement of plasma from the blood into the tissue. This fluid exudate is rich in proteins such as fibrinogen, kinins, complement, and immunoglobulins that activate coagulation, promote pathogen killing, and generally contribute to the inflammatory response. Moreover, fluid loss concentrates erythrocytes in the vasculature and reduces the local blood flow. This condition is called stasis and facilitates the rolling of leukocytes along the endothelium and their subsequent migration into the tissue.

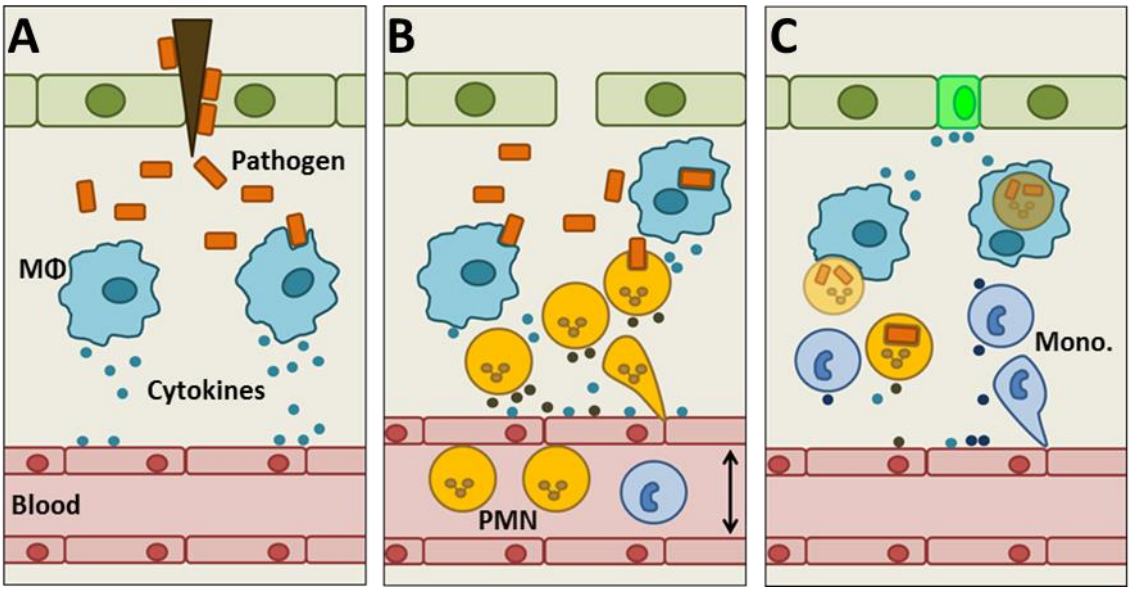

**Figure 1.1: Phases of acute inflammation.** Acute inflammation is a local response to tissue damage (e.g. getting a splinter) and comprises three main steps: detection of the insult (A), recruitment of effector molecules and cells (B) and restoration of tissue homeostasis (C). Inflammation is triggered immediately at the site of injury by resident cells of the innate immune system, mainly macrophages (MΦ) and DCs. These cells present on their surfaces pattern recognition receptors (PRRs) that recognise inflammatory inducer molecules associated with microbial pathogens and cellular damage. Engagement of PRRs induces cell activation and the release of cytokines and chemokines, which orchestrate the inflammatory response. Local blood vessels dilate and become more permeable, promoting the influx of blood plasma and leukocytes. Neutrophils (PMN) are typically recruited first and, along with tissue macrophages, constitute potent phagocytes. In addition, neutrophils release their own mediators and granule contents, directly mediating the recruitment of classical monocytes (mono.). These cells are highly plastic, capable of differentiating into both macrophages and DCs with both pro- and anti-inflammatory characteristics. Once neutrophils have successfully cleared the inciting stimulus, they undergo apoptosis (faded cells). This not only promotes continued monocyte influx but prevents further infiltration of neutrophils. The clearance of apoptotic neutrophils by macrophages prompts an anti-inflammatory programme, which includes the secretion of growth factors that helps to restore tissue homeostasis. Resolution of inflammation is marked by the emigration of monocyte-derived cells out of the inflamed site via the lymphatics.

Polymorphonuclear neutrophils (PMNs) are the earliest and most abundantly recruited leukocyte cell type during acute inflammation, typically reaching the site of damage after the first 6-24 hours. This is followed by a second wave of monocyte infiltration after 24-48 hours (Kumar et al., 2010). Upon recruitment to damaged tissue, leukocytes undergo activation by interacting with local inducer molecules and inflammatory mediators, resulting in the enhancement of their defensive functions. Monocytes generally differentiate into more specialised macrophages and DCs which, along with activated neutrophils, constitute potent phagocytes, engulfing microbes and dead cells and incorporating them into phagocytic vacuoles. Internalisation triggers an oxidative burst in which the multisubunit enzyme NADPH oxidase is assembled in the vacuole membrane prior to generating reactive oxygen species (ROS), potent microbicidal agents considered to be the major killing mechanism for most invading pathogens (Dale et al., 2008). The fusion of lysosomal granules with phagocytic vacuoles introduces a range of digestive and hydrolytic enzymes which further contribute to pathogen killing before catalysing their degradation. Activated leukocytes can also kill pathogens extracellularly independent of phagocytic uptake by secreting antimicrobial molecules and releasing the contents of their granules. Moreover, neutrophils have been shown to release extracellular traps (NETs), a sticky network of chromatin DNA and granule proteins that ensnare pathogens and promote their killing. In addition to exerting

antimicrobial effects, activated leukocytes also release a plethora of inflammatory mediators that amplify the inflammatory response and perpetuate leukocyte recruitment. Extravasated neutrophils for example release preformed granule proteins, which promote monocyte recruitment both directly by activating receptors on their surfaces and indirectly by stimulating the secretion of monocyte-specific chemokines by resident macrophages and endothelial cells (Soehnlein and Lindbom, 2010).

Once the offending stimulus has been successfully removed, the inflammatory response begins to resolve. Vessel permeability and calibre returns to a normal status and the local production of pro-inflammatory cytokines is suppressed, abating further neutrophil recruitment. This is supported by the active secretion of mediators possessing pro-resolution and anti-inflammatory properties. These include interleukin (IL)-10, an inhibitor of the pro-inflammatory transcription factor NF-κB, and members of the lipoxin, protectin and resolvin families, which selectively block neutrophil chemotaxis and more generally contribute to the resolution phase by promoting the nonphlogistic (i.e. non-inflammatory) recruitment of monocytes and activating macrophages to engulf apoptotic neutrophils and cellular debris (Serhan et al., 2008). As inflammation subsides other secreted mediators orchestrate wound healing, ideally by initiating tissue regeneration. In this context, residual cells are stimulated to deposit extracellular matrix (ECM) proteins and undergo proliferation, thereby re-filling the wound area and restoring tissue homeostasis, integrity and function (Kumar et al., 2010). This is supported by local angiogenesis, which functions to re-establish the vasculature and provide nutrients and oxygen crucial for anabolic processes. Macrophages eventually leave the site of injury, predominantly by draining into the lymph nodes, marking the end of the resolution phase (Serhan and Savill, 2005).

*b) Chronic inflammation:*

Acute inflammation typically lasts for hours or days. If however the noxious stimulus is not quickly removed or the regulation of the inflammatory or healing response becomes impaired, inflammation can persist for weeks, months or even years. During such prolonged, or chronic, inflammation continuing leukocyte infiltration and attempted tissue healing occur at the site of injury simultaneously. Chronic inflammation can be caused by persistent infections by microorganisms that are difficult to eliminate (e.g. *Mycobacterium tuberculosis*, the causative pathogen of Tuberculosis), prolonged

exposure to toxic agents (e.g. silica particles), or self-antigens that induce an autoimmune response. In addition to succeeding single or repeated bouts of acute inflammation, chronic inflammation can also develop insidiously as a low-grade, smouldering, often asymptomatic response.

While acute inflammation is mediated by abundant neutrophil recruitment, during chronic inflammation there is a shift in type of leukocyte to mononuclear cells, predominantly monocytes/macrophages and lymphocytes. As these cells accumulate and proliferate at the site of injury they produce a range of chemical mediators that induce the hallmarks of chronic inflammation. Proteolytic enzymes and ROS are secreted in an attempt to clear the inciting agent, however, acting largely non-specifically, their continuous release during chronic inflammation often results in collateral damage to otherwise healthy tissue. Subsequent healing can often not be accomplished by regeneration and instead occurs by fibrosis, a hardening or scarring of the tissue resulting from the excess deposition of collagens and other ECM proteins. Stimulated by macrophage-derived growth factors, fibrosis can severely impair tissue architecture and function, potentially culminating in organ failure. Other mediators, such as bradykinin and histamine, excite local nociceptive neurons causing persistent pain, while extensive systemic effects are also associated with chronic inflammation including fever, fatigue, weight loss and wasting (Kumar & Wakefield, 2010).

In this context, inflammation may no longer benefit the host but instead be detrimental. Indeed, chronic inflammation underlies the pathology of many common and clinically important diseases including rheumatoid arthritis, asthma, Alzheimer’s disease, and atherosclerosis. Moreover, persistent inflammation promotes carcinogenesis by causing DNA damage and generating proliferative and anti-apoptotic signals, thereby enhancing the risk of developing cancer (Fitzpatrick, 2001). Responsible globally for over 35 million deaths a year, these chronic disorders now represent the leading cause of morbidity and mortality worldwide, affecting the young and the old, the rich and the poor, and different ethnicities alike. In addition, they have a substantial economic impact both on patients' families and society as a whole. In the United States for example, healthcare spending and lost business productivity due to chronic disease totals over $250 billion and $1 trillion per year, respectively (DeVol & Bedroussian, 2007). With current treatments proving largely ineffective and the burden of chronic diseases projected to increase there is a great emphasis on further understanding the

mechanisms of chronic inflammation in the hope that this will catalyse the development of novel therapeutic strategies (Mackay, 2008). This particular study focusses on monocytes, whose continuous recruitment, activation and differentiation into tissue macrophages and DCs is a typical hallmark of chronic inflammation.

### *1.2 Monocytes*

*a) Monocyte heterogeneity:*

Monocytes are generally the largest leukocyte cell type in the blood, morphologically characterised by an abundant and moderately granular cytoplasm and a kidney-shaped nucleus. There are two major subsets of monocytes in humans, originally distinguished by size, function and differential expression of the surface markers CD14 (a co-receptor for LPS) and CD16 (a low affinity Fc receptor) (Grage-Griebenow et al., 2001). Described first and accounting for ~90% of the total monocyte population in healthy individuals, classical monocytes were large cells with relatively high phagocytic activity, superoxide release, and CD14 expression but absent for CD16 ($CD14^{++}$ CD16). Conversely, non-classical monocytes, comprising only ~10% of monocytes, were smaller in size, had low peroxidase activity, and were CD14 low, CD16 high ($CD14^{+}$ $CD16^{++}$). Numerous other phenotypic differences have since been elucidated, including distinct chemokine receptor expression profiles. Classical monocytes are $CCR2^{+}$, $CCR5^{-}$ and $CX_3CR1^{low}$, while non-classical monocytes are $CCR2^{-}$, $CCR5^{+}$ and $CX_3CR1^{hi}$ (Ingersoll et al., 2010).

Two major monocyte subsets have been reported in other mammals including pigs, rats and mice. Murine monocytes have been particularly well characterised and are collectively identified as $CD115^{+}$, $CD11b^{+}$, $F4/80^{int}$ blood cells (Sunderkötter et al., 2004). Represented in roughly equal proportion in the circulation, the two murine monocyte subsets are typically distinguished by the marker lymphocyte antigen 6C (Ly6C), a protein with unknown function. $Ly6C^{+}$ monocytes are also $CCR2^{hi}$ and $CX_3CR1^{med}$, resembling human classical monocytes. Likewise, $Ly6C^{-}$ monocytes are $CCR2^{low}$, $CX_3CR1^{hi}$ and $CD16^{+}$ similar to human non-classical monocytes. It was consequently proposed that homologous monocyte subsets exist in humans and mice. Indeed, similar morphological features, comparable gene expression profiles and the identification of other common surface markers reveal both subsets (herein collectively

referred to as classical and non-classical monocytes) are broadly conserved between the two species (*Figure 1.2*) (Ingersoll et al., 2010). Accordingly, mouse models have been and continue to be routinely used to characterise monocyte biology.

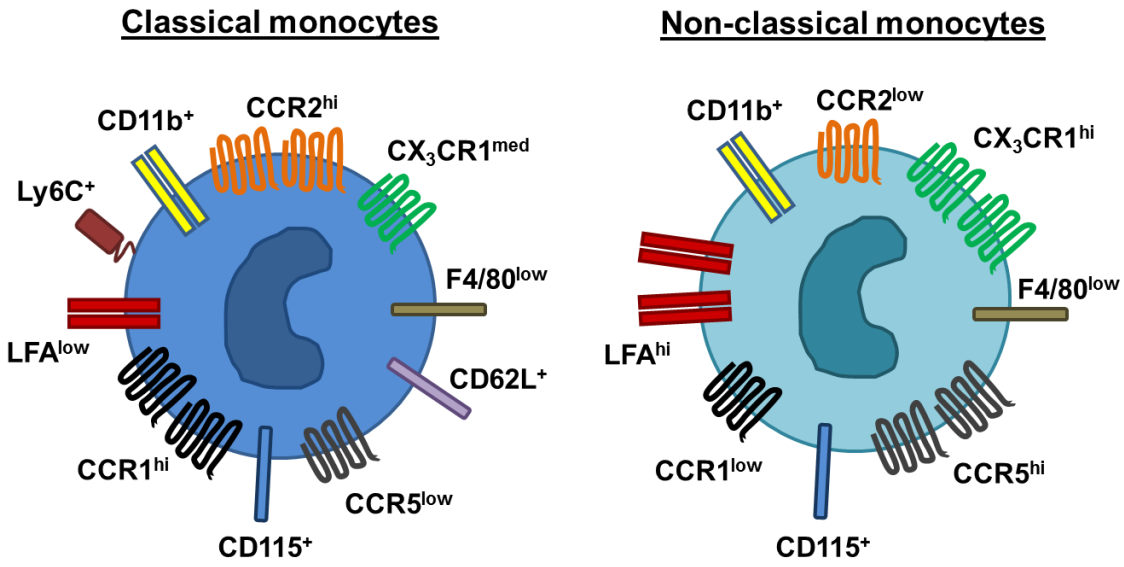


**Figure 1.2: Phenotype of murine monocyte subsets:** Classical and non-classical monocytes possess characteristic expression profiles of adhesion molecules and chemokine receptors, which govern distinct recruitment mechanisms. These profiles are largely conserved in humans and mice.

*b) The mononuclear phagocyte system:*

Monocytes, like all other leukocytes develop from pluripotent haematopoietic stem cells (HSCs) that reside in the bone marrow. Changes in gene expression enable HSCs to commit to alternative differentiation pathways culminating in the production of distinct leukocyte subsets. For monocytes, maturation occurs via several intermediate progenitors, namely the common myeloid progenitor (CMP), the granulocyte/macrophage progenitor (GMP), and the macrophage/DC progenitor (MDP). These progenitor cells, along with mature monocytes and their macrophage and DC derivatives comprise the mononuclear phagocyte system (MPS) (*Figure 1.3*). Commitment to the mononuclear phagocyte lineage is critically dependent on the transcription factor PU.1. When sufficiently activated by the cytokine macrophage colony-stimulating factor (M-CSF), PU.1 functions to antagonise the transcription factor C/EBP-α, imperative for the development of neutrophils, while also promoting monocyte maturation more directly by inducing secondary transcription factors and

other genes characteristic of monocytes, such as CD14, scavenger receptors, and the adhesion molecules CD11b and CD18 (Valledor et al., 1998). Classical monocytes are reportedly the first subset to develop in the bone marrow, differentiating directly from MDPs. Classical monocytes in turn give rise to non-classical monocytes. This appears to occur via a distinct 'intermediate' subset, which, in addition to acting as a transitional population, also possesses discrete biological functions (Wong et al., 2011).

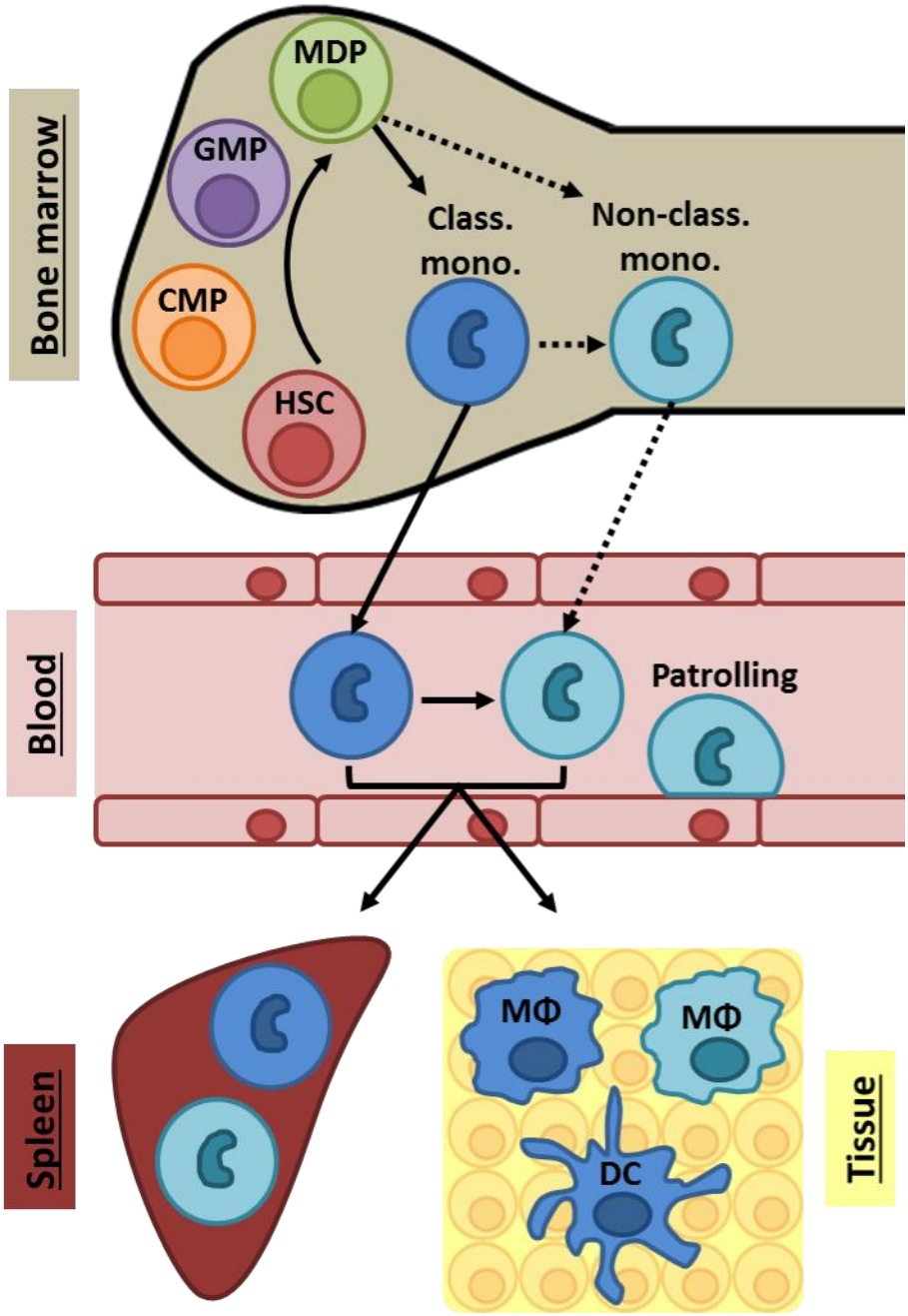

**Figure 1.3: The mononuclear phagocyte system.** The mononuclear phagocyte system (MPS) comprises monocytes and their bone marrow (BM) progenitors, as well as tissue macrophages (MΦ) and dendritic cells (DC). Classical monocytes are developed directly in the BM, differentiating from several intermediate progenitors, including the common myeloid progenitor (CMP), the granulocyte/macrophage progenitor (GMP), and the macrophage/DC progenitor (MDP). Upon maturation, classical monocytes enter the bloodstream in a CCR2-dependent manner, wherein they may differentiate further into non-classical monocytes, seemingly via a distinct intermediate population. It has also been postulated that non-classical monocytes can develop directly in the BM, either from classical monocytes or other progenitor cells. In addition to circulating freely, a large proportion of mature monocytes home to the spleen. Under steady state conditions, classical monocytes maintain populations of resident macrophages and DCs in the peripheral tissues, while non-classical monocytes patrol blood vessels for damage. During inflammation, classical monocytes egress from the BM and spleen and are extensively recruited to the damaged tissue where they differentiate into pro-inflammatory TipDCs or M1-like macrophages. Non-classical monocytes are also recruited to sites of inflammation and possibly contribute to wound healing by differentiating into M2-like macrophages.

Upon maturation, monocytes emigrate out of the bone marrow and enter the bloodstream. For classical monocytes, this process is dependent on the activation of C-C chemokine receptor 2 (CCR2) by its ligands CCL2 and CCL7 (Tsou et al., 2007). This differs for non-classical monocytes which express considerably lower levels of CCR2, however an analogous mechanism has yet to be elucidated (Ingersoll et al., 2011). Alternatively, it has been postulated that the conversion of classical monocytes to non-classical monocytes can occur directly in the bloodstream (Sunderkötter et al., 2004). As well as circulating freely in the blood, a large proportion of mature monocytes have been shown to collect in the subcapsular red pulp of the spleen, in both humans and mice (van der Laan et al., 2014). These monocytes remain in an undifferentiated state and have an identical morphology and transcriptome compared to their blood counterparts (Swirski et al., 2009a).

In the steady state monocytes constitute approximately 10% of total blood leukocytes in humans and 4% in mice. They typically circulate for several days, after which they die, return to the bone marrow, or move into tissues to replenish resident macrophages and DCs. Found throughout the body, these mononuclear phagocytes fulfil many important physiological functions during homeostasis, for example removing senescent cells and cellular debris, tissue remodelling, and serving as sentinels to invading microbes. While both monocyte subsets are capable of differentiating into both macrophages and DCs *in vitro* (Geissmann et al., 2003), it appears classical monocytes are the dominant precursors in the steady state *in vivo.* Indeed, classical murine monocytes have been

shown to repopulate macrophages and DCs in the skin, lungs, and digestive tract, though other populations appear to be predominantly maintained by local proliferation (Auffray et al., 2009). While non-classical monocytes have for example been shown to reconstitute a subpopulation of pulmonary DCs (Jakubzick et al., 2008), it appears their primary function under homeostatic conditions is immunosurveillance. Non-classical murine monocytes are known to reside in resting tissues and have also been observed by intravital microscopy to constitutively crawl on the luminal side of the endothelium in blood vessels in the dermis and mesentery (Auffray et al., 2007). As such, they are ideally located to scavenge microparticles and cellular debris, as well as survey their surroundings for tissue damage (Carlin et al., 2013).

*c) Monocytes during inflammation:*

As part of the inflammatory response, circulating monocytes mobilise to damaged tissues where they play an essential role in clearing the inciting stimulus and restoring tissue homeostasis. The recruitment of monocytes during inflammation is supported by a transient increase in the total number of monocytes in the blood. Mature monocytes residing in the spleen and bone marrow enter the bloodstream en masse in an angiotensin II and CCL2-dependent manner, respectively (Shi and Pamer, 2011). In addition, monocyte production in the bone marrow is heightened (Robbins and Swirski, 2010). The spleen and bone marrow therefore serve as monocyte reservoirs, which, when deployed into the circulation, promote rapid and abundant monocyte accumulation. Generally during both acute and chronic inflammation the classical monocyte subset predominantly accumulates in the circulation and is extensively recruited to the site of injury (Ingersoll et al., 2011). This is observed in murine models of bacterial, viral, fungal and parasitic infection, wherein they contribute to the control of pathogen growth by partaking in phagocytosis and producing a combination of pro-inflammatory mediators including TNF-α, ROS, nitric oxide, and type 1 interferon (Robbins and Swirski, 2010). In addition, recruited classical monocytes and/or their DC-derivatives can enter draining lymph nodes and engage the adaptive immune system by priming T lymphocytes, as seen following infection with *Leishmania major* and *Mycobacterium tuberculosis* (Serbina et al., 2008).

Using a model of peritoneal infection with the bacterium *Listeria monocytogenes* (so called because it induces a strong monocyte response), Auffray et al. also report

abundant classical monocyte infiltration, however this was preceded by an influx of non-classical monocytes, entering the peritoneal cavity after just 1 hour. These cells initiated an early inflammatory response by releasing the potent inflammatory mediators TNF-α and interleukin-1 beta (IL-1β) and upregulating genes encoding chemokines, TLRs, defensins, and complement proteins (Auffray et al., 2007). A direct result of this response was the recruitment of classical monocytes, which were shown to release large quantities of their own inflammatory mediators before differentiating into inflammatory cells resembling TIP (TNF-α/ inducible nitric oxide synthase (iNOS)-producing) DCs. This coincided with a shift in gene expression in the non-classical monocytes: pro-inflammatory genes were turned off and instead an M2-like macrophage differentiation programme was initiated. M2-like, or alternatively activated macrophages are involved in tissue remodelling, wound repair, and immunomodulation.

This latter study describes distinct biological functions for classical and non-classical monocytes in response to bacterial infection: classical monocytes were recruited more extensively and initiated pro-inflammatory activities, while non-classical monocytes, despite developing an early pro-inflammatory response, ultimately adopted an anti-inflammatory phenotype. Comparable observations have been made in several models of sterile injury. Using a mouse model of myocardial infarction, Nahrendorf et al. observed a biphasic recruitment of monocytes to the healing myocardium (Nahrendorf et al., 2007). Large numbers of classical monocytes were initially recruited in a CCR2-dependent manner and exhibited phagocytic, proteolytic and pro-inflammatory activity. This was followed by a less pronounced $CX_3CR1$-dependent influx of non-classical monocytes, which displayed anti-inflammatory properties and promoted tissue healing via myofibroblast accumulation, angiogenesis, and collagen deposition. Similarly, using a model of notexin-mediated skeletal muscle injury, Arnold et al. revealed an early recruitment of classical monocytes which expressed the inflammatory mediators TNF-α and IL-1β (Arnold et al., 2007). After several days however the proportion of non-classical monocytes increased and began to exhibit features of anti-inflammatory macrophages. This phenomenon was not attributed to a secondary wave of non-classical monocyte recruitment, but instead resulted from the local differentiation of classical monocytes into non-classical monocytes. These and other studies suggest classical and non-classical monocytes have divergent and complementary functions during inflammation. Classical monocytes are more extensively recruited to damaged tissues,

acquire a pro-inflammatory profile resembling TIP-DCs or inflammatory M1-like macrophages, and promote pathogen clearance. Conversely, non-classical monocytes are recruited in smaller numbers, acquire an anti-inflammatory profile resembling M2-like macrophages, and promote wound healing.

It is emerging that while monocytes do contribute directly to inflammation by performing phagocytosis and releasing inflammatory cytokines, their most significant attribute is their mobility. By circulating in the blood, monocytes can undergo extravasation and enter tissues throughout the body. This is facilitated through the expression of a broad array of chemotactic receptors, enabling monocytes to respond to a variety of chemoattractants including chemokines, chemotactic lipids, and complement fragments (Bachelerie et al., 2013). The two monocyte subsets differentially express these receptors and hence exhibit distinct migration patterns. In general however, the receptors CCR2 and $CX_3CR1$ appear to be commonly and critically employed in the migration of classical and non-classical monocytes, respectively (Domínguez and Ardavín, 2010). Once they infiltrate the site of inflammation, monocytes inevitably differentiate into macrophages and dendritic cells. These cells, though harbouring a limited migration potential, are longer living with more specialised immune functions. Macrophages are larger than monocytes with more lysosomal granules and consequently have a greater capacity for phagocytosis. They also display great plasticity, adopting a range of activation states, both pro- and anti-inflammatory, depending on the environmental signals they receive. DCs are the premier antigen-presenting cells, although macrophages and certain B-lymphocytes share this capability. DCs engulf foreign matter and pathogens by phagocytosis, migrate to regional lymph nodes, and activate lymphocytes by displaying digested protein fragments, or antigens, on their surfaces. DCs therefore play a key role in activating and regulating the adaptive immune system and by extension contribute to establishing immunologic memory.

It is clear that monocytes and their derivatives are key players in the inflammatory response. They not only directly promote the killing and clearance of a diverse range of bacterial, fungal and protozoal pathogens, but also activate adaptive immunity and participate in tissue healing (Shi and Pamer, 2011). Like a double-edged sword however, their excessive and/or prolonged recruitment and/or activation can be harmful and is known to contribute to the pathogenesis of various infections, cancers,

neurodegenerative diseases and inflammatory diseases. In particular, as monocytes/macrophages are recognised as the dominant cells during chronic inflammation, they have been strongly implicated in the development of many chronic inflammatory diseases. These include rheumatoid arthritis, during which synovial infiltration of monocytic cells damages cartilage and propagates inflammation through the release of pro-inflammatory mediators, proteases and ROS (Kawanaka et al., 2002), and asthma, where recruited monocytes and macrophages promote destruction of the alveolar walls and induce mucus hypersecretion (Rivier et al., 1995). Most importantly, monocytes contribute greatly to the pathogenesis of atherosclerosis, a chronic inflammatory condition of the arterial wall (*Figure 1.4*). As the most common cause of cardiovascular disease, atherosclerosis underlies the leading cause of morbidity and mortality in the developed world and is threatening to attain this status worldwide (Lloyd-Jones et al., 2010).

*d) Monocytes and atherosclerosis:*

Atherosclerosis usually develops slowly over many years and is characterised by the deposition of fatty deposits in the walls of large arteries, typically at sites of disturbed laminar flow. It is initiated by the activation and dysfunction of the arterial endothelium. Alterations in its cellular structure and composition, as well as an increased permeability enables low-density lipoprotein (LDL), the major cholesterol-carrying lipoprotein in the blood, to accumulate in the subendothelial intima (Weber and Noels, 2011). As LDL is retained it becomes susceptible to oxidation, cleavage and aggregation. These modifications turn LDL toxic to the endothelial cells, thereby further increasing their immune activity and promoting inflammation. This involves up-regulating the expression of adhesion molecules and secreting chemokines, which together promote the recruitment of blood leukocytes, particularly monocytes, to the arterial wall (Weber and Noels, 2011). Here monocytes engulf modified LDL through scavenger receptors and differentiate into macrophages and/or DC-like cells. These cells continue to take-up LDL and other lipids, soon transforming into lipid-laden foam cells. Unable to migrate out of the intima, foam cells accumulate in the evolving lesion and form early plaques. Foam cells secrete chemokines and other mediators, thereby perpetuating the inflammatory response, and stimulate local cell proliferation. This collectively causes the plaque to grow in size, narrowing the artery lumen and

restricting the flow of blood. The secretion of matrix-degrading proteases and the formation of a necrotic core, driven largely by the death of resident foam cells, render the atherosclerotic plaque unstable. Ultimately the plaque may rupture with the ensuing release of debris often resulting in occlusive luminal thrombosis, culminating in heart attack, stroke, and sudden cardiac death.

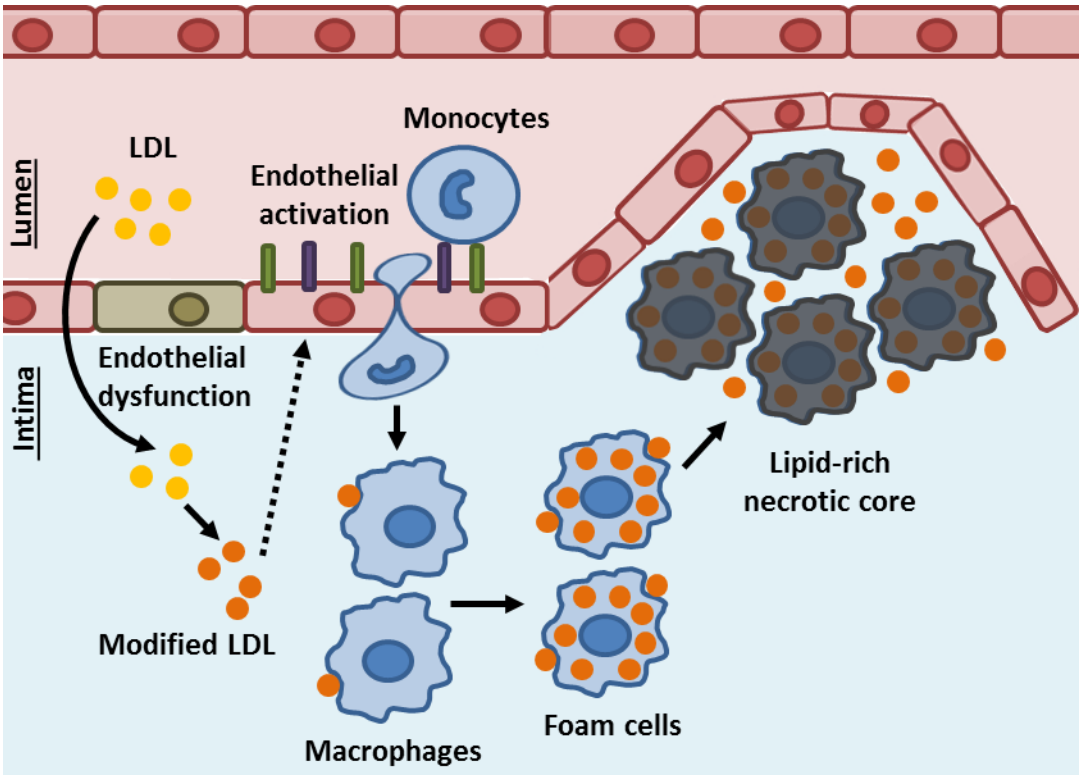


**Figure 1.4: Stages in the development of atherosclerotic plaques.** Atherosclerotic plaques typically develop in the walls of large arteries and are initiated by the accumulation of circulating low-density lipoprotein (LDL) within the subendothelial intima. This is promoted by local endothelial dysfunction or injury, as well as excess levels of LDL in the blood. Trapped LDL is subjected to chemical modifications, which promote its retention in the tissue and incite a local inflammatory response characterised by cytokine and chemokine secretion and the up-regulation of luminal adhesion molecules by overlying endothelial cells. These collectively promote the recruitment of circulating monocytes to the intima, which undergo subsequent differentiation into macrophages. Highly phagocytic, macrophages become laden with engulfed LDL and other lipids, resulting in foam cell formation. These cells constitute potent secretors of inflammatory cytokines that perpetuate the infiltration of monocytes and other cell types, including circulating T-cells and underlying smooth muscle cells. They are unable however to process the excess lipids and eventually undergo cell death, generating a lipid-rich necrotic core. As the plaque grows, the artery lumen narrows, restricting blood flow. More severely, weakening of the plaque cap by proteases can cause the plaque to rupture, spilling thrombogenic material into the circulation, potentially culminating in a heart attack or stroke.

Work on mice has provided an insight into the mechanisms that underlie the development of atherosclerosis. Using apolipoprotein E–deficient ($ApoE^{-/-}$) mice, which exhibit high levels of circulating cholesterol and spontaneously develop atherosclerosis on a high-fat diet, the classical monocyte subset was shown to be proportionally elevated in the blood. This was attributed to an increase in the survival and proliferation of these cells, as well as impaired conversion to the non-classical subset (Swirski et al., 2007). Classical monocytes were also shown to be predominantly and continually recruited to atherosclerotic plaques in a CCR2, CCR5 and $CX_3CR1$-dependent manner, with their accumulation increasing proportionally with lesion size (Tacke et al., 2007). Upon infiltration, classical monocytes secrete inflammatory mediators, ROS, and proteases prior to undergoing differentiation into macrophages and eventually foam cells (Robbins et al., 2012). Non-classical monocytes also infiltrate plaques, albeit less frequently. Their recruitment relies on CCR5 but surprisingly not on $CX_3CR1$. While their precise role in disease progression remains largely unknown, non-classical monocytes do exhibit phagocytic and proangiogenic functions upon recruitment (Swirski et al., 2009b). Moreover, they selectively upregulate CD11c, a marker for DCs, and have therefore been postulated to mediate local adaptive immune responses (Tacke et al., 2007).

The majority of currently available therapeutics against atherosclerosis serve to alleviate hypertension (e.g. β-blockers) and hyperlipidemia (e.g. statins) (Weber and Noels, 2011). While these drugs do reduce the risk of atherosclerosis, they do not fully inhibit the formation of atherosclerotic plaques. Moreover, they do not adequately protect patients with pre-existing coronary artery disease from secondary cardiovascular events. This is thought to be due, in part, to the fact that existing therapeutics do not directly address the inflammatory mechanisms that underlie atherosclerosis (Charo and Taub, 2011). In this context, and considering the critical role played by monocytes in the initiation, propagation, and progression of atherosclerosis, broadening our understanding of the mechanisms that govern monocyte migration could uncover novel therapeutic targets. In support of this, inhibiting monocyte-associated chemokine pathways almost abolishes atherosclerosis in $ApoE^{-/-}$ mice (Combadière et al., 2008). Moreover, several anti-inflammatory drugs have now entered late phase clinical trials, some of which are directed at blocking monocyte trafficking into atherosclerotic plaques (Charo and Taub, 2011). Manipulating monocyte infiltration could also offer

new paradigms for the treatment of other monocyte-driven inflammatory disorders. Indeed, selectively disrupting leukocyte migration appears to represent a particularly promising therapeutic avenue for a variety of inflammatory conditions, both in animal models and more importantly in clinical trials (Mackay, 2008). Further still, when regarding the essential role played by monocytes in host defence, delineating the mechanisms underlying monocyte migration could inspire new ways to enhance their activities, thereby improving the treatment of various cancers and infectious diseases (Nourshargh et al., 2010).

### *1.3 Leukocyte adhesion cascade*

In order to enter peripheral tissues, both in the steady state and during inflammation, circulating monocytes partake in a multi-step process in which they adhere to and subsequently traverse the walls of endothelial-lined blood vessels. This process has been similarly described for many kinds of leukocytes and is generally termed the leukocyte adhesion cascade. Originally encompassing three steps of leukocyte rolling, activation and firm adhesion, the leukocyte adhesion cascade has since been updated to include additional steps of leukocyte tethering, slow rolling, adhesion strengthening, intraluminal crawling, transcellular and paracellular transendothelial migration, and migration through the basement membrane and pericyte sheath (Ley et al., 2007) (*Figure 1.5*). Both the leukocyte and the endothelium play an active role during the leukocyte adhesion cascade by engaging complex signalling pathways and undergoing distinct molecular and structural changes.

*a) Leukocyte adhesion to the endothelium:*

Leukocyte extravasation *in vivo* occurs primarily at post-capillary venules. These blood vessels support TEM by exhibiting relative low haemodynamic shear forces, which are reduced further still during inflammation with the onset of stasis. Under these conditions, leukocytes are displaced to the inner endothelial lining of the venule wall by faster circulating erythrocytes, predisposing them to chemokines and adhesion molecules actively upregulated by post-capillary venules in inflamed tissues (Springer, 1994). These include adhesion molecules of the selectin family, which mediate leukocyte tethering and rolling on the endothelium, the initial steps in the adhesion cascade. In response to inflammatory cytokines such as TNF-α and IL-1β, endothelial

cells (ECs) specifically and sequentially mobilise P-selectin and E-selectin to their luminal surfaces where, through use of an amino terminal carbohydrate recognition domain, they bind glycosylated ligands displayed on the surface of circulating leukocytes. P-selectin glycoprotein ligand 1 (PSGL1) is a major ligand for all selectins and is constitutively expressed by the majority of leukocytes (Laszik et al., 1996). Some ECs also express mature PSGL1 which, along with other inducible glycoproteins (e.g. CD34), serve as ligands for L-selectin, the third member of the selectin family and constitutively expressed by most leukocyte subtypes.

Selectins bind their ligands with high tensile strength, enabling bonds to be formed even under the shear stress exerted by blood flow (Alon et al., 1995). In addition, selectin-ligand bonds have characteristically fast association and dissociation rates. As the leukocytes repeatedly tether to and detach from the endothelium they slow down and begin to 'roll' along the inner surface of the vessel wall. While this process is reversible and does not commit the leukocyte to transmigration – rolling leukocytes often dissociate entirely from the endothelium and re-enter the circulation – selectin-binding is a pivotal step for normal leukocyte trafficking. Indeed, mice deficient in the selectins show drastic reductions in leukocyte rolling and extravasation and develop spontaneous skin infections culminating in death (Jung and Ley, 1999). Specifically regarding monocytes, L-selectin appears to play a prominent role in the migration of classical monocytes as their recruitment following thioglycollate-induced peritonitis is reduced by more than 70% in L-selectin-deficient mice compared to wild-type controls (Tedder et al., 1995). Moreover, $ApoE^{-/-}$ mice also deficient for P-selectin develop delayed onset, smaller atherosclerotic plaques containing fewer monocytes when fed a high-fat diet, emphasising its role in monocyte recruitment and suggesting similar mechanisms govern leukocyte transmigration through both venular and arterial vessel walls (Dong et al., 2000).

While selectins constitute the most important rolling molecules, members of the integrin family of alpha/beta heterodimeric adhesion molecules are also involved. The integrin very late antigen-4 (VLA-4) for example is located on the surface of monocytes and mediates cell rolling by binding its receptor vascular cell adhesion molecule-1 (VCAM-1) expressed on ECs (Gerszten et al., 1998). In addition, some integrins, including lymphocyte function-associated antigen-1 (LFA-1) and macrophage receptor 1 (Mac-1), appear to work in synergy with selectins to mediate slow rolling, a separate step in

which the speed of the rolling leukocyte is further reduced (Dunne et al., 2002). This serves to facilitate the subsequent firm arrest of leukocytes on the endothelium, which is nearly exclusively mediated by the integrins and constitutes their primary function during the adhesion cascade.

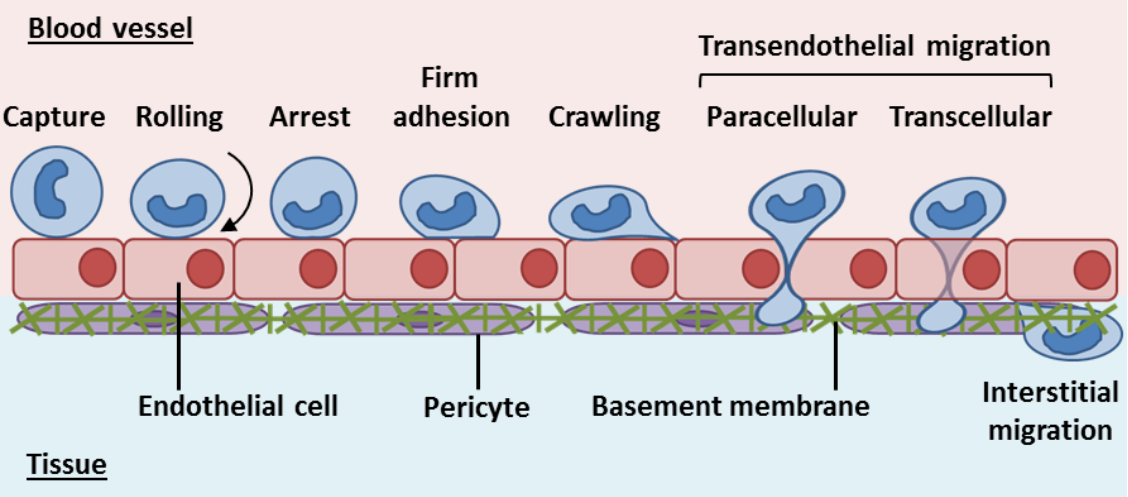


**Figure 1.5: The leukocyte adhesion cascade.** The leukocyte adhesion cascade is employed by monocytes and other leukocyte subsets to egress out of the bloodstream and enter tissues. This process is mediated by a series of interactions formed between the migrating leukocyte and the vessel wall. Originally encompassing steps of rolling, activation and firm adhesion, advances in real-time imaging have enabled additional steps to be defined which are collectively and sequentially described as follows: leukocyte capture, slow rolling, adhesion strengthening, intraluminal crawling, paracellular or transcellular transendothelial migration (TEM) and migration into the interstitial space through the pericyte layer and basement membrane. Image is adapted from Nourshargh et al., 2010.

During inflammation, leukocyte arrest is triggered by the binding of chemokines and lipid chemoattractants to corresponding G protein-coupled receptors (GPCRs) located on the surface of rolling leukocytes. Such chemokine receptors are differentially expressed by leukocyte subtypes and ultimately dictate their responsiveness to specific chemotactic molecules produced at the site of injury, predominantly by activated ECs and resident immune cells. Upon secretion, chemokines have been shown to interact with glycosaminoglycan chains of endothelial proteoglycans, which is thought to facilitate their retention on the vessel wall, even under shear stress, and promote leukocyte engagement (Proudfoot et al., 2003). Chemokine binding to leukocyte receptors elicits a rapid integrin-activation signal in the leukocyte, inducing dramatic conformational changes in their integrin ectodomains that results in an increased affinity

for counter-ligands expressed by ECs (Calderwood, 2004). This can be similarly and cooperatively triggered by certain selectin interactions and in monocytes is transduced by phospholipase C and changes in intracellular calcium stores (Ley et al., 2007). Upon ligand recognition, integrins typically cluster together in the leukocyte membrane. This reinforces the existing adhesive interactions via cooperative binding and promotes the tight attachment of leukocytes to the inflamed endothelium.

Integrins belonging to the $\beta_1$- and $\beta_2$-subfamilies are most relevant to leukocyte arrest. $\beta_2$-integrins may however be less involved on monocytes as blockade of LFA-1 ($\alpha L\beta 2$) and Mac-1 ($\alpha M\beta 2$), as well as their ligands ICAM-1 and ICAM-2, did not prevent monocyte arrest (Schenkel et al., 2004). Instead, monocyte firm adhesion appears to be more substantially mediated by the $\beta_1$-integrins, in particular VLA-4 ($\alpha 4\beta 1$). Inhibition of VCAM-1, the principal ligand of VLA-4, but not ICAM-1 reduced both monocyte adhesion and early lesion formation in the arteries of $ApoE^{-/-}$ mice (Cybulsky et al., 2001). Similarly, the recruitment of classical monocytes in response to thioglycollate in a mouse peritonitis model was shown not to depend on LFA-1 or Mac-1 but on VLA-4, as well as CCL2 (Henderson et al., 2003). Indeed, CCR2-CCL2 signalling in classical monocytes has been reported to elicit activating conformational changes in VLA-4 (Yang et al., 2014).

*b) Transendothelial migration:*

Leukocyte firm adhesion is a prerequisite for transendothelial migration (TEM), the subsequent step in the leukocyte adhesion cascade in which leukocytes penetrate the endothelial cell monolayer, or endothelium, that lines the vessel lumen. For this to be achieved, arrested leukocytes initially undergo cell spreading and polarisation, whereby they change from a spherical to a flattened morphology and form invading membrane protrusions, or pseudopodia, at their leading edge and a contractile uropod at the rear. In this state, leukocytes are able to travel laterally over the surface of the endothelium by establishing transient and sequential contacts with endothelial substrates. This process is termed intraluminal crawling and is mediated by integrin binding and the active reorganisation of the cytoskeleton (Phillipson et al., 2006). Guided by an intravascular chemokine gradient sequestered on the endothelium, leukocytes crawl towards the site of inflammation while scanning for optimal sites of TEM (Massena et al., 2010). Leukocytes typically crawl to and then along the cell-cell borders of adjacent ECs

through which they can subsequently squeeze towards the basal side of the endothelium (paracellular TEM). When crawling is inhibited however, leukocyte TEM is delayed and instead occurs primarily by passing directly through the body of an individual EC (transcellular TEM) (Phillipson et al., 2006). While both migration pathways are used by leukocytes under normal circumstances *in vivo*, the paracellular pathway seems to represent the most common route of emigration (Ley et al., 2007).

The endothelium does not merely represent a barrier to migrating leukocytes but actively contributes to and regulates the transmigration process. Adherent leukocytes can induce the formation of endothelial-cell projections rich in the integrin ligands ICAM-1 and VCAM-1 and various cytoskeletal components. Termed transmigratory cups, these structures partially embrace the leukocyte and facilitate TEM, through both migration pathways, by providing a physical scaffold that is aligned parallel to the direction of extravasation (Carman and Springer, 2004). In addition, ICAM-1 and VCAM-1 clustering triggers endothelial signalling pathways, leading to an increase in cytosolic calcium and phosphorylation of vascular endothelial (VE)-cadherin and myosin light chain (MLC). Constituting the major adhesion molecule of endothelial adherens junctions, VE-cadherin does not support leukocyte TEM but rather acts as an obstacle to emigrating cells. Upon phosphorylation however, VE-cadherin interactions are destabilised, loosening EC junctions. This is supported by phosphorylated MLC, which triggers actin–myosin fibre contractions causing neighbouring ECs to pull apart. Collectively, these events induce small gaps at endothelial junctions and promote the paracellular transit of leukocytes through the endothelium (Muller, 2011).

Numerous other endothelial molecules are functionally active during leukocyte TEM. The majority of these molecules localise to EC junctions and were originally implicated in paracellular migration, though it appears they may be similarly involved in transcellular migration. Platelet endothelial cell adhesion molecule-1 (PECAM-1, also known as CD31) was the first molecule reported to play a role exclusively at the point of leukocyte TEM both *in vitro* and *in vivo* (Muller, 2013). The extracellular domain of PECAM-1 engages in homophilic interactions. While this typically occurs between adjacent cells along the endothelial border, during TEM endothelial PECAM-1 can similarly interact with PECAM-1 expressed on the surface of leukocytes. This is crucial to the process of monocyte extravasation as blocking PECAM-1 reduces monocyte TEM by 70-90% (Muller et al., 1993). A similar phenotype is observed upon inhibition

of CD99 (Schenkel et al., 2002). As with PECAM-1, CD99 is expressed on ECs and leukocytes and undergoes homophilic binding during TEM. It appears endothelial PECAM-1 and CD99 sequentially engage their leukocyte counterparts, effectively guiding the leukocyte to the basal side of the endothelium (Schenkel et al., 2002).

In a similar fashion, junctional adhesion molecules (JAM)-A and -C promote transmigration by binding the leukocyte integrins LFA-1 and Mac-1, respectively, while putative functions have also been described for endothelial cell-selective adhesion molecule (ESAM), CD99L2, vascular adhesion protein 1 (VAP1), and poliovirus receptor (Ley et al., 2007). Considering the broad array of molecules implicated in leukocyte TEM (*Table 1.1*), it was hypothesised that they may operate synergistically as a large "transmigration complex" that collectively constitutes a platform for migrating leukocytes (Muller, 2013). Indeed, a reticulum of interconnected vesicles rich in EC junctional molecules including PECAM-1, CD99 and JAM-A has been described in ECs, residing under the plasma membrane at the endothelial border. This lateral border recycling compartment (LBRC) is recruited to and exteriorised at the site of leukocyte transmigration. This serves to push endothelial cell-cell interactions and other obstructive structural components of the junction aside, as well as present unligated endothelial molecules to their corresponding molecules on the leukocyte cell surface. As the LBRC surrounds the leukocyte, it provides a passageway through which it can migrate. In this same manner, the LBRC, in accordance with other vesicular compartments such as vesiculo-vacuolar organelles (VVOs), has also been shown to facilitate the movement of leukocytes through the body of individual ECs via the transcellular pathway. It appears the LBRC is governed by a different set of molecules, depending on the inflammatory stimulus or the leukocyte subtype. For example, unlike monocytes, lymphocytes do not seem to require PECAM-1 for transmigration *in vitro* (Muller, 2001), while PECAM-1, ICAM-2 and JAM-A are involved in the migration of neutrophils in the cremaster muscle in response to IL-1β but not TNF-α (Woodfin et al., 2009).

Leukocytes typically travel to the abluminal side of the endothelium without pause. Under some circumstances however the transmigration process is disrupted. Leukocytes may move back and forth in the EC junction numerous times prior to entering the sub-endothelial space (hesitant TEM), and have even been shown to migrate back through the junction in an abluminal-to-luminal direction and re-enter the blood (reverse TEM).

These phenomena have been best characterised *in vivo* in neutrophils and appear to be regulated by the junctional adhesion molecule JAM-C – the pharmacological blockade or genetic deletion of JAM-C in ECs results in enhanced disrupted TEM (Woodfin et al., 2011). Blocking JAM-C also increases reverse transmigration of monocytes through cultured ECs *in vitro*, however this has yet to be thoroughly explored *in vivo* (Bradfield et al., 2007).

**Table 1.1: Key endothelial cell-leukocyte interactions during transmigration.**

| Endothelial molecule | Leukocyte ligand | Transmigration step |
|---|---|---|
| CD34 | L-selectin | Tethering, rolling |
| P-selectin | PSGL-1 | Tethering, rolling |
| E-selectin | ESL-1, PSGL-1 | Tethering, rolling |
| VCAM-1 | VLA-4 | Rolling, arrest |
| ICAM-1 | LFA-1 | Rolling, arrest, crawling |
| MAdCAM-1 | α4β7-integrin | Arrest |
| ICAM-2 | MAC-1, LFA-1 | Crawling |
| PECAM-1 | PECAM-1 | Transendothelial migration |
| CD99 | CD99 | Transendothelial migration |
| CD99L2 | CD99L2 | Transendothelial migration |
| JAM-A | LFA-1, JAM-A | Transendothelial migration |
| JAM-B | VLA-4 | Transendothelial migration |
| JAM-C | MAC-1 | Transendothelial migration |
| ESAM | unknown | Transendothelial migration |

*c) Transmigration beyond the endothelium:*

Upon successfully crossing the endothelium, migrating leukocytes need to subsequently bypass the endothelial basement membrane (EBM) and, in most venules, the pericyte sheath. The pericyte sheath consists of a discontinuous network of pericyte cells that wrap themselves around ECs and aid in regulating their development and maintenance. Both cell types contribute to the formation of the EBM, which provides structural stability to the vessel wall and provides adhesive support to neighbouring cells. The EBM constitutes a thick layer of tightly packed and interconnected proteins, including laminins and collagen type IV. As such, it represents a substantial physical barrier to emigrating leukocytes that takes considerably longer to breach (> 15 minutes) compared to the endothelium (~5 minutes) (Ley et al., 2007). To facilitate its penetration,

leukocytes use ventral membrane protrusions to identify areas of the EBM with reduced levels of matrix proteins. Such low expression regions (LERs) represent preferred sites of leukocyte transmigration as they are not only easier to breach but are also more likely to be permeated by chemoattractants produced by the inflamed tissue. Moreover, LERs are closely associated with gaps in the pericyte sheath, which become enlarged during inflammation, acting essentially as gates for migrating leukocytes (Proebstl et al., 2012). In contrast to neutrophils, which employ matrix-degrading proteases to widen the LERs and ease their passage, monocytes appear to squeeze directly through LERs by dramatically changing their cellular shape (Voisin et al., 2009).

Several molecules have been implicated in regulating the movement of leukocytes through the pericyte sheath and venular EBM including Mac-1, LFA-1 and ICAM-1, which collectively support leukocyte crawling along pericyte processes (Proebstl et al., 2012), and integrin α6β1, the main receptor for vascular laminins (Dangerfield et al., 2002). Once the leukocyte has successfully detached from the EBM, it can subsequently traffic through the interstitial space to the site of tissue damage. Actin protrusions formed at the leading edge of the cell intercalate with the porous network of the extracellular matrix, propelling the leukocyte forward (Weninger et al., 2014). This is termed amoeboid movement and may be supported by the actomyosin-mediated retraction of the cell rear. In this manner, leukocytes travel along a gradient of chemotactic agents to the site of inflammation where they subsequently exert their effector functions.

The multi-step adhesion cascade has proved to be remarkably robust and has been observed for all kinds of leukocytes in a variety of inflammatory scenarios. This has posed somewhat of a hurdle for developing effective anti-inflammatory treatments as many potential therapeutic targets have widespread functions that are central to maintaining the protective functions of the immune system. Natalizumab for example is a monoclonal antibody that binds to the α4-subunit of α4β1 and α4β7 integrins expressed on the surface of most leukocytes. While it has been used successfully for the treatment of multiple sclerosis and Crohn's disease it also rendered patients more susceptible to severe viral and bacterial infections. To circumvent such issues, researchers are now beginning to delineate leukocyte-specific, and even tissue- and stimulus-specific molecules and mechanisms of transmigration. These can be therapeutically targeted to interfere only with the cellular subsets that possess disease

activity while leaving other immune cells largely undisturbed. This should keep unwanted side-effects to a minimum and ensure the immune system as a whole is not severely compromised.

In this light there is an emphasis on furthering our understanding of the specific mechanisms that regulate monocyte transmigration in the hope this will identify novel therapeutic targets for monocyte-driven pathologies. Whilst the roles of adhesion molecules and chemokine receptors in monocyte trafficking have been extensively researched, very little attention has been placed on the potential roles of proteases, which have been implicated in virtually every step of the inflammatory response including leukocyte transmigration. To address this issue, we have initially focussed on neutrophil elastase, a protease which has been routinely studied in neutrophils but whose function in monocytes has received little attention.

### *1.4 Neutrophil elastase*

*a) Biochemical properties of NE:*

As its name may suggest, neutrophil elastase (NE) was initially identified in neutrophils as a protease that could cleave the extracellular matrix protein elastin (Janoff and Scherer, 1968). NE has since been detected in other leukocyte subtypes and been shown to cleave virtually every type of matrix protein, including fibronectin, laminin, proteoglycans, and several types of collagen (Chua and Laurent, 2006). Its broad substrate specificity extends to other groups of proteins with various cytokines (e.g. IL-1β and TNF-α), adhesion molecules (e.g. ICAM-1 and VCAM-1), and other proteases (e.g. MMP-2 and MMP-9) also liable to cleavage. NE belongs to the chymotrypsin superfamily of serine proteases, which cleave peptide bonds by forming a charge relay system composed of a catalytic triad of conserved histidine, aspartate, and serine residues. The active site in NE is lined with a series of bulky hydrophobic residues which accounts for its preference in cleaving small hydrophobic residues within its substrate molecules (Korkmaz et al., 2010).

In neutrophils, NE primarily localises to cytoplasmic azurophil granules but has also been detected in the nucleus and in association with the plasma and other subcellular membranes. Azurophil granules contain two other structurally related serine proteases, cathepsin G (CG) and proteinase 3 (PR3). The expression and storage of all three

proteases peaks during the promyelocytic stage of neutrophil differentiation in the bone marrow and switches off upon maturation. NE is initially synthesised in the endoplasmic reticulum as a zymogen of 267 amino-acid residues in humans and 265 in mice (*Figure 1.6*). NE activation and packaging into granules is dependent on two separate amino-terminal processing steps. The signal sequence is first removed by signal peptidase, exposing a two-residue pro-sequence that is subsequently cleaved by dipeptidyl peptidase I (DPPI), rendering the active site accessible to substrate. In addition, NE can undergo carboxy-terminal processing by an unknown enzyme, however this is not required for NE activation. It does however expose a docking site that is thought to mediate NE trafficking to azurophil granules, as retention of the C-terminus re-routes NE to the plasma membrane (Horwitz et al., 2004). Fully processed active NE constitutes a 218 amino-acid monomeric protein in humans and 219 in mice. It is highly cationic and in azurophil granules associates with a matrix of negatively charged proteoglycans. This matrix, in combination with the low pH of the granule's interior, sequesters NE, a neutral-acting protease, in an inactive state until it is functionally required.

The gene encoding NE is found on chromosome 19 in humans and chromosome 10 in mice in a gene-cluster that includes PR3. It consists of 5 exons of identical size and 4 introns which are collectively larger in humans. Exon IV encodes two potential N-glycosylation sites resulting in an apparent protein mass of 29-33 kDa upon SDS-polyacrylamide gel electrophoresis (Korkmaz et al., 2010).

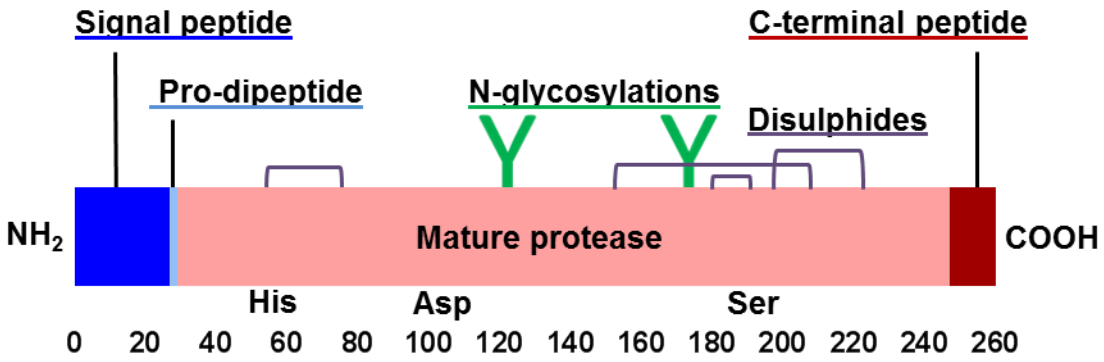


**Figure 1.6: Structure of neutrophil elastase.** The mature NE protein is formed following the proteolytic removal of a signal peptide (by signal peptidase) and pro-dipeptide (by DPPI) at the N-terminus and typically a pro-peptide at the C-terminus (enzyme unknown). It contains four disulphide bridges and two N-glycosylation sites. Its secondary structure consists of two homologous β-barrels and a C-terminal α-helix. The catalytic triad of histidine, aspartate, and serine residues converge at the junction of the two β-barrels (Korkmaz et al., 2010).

*b) Physiological and pathological activities of NE:*

Mapping the NE gene locus has enabled its physiological functions to be studied more rigorously through the generation of NE deficient ($NE^{-/-}$) mice. In brief, this was achieved by replacing exon II of the NE gene with the neomycin phosphotransferase cDNA, thereby terminating NE transcript expression (Belaaouaj et al., 1998). While the $NE^{-/-}$ mice were not immunocompromised, that is, they did not spontaneously develop infections, they did demonstrate a greater susceptibility to sepsis and death following intraperitoneal infection with Gram negative, though not Gram positive bacteria compared to wild-type littermates. This was attributed to an inability of $NE^{-/-}$ neutrophils to successfully degrade engulfed bacteria. Typically following phagocytosis, azurophil granules fuse with the phagosome with the ensuing generation of reactive oxygen species inducing an increase in local pH. This in turn activates NE and other degradative enzymes, culminating in the death and breakdown of the bacterium. This fate was avoided however upon infection of $NE^{-/-}$ neutrophils, the bacteria instead being seen to remain intact in the phagosome and even divide. Subsequent studies have shed light on the mechanisms that underlie NE-mediated intracellular bactericidal activity. NE was shown to directly mediate the killing of *Escherichia coli* by degrading outer membrane protein A (OmpA), a structural membrane protein that is highly conserved in a wide range of Gram-negative bacteria. Moreover, NE can cleave virulence factors of enterobacteria, such as *Shigella flexneri* and *Yersinia enterocolitica*, preventing their escape from phagolysosomes and promoting their clearance (Weinrauch et al., 2002). As well as targeting Gram negative bacteria, NE has also been shown to display potent antimicrobial activity against spirochaetes (Garcia et al., 1998) and fungi (Tkalcevic et al., 2000).

NE is stored in azurophil granules at extremely high concentrations (~5 mM) and is thought to contribute mainly to the intracellular degradation of phagocytosed microorganisms. That being said, the anti-microbial functions of NE can also be exerted extracellularly. NE and other serine proteases can escape azurophil granules, translocate to the nucleus and form neutrophil extracellular traps (NETs) by interacting with chromatin DNA. Once deployed by the cell, these sticky structures capture and kill bacteria, fungi, and parasites (Papayannopoulos et al., 2010). NE can also be released straight into the extracellular environment, either via the stimulated exocytosis of azurophil granules, or indirectly during frustrated phagocytosis or following neutrophil

apoptosis. In this state, NE has been shown to cleave the bacterial virulence factor flagellin, relinquishing its biological activity (López-Boado et al., 2004). Neutrophil degranulation freely releases only up to 25% of total NE stores into the extracellular space. A much greater proportion of NE instead associates with the neutrophil cell surface by binding to negatively charged sulphate groups of chondroitin sulphate- and heparan sulphate-containing proteoglycans (Campbell and Owen, 2007). Here it remains in an active state and, importantly, becomes inaccessible, and therefore resistant, to $\alpha_1$-antitrypsin ($\alpha_1$-AT), the major endogenous NE inhibitor, which is abundantly expressed in the plasma and interstitial fluid. Thus, membrane-bound NE is thought to represent the predominant and most active form of extracellular NE.

While clearly involved in host defence, NE, particularly in its extracellular form, has also been implicated in other inflammatory processes. One such function involves modulating the activity of chemokines and cytokines by proteolysis. The removal of a C-terminal peptide from chemerin for example converts it into a potent agonist for its receptor ChemR23 expressed by DCs and macrophages (Wittamer et al., 2005). In contrast, the N-terminal processing of CXCL12 results in a loss of chemotactic activity, attenuating T-lymphocyte migration (Rao et al., 2004). The pro-inflammatory cytokines TNF-α, IL-1β and IL-6 are also inactivated by NE. As well as directly cleaving cytokines, released NE has also been shown to modulate cytokine expression. In a model of *P. aeruginosa* infection, TNF- α, MIP-2, and IL-6 were all induced by NE, possibly through the cleavage of TLR-4, and shown to actively contribute to host protection (Benabid et al., 2012). Young et al. also show an impaired generation of the pro-inflammatory mediators IL-1β, KC and MIP-1α in zymosan-stimulated tissues in $NE^{-/-}$ mice, resulting in a reduction in neutrophil recruitment (Young et al., 2004). As neutrophils are typically the first cells to infiltrate sites of inflammation, their ability to regulate the activity and expression of cytokines through NE enables them to influence subsequent leukocyte recruitment. This may result in the dampening or enhancement of the inflammatory response as necessary.

Neutrophil degranulation occurs during transmigration in response to numerous inflammatory mediators, particularly leukotriene $B_4$ ($LTB_4$) and formyl tripeptide (fMLP). Upon release, NE has been shown to mobilise to the migrating front of the cell (Cepinskas et al., 1999). This same study reported an 80% reduction in neutrophil migration when NE was pharmacologically blocked, implicating NE as a key regulator

of transmigration. As outlined earlier, the molecules PSGL-1, ICAM-1 and VCAM-1 are important in several steps of the leukocyte adhesion cascade and are all liable to cleavage by NE. This may function to regulate the sequential movement of neutrophils through the vessel wall by removing existing cell-cell or cell–ECM interactions or by influencing EC signalling pathways (Pham, 2006). In addition, NE-mediated proteolysis may also help regulate integrin binding (Si-Tahar et al., 1997). Its ability to cleave virtually every type of matrix protein also identified NE as a potential mediator of migration through the dense endothelial basement membrane. Supporting this, NE inhibitors have been shown to reduce matrix-protein degradation (Heck et al., 1990), as well as neutrophil migration through EBM-like structures *in vitro* (Delacourt et al., 2002). Inhibiting NE also arrested migrating neutrophils at the level of the venular EBM *in vivo* in the cremaster muscle, possibly owing to an inability to enlarge LERs (Young et al., 2007).

Other putative functions of NE have also been reported. NE for example can release soluble complement receptor 1 (CR1) from the surface of erythrocytes, which can subsequently inhibit complement proteins (Sadallah et al., 1999). NE has also been shown to influence cell signalling through protease activated receptors (PARs), a subfamily of GPCRs that mediate a number of pathways involved in the inflammatory response. They are expressed by a variety of cells including ECs and leukocytes and are functionally regulated through proteolysis of their extracellular domains. In this manner, NE has been shown to inhibit canonical signalling pathways downstream of PAR-1 and PAR-2, triggering instead MAP kinase signalling, resulting in a decrease in vascular permeability (Mihara et al., 2013). NE may also contribute to wound healing by releasing growth factors, digesting cellular debris and remodelling components of the extracellular matrix (Barrick and Campbell, 1999).

This same ability to cleave matrix proteins can however cause tissue damage if NE is excessively or inappropriately released. Furthermore, NE can activate the degradative matrix metalloproteinases MMP-2, MMP-3, and MMP-9, and disarm their inhibitor, TIMP-1. Accordingly, NE has been implicated in several human pathologies which feature neutrophil-mediated inflammation. Chronic obstructive pulmonary disease (COPD) constitutes the fourth leading cause of death worldwide and is characterised by a persistent blockage of airflow from the lungs. Disease progression is associated with NE-mediated pulmonary tissue destruction and mucus secretion, resulting from

neutrophil accumulation and activation. Tobacco smoking is the most common cause of COPD, though it can also be caused by a genetic deficiency in the NE inhibitor α1-antitrypsin, which typically protects against unregulated proteolysis in the lung. NE has similarly been implicated in other lung conditions, including acute lung injury (ALI), cystic fibrosis and adult respiratory distress syndrome (ARDS). Administration of the synthetic NE inhibitor Sivelestat (ONO-5046) has been shown to attenuate pulmonary disorders and improve pulmonary function, however its clinical application is limited to the treatment of ALI and ARDS, and only in Japan (Lucas et al., 2013).

Elevated levels of NE have likewise been found in the synovial fluid of rheumatoid arthritis patients, where it contributes to cartilage degradation (Elsaid et al., 2003). Moreover, NE has been implicated in the development and rupture of atherosclerotic plaques (Henriksen and Sallenave, 2008) and in the metastasis of some breast and lung cancers (Sato et al., 2006). Mutations in the NE gene have also attracted great interest due to their affiliation with neutropenia, a disorder characterised by an abnormally low number of neutrophils predisposing patients to recurrent bacterial infections. Though the precise mechanisms underpinning neutropenia remain to be clarified, it appears mutant NE proteins either misfold or are mislocalised, culminating in the diminished production of neutrophils from progenitor cells in the bone marrow (Horwitz et al., 2007).

*c) NE and monocytes:*

The biochemical properties of NE, with regards to both its physiological and pathological functions, have almost entirely been studied in neutrophils. In contrast, very few studies have explored NE in the context of monocytes. A subpopulation of human monocytes have however been shown to store NE and other enzymes traditionally associated with neutrophils in cytoplasmic granules (Owen et al., 1994). This was corroborated by Dollery et al. who demonstrated NE mRNA and protein expression in human blood monocytes and their macrophage derivatives (Dollery et al., 2003). Moreover, they show abundant NE in the macrophage-rich areas of vulnerable atherosclerotic plaques where it presumably promotes plaque rupture. As with neutrophils, NE has also been implicated in the migration of monocytes, though this too remains unclear. Supporting a role for NE in monocyte transmigration, it has been shown that monocytes deficient in NE exhibit reduced motility through matrix

structures *in vitro* and cigarette smoke-induced recruitment of monocytes to the lung is impaired in $NE^{-/-}$ mice (Shapiro et al., 2003). Conversely, the presence of the NE-specific inhibitor ONO-5046 had no effect on CCL2-induced monocyte migration in the mouse cremaster muscle *in vivo* (Voisin et al., 2009). Taken together, it is possible that NE is only functional in a stimulus- and/or tissue-specific manner.

### *1.5 Hypothesis and aims of the study*

Confirming a role for NE in monocyte transmigration may uncover novel therapeutic avenues to treat monocyte-driven pathologies, such as atherosclerosis. In this light, and given the limited and contradicting results that currently exist, we sought to continue to explore NE as a potential regulator of monocyte transmigration *in vivo* in this study. The overriding objectives we want to address are as follows:

**(i) Establishing a mouse model to facilitate the concurrent study of NE and monocyte biology.**

Transgenic $CX_3CR1$-eGFP-knock-in mice exhibit eGFP-fluorescent monocytes enabling them to be accurately distinguished from other leukocyte subsets. Classical and non-classical monocytes can be further differentiated through differences in eGFP intensity and Ly6C expression. These mice will be crossed with $NE^{-/-}$ mice in order to robustly study NE specifically in the context of monocytes.

**(ii) Investigating the expression of NE in murine monocytes.**

While NE has been identified in human monocytes, this has yet to be confirmed in their murine counterparts. As such, we plan to harvest total leukocytes from $CX_3CR1$-eGFP mice and extract pure populations of classical and non-classical monocytes. Quantitative real-time PCR and Western blot analysis will subsequently be employed to determine NE transcript and protein levels, respectively.

**(iii) Investigating the functional role of NE in monocyte trafficking *in vivo*.**

To broadly determine if NE is involved in monocyte recruitment, monocyte infiltrates will be compared in a peritonitis model of inflammation between $NE^{-/-}$

and $NE^{+/+}$ mice. To elucidate a specific role for NE during monocyte TEM, immunofluorescent labelling and confocal microscopy will be employed to track $CX_3CR1$-eGFP monocytes in the mouse cremaster muscle and ear dermis *ex vivo*. This will enable the mechanisms of monocyte extravasation to be explored, including how and where the monocytes interact with the vasculature.

**(iv) Characterising the mode and dynamics of monocyte transmigration *in vivo*.**

Our lab has recently established a confocal intravital microscopy imaging platform to track leukocyte transmigration through cremasteric venules in real time. This technique offers outstanding spatial and temporal resolution, which should enable monocyte behaviour to be rigorously analysed during transmigration *in vivo* for the first time. Once optimised, we can subsequently investigate how NE, and indeed other molecules, may regulate monocyte transmigration over the course of an inflammatory insult.

# CHAPTER 2: Materials and Methods

### *2.1 Reagents*

*a) Antibodies:*

| Name | Description | Application (working conc.) |
|---|---|---|
| **Primary antibodies** | | |
| α-SMA | Monoclonal mouse anti-mouse α-SMA, clone 1A4, conjugated to Cy3, Sigma-Aldrich (St. Louis, USA) | Confocal imaging (CI) (6.5 μg/ml) |
| β-actin | Monoclonal mouse anti-β-actin, clone AC-15, Sigma-Aldrich (St. Louis, USA) | Western blot (WB) (1 μg/ml) |
| CCR1 | Monoclonal rat anti-mouse CCR1, clone 643854, conjugated to PE, R&D Systems (Abingdon, UK) | Flow cytometry (FC) (1 μg/ml) |
| CCR2 | Monoclonal rat anti-mouse/rat CCR2, clone 475301, conjugated to PE, R&D Systems (Abingdon, UK) | FC (1 μg/ml) |
| CCR5 (CD195) | Monoclonal hamster anti-mouse CD195, clone HM-CCR5, conjugated to PE, Biolegend (San Diego, USA) | FC (1 μg/ml) |
| CD115 | Monoclonal rat anti-mouse CD115, clone AFS98, conjugated to PE or Alexa Fluor-488, eBioscience (Hatfield, UK) | FC, CI (0.67 μg/ml) |
| CD45 | Monoclonal rat anti-mouse CD45, clone 30-F11, conjugated to APC, Biolegend (San Diego, USA) | FC, CI (0.5 μg/ml) |
| F4/80 | Monoclonal rat anti-mouse F4/80, clone BM8, conjugated to PE, eBioscience (Hatfield, UK) | FC (0.67 μg/ml) |
| Fc Block™ | Monoclonal rat anti-mouse CD16/CD32, clone 2.4.G2, Pharmingen (Oxford, UK) | FC (1-5 μg/ml) |
| GR1 | Monoclonal rat anti-mouse Ly6G and Ly6C (GR1), clone RB6-8C5, conjugated to e660 or PE, BD Pharmingen (Oxford, UK) | FC, CI (0.1 μg/ml) |
| Integrin β2 (CD18) | Monoclonal rat anti-mouse CD18, clone C71/16, conjugated to PE, BD Pharmingen (Oxford, UK) | FC (1 μg/ml) |
| JAM-C | Polyclonal rabbit anti-mouse JAM-C, Nr. 526, a kind gift from Prof. Beat Imhof (University of | CI (1:100) |

| | | |
|---|---|---|
| | Geneva, Geneva, Switzerland) | |
| L-selectin (CD62L) | Monoclonal rat anti-mouse CD62L, clone MEL-14, conjugated to PE, BD Pharmingen (Oxford, UK) | FC (0.5 μg/ml) |
| Ly6G | Monoclonal rat anti-mouse Ly6G, clone 1A8, conjugated to PE or Alexa Fluor-647, Biolegend (San Diego, USA) | FC, CI (0.2 μg/ml) |
| MRP-14 | Monoclonal rat anti-mouse MRP-14, clone 2B10, conjugated in house to Alexa Fluor-647, a kind gift from Dr. Nancy Hogg (Cancer Research UK, London Research Institute, London, UK) | CI (~7 μg/ml) |
| NE | Polyclonal rabbit anti-human NE, Abcam (Cambridge, UK) | FC (1-5 μg/ml), CI (10 μg/ml), WB (1 μg/ml) |
| PECAM-1 (CD31) | Monoclonal rat anti-mouse CD31, clone 390, conjugated in house to Alexa Fluor-555 and 647, eBioscience (Hatfield, UK) | CI (~5 μg/ml) |
| VE-cadherin (CD144) | Monoclonal rat anti-mouse CD144, clone eBioBV13 (BV13), conjugated in house to Alexa Fluor-555 and 647, eBioscience (Hatfield, UK) | CI (~5 μg/ml) |
| **Secondary antibodies** | | |
| Mouse IgG | Polyclonal rabbit anti-mouse IgG, conjugated to HRP, Dako (Copenhagen, Denmark) | WB (0.2 μg/ml) |
| Rabbit IgG | Goat anti-rabbit IgG, conjugated to Alexa Fluor-488 or 555, Invitrogen (Paisley, UK) | FC (0.8-4 μg/ml), CI (0.8 μg/ml) |
| Rabbit IgG | Goat anti-rabbit IgG, conjugated to HRP, Invitrogen (Paisley, UK) | WB (0.2 μg/ml) |
| **Isotype controls** | | |
| Hamster IgG | Monoclonal Armenian hamster anti-trinitrophenol -KLH IgG isotype control, clone HTK888, conjugated to PE, Biolegend (San Diego, USA) | FC |
| Rabbit IgG | Polyclonal rabbit IgG isotype control, Abcam (Cambridge, UK) | FC, CI |
| Rat $IgG_{2A}$ | Monoclonal rat anti-keyhole limpet hemocyanin (KLH) $IgG_{2A}$ isotype control, clone 54447, conjugated to PE, R&D Systems (Abingdon, UK) | FC |

N.B. In house antibody conjugations were performed using Molecular Probes Antibody Labeling Kits (see below).

*b) Inflammatory stimuli:*

| Name | Description |
|---|---|
| CCL2 | Recombinant Mouse CCL2/JE/MCP-1-CF, Cat. No.: 479-JE/CF, R&D Systems (Abingdon, UK) |
| CCL2 | Recombinant Human CCL2/MCP-1-CF, Cat. No.: 279-MC-010/CF, R&D Systems (Abingdon, UK) |
| IFN-γ | Recombinant Mouse IFN-gamma-CF, Cat. No.: 485-MI-100/CF, R&D Systems (Abingdon, UK) |
| LPS | LPS from *Escherichia coli* 0111:B4, Cat. No.: L4391, Sigma-Aldrich (St. Louis, USA) |
| $LTB_4$ | $LTB_4$, Cat. No.: 434625, Merck (Hoddeston Hets, UK) |
| TNF-α | Mouse TNF-α, Cat. No.: 401-ML-010/CF, R&D Systems (Abingdon, UK) |

*c) Inhibitors:*

| Name | Description |
|---|---|
| GW311616A | NE inhibitor, Cat. No. sc-215120, Santa Cruz Biotechnology, Inc. (Santa Cruz, USA) |
| H33 | JAM-C blocking antibody, monoclonal rat anti-mouse JAM-C, clone H33, Millipore (Hoddeston Hets, UK) |
| ONO-5046 | NE inhibitor, kind gift from ONO Pharmaceuticals (Osaka, Japan) |
| Protease inhibitors | Halt™ Protease and Phosphatase Inhibitor Cocktail (100×), Thermo Scientific (Rockford, USA) |

*d) Kits:*

| Name | Description |
|---|---|
| BCA™ Protein Assay Kit | Cat. No.: 23227, Thermo Scientific (Rockford, USA) |
| Leucoperm™ Fixation and Permeabilization Kit | Cat. No.: BUF09C, AbD Serotec (Kidlingdon, UK) |
| Molecular Probes® Antibody Labeling Kits | Cat. No.: A2018-1/6/7, Invitrogen (Paisley, UK) |
| Monocyte Isolation Kit (BM), mouse | Cat. No.: 130-100-629, Miltenyi Biotec (Bergisch-Gladbach, Germany) |

| | |
|---|---|
| RNeasy® Micro Kit | Cat. No.: 74004, QIAGEN (Valencia, USA) |
| iScript™ cDNA Synthesis Kit | Cat. No.: 170-8890, Bio-Rad (Hemel Hempstead, UK) |

*e) Miscellaneous:*

| Name | Description |
|---|---|
| 7-Aminoactinomycin D (7-AAD) | ~97% pure, reconstituted in PBS to 5 mg/ml, Sigma-Aldrich (St. Louis, USA) |
| Agarose | UltraPure™ Agarose, Invitrogen (Paisley, UK) |
| Bovine serum albumin (BSA) | Cohn fraction V, 95% standard powder pH 7.0, New England Biolabs (Hitchin, UK) |
| DAPI | 4′,6-Diamidino-2-phenylindole dihydrochloride, Sigma-Aldrich (St. Louis, USA) |
| Deoxynucleotide triphosphates (dNTPs) | Bioline Reagents Ltd. (London, UK) |
| DNA Ladder | SmartLadder SF, Eurogentec (Southampton, UK) |
| Draq5™ nuclear dye | 5 mM, Biostatus Ltd. (Shepshed, UK) |
| Dulbecco's Modified Eagle's Medium (DMEM) | High glucose, Gibco (Paisley, UK) |
| EZview™ Red Protein G Affinity Gel | Sigma-Aldrich (St. Louis, USA) |
| Foetal bovine serum (FBS) | Gibco (Paisley, UK) |
| Gelatin | From bovine skin, Type B, Sigma-Aldrich (St. Louis, USA) |
| GelRed ™ nuclear dye | 10,000×, Cambridge BioScience (Cambridge UK) |
| Ham's F12 Nutrient Mixture | Gibco (Paisley, UK) |
| iQ™ SYBR® Green SuperMix | Bio-Rad (Hemel Hempstead, UK) |
| Ketamine | Ketaset® solution, 100 mg/ml, Fort Dodge Animal Health Ltd. (Southampton, UK) |
| L-Glutamine | 200 mM, Gibco (Paisley, UK) |
| MEM Non-Essential Amino Acids Solution | 100×, Gibco (Paisley, UK) |
| Neutrophil Elastase | Recombinant Mouse Neutrophil Elastase/ELA2, CF, |

| | |
|---|---|
| | R&D Systems (Abingdon, UK) |
| Neutrophil Elastase 680 FAST™ | Perkin-Elmer (Norwalk, USA) |
| Normal goat serum (NGS) | AbD Serotec (Kidlingdon, UK) |
| Paraformaldehyde (PFA) | 95%, VWR, (Soulbury, UK) |
| Penicillin/Streptomycin | 10 000 units of penicillin and 10 mg/ml streptomycin, Gibco (Paisley, UK) |
| Phorbol 12-myristate 13-acetate (PMA) | ≥ 99%, Sigma-Aldrich (St. Louis, USA) |
| Polyacrylamide gels | Mini-Protean® TGX™ precast polyacrylamide gels, Bio-Rad (Hemel Hempstead, UK) |
| Poly-L-lysine solution | 0.1% (w/v) in $H_2O$, Sigma-Aldrich (St. Louis, USA) |
| ProLong® Gold Antifade Mountant | Invitrogen (Paisley, UK) |
| Proteinase K | 10 mg/ml, Bioline Reagents Ltd. (London, UK) |
| Protein ladder | SeeBlue® Plus2 Pre-stained Protein Standard, Invitrogen (Paisley, UK) |
| RIPA buffer | Sigma-Aldrich (St. Louis, USA) |
| RPMI Media 1640 | Gibco (Paisley, UK) |
| Saline | Sodium chloride, 0.9% w/v, Baxter Healthcare (Northampton, UK) |
| Sodium dodecyl sulphate (SDS) | 10% SDS solution, Severn Biotech Ltd. (Kidderminister, UK) |
| SuperSignal™ West Pico Chemiluminescent Substrate | Thermo Scientific (Rockford, USA) |
| TAQ polymerase | Biotaq DNA polymerase, 5 U/µl, Bioline Reagents Ltd. (London, UK) |
| Tetramethylbenzidine (TMB) | Peroxidase substrate for ELISA, Sigma-Aldrich (St. Louis, USA) |
| Tris-Acetate-EDTA (TAE) | UltraPure 10× TAE buffer, Invitrogen (Paisley, UK) |
| Tris-HCl | 1 M Tris-HCl solution, pH 8.5, Severn Biotech Ltd. (Kidderminister, UK) |
| Triton™ X-100 | Sigma-Aldrich (St. Louis, USA) |
| Trypan blue | 0.4%, Gibco (Paisley, UK) |
| Xylazine | Rompun® 2% (w/v), 20 mg/ml, Bayer plc. (Newbury, UK) |

### *2.2 Animals*

*a) Maintenance of mice:*

All mice were housed in individually ventilated cages under conditions of controlled lighting (12 hour light, 12 hour dark) and temperature (20 – 23°C) and fed an *ad libitum* standard chow diet. Both male and female mice were used for experiments at an age between 6 and 15 weeks. All experiments were approved by the United Kingdom Home Office according to the Animals Scientific Procedures Act 1986. Mice were humanely culled by cervical dislocation at the completion of each study.

*b) Mouse strains:*

**C57/BL6:** Wild-type (WT) C57BL/6 mice were purchased from Charles River Laboratories (Margate, United Kingdom). All transgenic mouse strains used in this study were backcrossed onto the C57/BL6 genetic background.

**$CX_3$CR1-eGFP-knock-in:** These mice express the reporter gene enhanced green fluorescence protein (eGFP) under control of the endogenous $CX_3$CR1 locus (Jung et al., 2000). $CX_3$CR1-eGFP-ki mice exhibit fluorescently labelled classical and non-classical monocytes, enabling their identification and tracking *in vivo*. The mice were initially obtained from the European Mutant Mouse Archive (Orleans, France).

**Neutrophil elastase knock-out:** Homozygous KO mice are deficient for neutrophil elastase transcript and protein (Belaaouaj et al., 1998). The mice were initially received as a gift from Professor Steven Saphiro, MD (Department of Medicine, University of Pittsburgh, Pittsburgh, USA). NE KO mice were crossed with $CX_3$CR1-eGFP-ki mice in order to study the role of NE in monocyte trafficking.

**LysM-eGFP-knock-in:** These mice express eGFP under control of the endogenous lysozyme M (LysM) locus (Faust et al., 2000). LysM-eGFP-ki mice exhibit particularly bright neutrophils, enabling their identification and tracking *in vivo*. The mice were initially received as a gift from Professor Markus Sperandio (Walter Brendel Center of Experimental Medicine, Ludwig-Maximillians-Universität, Munich, Germany).

*c) Genotyping transgenic mice:*

To determine the genotype of individual transgenic mice, a polymerase chain reaction (PCR)-based assay was performed on genomic DNA isolated from ear notches. The ear notches were initially digested overnight at 55°C in 250 µl lysis buffer containing 100 mM Tris-HCl (pH 8.5), 5 mM EDTA, 200 mM NaCl, 0.2% SDS and 100 µg/ml Proteinase K. The cellular debris was pelleted by centrifugation at 17,000 relative centrifugal force (RCF) for 10 minutes at room temperature (RT) after which the supernatant was removed, added to 250 µl isopropanol in a fresh eppendorf tube and shaken to precipitate the DNA. The DNA was subsequently pelleted by centrifugation at 17,000 RCF for 5 minutes at RT and washed in 70% ethanol. The ethanol was removed and the tubes left open for 5 minutes to air-dry, after which the DNA was resuspended in 50 µl DNAse free $H_2O$.

Two separate multiplex PCR assays were designed to distinguish WT and transgenic alleles of NE KO and $CX_3CR1$-eGFP-ki mice. For each, PCR was performed on a DNAEngine® Peltier Thermal Cycler (Bio-Rad, Hemel Hempstead, UK) using a common forward primer and separate reverse primers specific for the WT and transgenic allele (*Table 2.1*). Details of the PCR reaction mixtures and cycling parameters are outlined below (*Tables 2.2 – 2.4*).

**Table 2.1: PCR primers used to genotype $CX_3CR1$-eGFP-ki and NE KO mice.**

| Gene (reference) | Primer type | Primer name | Melting temp. | Sequence 5'→ 3' | Amplicon size (bp) |
|---|---|---|---|---|---|
| **NE** | Common forward | oIMR7065 | 60.2°C | TGC ACA GAG AAG GTC TGT CG | - |
| | WT reverse | oIMR7064 | 59.8°C | GGA ACT TCG TCA TGT CAG CA | 230 |
| (Mouse Mutant Resource, 2012) | KO reverse | oIMR8162 | 65.4°C | TGG ATG TGG AAT GTG TGC GAG | 310 |
| **$CX_3CR1$** | Common forward | CX3CR1GFP_KL001 | 60.1°C | CAA CAG GGT TCC AAG CAA G | - |
| | WT reverse | CX3CR1GFP_KL002 | 59.9°C | GGA CAG GAA GAT GGT TCC AA | 438 |
| (Jung et al., 2000) | KO reverse | CX3CR1GFP_KL003 | 59.8°C | TGG TGC AGA TGA ACT TCA GG | 569 |

**Table 2.2: PCR reaction mixture used to genotype NE KO mice.**

| Reagents (units) | Stock conc. | Final conc. | Volume (n = 1, µl) |
|---|---|---|---|
| $dH_2O$ | - | - | 17.9 |
| oIMR7064 (pmol/µl) | 100 | 1 | 0.25 |
| oIMR7065 (pmol/µl) | 100 | 1 | 0.25 |
| oIMR8162 (pmol/µl) | 100 | 1 | 0.25 |
| dNTPs (mM) | 10 | 0.2 | 0.5 |
| $MgCl_2$ (mM) | 50 | 2.5 | 1.25 |
| $NH_4$ buffer (×) | 10 | 1 | 2.5 |
| Taq (U/µl) | 5 | 0.5 | 0.1 |
| **Total Volume** | | | **23** |
| *Total vol. (with 2µl DNA)* | | | *25* |

**Table 2.3: PCR reaction mixture used to genotype $CX_3CR1$-eGFP-ki mice.**

| Reagents (units) | Stock conc. | Final Conc. | Volume (n = 1, µl) |
|---|---|---|---|
| $dH_2O$ | - | - | 18.15 |
| CX3CR1GFP_KL001 (pmol/µl) | 100 | 0.5 | 0.125 |
| CX3CR1GFP_KL002 (pmol/µl) | 100 | 0.5 | 0.125 |
| CX3CR1GFP_KL003 (pmol/µl) | 100 | 1 | 0.25 |
| dNTPs (mM) | 10 | 0.3 | 0.75 |
| $MgCl_2$ (mM) | 50 | 2 | 1 |
| $NH_4$ buffer (×) | 10 | 1 | 2.5 |
| Taq (U/µl) | 5 | 0.5 | 0.1 |
| **Total Volume** | | | **23** |
| *Total vol. (with 2µl DNA)* | | | *25* |

**Table 2.4: PCR cycling conditions used for genotyping.**

| Step | Temperature | Time | Cycles |
|---|---|---|---|
| Initial denaturation | 94°C | 5 minutes | 1 |
| Denaturation | 94°C | 30 seconds | 30 (NE)<br>35 ($CX_3CR1$) |
| Annealing | 60°C | 30 seconds | |
| Extension | 72°C | 30 seconds | |
| Final extension | 72°C | 5 minutes | 1 |
| Storage | 4°C | hold | - |

Following PCR amplification, 3 µl ×10 DNA loading buffer (15% Ficoll/0.24% bromophenol blue/0.24% xylene cyanol FF) was added to the PCR reaction mixture and mixed well prior to loading 18 µl into a 1% agarose/1× Tris-acetate-EDTA (TAE) gel containing GelRed™ Nucleic Acid Stain. The gel was run on a Mupid®-One ADVANCE electrophoresis unit (Eurogentec, Southampton, UK) in 1× TAE buffer at 100 volts for 40 minutes and visualised using a BioDoc-It Imaging System (UVP, Upland, USA).

### *2.3 Cell sorting of leukocyte subsets*

*a) Harvesting primary leukocytes:*

Leukocytes were harvested from the bone marrow (BM) and spleens of mice. BM was extracted from both femur and tibia bones. The bones were dissected and rubbed with tissue paper to remove the surrounding muscle tissue. Both ends of the bones were cut off with scissors and the marrow flushed into a petri dish with 5-10 ml of cold PBS using a syringe with a 30 gauge needle. The marrow was gently homogenised with the plunger of a 5-ml syringe, passed through a cell strainer (40-µm-pore size) and collected in a 50 ml Falcon tube. Whole spleens were removed from mice and directly homogenised, as above. The resulting cell suspensions were pelleted by centrifugation at 1200 RCF at 8°C for 5 minutes. The supernatant was discarded and the pellet resuspended in 2 ml Ammonium-Chloride-Potassium (ACK) lysis buffer (150 mM $NH_4Cl$, 1 mM $KHCO_3$, 0.1 mM EDTA, pH 7.3) for 5 minutes at RT to lyse any erythrocytes. The remaining leukocytes were washed twice in PBS and stored at 4°C in the dark.

*b) FACS-sorting leukocyte subsets:*

Fluorescence activated cell sorting (FACS) was used to purify leukocyte subsets from spleens harvested from naïve $CX_3CR1$-eGFP-ki mice. Freshly prepared splenocytes were resuspended in 4 ml PBS and immunostained with 0.4 µg anti-GR1 monoclonal antibody conjugated to PE for 20 minutes on ice in the dark. The cell density was determined using a haemocytometer (see section *2.5b*) and adjusted accordingly to $1.5\times10^7$ cells per ml in PBS + 2% foetal calf serum (FCS). The live/dead marker DAPI was added at a final concentration of 80 ng/ml prior to sorting the splenocytes on a

FACSAria II cell sorter. Classical monocytes, non-classical monocytes, neutrophils and lymphocytes were distinguished based on GR1 and $CX_3CR1$-eGFP expression patterns. The cell subsets were sorted into pre-cooled polypropylene collection tubes coated with 1 ml pure sterile heat inactivated (HI) FCS and counted on a haemocytometer. Cell numbers were standardised (between $5\text{-}10\times10^5$ cells) and pelleted by centrifugation at 1300 RCF at 4°C for 20 minutes. The supernatants were discarded and the cells were either promptly used or snap frozen in liquid nitrogen and stored at -80°C.

*c) MACS-sorting classical monocytes:*

Monocytes were also purified from the spleen and BM of naïve $CX_3CR1$-eGFP-ki mice by MACS (magnetic-activated cell sorting)-separation using the Monocyte Isolation Kit, as per the manufacturer's instructions. Following cell preparation, up to $10^8$ leukocytes were passed through an LS column, placed in the magnetic field of a MidiMACS™ Separator. The magnetically labelled non-target cells are depleted by being retained within the MACS column, whilst the unlabelled monocytes pass through the column for collection. For increased purity, the cells were passed sequentially through two columns. The labelled non-monocytes were subsequently eluted by pipetting 5 ml MACS-buffer (PBS, 0.5% BSA, 2 mM EDTA) onto the column and firmly applying the provided plunger. Upon collection, cell numbers were determined using a haemocytometer (see section *2.5b*). $5\times10^4$ cells from each fraction were prepared for analysis by flow cytometry to ascertain the purity of the MACS-sort (see section *2.5c*). The remaining cells were kept on ice and used promptly for transmigration and gene expression assays.

### *2.4 NE expression analysis*

*a) RT-qPCR:*

NE transcript expression was assayed by reverse transcription quantitative PCR (RT-qPCR). Frozen pellets of FACS-sorted leukocytes were thawed and total RNA extracted using an RNeasy® Micro Kit as per the manufacturer's instructions. The concentration of isolated RNA was determined by measuring its absorbance at 260 nm using a NanoDrop ND-1000 spectrophotometer (NanoDrop Technologies, Labtech International Ltd., Ringmer, UK). 150 ng RNA was converted into cDNA in a 20 µl

volume using the iScript cDNA Synthesis Kit as per the manufacturer's instructions. qPCR reactions were subsequently performed on a 96-well StepOne real-time PCR System (Applied Biosystems, Foster City, USA). Details regarding the primers used to measure the expression of NE, as well as the housekeeping genes GAPDH and cyclophilin, are shown below, along with details of the qPCR reaction mixtures and cycling parameters, which remained constant (with the exception of the primers) for all genes analysed (*Tables 2.5 – 2.7*).

**Table 2.5: qPCR primers used for mRNA quantification.**

| Gene (reference) | Primer type | Primer name | Melting temp. | Sequence 5'→ 3' | Amplicon size (bp) |
|---|---|---|---|---|---|
| **NE** | Forward | 5'NE | 57.3°C | CAC TGT GTG AAC GGC CTA AA | 171 |
| (Access. No. NM_015779.2) | Reverse | 3'NE | 56.7°C | GGA GCC ATT GAG CTG GAT A | |
| **GAPDH** | Forward | 5'GAPDH | 67.8°C | TCG TGG ATC TGA CGT GCC GCC TG | 251 |
| (Access. No. M32599) | Reverse | 3'GAPDH | 66.3°C | CAC CAC CCT GTT GCT GTA GCC GTA T | |
| **Cyclophilin** | Forward | 5'Cyclo | 57.9°C | CCA CCG TGT TCT TCG ACA T | 114 |
| (Access. No. M60456.1) | Reverse | 3'Cyclo | 57.5°C | CAG TGC TCA GAG CTC GAA AG | |

**Table 2.6: qPCR cycling conditions used for transcript quantification.**

| Step | Temperature | Time | Cycles |
|---|---|---|---|
| Initial denaturation | 95°C | 15 minutes | 1 |
| Denaturation | 95°C | 15 seconds | 40 |
| Annealing/Extension | 60°C | 1 minute | |
| DNA dissociation | 95°C | 15 seconds | 1 |
| | 60°C | 15 seconds | 1 |
| | 95°C | 15 seconds | 1 |

**Table 2.7: qPCR reaction mixtures used for transcript quantification.**

| Reagents (units) | Stock conc. | Final conc. | Volume (n = 1, µl) |
|---|---|---|---|
| $dH_2O$ | - | - | 8.2 |
| SYBR green mix (×) | 2 | 1 | 10 |
| Forward primer (µM) | 5 | $1\times10^{-4}$ | 0.4 |
| Reverse primer (µM) | 5 | $1\times10^{-4}$ | 0.4 |
| cDNA (×) | 20 | 1 | 1 |
| **Total Volume** | | | **20** |

*b) Western blot:*

Cellular NE protein expression was assayed by Western blotting. Pellets of pre-sorted or whole leukocytes (1-$10\times10^5$ total cells) were lysed with 25 µl sodium dodecyl sulphate (SDS) loading buffer (250 mM Tris pH6.8, 6% SDS, 10% glycerol, 0.05% Bromophenol blue) supplemented with 10 µl/ml beta-mercaptoethanol (β-ME). Lysates were sonicated for 10 minutes and passed through a 0.3 ml insulin syringe (31G needle) several times to shear genomic DNA and reduce viscosity. After 10 minutes of boiling at 100°C, 20 µl of each lysate and 5 µl of SeeBlue® Plus2 Pre-stained Protein Standard was loaded onto a Mini-Protean® TGX™ precast polyacrylamide gel and proteins separated by SDS-polyacrylamide gel electrophoresis (PAGE) for 70 minutes at 120 volts on a Power Pac HC (Bio-Rad, Hemel Hempstead, UK) Upon completion, the gel was equilibrated in cathode buffer (25 mM Tris base, 192 mM glycine, 10% methanol) for 15 minutes and proteins transferred to a methanol-activated hydrophobic PVDF membrane equilibrated in anode buffer (25 mM Tris base, 10% methanol) by electroblotting at 0.25A for 1.5 hours. The membrane was subsequently blocked in 5% milk (in PBS) for 1 hour and incubated with a primary rabbit anti-NE polyclonal antibody (1 µg/ml) on a rocker overnight at 4°C. After washing with PBS containing 0.05% Tween (PBST) four times for 5-10 minutes, the membrane was incubated with a secondary goat anti-rabbit IgG polyclonal antibody conjugated to horseradish peroxidise (HRP) (0.2 µg/ml) on a rocker for 2 hours at RT. The membrane was washed as before, incubated with 1-2 ml SuperSignal® West Pico Chemiluminescent Substrate and developed on a SRX-101A Medical Film Processor (Konica-Minolta, Ramsey, USA). To provide a protein loading control, the membrane was washed once more, re-probed sequentially with a primary mouse anti-β-actin monoclonal antibody (1 µg/ml, 2 hours

at RT) and secondary rabbit anti-mouse IgG polyclonal antibody (0.2 µg/ml, 1 hour at RT), and processed and developed, as before.

*c) Slot blot:*

To determine levels of secreted NE protein, 250 µl leukocyte-conditioned media (see section *2.8a*) was loaded into the centre of the wells of a PR 648 slot blot apparatus (Hoefer Scientific Instruments, San Francisco, USA) overlaying a methanol-activated hydrophobic PVDF membrane equilibrated in PBS. Suction was applied to draw the liquid through the membrane, adsorbing any proteins onto its surface. This process was repeated with 1 ml PBS to clean the membrane. As with Western blot analysis, the membrane was subsequently blocked, probed sequentially with an anti-NE primary and anti-rabbit secondary antibody, incubated with chemiluminescent substrate and developed on a SRX-101A Film Processor.

*d) Immunoprecipitation:*

To determine if immunoprecipitation could be implemented to measure levels of secreted NE, 10 ng recombinant mouse NE in 500 µl RPMI-1640 SF media was initially incubated with 50 µl EZview™ Red Protein G Affinity Gel beads for 1 hour at RT on a rotating wheel. The beads were pelleted by centrifugation at 4000 RCF at RT for 2 minutes. The supernatant was subsequently incubated with a further 50 µl beads supplemented with 1 µg polyclonal rabbit anti-NE antibody overnight at 4°C on a rotating wheel. The beads were pelleted as before and the supernatant discarded. To elute the adsorbed proteins, the beads were either boiled for 10 minutes in 25 µl SDS loading buffer or incubated twice in 15 µl 0.2 M glycine buffer (pH 2.5) for 10 minutes. The beads were pelleted once more and the supernatants analysed by Western blot, as before.

*e) ELISA:*

To determine if secreted NE could be quantified by an enzyme-linked immunosorbent assay (ELISA), pellets of whole bone marrow leukocytes ($10^6$ total cells) harvested from $NE^{+/+}$ and $NE^{-/-}$ mice were lysed in RIPA buffer and adjusted to a volume of 200 µl with PBS. The lysates were serially diluted 2-fold in PBS (9 final dilutions, total

volume of 100 µl per well) across a 96 well plate and incubated overnight at 4°C. The lysates were subsequently poured off, washed twice with 200 µl PBS and blocked with 1% BSA (100 µl, in PBS) for 1 hour at RT. The wells were washed three times, as before, and incubated with a primary rabbit anti-NE polyclonal antibody (50 µl, 1 µg/ml) for 1 hour at RT. The wells were washed three more time and incubated with a secondary goat anti-rabbit IgG polyclonal antibody conjugated to HRP (50 µl, 0.2 µg/ml) for 1 hour at RT. After a final round of washing, the wells were incubated sequentially with 50 µl TMB peroxidase substrate and 50 µl hydrochloric acid (1 M, after 2 minutes). NE protein expression levels were quantified by spectroscopy at 450 nm using a Spectra MR spectrometer (Dynex technologies Ltd., West Sussex, UK).

*f) Immunofluorescence:*

Immunofluorescence (IF) analysis was employed to investigate the cellular localisation of NE protein in murine leukocytes. $2\times10^5$ total or MACS-sorted leukocytes (in 80 µl PBS) were seeded onto coverslips and left to adhere at RT for 15 minutes. To facilitate cell attachment, the coverslips were initially coated with 90 µl 0.001% poly-L-lysine in $dH_2O$ for 30 minutes at 37°C, after which the excess liquid was removed and the coverslips allowed to air-dry completely (~15 minutes). Upon cell attachment, the PBS was removed and the cells immediately fixed either in 500 µl methanol (incubated at -20°C for 10 minutes) or 4% PFA in PBS (incubated at RT for 20 minutes). The cells were subsequently washed three times with 500 µl PBS. Cells fixed in PFA were permeabilised with 300 µl 0.1% Triton in PBS for 1 minute at RT, before being washed again, as before. The cells were next incubated in blocking solution (PBS, 10% goat serum, 1 µg/ml mouse BD Fc Block) overnight at 4°C and immunolabelled with a polyclonal rabbit anti-NE antibody (1 µg/ml), in conjunction with fluorophore-conjugated antibodies raised against different cell markers, including CD45 (general leukocyte marker), Ly6G (a neutrophil marker) and CD115 (a monocyte marker). The antibodies were prepared in 250 µl PBS + 1% FCS, in which the cells were incubated for at least 5 hours, if not overnight, at 4°C in the dark. The cells were washed as before and incubated with a secondary goat anti-rabbit polyclonal antibody conjugated to Alexa Fluor-555 (0.8 µg/ml) for 1.5 hours at RT. As appropriate, the cells were also stained with 250 µl of the nuclear dye DRAQ5 (1 mM) for a further 10 minutes. The coverslips were washed as before, immersed in two pots of sterile $H_2O$ to remove

excess PBS, and mounted onto microscope slides, cell side down, in a small drop of ProLong® Gold Antifade Reagent. The slides were allowed to cure overnight at RT, after which they were stored at 4°C in the dark.

NE expression and localisation was subsequently determined using a Zeiss LSM 5 PASCAL confocal laser-scanning microscope (Carl Zeiss Ltd, Welwyn Garden City, UK) incorporating either a ×20 water dipping objective lens (numerical aperture 0.5) or a ×63 oil dipping objective lens (numerical aperture 1.4). Z-stack images (0.7 µm optical sections) of cells were captured using the multiple track scanning mode and reconstructed *in silico* using the image processing software IMARIS (Bitplane, Zurich, Switzerland). $NE^{-/-}$ cells were included during analysis to establish levels of non-specific fluorescence.

*g) Flow cytometry:*

To investigate NE protein expression in murine leukocytes *ex vivo,* total leukocytes were harvested from the blood, BM, or peritoneal cavity of $CX_3CR1^{+/eGFP}$ mice and prepared for flow cytometric analysis (see section *2.5c*). Cell surface NE expression was assayed for on live cells, whilst immunostaining for intracellular NE stores required the cells to first undergo fixation and permeabilisation. This was initially achieved using methanol or a combination of PFA and Triton. $3\times10^5$ cells were pelleted at 1200 RCF at 8°C for 5 minutes, resuspended in 100 µl ice-cold methanol or 2% PFA in PBS, vortexed briefly, and incubated at RT for 20 minutes. Cells fixed in PFA were pelleted and subsequently permeabilised in 100 µl 0.1% Triton in PBS at RT for 5 minutes. Unfortunately, neither fixation method enabled successful immunostaining. As such cells were subsequently fixed/permeabilised using the Leucoperm kit (AbD Serotec, UK) as per the manufacturer's instructions, prior to undergoing receptor blocking, immunostaining, and flow cytometric analysis (see section *2.5c*). To label NE, the cells were initially incubated with a primary rabbit anti-NE polyclonal antibody (1 mg/ml; 1:100, 1:500 and 1:1000 dilutions were all tested) at RT for 20 minutes. The cells were washed twice in 500 µl PBS and incubated with a secondary goat anti-rabbit polyclonal antibody conjugated to Alexa Fluor-555 (2 mg/ml; 1:500, 1:1000 and 1:2500 dilutions were all tested) at RT for a further 20 minutes.

### *2.5 Mouse peritonitis model of inflammation*

*a) Induction of inflammation:*

Peritonitis was elicited in mice by intraperitoneal (i.p.) injection of a given inflammatory mediator prepared in 1 ml sterile PBS. Control mice were injected with PBS only. Upon completion of the stimulation period, the mice were anaesthetised by intramuscular (i.m.) injection of 1 ml/kg ketamine (40 mg) and xylazine (2 mg) prepared in saline solution and sacrificed by cervical dislocation. The heart was made accessible by thoracotomy and whole blood was collected by cardiac puncture into a 1-ml syringe pre-coated with 0.5 M EDTA and transferred into a 15 ml Falcon tube on ice containing 5 ml PBS. The peritoneal cavity of the mouse was next exposed and injected with 6 ml ice-cold lavage buffer (PBS, 0.25% BSA, 2 mM EDTA). The abdomen of the mouse was shaken for 30 seconds to dislodge adherent cells and the lavage was retrieved and transferred to a 15 ml Falcon tube on ice.

*b) Peritoneal lavage counts:*

The total number of leukocytes present in the peritoneal lavage was calculated using a haemocytometer (Neubauer, Wertheim, Germany). 10 µl of retrieved lavage buffer was mixed with 10 µl 0.4% trypan blue solution and transferred to a chamber on the haemocytometer. The number of viable cells (trypan blue negative) was counted under an Axiovert 40 CFL light microscope (Zeiss) using ×20 magnification and the cell concentration and total cell number was extrapolated using the manufacturer's instructions.

*c) Flow cytometric analysis of leukocyte recruitment:*

Following their collection, the leukocytes present in the blood and peritoneal lavage were analysed by flow cytometry. The cells in the samples were initially pelleted by centrifugation at 1200 RCF at 8°C for 5 minutes. The supernatant was discarded and the pellet resuspended either in itself (blood) or 500 µl PBS containing 1% heat inactivated normal goat serum (NGS) (lavage). 50 µl of cell-suspension was transferred to a 96 well FACS plate containing 5 µg/ml mouse Fc Block$^{TM}$ and incubated on ice for 20 minutes. The cells were subsequently immunostained for various cell surface markers of interest. Fluorophore-conjugated antibodies raised against these markers were prepared in 50 µl

PBS/NGS, added to the appropriate wells and incubated on ice in the dark for 20 minutes. The cells were next washed in 200 µl PBS/NGS and pelleted by centrifugation, as before. The supernatant was discarded and the pellet resuspended in 300 µl ACK lysis buffer at RT for 5 minutes to lyse the erythrocytes. The cells were washed twice in PBS/NGS, resuspended in 200 µl PBS/NGS and transferred to FACS tubes. 10 µl of the cell viability stain 7-AAD (25 µg/ml) in PBS was added and vortexed prior to acquiring sample data using a FACScalibur flow cytometer and CellQuest acquisition software (both from BD Biosciences, Mountain View, USA). The data was subsequently analysed using FlowJo7.6.4 software (Tree Star Inc., Ashland, USA). Leukocyte protein expression levels were represented as relative fluorescence intensity (RFI), measured as the ratio of the median fluorescence intensity (MFI) of the specific markers to the MFI of isotype controls.

### *2.6 Mouse cremaster muscle model of inflammation*

*a) Induction of inflammation*

To elicit inflammation in the mouse cremaster muscle, male mice were anaesthetised by an i.m. injection as before and administered an intrascrotal (i.s.) injection of a given inflammatory mediator prepared in 400 µl sterile PBS. 4 µg anti-PECAM monoclonal antibody conjugated to Alexa Fluor-555 was included for real-time intravital experiments. Control mice were injected with PBS only. In some experiments, mice were pre-treated with the NE-inhibitor GW311616A (2 mg/kg) or a vehicle control ($H_2O$) by gavage in 0.5 ml $H_2O$ 24 hours prior to i.s. stimulation.

*b) Confocal analysis of leukocyte recruitment:*

Upon completion of the stimulation period, the mice were sacrificed by cervical dislocation and the cremaster muscles surgically removed – a midline incision was made in the scrotum and the testicles gently drawn out, before the cremaster muscle was separated from the underlying connective tissue, opened via a longitudinal incision, and subsequently fully removed from the testis. The cremasters were next fixed by being pinned flat on a piece of dental wax and immersed in 4% PFA at 4°C for 1 hour. After two rounds of washing in PBS, the tissues were incubated in blocking/permeabilisation solution (PBS, 12.5% FCS, 12.5% GS, 0.5% Triton X-100) for 3 hours at RT on a

rotating wheel and immunostained for α-smooth muscle actin (SMA) (a pericyte marker) and either MRP-14 (a neutrophil marker) or VE-cadherin (an EC marker). Fluorophore-conjugated antibodies raised against these markers were prepared in 200 µl PBS + 10% FCS, in which the tissues were incubated at least overnight at 4°C in the dark. The tissues were washed three times in PBS, each for 30 minutes, at RT on a rotating wheel and stored in PBS at 4°C in the dark.

Leukocyte recruitment to the inflamed cremaster muscle was subsequently determined using a Leica TCS SP5 confocal microscope (Leica Microsystems, Milton Keynes, UK), incorporating a ×20 water dipping objective lens (numerical aperture 1). Z-stack images (0.7 µm optical sections) were captured of post-capillary venules (700 µm segments) with a diameter of 20-50 µm at a scanning frequency of 600 Hz and reconstructed *in silico* using the image processing software IMARIS (Bitplane, Zurich, Switzerland). Total numbers of monocytes and neutrophils within/attached to the vessel of interest or within 300 µm of the surrounding tissue were counted. 5-6 venules were analysed per cremaster and a mean average was calculated.

*c) Confocal intravital microscopy:*

Intravital microscopy (IVM) was conducted on the cremaster muscle of male $CX_3CR1^{+/eGFP}$ mice to study the mechanisms of monocyte migration in real time. The mice were anaesthetised and stimulated as before. Upon completion of the stimulation period, the mice were re-anaesthetised by i.p. injection of ketamine (100 mg/kg) and xylazine (10 mg/kg) prepared in saline solution. The mice were maintained at 37°C throughout the procedure by being placed on a custom-built heated microscope stage. Once in a deep sleep (after ~40 minutes) one of the testicles was exteriorised and the cremaster muscle opened, as before. The cremaster was carefully separated from the epididymis and, with the aid of pins, spread radially over the viewing window of the stage. A flow of warm Tyrodes buffered solution was continuously applied to the exteriorised cremaster muscle to preserve its moistness, while simultaneously accommodating the ×20 water dipping objective lens of the Leica TCS SP5 confocal microscope. As necessary, the Tyrodes solution was supplemented with a given inflammatory mediator to perpetuate the inflammatory response.

Straight post-capillary venules, 20-50 μm in diameter and exhibiting good blood flow were selected for analysis of monocyte extravasation. Z-stack images (1 μm optical sections) of half vessels were captured using a resonance scanner at 8,000 Hz at intervals of 1 min for a total of 60-90 minutes. The images were reconstructed using IMARIS, yielding high-resolution four-dimensional videos of monocytes interacting with the vasculature. This enabled the mode and duration of monocyte extravasation to be studied in response to different inflammatory stimuli.

### *2.7 Mouse ear model of inflammation*

*a) Induction of inflammation:*

To elicit inflammation in the mouse ear, $CX_3CR1^{+/eGFP}$ mice were anaesthetised i.m. as before and injected intradermally (i.d.) into the dorsal side of the ear pinnae (typically of the left ear) with a given inflammatory mediator prepared in 30 μl sterile PBS. 2.5 μg anti-PECAM-1 monoclonal antibody conjugated to Alexa Fluor-555 was also included to label the vasculature *in situ*. Control mice were injected with PBS only.

*b) Confocal analysis of leukocyte recruitment:*

Upon completion of the stimulation period, the mice were sacrificed by cervical dislocation, the stimulated ear(s) removed whole with scissors and fixed in 4% PFA at 4°C for 30 minutes. Following a brief wash in PBS, the ventral skin and cartilage of the ear were gently separated from the dorsal skin using forceps. The dorsal skin was subsequently pinned flat on a piece of dental wax and reimmersed in 4% PFA for a further 10 minutes. Each tissue was washed several times in PBS and stored at 4°C in the dark.

As with the cremaster muscle model, leukocyte recruitment to the inflamed ear was determined using a Leica TCS SP5 confocal microscope incorporating a ×20 water dipping objective lens. Z-stack images (0.7 μm optical sections) were captured of post-capillary venules (700 μm segments) with a diameter of 20-60 μm at a scanning frequency of 800 Hz and reconstructed *in silico* using the image processing software IMARIS. Total numbers of monocytes within/attached to the vessel of interest or within 300 μm of the surrounding tissue were counted. 6-7 venules were analysed per ear and a mean average was calculated.

*c) Confocal analysis of NE activity and expression:*

NE activity was assessed in the ear and cremaster muscle of $CX_3CR1^{+/eGFP}$ mice by administering the fluorescent imaging agent Neutrophil Elastase 680 FAST™ intravenously (i.v.) (2 nmols in 200 µl PBS) immediately prior to inducing local inflammation. After 4 hours, the tissues were harvested, processed and imaged, as before. NE activity was correlated to the fluorescence intensity measured at 640-700 nm following excitation at 633 nm. NE protein expression was also evaluated in stimulated ears. Following PFA-fixation and protein blocking (as before), tissues were immunostained with a primary rabbit anti-NE polyclonal antibody (10 µg/ml) overnight at 4°C. After washing with PBS three times for 30 minutes, the tissues was incubated with a secondary goat anti-rabbit IgG polyclonal antibody conjugated to Alexa Fluor-647 (0.8 µg/ml) for 1.5 hours at RT. Markers for MRP-14 and VE-cadherin were concurrently immunostained, as before (*see section 2.6b*). Using the surface function on IMARIS, the intensity of NE staining was measured in individual monocytes and neutrophils, following normalisation to $NE^{-/-}$ samples.

### *2.8 Cell culture*

*a) Stimulating leukocytes in vitro:*

In order to study NE expression in monocytes upon stimulation, $2\text{-}10\times10^5$ sorted monocytes were initially resuspended in 500 µl RPMI-1640 media supplemented with 10% heat-inactivated foetal bovine serum (HI-FBS), 2 mM L-glutamine, and 1% Penicillin (10,000 U/ml)/Streptomycin (10 mg/ml). The cells were either maintained in suspension in 1.5 ml Eppendorf tubes or adhered to a 12-well plate. Stimulation was performed in a humidified incubator adjusted to 37°C and 5% $CO_2$ using different combinations of cytokines (or appropriate vehicle controls) for varying durations (detailed in depth in the results chapters). The cells were pelleted by centrifugation at 1300 RCF at 4°C for 20 minutes. Secreted NE was assayed for in the recovered supernatant via slot blot analysis or immunoprecipitation (see sections *2.4c-d*), while cellular NE was analysed either by Western blotting (see section *2.4b*) or immunofluorescence (see section *2.4f*). NE activity was also evaluated in cells fixed with PFA (opposed to methanol) by incubating the coverslips in 250 µl PBS containing Neutrophil Elastase 680 FAST™ (1 µM) for 2 hours at 4°C.

*b) Murine leukocyte transmigration assay:*

Murine skin endothelial cells (sENDs) were routinely cultured in Dulbecco's modified Eagle's medium (DMEM), supplemented with 10% HI-FBS, 2 mM L-glutamine, 1% non-essential amino acids, 1 mM sodium pyruvate and 5 µM β-ME (all Invitrogen, UK). Transmigration assays were readied in 24-well plates by seeding $5\times10^4$ sEND cells onto Transwell filters (3 or 8 µm pore size) (VWR, Soulbury, UK) pre-coated with 150 µl gelatin (0.5%). The cells were placed in a humidified incubator (37°C, 5% $CO_2$) and allowed to reach confluency for two days. $1\text{-}5\times10^5$ total or sorted murine leukocytes suspended in 150 µl RPMI-1640 media supplemented with 0.5% HI-FBS, 2 mM L-glutamine, and 1% Penicillin (10,000 U/ml)/Streptomycin (10 mg/ml) were then added to the upper chamber of the Transwells. 1 ml of media was added to the lower chamber and supplemented either with FBS (total of 10%) or murine CCL2 (10 nM) to induce cell migration. Numbers of transmigrated cells were quantified after 4-16 hours by counting and combining the number of cells in the lower chamber in three separate and randomised fields of view using an Olympus IX81 inverted microscope (Olympus Medical, Southend-on-Sea, UK) (4× objective). Assays were run in triplicate.

*c) Human leukocyte transmigration assay:*

Human umbilical vein endothelial cells (HUVECs) were routinely cultured in a 50:50 mix of DMEM and Hams F12 media supplemented with 10% HI-FBS, 25 µg/ml endothelial mitogen (AbD Serotec, UK), 1 µg/ml heparin (Sigma-Aldrich, USA) and 1% Penicillin (10,000 U/ml)/Streptomycin (10 mg/ml). The human monocyte-like U937 cell line was routinely cultured in RPMI-1640 media supplemented with 10% HI-FBS, 2 mM L-glutamine and 1% Penicillin (10,000 U/ml)/Streptomycin (10 mg/ml). Transmigration assays were readied in 24-well plates by seeding $5\times10^5$ HUVEC cells onto Transwell filters (8 µm pore size) pre-coated with 150 µl gelatin (0.5%). The cells were placed in a humidified incubator (37°C, 5% $CO_2$) and allowed to reach confluency for two days. $5\times10^5$ U937 cells suspended in 150 µl supplemented RPMI-1640 media (containing a reduced 0.5% HI-FBS) containing either the NE-inhibitor ONO-5046 (50 µM) or PBS (vehicle control) were then added to the upper chamber of the Transwells. 1 ml of media supplemented with human CCL2 (10 nM) was added to the lower chamber to induce cell migration. Numbers of transmigrated cells were quantified after 4 hours as before. Assays were run in triplicate.

### *2.9 Statistical analysis*

Data analysis was performed using GraphPad Prism, version 6. Graphs are presented as a mean value ± standard deviation (SD) or standard error of the mean (SEM), as appropriate. An unpaired two-tailed T-test was used to compare data from two groups. A one sample T-test was used to compare a sample mean to a known value. P-values < 0.05 were considered to be statistically significant.

# CHAPTER 3: Establishing a mouse model to facilitate the concurrent study of NE and monocyte biology.

## *3.1 Introduction*

Particularly useful in dissecting complex signalling pathways and intricate molecular mechanisms, the implementation of *in vitro* techniques has contributed immensely to our current understanding of leukocyte transendothelial migration. That being said, there are major caveats to extrapolating *in vitro* data to *in vivo* physiology. Even the most elaborate *in vitro* models struggle to replicate the complex structure of vessel walls or take fully into account the contribution of environmental factors, such as the haemodynamic forces of the circulation or local cytokine production. Accordingly, and owing to the advent of established animal models, the mechanisms of leukocyte migration are now being increasingly studied directly *in vivo*.

Several strategies have been developed to study monocyte trafficking *in vivo*. Monocytes have been labelled with fluorescent beads or radioactive isotopes and adoptively transferred into recipient mice. Increasingly, transgenic mouse models expressing the enhanced green fluorescent protein (eGFP) reporter gene are being employed. Lysozyme-M eGFP-knock-in mice express eGFP specifically in myelomonocytic cells including neutrophils and monocytes, while the *c-fms*-eGFP transgene is expressed throughout the mononuclear phagocyte system (Sasmono et al., 2003). Probably the most commonly used transgenic model to study monocytes is the $CX_3CR1$ knockout mouse. $CX_3CR1$ constitutes a specific seven transmembrane G protein-coupled receptor for the chemokine $CX_3CL1$. $CX_3CR1$ is expressed by monocytes, subsets of natural killer (NK) and dendritic cells and the brain microglia (Imai et al., 1997). In order to disrupt the *$CX_3CR1$* gene, the second exon was replaced by the *eGFP* gene (Jung et al., 2000). This approach not only created a mutant *$CX_3CR1$* locus, but also fluorescently labelled all $CX_3CR1$-bearing cells. As such, $CX_3CR1$-eGFP-knock-in mice have been routinely used to identify and track monocytes and their derivatives *in vivo*.

$CX_3CR1$ is expressed by all murine monocytes, though to varying extents with classical and non-classical monocytes displaying intermediate and high levels of $CX_3CR1$ on their surfaces, respectively. $CX_3CR1$ has been implicated in the adhesion and migration

of both monocyte subsets through the endothelium, a potent source of $CX_3CL1$, though predictably appears to play a more dominant role in the trafficking of non-classical monocytes. Interestingly, the recognition of $CX_3CL1$ by $CX_3CR1$ on monocytes also confers an essential anti-apoptotic survival signal (Gautier et al., 2009). Accordingly, heterozygous $CX_3CR1^{+/eGFP}$ mice are most commonly used during intravital studies as they are devoid of any defects in monocyte migration and/or survival, while retaining sufficient fluorescence intensity. Monocyte trafficking has been monitored in these mice under physiological and inflammatory conditions both *ex vivo*, for example by analysing infiltrated cells in the peritoneal cavity, and *in vivo* in the mouse cremaster muscle (Soehnlein et al., 2008), kidney (Li et al., 2008), and spleen (Swirski et al., 2009a).

We aimed to similarly exploit $CX_3CR1$-eGFP-ki mice to investigate monocyte migration *in vivo* in this study. In particular, we were interested in how the protease neutrophil elastase may regulate this process. Through its ability to induce endothelial injury and cleave virtually every type of extracellular matrix protein, NE has been implicated as a potent mediator of vascular and tissue injury. This has led to the generation of numerous recombinant endogenous or synthetic NE-specific inhibitors, which, while ultimately intended as possible therapeutics for NE-mediated pathologies, have also been routinely used in research labs to better understand NE biology. Applied principally *in vitro*, the physiological roles of NE *in vivo* have however been most commonly and rigorously investigated in NE knock-out ($NE^{-/-}$) mice (Belaaouaj et al., 1998). While numerous studies conducted on these mice have identified NE as a regulator of neutrophil extravasation, the involvement of NE in the trafficking of monocytes has received almost no attention. To address this issue, NE KO mice were crossed, for the first time, with $CX_3CR1$-eGFP-ki mice. $CX_3CR1^{+/eGFP}$ mice carrying either mutant or wild-type copies of the NE gene were subsequently compared to investigate the expression and function of NE in monocyte migration *in vivo*.

For this study to be successful, it was imperative to initially establish a robust set of protocols for the effective application of all tools, reagents, and mouse models. Furthermore, though NE KO mice are reportedly normal in the absence of inflammatory stress, we felt it necessary to characterise the leukocyte profiles of naïve $NE^{-/-}$ and $NE^{+/+}$ mice to confirm there were no underlying differences that may influence their responses

during inflammation. We sought to achieve these general aims in this opening results chapter by addressing the following specific objectives:

- Optimise imaging techniques to reliably identify and track $CX_3CR1$-eGFP$^+$ monocytes both *ex vivo* in suspension and *in situ* at sites of inflammation.
- Develop gene expression assays specific for NE.
- Develop genotyping assays to distinguish mutant and wild-type alleles of *$CX_3CR1$* and *NE*.
- Determine the number, proportion and distribution of leukocyte subsets in NE$^{-/-}$ and NE$^{+/+}$ mice under naïve conditions.

### *3.2 Results*

#### *a) Blood monocytes and neutrophils from $CX_3CR1$-eGFP-ki mice can be reliably identified by flow cytometry.*

Flow cytometry is a commonly used technique to identify discrete leukocyte populations within a heterogeneous sample of cells based on their physical and biochemical characteristics. It uses laser light to gauge the size and granularity of cells and to detect fluorescently-labelled antigens expressed specifically or distinctly by a cell type of interest. In this manner, mouse blood monocytes are traditionally classified as $CD115^+$, $CD11b^+$, $F4/80^{int}$ (Sunderkötter et al., 2004). They can also be crudely distinguished from other blood leukocytes by their relatively large size and moderately granular cytoplasm, reflected respectively in their forward and side scatter profiles ($FSC^{int}$, $SSC^{int}$). The two major monocyte subsets can be subsequently divided according to CD62L, Ly6C, and CCR2 expression.

The generation of $CX_3CR1$-eGFP-ki mice has provided a new approach to classify monocytes by flow cytometry. Not only are all monocytes in these mice intrinsically fluorescent, the two subsets can be distinguished by eGFP intensity. As fewer monocyte-specific markers are required, there is also a greater scope to simultaneously stain for other markers of interest. While monocytes have been identified in $CX_3CR1$-eGFP-ki mice by flow cytometry in other studies, we have yet to optimise a gating strategy in our group. Using blood harvested from $CX_3CR1^{+/eGFP}$ mice, we sought to gate both monocyte subsets, as well as neutrophils, according to $CX_3CR1$ and GR-1 expression. GR-1 is a GPI-anchored protein of unknown function consisting of two epitopes, Ly6G and Ly6C. Ly6G represents a specific marker of neutrophils, while Ly6C is expressed by classical monocytes (as well as neutrophils) but not non-classical monocytes.

Cell analysis was performed on a BD FACSCalibur. This particular flow cytometer is capable of detecting up to four colours at the same time. Three of the colour detectors (FL-1, FL-2, and FL-3), in addition to the forward and side scatter detectors, are excited with a 488 nm blue laser, while the fourth colour detector (FL-4) is excited with a 635 nm red laser. eGFP emits green light ($\lambda_{max}$ = 510 nm) when excited with the blue laser, which is detected in the FL1 channel. GR-1 was immunostained with an anti-mouse monoclonal antibody (clone RB6-8C5) conjugated to eFluor-660, detected in the FL4 channel. In addition, all cells were stained for the platelet-marker CD41 and the

viability stain 7-AAD, which intercalates DNA of dying or dead cells only. Platelets often stick to leukocytes, influencing their light scattering properties, while dead cells tend to bind antibodies non-specifically, giving rise to false positive results. Only cells negative for CD41-PE-Cy7 and 7-AAD, both of which are detected by the FL3 channel, were gated for analysis. All other cell markers were conjugated with fluorophores detected in the FL2 channel (*Appendix 3.1*).

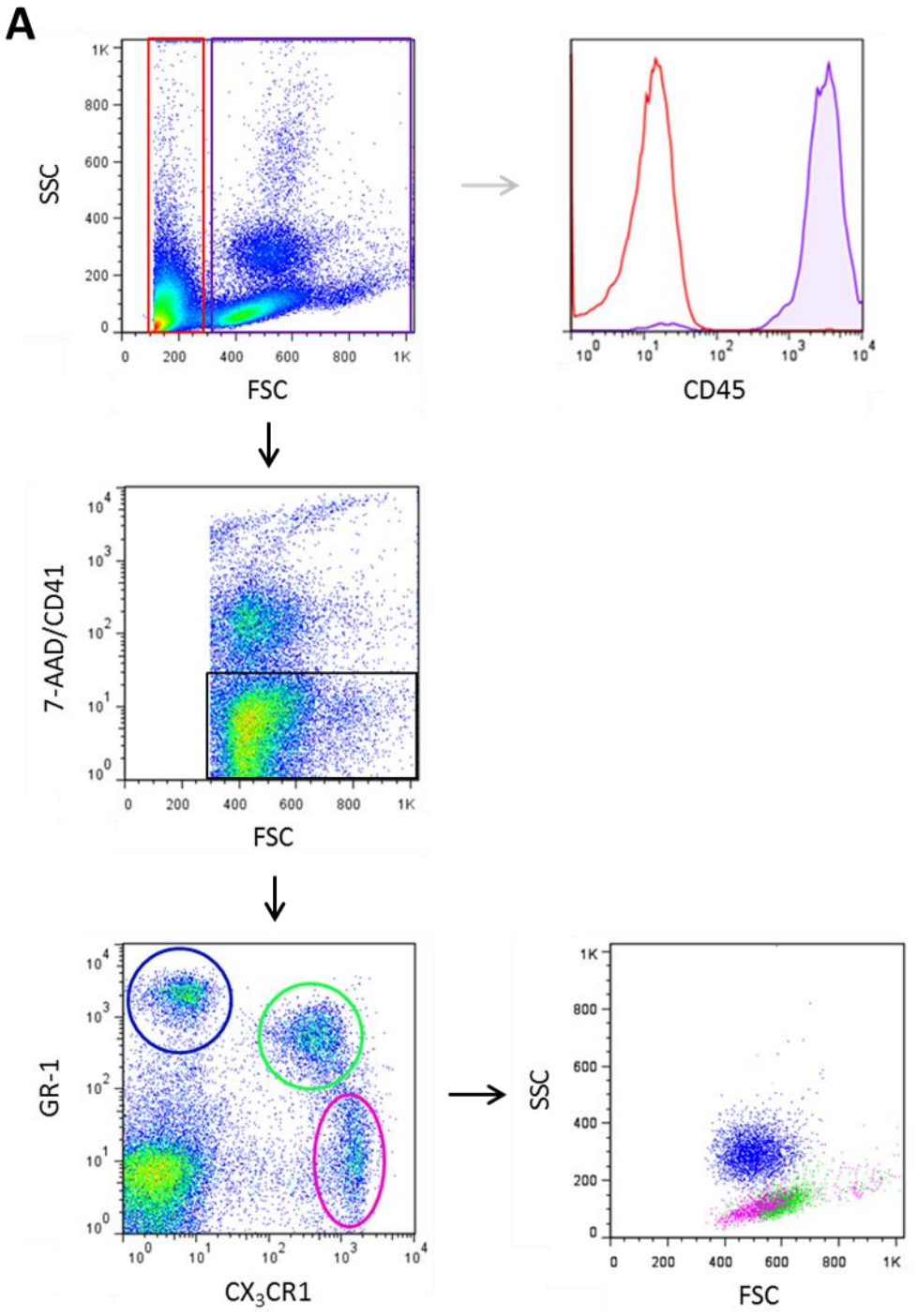

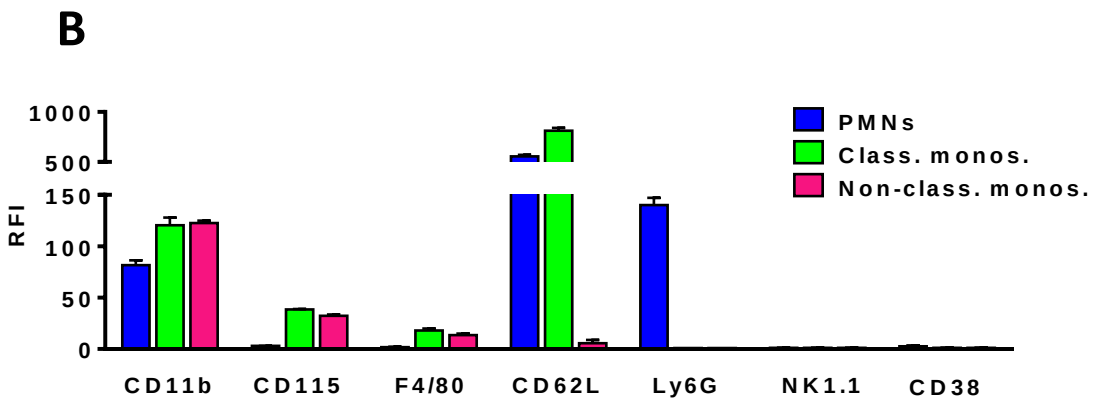


**Figure 3.1: Flow cytometric gating strategy for discerning leukocytes in $CX_3CR1$-eGFP-ki mice.** Blood harvested from $CX_3CR1^{+/eGFP}$ mice was lysed, immunostained and analysed by flow cytometry. $CD45^+$ leukocytes were separated from residual erythrocytes by their FSC/SSC profile. Upon the exclusion of dead cells and platelet complexes, classical monocytes (green), non-classical monocytes (pink) and neutrophils (blue) were distinguished according to GR-1 and $CX_3CR1$ expression (A), as confirmed by their SSC properties and relative fluorescence intensities (RFI) of CD11b, CD115, F4/80, CD62L, Ly6G, NK1.1 and CD38 (B). Data are represented as the mean ± SEM (n = 2 mice, average of 2-3 FACS readings per mouse).

In running blood samples from $CX_3CR1^{+/eGFP}$ mice through the flow cytometer, total leukocytes were initially separated from erythrocytes and cellular debris by their FSC and SSC profiles, as verified by expression of the general leukocyte marker CD45. Dead cells and platelet complexes were subsequently excluded and the remaining cells plotted according to $CX_3CR1$ and GR-1 expression. This revealed four distinct populations of cells (*Figure 3.1*). The two $CX_3CR1^+$ populations were also positive for CD11b, CD115 and F4/80, and displayed an intermediate FSC/SSC profile, confirming them as monocytes. The $CX_3CR1^{med}$ but not $CX_3CR1^{hi}$ cells also expressed GR-1 and CD62L, signifying these cells correspond to classical and non-classical monocytes, respectively. Those cells negative for $CX_3CR1$ but positive for GR-1 were also highly granular ($SSC^{hi}$), positive for CD11b and Ly6G, but negative for F4/80 and CD115, all indicative of neutrophils. The remaining $CX_3CR1^-$, GR-$1^-$ double-negative population represents all other leukocytes, including $CD38^+$ lymphocytes and $NK1.1^+$ NK cells.

***b) Monocytes in $CX_3CR1$-eGFP-ki mice can be visualised undergoing TEM in the cremaster muscle and ear dermis.***

Having established a rigorous approach to identify and quantify both monocyte subsets *ex vivo* in the blood of $CX_3CR1^{+/eGFP}$ mice, we next sought to directly study monocyte trafficking *in situ* at sites of inflammation. Using a combination of immunofluorescence

and confocal microscopy, our group has previously imaged $CX_3CR1\text{-}eGFP^+$ monocytes migrating out of stimulated post-capillary venules in the cremaster muscle (Voisin et al., 2009). Found only in males, the cremaster muscle envelops the testis and helps regulate its movement. Due to its thin, transparent, and highly vascularised nature, the mouse cremaster muscle is often exploited to record high resolution images of the microcirculation during inflammation. This enables leukocyte extravasation to be directly visualised and its underlying mechanisms characterised, including how and where the leukocytes interact with the vasculature and each other. We sought to use the cremaster muscle of $CX_3CR1^{+/eGFP}$ mice, as before, to analyse monocyte transendothelial migration in this study. Furthermore, we applied the same imaging protocols to the thin dorsal skin of the mouse ear, another preparation commonly used to study leukocyte trafficking.

We initially stimulated both the cremaster muscles and ears of $CX_3CR1^{+/eGFP}$ mice with LPS, a reaction previously shown to induce both monocyte and neutrophil infiltration (Voisin et al., 2009). After 4 hours the tissues were harvested, immunostained, and analysed by three-colour confocal microscopy. Vascular endothelial cells were identified by immunostaining for the junctional molecules VE-cadherin or PECAM-1. Arterioles, venules and capillaries were distinguished according to the distinct morphology of their endothelium or associated layer of pericytes, as identified by α-SMA staining (*Appendix 3.2*). In order to identify neutrophils, we stained for MRP-14, a cytoplasmic calcium binding protein highly expressed by neutrophils (Newton and Hogg, 1998). Using this approach, monocytes and neutrophils could be clearly visualised and counted, both in the cremaster muscle and ear, as they emigrated out of post-capillary venules (*Figure 3.2*).

***c) NE transcript can be accurately detected in murine samples by PCR.***

As part of this study we intended to characterise NE expression in murine monocytes by measuring levels of both NE transcript and protein. This was principally achieved *in vitro* by qRT-PCR and Western blotting, respectively. Both of these techniques, though commonly employed by our group, had to be re-optimised specifically for NE. Ideal as negative controls, samples from NE KO mice were included in all analyses to ensure NE was reliably detected in WT mice.

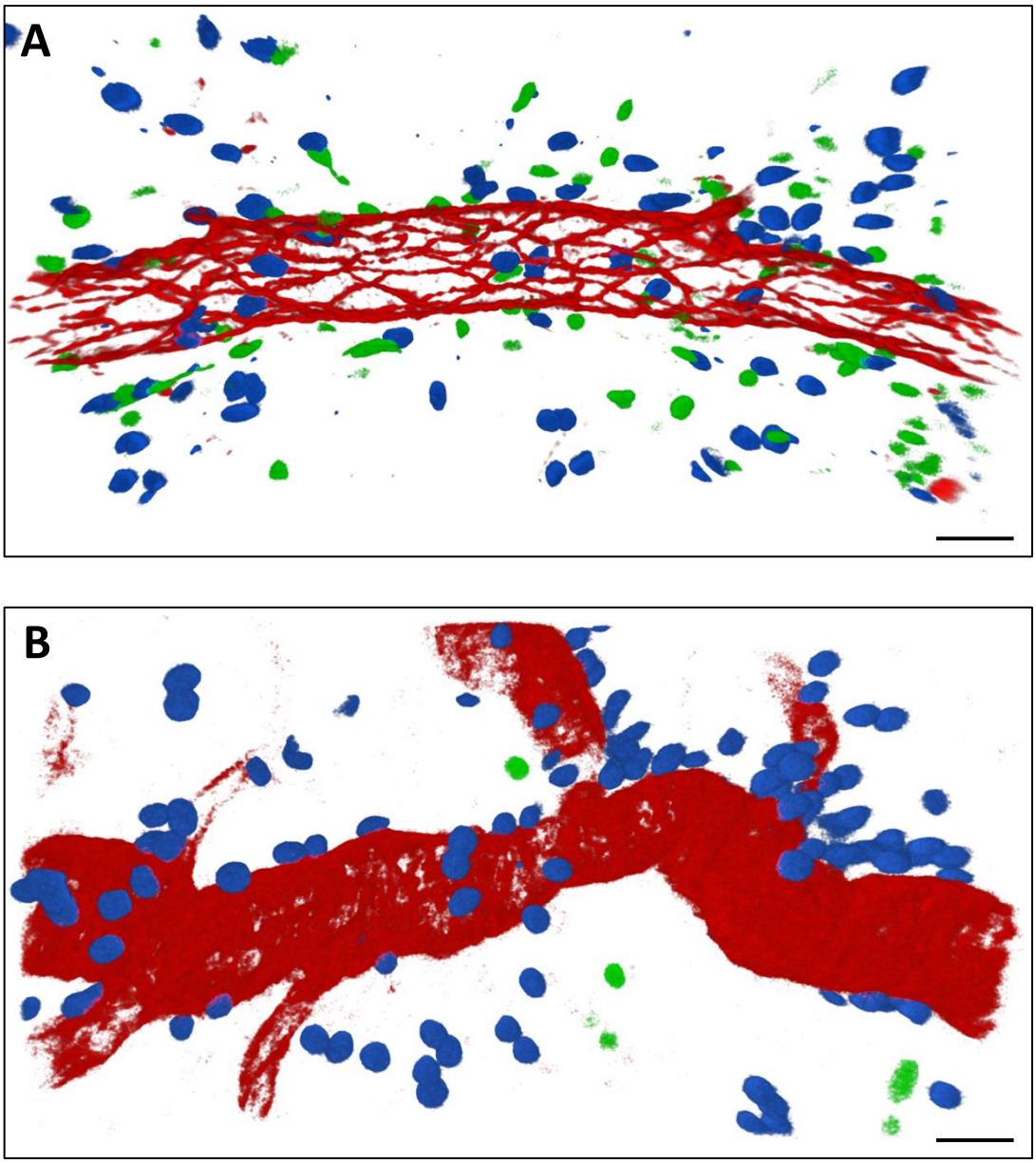


**Figure 3.2: Confocal imaging of monocyte and neutrophil transendothelial migration *in vivo* in $CX_3CR1$-eGFP-ki mice.** Representative reconstructed confocal images of post-capillary venules in the cremaster muscle (A) and ear (B) of $CX_3CR1^{+/eGFP}$ mice stimulated with LPS for 4 hours. Upon culling the mice, tissues were harvested, fixed in PFA and immunostained for neutrophils (MRP-14, blue) and either VE-cadherin (cremaster, red) or α-SMA (ear, red). $CX_3CR1$-$eGFP^+$ monocytes are shown in green. Scale bar, 30 μm.

Quantitative reverse transcription PCR (qRT-PCR) is the most common approach for measuring mRNA abundance. In this method, total RNA is first transcribed into complementary DNA (cDNA), which is subsequently used as a template for qPCR. Incorporating DNA-binding fluorescent dyes, during qPCR the amount of PCR product is assessed throughout the reaction. By establishing the critical threshold ($C_T$) cycle, i.e.

the first PCR cycle in which a tangible fluorescent signal can be detected, the amount of starting RNA material can be derived. Sequence-specific primers are essential in qPCR to ensure only the target transcript is amplified and detected. In order to measure transcript levels of NE, we were first required to design an appropriate pair of primers. To reduce amplification from contaminating genomic DNA, we targeted sequences that span exon-exon boundaries. Specifically, the chosen forward and reverse primers corresponded to the boundaries of exons II/III and exons III/IV of the NE transcript, respectively (*Table 2.5* and *Appendix 3.3*). In keeping with the recommended guidelines for qPCR, the primers were also 18-25 nucleotides long (19 and 20), exhibited similar melting temperatures (56 and 54°C), contained a GC content between 50 and 60% (50 and 53%), and yielded an amplicon between 100 and 300 bp (171 bp).

To confirm the chosen primers generated PCR products specific to NE, conventional PCR was performed on cDNA obtained from $NE^{+/+}$ and $NE^{-/-}$ mice. As NE is transcribed predominantly in developing myeloid cells, RNA was originally isolated from whole bone marrow leukocytes. Upon resolving the PCR products on a gel, a single band of appropriate size could be seen in the $NE^{+/+}$ lane only (*Figure 3.3A*). A specific and uniform PCR product is imperative during qPCR to achieve accurate template quantification. This was achieved specifically by employing the comparative $C_T$ method of relative quantification, in which levels of a target gene (in this case NE) are normalised to an endogenous housekeeping gene (GAPDH). For this to be valid, the PCR efficiencies, i.e. the rate at which a PCR amplicon is generated, have to be equal for both genes at approximately 100%. Under such circumstances, levels of PCR products double every cycle during the exponential phase of amplification. When represented as a semi-log regression line plot of $C_T$ value vs. log of input cDNA, a 100% efficient reaction is indicated by a standard curve slope of -3.32. With PCR efficiencies for NE and GAPDH measuring at -3.15 (107%) and -3.27 (102%), respectively, we can be confident that these same primers enabled cellular NE expression to be reliably assessed, as described later on in the study (*Figure 3.3B*).

***d) NE protein can be accurately detected in murine samples by Western blotting.***

Western blotting is the most commonly used technique to analyse relative levels of individual proteins. Whole protein samples are initially separated according to size by gel electrophoresis and transferred to a membrane, where they are subsequently probed

with primary antibodies specific to the target protein. Enzyme-conjugated secondary antibodies are most commonly used as a means of generating a detectable signal. The intensity of this signal is proportional to the quantity of protein present on the blot. A successful Western blot is reliant on a primary antibody that is not only specific to the protein of interest, but also offers a high signal-to-noise ratio that can be detected with minimal background.

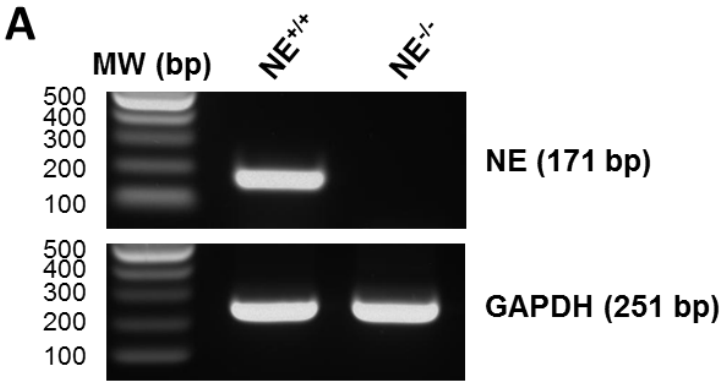


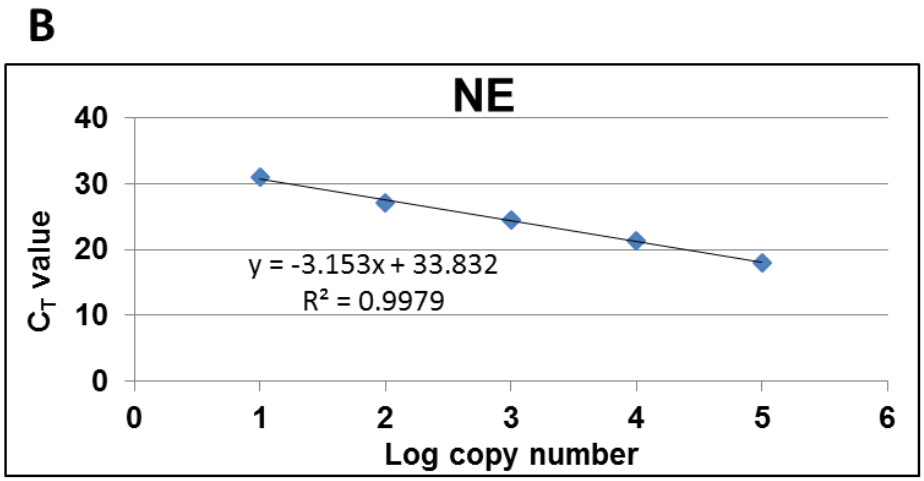


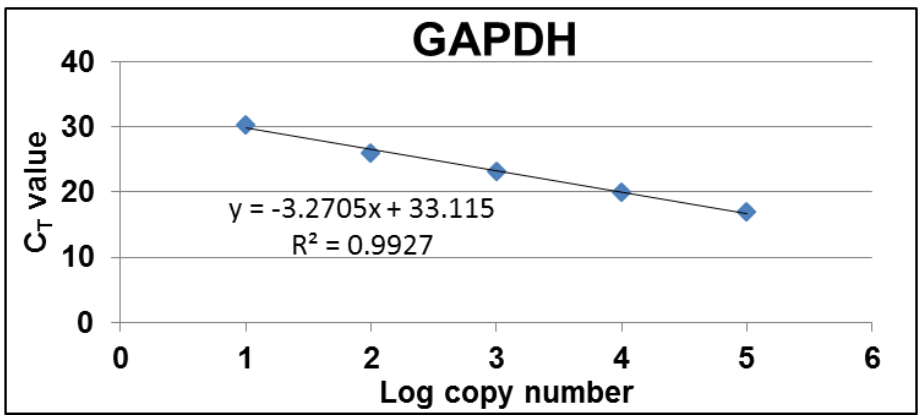

**Figure 3.3: Validation of qPCR primers for NE transcript quantification.** Total cellular RNA was extracted from whole BM leukocytes from $NE^{-/-}$ and $NE^{+/+}$ mice and converted into cDNA. Conventional PCR was initially performed with primers specific for NE and the housekeeping gene glyceraldehyde 3-phosphate dehydrogenase (GAPDH). PCR products were resolved on a 1.5% agarose gel (A). qRT-PCR was subsequently performed across a serial dilution of cDNA to determine PCR amplification efficiencies (B).

In the specific context of murine NE, it appears from the literature that most groups conduct Western blots with their own self-raised antibodies, presumably due to the lack of a suitable commercially available antibody. Our group too has recently raised an anti-murine NE antibody, achieved by immunising rabbits with a synthetic peptide analogous to residues 84-98 of the mouse NE protein (*Appendix 3.4*). This sequence was chosen as it not only localises to the protein surface, but is also unique to murine NE. This was desirable as, despite sharing an identity of 73%, most anti-human NE Abs do not cross-react well with murine NE. Total antibodies were purified from the final immunised serum, effectively yielding a rabbit anti-mouse NE polyclonal antibody, termed SY0049.

We initially trialled SY0049, as well as two newly available anti-human NE antibodies, to determine which, if any, were suitable for quantifying mouse NE via Western blotting. Starting with SY0049, while recombinant mouse NE could be detected (runs at ~34 kDa under reducing conditions), it failed to detect native mouse NE (29-33 kDa) in the lysates of $NE^{+/+}$ leukocytes (*Figure 3.4*). While the mouse anti-human NE mAb (from Sigma) did manage to detect a band at ~30 kDa, this band was similarly observed for $NE^{-/-}$ leukocytes suggesting it was unspecific to NE. In contrast, the rabbit anti-human NE pAb (from Abcam), in addition to recognising recombinant NE, generated bands in the $NE^{+/+}$ lane only, running at ~22, 24 and 32 kDa. As all three of these bands are seemingly NE-specific, we propose that only the top band represents the full-length protein, with the two subsequent bands corresponding to lower molecular weight protein fragments. This is in keeping with a previous study on human neutrophils, in which NE is shown to generate several autolysis peptides during SDS gel electrophoresis (Liau et al., 1993). Due to its ability to react specifically with murine NE, only the rabbit anti-human NE pAb was used in future Western blot analyses.

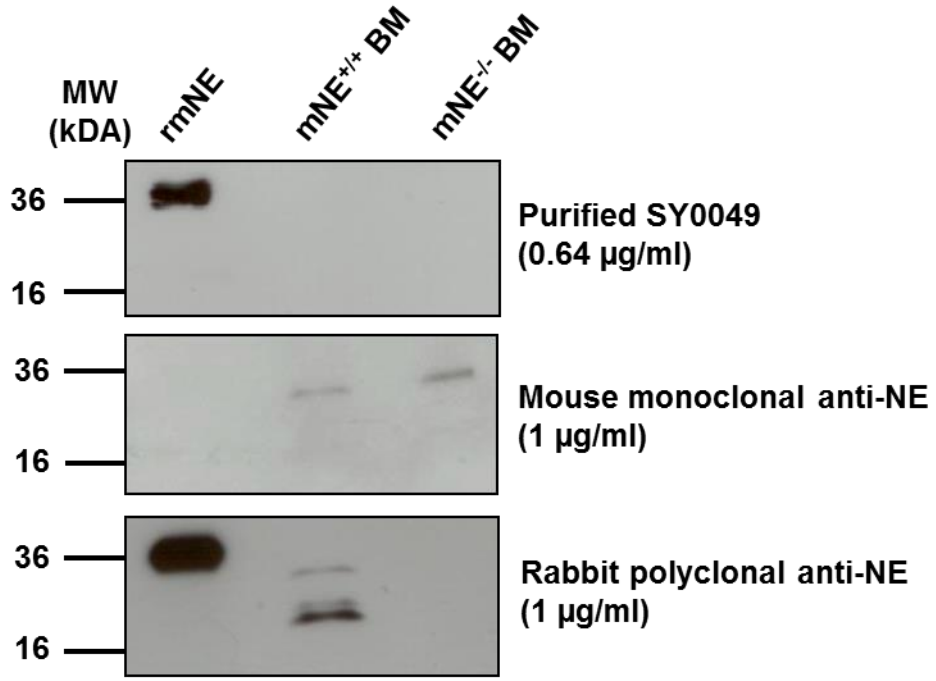


**Figure 3.4: Characterisation of anti-NE antibodies by Western blot analysis.** Protein lysates of $10^6$ whole BM leukocytes from $NE^{-/-}$ and $NE^{+/+}$ mice were separated by gel electrophoresis along with 50 ng recombinant murine NE, transferred to a PVDF membrane and immunoprobed with three separate anti-NE primary Abs. All blots were subsequently and sequentially developed using an appropriate HRP-conjugated secondary Ab (0.2 µg/ml) and chemiluminescence detection reagents.

***e) $CX_3CR1$-eGFP-ki mice were successfully crossed with NE KO mice.***

The advent of NE KO mice has provided an elegant and robust tool to study the biological properties of NE *in vivo*. In order to characterise NE specifically in the context of monocytes, NE KO mice were crossed with $CX_3CR1$-eGFP-ki mice. This was conducted with the assistance of Dr. Martina Beyrau. We ultimately sought to generate, and then compare, $CX_3CR1^{+/eGFP}$ mice carrying either double mutant ($NE^{-/-}$) or wild-type ($NE^{+/+}$) copies of the NE gene. For this to be achieved, we were initially required to establish genotyping assays for *$CX_3CR1$* and *NE*. In multiplex PCR, several DNA target sequences are amplified in a single PCR reaction. This technique has been commonly used to detect different alleles of an individual gene and was similarly applied here for *$CX_3CR1$* and *NE*. For each, PCR was conducted using a common forward primer and separate reverse primers specific for the WT and transgenic allele (*Table 2.1*). Importantly, the primers were designed to produce PCR products of unique sizes that could be distinguished when run on a gel (*Figure 3.5*). This enables the

specific genotypes of individual mice to be deduced, ensuring the correct mice are utilised, both for breeding and experimental purposes.

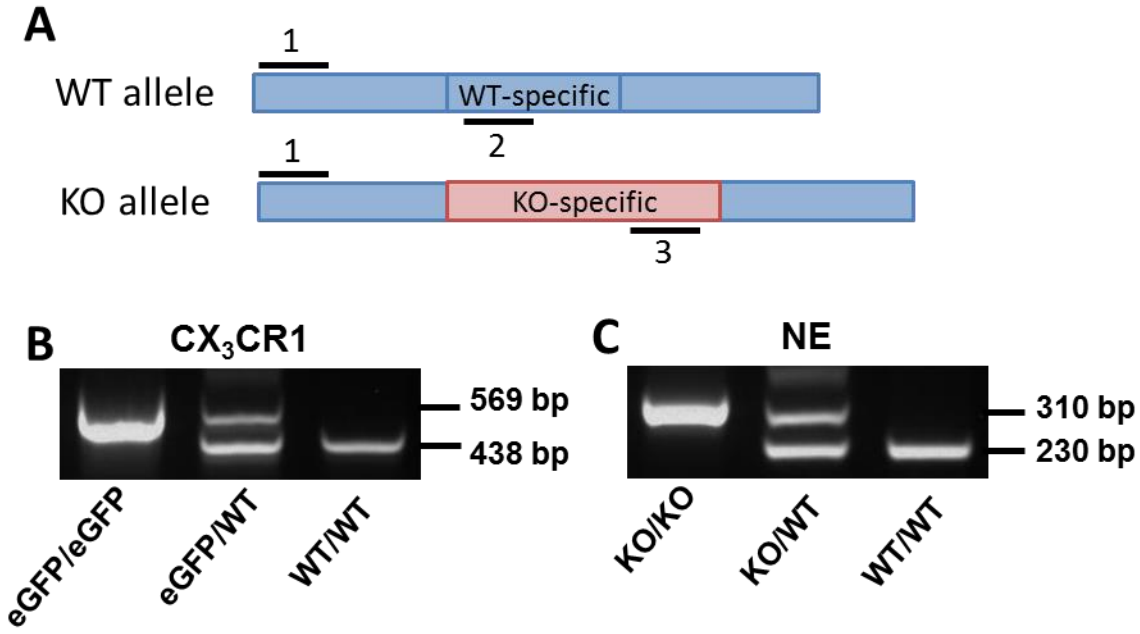


**Figure 3.5: PCR genotyping of $CX_3CR1$-eGFP-ki and NE KO mice**. Separate multiplex PCR reactions were employed to assay for WT and KO alleles of $CX_3CR1$-eGFP-ki and NE KO mice. PCR was performed on genomic DNA isolated from ear notches using a common forward primer (1) and separate reverse primers specific to the WT (2) and KO (3) alleles (A). Importantly, each of the reactions generated a PCR product of unique size that could be distinguished when resolved on a 1.5% agarose gel. Representative homozygous KO, heterozygous and homozygous WT genotypes are shown for the *$CX_3CR1$* (B) and *NE* (C) genes.

### *f) $NE^{-/-}$ and $NE^{+/+}$ mice display comparable leukocyte profiles under naïve conditions.*

$NE^{-/-}$ mice have been reported to record normal counts of circulating neutrophils, monocytes and lymphocytes under naïve conditions (Hirche et al., 2004). As mice from different institutions do sometimes exhibit contrasting phenotypes, and considering we crossed NE KO mice with $CX_3CR1$-eGFP-ki mice, we sought to re-establish the number, proportion and distribution of leukocyte subsets in naïve $NE^{-/-}$ and $NE^{+/+}$ mice, not only in the blood but in the bone marrow, spleen, and peritoneal cavity. The spleen and bone marrow comprise extensive leukocyte reservoirs that can be deployed into the circulation, as necessary, while the peritoneal cavity, to be used later as a model of inflammation, also contains a large resident population of leukocytes. It is imperative to characterise the resting leukocyte profiles of these mice and identify any significant differences as these may influence how the mice respond in subsequent models of

inflammation. In this same regard, we also measured the resting expression levels of the key monocyte chemokine receptors CCR1, CCR2, CCR5 and $CX_3CR1$, though only in the blood (*Table 3.1*).

Total leukocytes were harvested from the blood, spleen, bone marrow and peritoneal cavity of naïve mice and counted using a haemocytometer. For each, similar numbers were observed for $NE^{-/-}$ and $NE^{+/+}$ mice (*Figure 3.6A*). Flow cytometry was subsequently employed, as before, to determine the relative proportions of neutrophils, classical monocytes and non-classical monocytes (*Figure 3.6B*). Peritoneal macrophages were also analysed, as identified by their high F4/80 expression (*Figure 3.6C*). No statistically significant differences were observed between the two genotypes in each of the tissues, across all cell types. Likewise, the chemokine receptor expression profiles of circulating monocytes were largely identical.

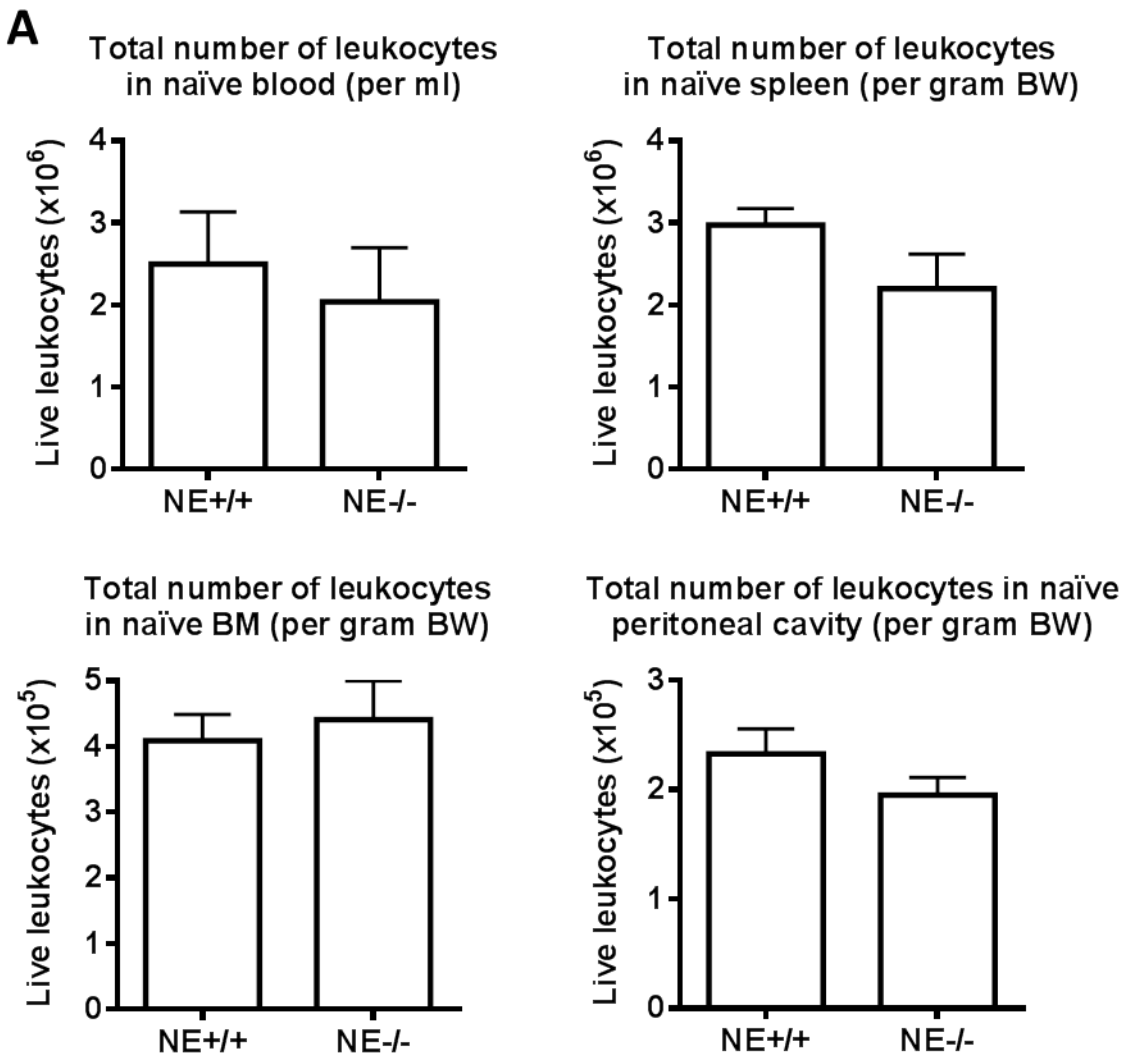

**B**

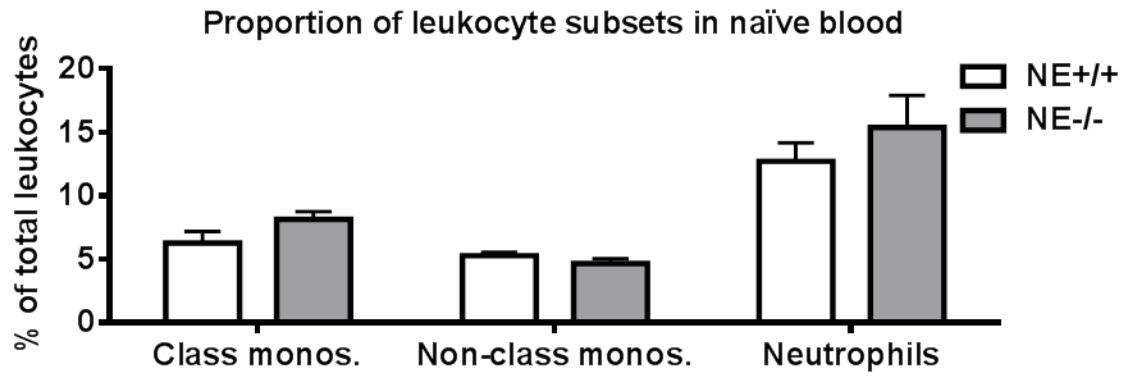
Proportion of leukocyte subsets in naïve blood
% of total leukocytes
20
15
10
5
0
Class monos.
Non-class monos.
Neutrophils
NE+/+
NE-/-

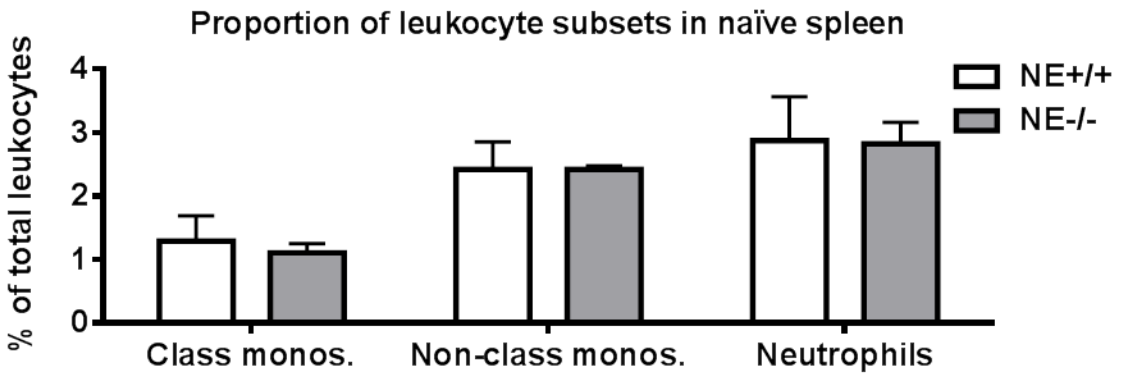
Proportion of leukocyte subsets in naïve spleen
% of total leukocytes
4
3
2
1
0
Class monos.
Non-class monos.
Neutrophils
NE+/+
NE-/-

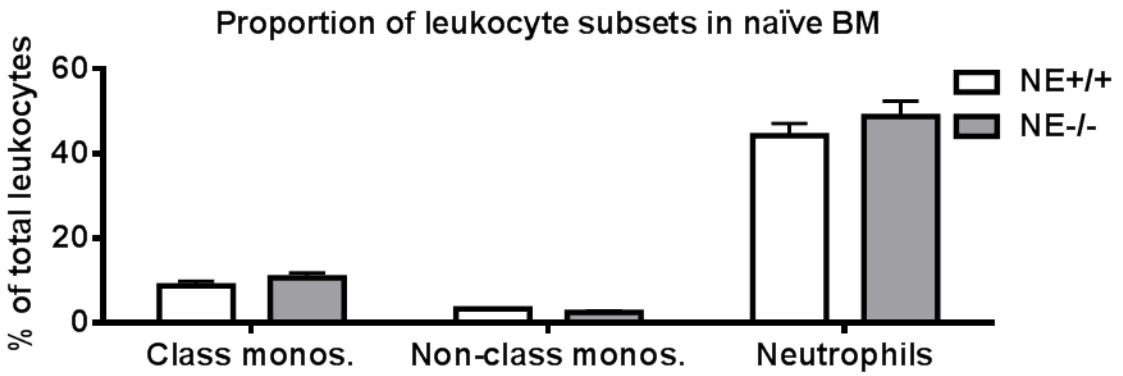
Proportion of leukocyte subsets in naïve BM
% of total leukocytes
60
40
20
0
Class monos.
Non-class monos.
Neutrophils
NE+/+
NE-/-

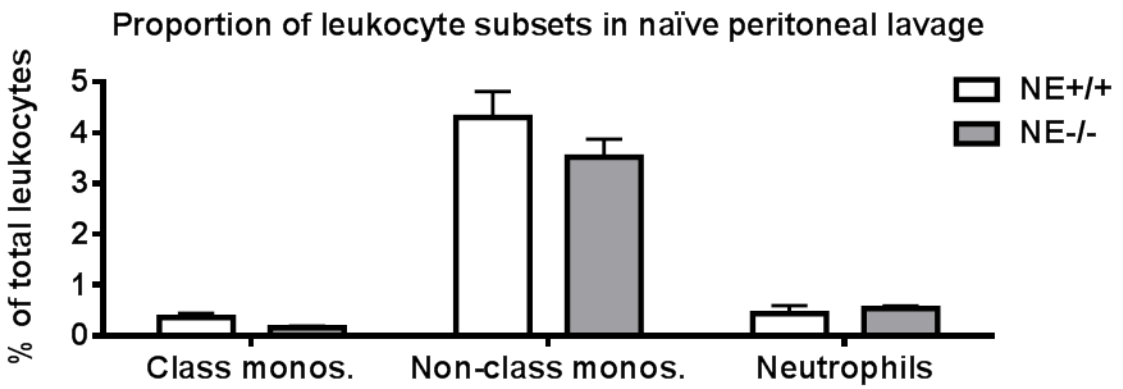
Proportion of leukocyte subsets in naïve peritoneal lavage
% of total leukocytes
5
4
3
2
1
0
Class monos.
Non-class monos.
Neutrophils
NE+/+
NE-/-

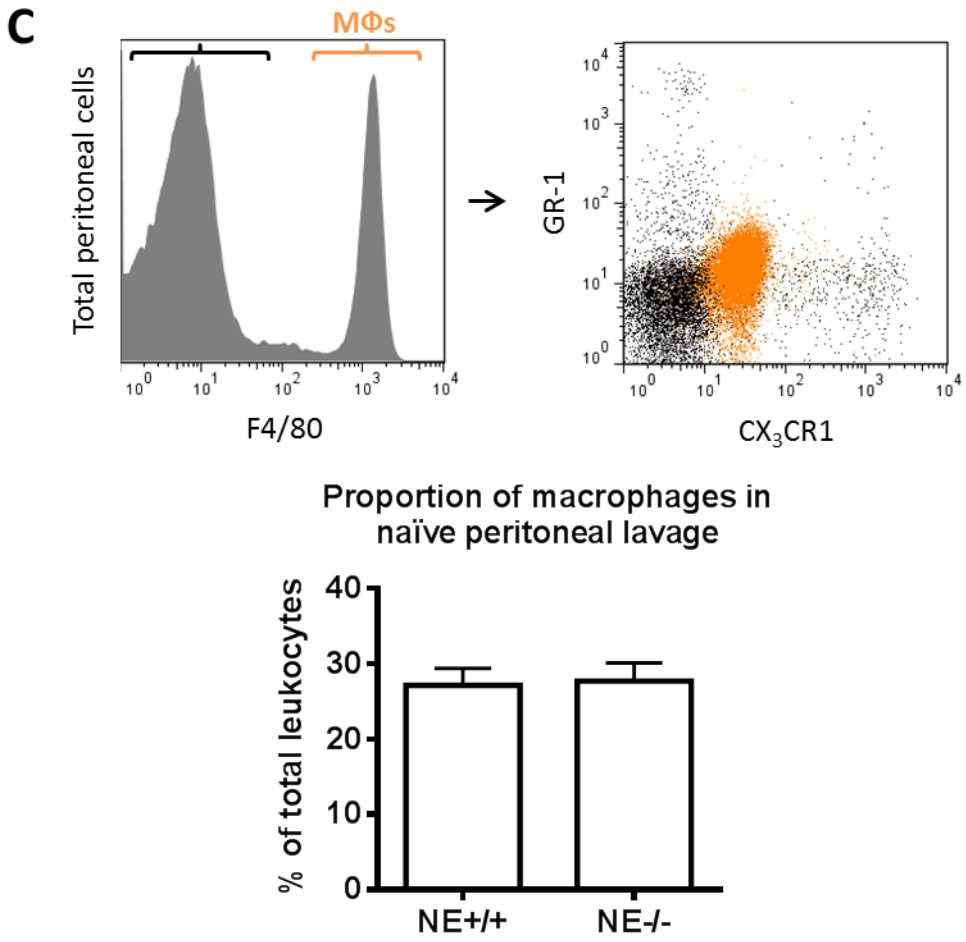


**Figure 3.6: Characterising the number and relative proportion of leukocytes in naïve NE$^{-/-}$ and NE$^{+/+}$ mice.** Total leukocytes were harvested from the blood, spleen, bone marrow (BM) and peritoneal cavity of NE$^{-/-}$ and NE$^{+/+}$ mice and counted using a haemocytometer (A). Flow cytometry was subsequently employed to assess the relative proportion of classical monocytes (GR-1$^{+}$, $CX_3CR1^{med}$), non-classical monocytes (GR-1$^{-}$, $CX_3CR1^{hi}$) and neutrophils (GR-1$^{+}$, $CX_3CR1^{-}$) (B). Proportions of peritoneal macrophages (F4/80$^{hi}$, $CX_3CR1^{low}$, GR-1$^{low}$) were also assessed (C). All data are represented as the mean ± SEM (n = 3 mice, FACS-data are averaged across 2-3 readings per mouse).

**Table 3.1: Cell surface expression of chemokine receptors on blood leukocytes.**

| | | CCR1 | CCR2 | CCR5 | $CX_3CR1$ |
|---|---|---|---|---|---|
| Class. monos. | NE$^{+/+}$ | 1.63 ± 0.15 | 106 ± 11.9 | 1.11 ± 0.004 | 221 ± 12.4 |
| | NE$^{-/-}$ | 1.58 ± 0.27 | 140 ± 44.9 | 1.07 ± 0.058 | 201 ± 24.2 |
| Non-class. monos. | NE$^{+/+}$ | 1.43 ± 0.15 | 10.2 ± 2.20 | 1.09 ± 0.073 | 478 ± 5.46 |
| | NE$^{-/-}$ | 2.03 ± 0.45 | 9.79 ± 1.48 | 1.16 ± 0.111 | 437 ± 29.7 |
| Neutrophils | NE$^{+/+}$ | 1.13 ± 0.03 | 1.18 ± 0.02 | 1.06 ± 0.039 | 2.41 ± 0.34 |
| | NE$^{-/-}$ | 0.97 ± 0.05 | 1.05 ± 0.05 | 0.94 ± 0.049 | 2.12 ± 0.09 |

Expression levels were assessed by flow cytometry and expressed in RFI. Data are represented as the mean ± SEM (n = 3 mice, average of 2 FACS readings per mouse).

### *3.3 Discussion*

The use of transgenic $CX_3CR1$-eGFP-knock-in and NE knock-out mice have contributed immensely to our current understanding of the physiological properties of monocytes and NE, respectively. Exhibiting eGFP-fluorescent monocytes, $CX_3CR1^{+/eGFP}$ mice are routinely used to study monocyte migration and trafficking *in vivo*. The two major monocyte subsets can even be selectively monitored, as distinguished by eGFP intensity. Similarly, homozygous NE KO mice represent a valuable tool for assessing NE disruption. In order to characterise the expression and function of NE specifically in murine monocyte migration in this study, $CX_3CR1$-eGFP-ki and NE KO mice were crossed together.

In this opening results chapter we initially sought to establish a set of protocols to effectively utilise and cross $CX_3CR1$-eGFP-ki and NE KO mice. In this context, we first developed imaging techniques to successfully identify and track monocytes in $CX_3CR1$-eGFP-ki mice. Four-colour flow cytometry was used to distinguish both monocyte subsets from other leukocytes according to their physical and biochemical characteristics. Analysing the blood of $CX_3CR1^{+/eGFP}$ mice, we found the vast majority of eGFP-fluorescent cells were also positive for CD11b, CD115 and F4/80, and displayed an intermediate FSC/SSC profile, typical of monocytes. Though a subset of natural killer cells has been reported to express $CX_3CR1$, all NK1.1-posititve cells (a pan NK marker) were eGFP-negative. The two major monocyte subsets could be further differentiated according to eGFP intensity and GR-1 expression: classical monocytes displayed intermediate levels of $CX_3CR1$ and GR-1, while non-classical monocytes were $CX_3CR1^{hi}$, GR-$1^{-}$. A third distinct population of $CX_3CR1^{-}$, GR-$1^{hi}$ cells was also observed, corresponding to $CD11b^{+}$, $Ly6G^{+}$ neutrophils. Thus, by plotting $CX_3CR1$ and GR-1 expression both monocyte subsets and neutrophils could be simultaneously and reliably identified.

Using this approach relative and total numbers of monocytes and neutrophils could be determined, not only in blood, but in cell suspensions prepared from the bone marrow, spleen, and peritoneal cavity. While the samples in this instance were all isolated from naïve mice, we recognised that analysing corresponding samples from immune-challenged mice would enable us to broadly monitor the mobilisation of these cells during inflammation. Indeed, in this manner flow cytometry was used in conjunction

with the mouse peritonitis model to track monocyte numbers in the blood and inflammatory exudate, as described further in Chapter 5. Changes in the phenotypes of these cells were simultaneously assessed by staining for different markers of interest. Moreover, through the use of fluorescence-activated cell sorting (FACS), a specialised type of flow cytometry, distinct populations of monocytes and other leukocytes could be retrieved for subsequent analysis.

Flow cytometry represents a powerful method for quantifying, characterising and isolating leukocytes *ex vivo* in suspension. In order to directly study leukocytes *in situ* at sites of inflammation, immunofluorescent labelling and three-colour confocal microscopy were combined to capture leukocytes as they migrated through stimulated venules. In $CX_3CR1$-eGFP-ki mice, endogenously fluorescent monocytes, as well as fluorescently-labelled neutrophils, could be seen infiltrating both the cremaster muscle and ear dermis in response to LPS. Through the use of Imaris imaging software, stacks of high-resolution confocal images were reconstructed into virtual 3-dimensional models, which could be subsequently manipulated, for example by adjusting the zoom, rotation or colour intensity. In this manner individual leukocytes could be analysed in great detail, providing information not only on their size and morphology, but on how they interact with the vasculature and each other. Leukocyte transmigration could also be quantitatively evaluated by counting the number of extravasated cells. Using this approach, $CX_3CR1$-eGFP-ki mice have already been exploited by our group to study the mechanisms that govern monocyte migration through the vascular basement membrane (Voisin et al., 2009).

In order to investigate the expression and function of NE in monocyte migration in this study we generated and compared $CX_3CR1^{+/eGFP}$ mice either deficient or normal for NE. This required the mice to be reliably genotyped, as achieved by employing the multiplex PCR assays developed in this chapter. Experimental mice were bred by mating $CX_3CR1^{eGFP/eGFP}$, $NE^{+/-}$ males with $CX_3CR1^{+/+}$, $NE^{+/-}$ females, thereby yielding $CX_3CR1^{+/eGFP}$ progeny, as required, carrying either one ($NE^{+/-}$), two ($NE^{-/-}$) or no ($NE^{+/+}$) copies of the mutant NE allele. Using this approach, littermates could be directly compared, limiting genetic and environmental variables. Indeed, this was exploited in order to evaluate the leukocyte profiles of naïve $NE^{-/-}$ and $NE^{+/+}$ mice and confirm there were no underlying differences that may influence their responses in subsequent models of inflammation. Leukocytes were analysed from the blood, spleen,

bone marrow and peritoneal cavity. While leukocytes ultimately mobilise to peripheral tissues from the blood, during inflammation the spleen and bone marrow are known to release their leukocyte stores into the circulation, thereby promoting their rapid and abundant infiltration. Monocytes are stored in particularly large quantities in the spleen while also being continuously produced in the bone marrow. Both tissues have been shown to serve as a rapid source of monocytes in murine studies for example, and respectively, in response to myocardial infarction (Swirski et al., 2009a) and bacterial infection (Serbina and Pamer, 2006).

Importantly, and in keeping with their original description, no significant differences were observed in the total number or relative proportion of leukocytes across all tissues in $NE^{-/-}$ mice compared to $NE^{+/+}$ controls. Looking specifically at monocytes, both the classical and non-classical subset could be detected in the blood, comprising around 7% and 5% of total circulating leukocytes, respectively. Relative to each other, the proportion of the two monocyte subsets (split roughly 60/40) is in keeping with previous studies. Levels of total blood monocytes are however higher than the 4% commonly reported, possibly due to the exclusion of all dead cells and platelet complexes during flow cytometric analysis. In the bone marrow, classical monocytes predominate supporting the theory that non-classical monocytes undergo differentiation principally in the blood. In contrast, slightly higher levels of non-classical monocytes could be seen in the spleen, consistent with a recent study (Swirski et al., 2009a).

Surface expression levels of the major monocyte chemokine receptors CCR1, CCR2, CCR5 and $CX_3CR1$ were also compared on circulating classical and non-classical monocytes in naïve $NE^{-/-}$ and $NE^{+/+}$ mice. The engagement of such receptors by chemokines is involved not only in monocyte extravasation but in their mobilisation from the bone marrow and spleen, as well as their life span (Gautier et al., 2009). Importantly, as comparable expression profiles were generated for both genotypes across all receptors, it is likely that their respective monocytes will have the same capacity to respond to stimulation in future models of inflammation. In this context, CCR2 plays a dominant role in mediating the early migration of classical monocytes by binding its cognate ligand CCL2. Indeed, CCR2 expression was ~10-fold higher in classical monocytes compared to non-classical monocytes, in keeping with the literature. Moreover, negligible amounts of CCR2 were observed on the surface of neutrophils, presumably rendering them unresponsive to exogenously administered

CCL2. Monocytes typically also express CCR1 and CCR5, which bind to a variety of chemokines, including the shared ligands CCL3 and CCL5. These receptors could be scarcely detected in our hands however, on either monocyte subset, calling into doubt the suitability of the specific detection antibodies used during flow cytometric analysis.

As a means of characterising NE expression later on in this study, in this chapter we initially designed and optimised PCR and Western blotting assays to quantify NE transcript and protein, respectively. For each, NE could be detected in the lysates of leukocytes harvested from the bone marrow of WT mice. The specificity of these signals was corroborated using $NE^{-/-}$ mice. Collectively, these results confirm $NE^{-/-}$ mice as full knockouts and identify BM leukocytes as a suitable positive control for subsequent analyses. Moreover, as immunostaining was successfully employed in Western blotting, we recognised that the same polyclonal rabbit anti-NE antibody might also be applicable to other expression assays, such as flow cytometry and confocal microscopy.

In conclusion, in this chapter we have successfully crossed $CX_3CR1$-eGFP-ki and NE KO mice, thereby establishing a valuable mouse model to rigorously, specifically and concurrently study NE and monocyte biology. In subsequent chapters, $CX_3CR1^{+/eGFP}$ mice carrying either mutant or WT copies of the NE gene were directly compared (by employing the various methods we have just optimised) to investigate the expression and function of NE in monocyte migration *in vivo*.

# CHAPTER 4: Investigating the expression of NE in murine monocytes.

## *4.1 Introduction*

The most significant insights into the expression profile of neutrophil elastase have arisen from studies performed on human neutrophils, where this protein was first discovered (Janoff and Scherer, 1968). Encoded by a single-copy gene, NE is transcribed almost entirely during the promyelocytic stage of neutrophil development in the bone marrow and is switched off completely upon maturation. The translated protein, detected in promyelocytes and thereafter, originally constitutes an inactive pro-enzyme. Activation requires the removal of specific peptides from the N- and C-termini, after which the protein is targeted to azurophil granules along with the structurally related proteinase 3 and cathepsin G. NE is stored in azurophil granules at millimolar concentrations and therefore represents a major protein component of neutrophils. Although the majority of NE is packaged inside the lumen of azurophil granules amongst a matrix of negatively charged proteoglycans, it is emerging that some NE also localises to a protein complex in the granule outer membrane (Metzler et al., 2014).

For the most part NE is restricted to azurophil granules until actively released following neutrophil exposure to inflammatory stimuli. NE has been shown to be released *in vitro* in response to a range of mediators including formyl tripeptide (fMLP), interleukin-8 (IL-8), and activated complement fragment C5a. Such release can be dramatically increased by priming the cells for example with LPS or TNF-α (Owen et al., 1997). NE release has also been shown to be greatly amplified by integrin-mediated cell adhesion (Rainger et al., 1998). Even under such optimal conditions, neutrophils only release up to 25% of their total NE contents into the extracellular milieu, though a considerably larger proportion (up to 6-fold more) does typically become sequestered on the outer cell membrane (Owen et al., 1997). Moreover, NE can translocate to the nucleus and be incorporated into neutrophil extracellular traps (NETs).

The expression profile of NE appears to be largely conserved in mice. The gene for mouse *NE* is composed of five exons and four introns, analogous to human *NE*. Transcripts can be abundantly detected in developing granulocytes in the bone marrow of mice, while mature blood neutrophils display intracellular stores of the NE protein

(Belaaouaj et al., 1998). Originally encompassing a larger pro-enzyme, the protein undergoes almost identical processing steps as seen in humans prior to being packaged into azurophil granules. These granules can be stimulated for secretion, with the lipid mediator $LTB_4$ particularly potent in inducing NE release both freely into the surroundings and to the neutrophil cell surface (Young et al., 2007).

Despite its name, neutrophil elastase is not exclusively expressed by neutrophils. NE has also been detected in U937 cells, a human cell line with many characteristics of the mononuclear phagocyte lineage, as well as primary human blood monocytes and macrophages and endothelial cells of atherosclerotic plaques (Dollery et al., 2003). These cells were shown to contain not only the NE protein but the NE transcript, refuting the dogma that NE synthesis occurs only in the bone marrow. In culturing human blood monocytes, NE expression appeared to diminish as the cells differentiated into macrophages. Monocytes also demonstrated a greater capacity to secrete their NE stores in response to CD40 ligand, a member of the TNF superfamily of molecules. The expression of NE by human monocytes has been similarly observed in a handful of other studies. These collectively indicate NE synthesis is not ubiquitous. Owen et al. detect NE only in a distinct subset of 'pro-inflammatory' monocytes representing 20-30% of the circulating monocyte pool (Owen et al., 1994). Similarly, Kargi et al. only found ~40% of blood monocytes to be NE-positive, though to varying extents (Kargi et al., 1990). In these cells, NE localised to cytoplasmic granules, akin to azurophil granules of neutrophils.

Neutrophils aside, mouse NE transcript, protein, and activity have also been recorded in resident peritoneal macrophages and mast cells (Kolaczkowska et al., 2009). In contrast, in comparing the transcriptomes of mouse and human monocytes, NE could not be significantly detected in mouse monocytes using a microarray approach, though, surprisingly, nor could it be significantly detected in the corresponding human samples (Ingersoll et al., 2010). Considering these inconsistencies, and the lack of any supporting studies, we believe there is a need to rigorously and explicitly investigate the expression of NE in murine monocytes. We sought to achieve this goal in this chapter. The specific objectives we wanted to address are as follows:

- Assess the relative levels of NE transcript in classical and non-classical monocytes.

- Assess the relative levels of NE protein in classical and non-classical monocytes.
- Establish the cellular localisation of NE in monocytes.
- Develop assays for measuring levels of secreted NE.

### *4.2 Results*

#### *a) Murine classical monocytes express high levels of NE transcript.*

Through fluorescence-activated cell sorting (FACS), distinct sub-populations of cells can be retrieved upon flow cytometric analysis. Using this approach, the two monocyte subsets, as well as neutrophils and a crude lymphocyte population were isolated from total splenic leukocytes harvested from naïve $CX_3CR1$-eGFP-ki mice. Individual cell types were distinguished according to $CX_3CR1$ and GR-1 expression, as before (see *Chapter 3.1*). Spleen-derived monocytes were chosen for gene analysis as they outnumber their equivalents in the circulation and are more amenable to extraction (Swirski et al., 2009a). Yielding cell purities of more than 90% (*Appendix 4.1*), the FACS-sorted cells were subsequently screened for NE expression.

Quantitative real-time PCR (qRT-PCR) was initially employed to evaluate NE expression at the transcript level. Relative levels of NE mRNA were measured in each leukocyte cell type, following normalisation to the housekeeping gene GAPDH or cyclophilin. Specifically, the comparative $C_T$ method was applied, in which the $C_T$ (cycle threshold) value of a target gene, in this case NE, is compared to that of the reference gene. The $C_T$ value corresponds to the cycle number at which the amplification curve crosses a uniform threshold line. For both genes, the threshold line was manually set to lie in the middle of the exponential phase of the amplification plot, as required for accurate quantification. Upon calculating $\Delta C_T$ scores for each sample, fold-expression changes in NE were subsequently calculated using the formula $2^{\Delta\Delta CT}$, which reflects the effective doubling of PCR product with each amplification cycle. Fold changes were presented relative to the neutrophil population, displaying an effective expression of 1 (*Figure 4.1*).

NE transcripts were detected in each of the leukocyte subsets analysed, as validated by $NE^{-/-}$ controls, which failed to penetrate the threshold line. While lymphocytes and non-classical monocytes contained marginally lower levels of NE transcript compared to neutrophils, significantly higher levels were recorded for classical monocytes. Taken together our results indicate that while both subsets of murine monocytes are seemingly capable of expressing the NE gene, there is a striking heterogeneity as to the level of expression.

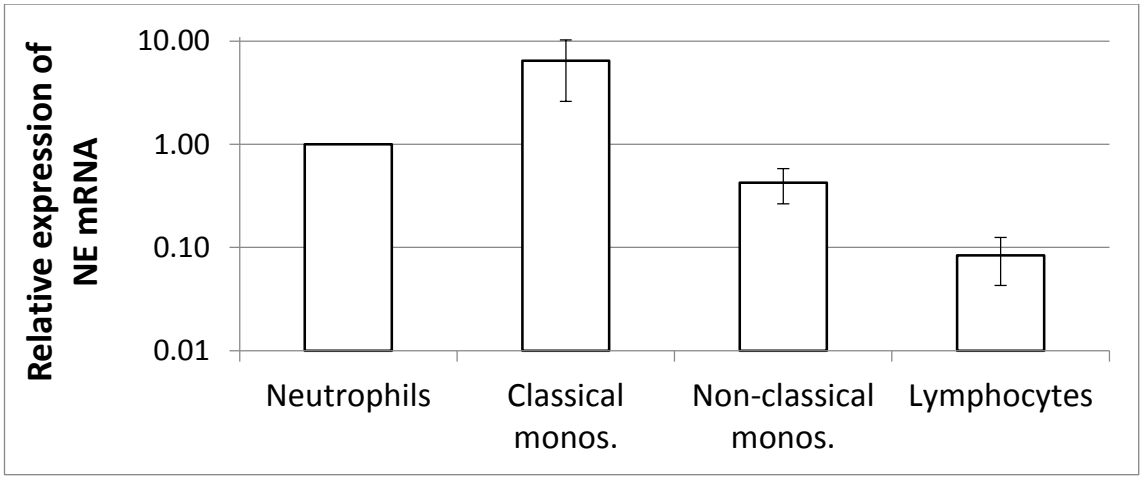


**Figure 4.1: Quantifying NE transcript levels in different leukocyte subsets of $NE^{+/+}$ mice.** Quantitative real-time PCR was employed to determine relative levels of NE transcript in splenic leukocyte homogenates. Total RNA was extracted from $5\times10^5$ FACS-sorted classical monocytes, non-classical monocytes, neutrophils and lymphocytes, converted into cDNA and used as a template for qRT-PCR. NE expression was specifically calculated using recorded $C_T$ values normalised to the housekeeping genes GAPDH and/or cyclophilin. cDNA from $NE^{-/-}$ BM leukocytes was used as a negative control. Fold changes are presented (on a log scale) relative to neutrophils (set to 1). Data are represented as the mean ± SEM (n = 5 runs, 6 mice). Each run was performed in triplicate. Some runs were coordinated by Dr. Martina Beyrau.

***b) Classical monocytes retain NE protein after MACS- but not FACS- sorting.***

To determine if murine monocytes also express the NE protein, naïve splenic leukocytes were FACS-sorted as before and assayed for cellular NE protein expression by Western blotting. This was achieved using an anti-human NE rabbit polyclonal antibody that we previously confirmed to cross-react with murine NE. As expected, neutrophils were shown to contain an abundance of NE protein. Interestingly, no protein could be detected in the remaining leukocyte types including either monocyte subset (*Figure 4.2A*). As NE translation may only be initiated in these cells upon stimulation, we incubated sorted cells with a cocktail of pro-inflammatory cytokines and chemokines for 24 hours *in vitro* prior to Western blot analysis. As before however, no protein could be detected in the lymphocyte or monocyte populations (*Figure 4.2B*).

Speculating that the NE protein might be released by monocytes during FACS-sorting, we next sought to purify monocytes using MACS technology. In magnetic activated cell sorting, individual cell types can be isolated from a heterogeneous mixture according to their extracellular protein profiles. Total cells are initially incubated with magnetic nanoparticles coated with antibodies against distinct surface antigens. Upon passing the cells through a column placed in a strong magnetic field, those labelled with antibody

are retained in the column while the remaining 'negative fraction' flows through unimpeded. In order to purify monocytes in this study, we used a specific monocyte isolation kit, in which unlabelled monocytes are freely collected as the remaining leukocytes are held in the column. Isolating monocytes in this manner via negative selection is preferable as the cells remain largely 'untouched' and hence are less likely to be activated.

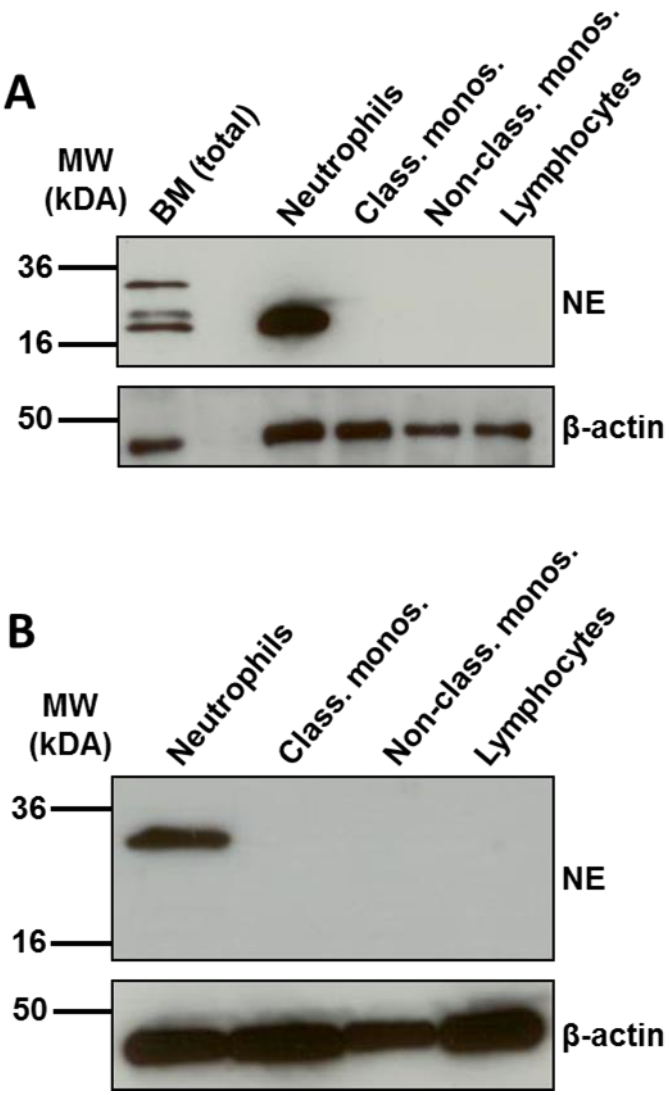


**Figure 4.2: NE protein expression in FACS-sorted leukocytes.** Western blot analysis was employed to assay for intracellular levels of NE protein in splenic leukocytes. Total protein lysates from $5\times10^5$ FACS-sorted classical monocytes, non-classical monocytes, neutrophils and lymphocytes were resolved by gel electrophoresis, transferred to a PVDF membrane and immunoprobed for NE. Analysis was conducted either immediately after FACS-sorting (A) or following 24 hours stimulation with a cocktail of LPS, IFN-γ and CCL2 (each at 100 ng/ml) in a 24-well plate in 500 µl RPMI-1640 media (B). Mouse NE runs at 22-32 kDa. β-actin (42 kDa) was used as a loading control.

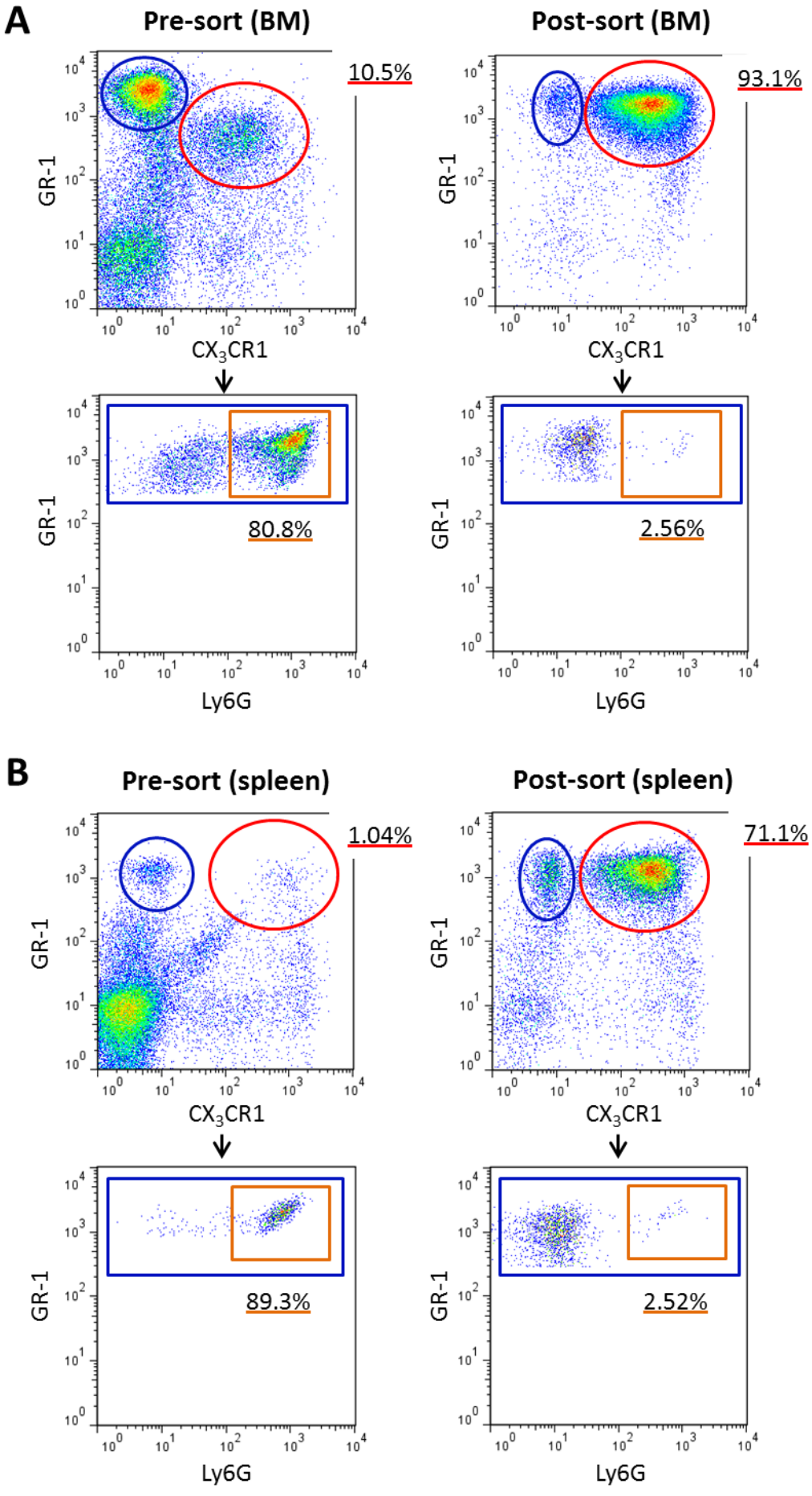
A
Pre-sort (BM)
Post-sort (BM)
10.5%
93.1%
GR-1
CX3CR1
80.8%
2.56%
Ly6G
B
Pre-sort (spleen)
Post-sort (spleen)
1.04%
71.1%
89.3%
2.52%

**Figure 4.3: Flow cytometric analysis of leukocytes pre- and post-MACS-sorting.** Flow cytometry was employed to determine the purity of classical monocytes (GR-1$^{+}$, $CX_3CR1^{med}$, red) following their MACS-sorting from whole leukocyte samples harvested from the bone marrow (BM) (A) or spleen (B) of $CX_3CR1^{+/eGFP}$ mice. Relative levels of neutrophils (GR-1$^{+}$, $CX_3CR1^{-}$, Ly6G$^{+}$, orange) were also assessed. Shown are representative FACS plots from one round of experiments.

Using this isolation kit, monocytes were MACS-sorted from the mouse bone marrow, as recommended by the manufacturer, as well as the spleen. Cells were harvested from $CX_3CR1$-eGFP-ki mice, enabling the purity of the sorted cells to be rigorously assessed by flow cytometry. Samples from the spleen and particularly the bone marrow were shown to be significantly enriched for monocytes following MACS-separation (*Figure 4.3*). These monocytes were almost entirely of the classical subset, in keeping with the manufacturer's description. While classical monocytes typically represent only 8-15% of total leukocytes in the bone marrow and 1-2% in the spleen, this was increased after MACS-sorting to more than 90% and 70%, respectively. Importantly, the small fraction of remaining cells were almost entirely depleted of neutrophils (< 0.5%). Owing to its greater purity, classical monocytes sorted from the bone marrow were subsequently subjected to Western blot analysis to examine NE protein expression. In stark contrast to FACS-sorted monocytes, MACS-sorted monocytes were found to contain the NE protein, at a level similar to whole bone marrow leukocytes (*Figure 4.4*).

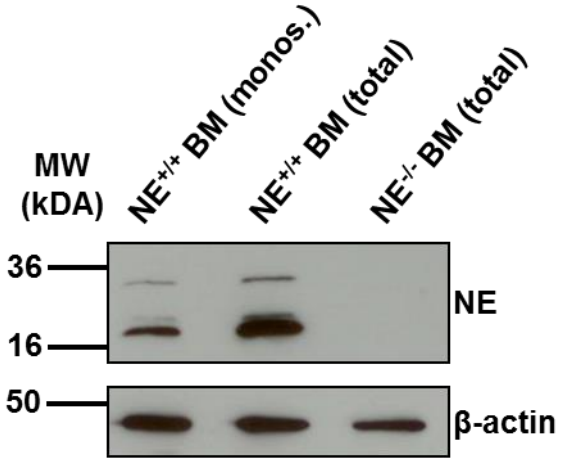


**Figure 4.4: NE protein expression in MACS-sorted leukocytes.** Western blot analysis was employed to assay for intracellular levels of NE protein in bone marrow (BM)-derived leukocytes. Total protein lysates from $3.5\times10^5$ whole BM leukocytes or MACS-sorted classical monocytes were resolved by gel electrophoresis, transferred to a PVDF membrane and immunoprobed for NE. Whole BM leukocytes from $NE^{-/-}$ mice were used as a negative control. Mouse NE runs at 22-32 kDa. β-actin (42 kDa) was used as a loading control.

***c) Monocyte NE is stored in cytoplasmic granules.***

Having established murine classical monocytes do express the NE protein, we next set out to elucidate its cellular localisation by immunofluorescence microscopy. For this to be achieved we hoped to exploit the same anti-NE antibody as used for Western blotting. We initially attempted to visualise NE in whole bone marrow leukocytes harvested from $CX_3CR1$-eGFP-ki mice. The cells were fixed onto cover slips with PFA, permeabilised with Triton X-100 and subsequently stained for NE and the neutrophil marker Ly6G. $NE^{-/-}$ leukocytes were used as a negative control. Though the neutrophils and monocytes could be clearly identified, the NE staining appeared largely non-specific as fluorescence could be observed for $NE^{+/+}$ and $NE^{-/-}$ cells alike (*Appendix 4.2*). As this could not be resolved by lowering the working concentration of the primary anti-NE antibody and/or the secondary anti-rabbit antibody (data not shown), we next revised our choice of fixative and permealising agent and exchanged PFA/Triton for methanol. Using this approach, NE staining could be seen in $NE^{+/+}$ cells only (*Figure 4.5*). As expected, NE in neutrophils appeared to localise to intracellular granules, though interestingly this same expression pattern was also noted for other $Ly6G^{-}$ cells. Unfortunately, as methanol causes irreversible bleaching of eGFP, the cellular localisation of NE specifically in monocytes could not be confirmed.

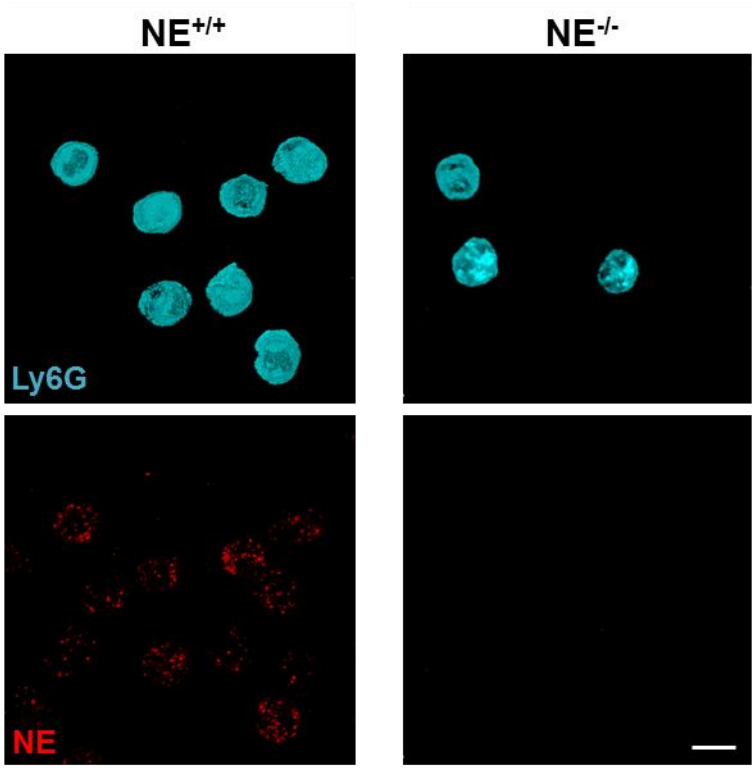

**Figure 4.5: NE protein localisation in murine leukocytes.** Whole bone marrow leukocytes were harvested from $CX_3CR1^{+/eGFP}$ mice, seeded onto cover slips, and fixed/permeabilised with methanol. The cells were subsequently immunostained for NE (red) and the neutrophil marker Ly6G (blue) and analysed by confocal microscopy. $NE^{-/-}$ leukocytes were used as a negative control. Scale bar, 5 µm.

As a means of exploring the sub-cellular localisation of NE in monocytes, we initially tried to identify monocytes by incubating whole BM leukocytes with antibodies against the monocyte markers CD115 and eGFP (in $CX_3CR1^{+/eGFP}$ mice), however none of these provided specific staining (data not shown). Taking a different approach, we next stained for NE directly in MACS-sorted monocytes, harvested both from the bone marrow and the spleen (*Figure 4.6A-B*). Irrespective of their origin, 100% of the sorted monocytes displayed intracellular stores of NE, akin to those seen in neutrophils. By concurrently staining for the pan-leukocyte surface marker CD45 and by incorporating the nuclear stain DRAQ5, it appears the NE-positive granules are largely confined to the monocyte cytoplasm (*Figure 4.6C*).

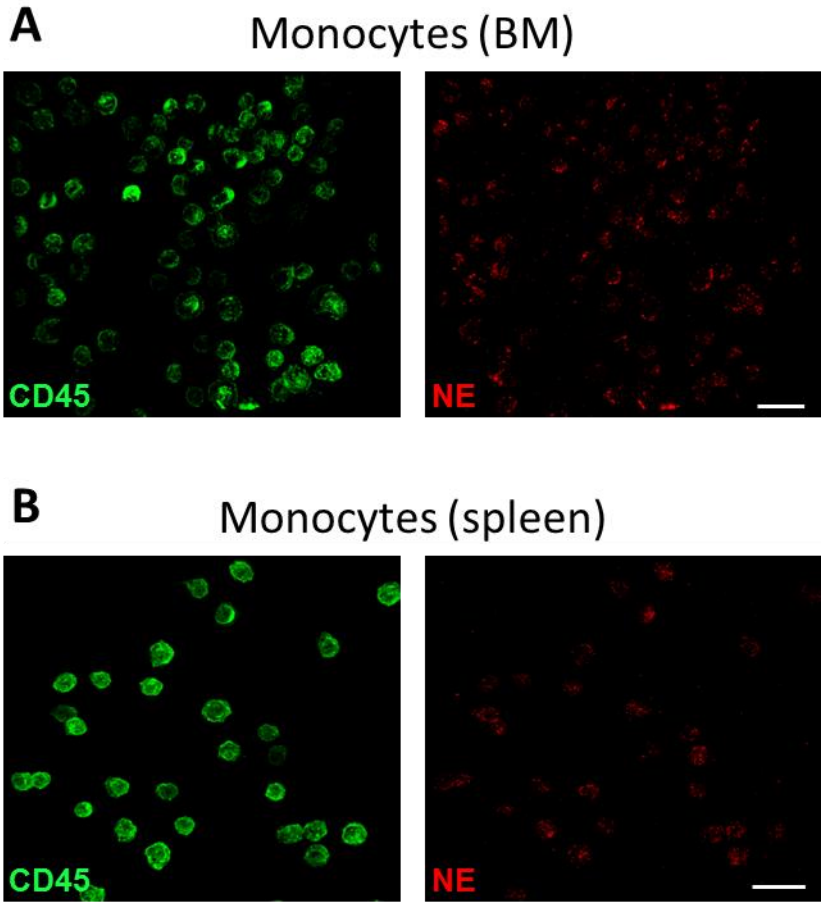

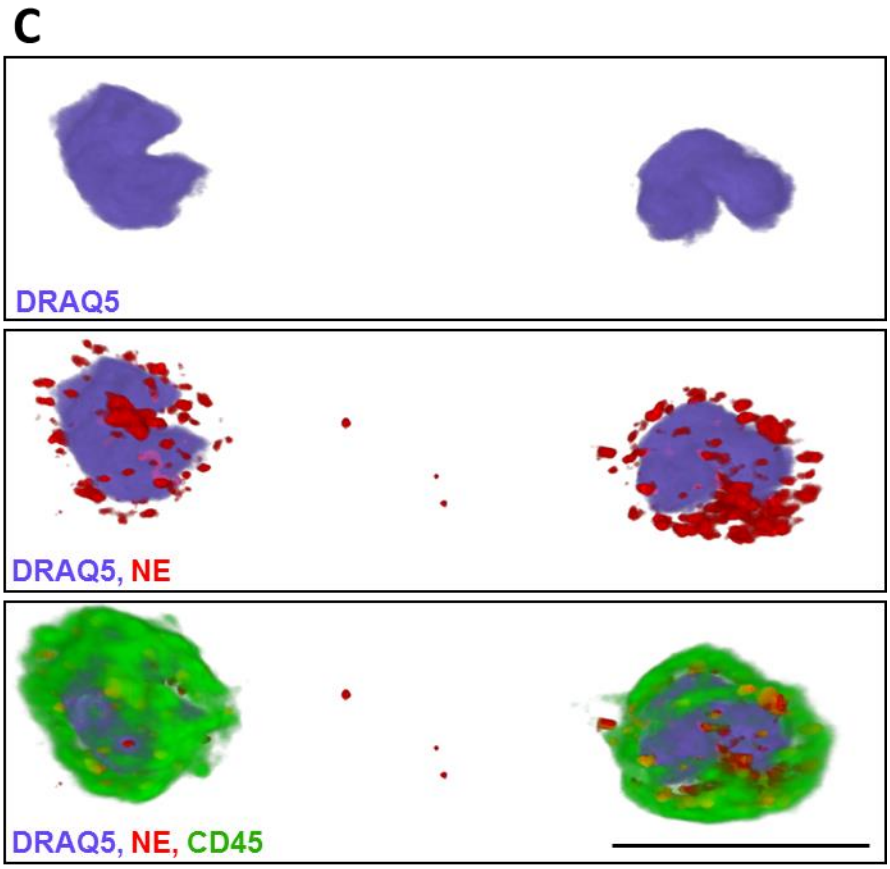


**Figure 4.6: Sub-cellular localisation of NE in classical monocytes.** Classical monocytes were MACS-sorted from the bone marrow (A) and spleen (B) of $CX_3CR1^{+/eGFP}$ mice, seeded onto cover slips, and fixed/permeabilised with methanol. The cells were subsequently immunostained for NE (red) and the pan-leukocyte surface marker CD45 (green), incubated with the nuclear stain DRAQ5 (blue) and analysed by confocal microscopy. Higher magnification images of BM monocytes reveals NE is expressed in cytoplasmic granules (C). Scale bar, 10 μm.

***d) Levels of secreted NE could not be precisely measured.***

In neutrophils, while NE is constrained to azurophil granules under naïve conditions, upon stimulation these intracellular stores have been shown to be actively released. In order to rigorously investigate the potential release of NE by murine monocytes, we sought to establish an assay capable of accurately detecting NE in solution. We initially tried developing an enzyme-linked immunosorbent assay (ELISA) in which dissolved proteins are immobilised onto a microtitre plate. A detection antibody is subsequently added, forming a complex with a particular protein of interest, while an enzyme-conjugated secondary antibody produces a signal readout proportional to the amount of target complex present in the sample. To determine if NE could be quantified by ELISA, whole cell lysates harvested from the bone marrow of $NE^{+/+}$ and $NE^{-/-}$ mice

were immobilised onto a 96-well plate and incubated with the rabbit anti-NE antibody. Essentially representing a negative control, we were surprised to see a signal be generated at all in the $NE^{-/-}$ mice, yet alone a signal equal in intensity to its $NE^{+/+}$ counterpart (*Figure 4.7*). Though we tried increasing the concentration of blocker and denaturing the lysates prior to analysis, this was not sufficient to remove the non-specific signal from the $NE^{-/-}$ samples (data not shown).

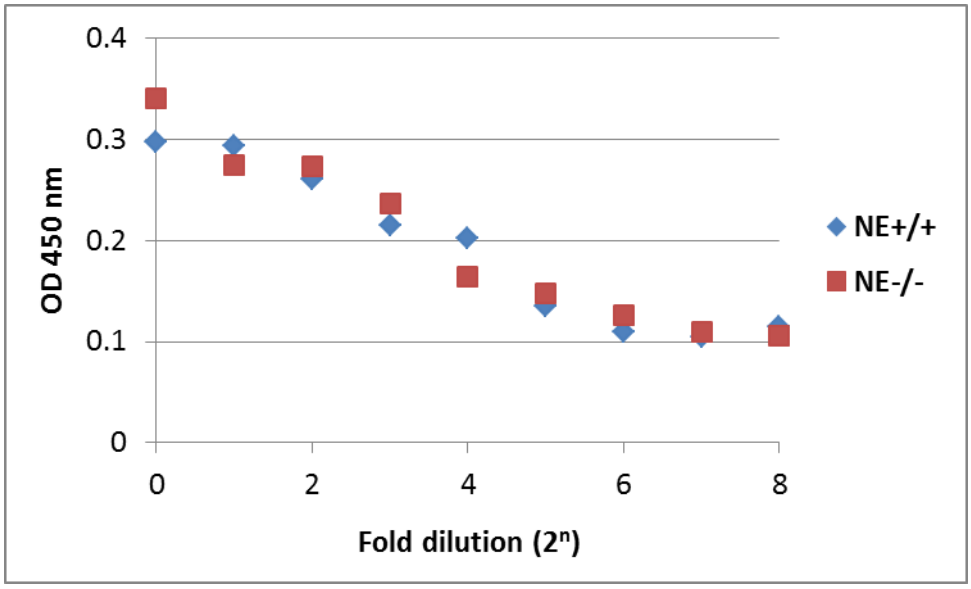


**Figure 4.7: Assaying for NE protein by ELISA.** Whole bone marrow leukocytes from $NE^{+/+}$ (♦) and $NE^{-/-}$ (■) mice were lysed, serially diluted 2-fold across an ELISA plate, and immunoprobed for NE. Sample absorption at 450 nm was characterised to determine relative levels of NE protein expression.

Though only considered to produce semi-quantitative results, we next attempted to assay for soluble NE via slot blot analysis. In a slot blot, a dissolved protein sample is applied directly onto a nitrocellulose membrane. As the sample is drawn through the membrane via a vacuum pump the proteins become adsorbed onto the membrane surface while the remaining components pass freely through. This approach enables large sample volumes to be analysed in their entirety. As with Western blotting and ELISA, the expression of a single target protein can be subsequently explored by immunodetection. To determine if levels of soluble NE could be measured by slot blot analysis, 5 and 50 ng of recombinant murine NE in 1 ml of PBS were processed in parallel using the rabbit anti-NE antibody. Encouragingly, differences in the amount of total NE were reflected in the intensity of the chemiluminescent signals generated by

the two samples (*Figure 4.8A*). To validate its application for endogenous murine NE, a subsequent slot blot was performed on the lysates of bone marrow leukocytes isolated from $NE^{+/+}$ and $NE^{-/-}$ mice (*Figure 4.8B*). Regrettably, a comparable signal was generated for both genotypes. Similarly observed for the ELISA, it is clear that NE is not the only cellular component detected by the anti-NE antibody.

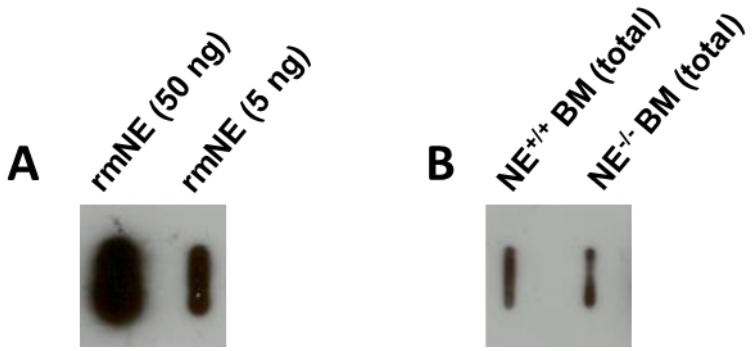


**Figure 4.8: Assaying for NE protein by slot blot.** Relative expression levels of recombinant (A) and endogenous (B) murine NE were assessed by slot blot analysis. 5 and 50 ng recombinant murine NE and protein lysates of $2.5\times10^5$ whole bone marrow (BM) leukocytes from $NE^{-/-}$ and $NE^{+/+}$ mice were denatured, transferred to a nitrocellulose membrane in 1 ml PBS, and immunoprobed for NE.

In contrast to an ELISA or slot blot which are unable to differentiate bona fide and artifactual signals, during Western blot analysis non-specific protein bands can be resolved by gel electrophoresis. In this light, we next attempted to extract and concentrate soluble NE by immunoprecipitation prior to evaluating its expression by Western blot analysis, as before. To gauge its feasibility, we initially attempted to precipitate recombinant murine NE using the anti-NE antibody in conjunction with protein G sepharose beads. The beads were subsequently boiled to elute the attached proteins (*Figure 4.9A*). In assaying for NE, two large non-specific bands at ~25 and 35 kDa could be detected in each of the samples, including the appropriate negative controls. We initially speculated that these bands derived from the sepharose beads which were commonly present in all of the samples. Specifically, we theorised they resulted from the deterioration of the beads through boiling. Accordingly, a second elution protocol encompassing a low pH glycine buffer was tested instead, however the miscellaneous bands persisted (*Figure 4.9B*). Considering these bands run at a similar

size to endogenous murine NE, immunoprecipitation does not constitute a viable method for measuring levels of secreted NE.

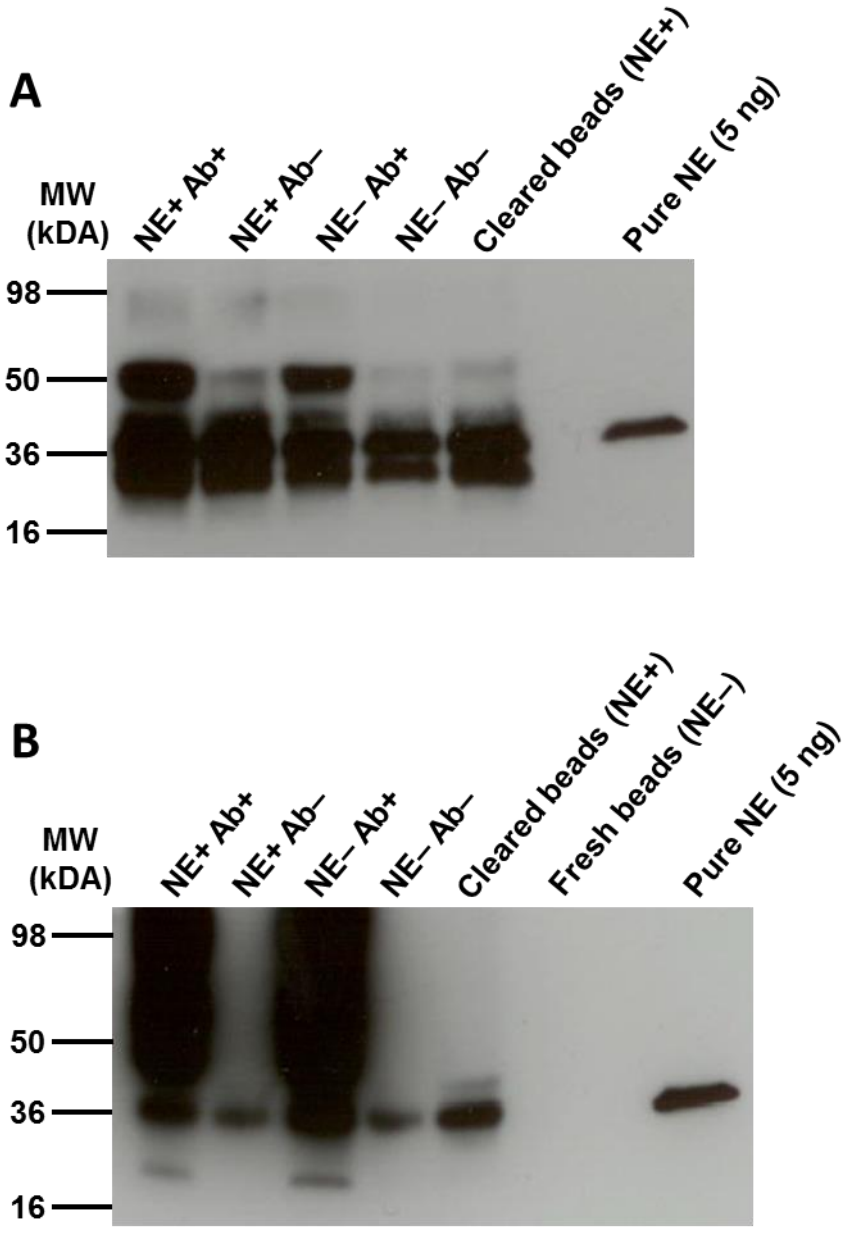


**Figure 4.9: Assaying for NE protein by immunoprecipitation.** We attempted to immunoprecipitate 10 ng recombinant murine NE (NE+) suspended in 500 µl RPMI-1640 media. Control samples lacking NE (NE–) were also processed. NE was sequestered onto Protein G beads via an anti-NE antibody (Ab+). All attached proteins were subsequently eluted from the beads either through boiling (A) or by using a low pH glycine buffer (B). The samples were subsequently resolved by gel electrophoresis, transferred to a PVDF membrane and immunoprobed for NE. Regrettably, both approaches ubiquitously yielded non-specific bands of a similar size to endogenous murine NE (22-32 kDa).

***e) NE secretion could not be induced in monocytes in vitro.***

Rather than directly measuring secreted NE in solution, we next sought to monitor the depletion of NE stores from leukocytes using flow cytomtery. This approach should enable relative levels of NE to be quantified both within the cell body and displayed on the outer cell surface upon stimulation. To determine if cellular NE could indeed be identified by flow cytometry, leukocytes from the blood and bone marrow of naïve $CX_3CR1$-eGFP mice were fixed, permeabilised and immunostained for NE. While neutrophils and monocytes could still be clearly defined upon fixing, neither cell type demonstrated positive staining for NE (*Figure 4.10*). Though we tried increasing the working concentrations of the detection antibodies and adding secondary permeabilising agents for a deeper penetration, no NE-staining could be observed. Likewise, no NE could be detected sequestered on the outer cell surface of any leukocyte subset, either in the circulation or following recruitment during peritonitis (*Appendix 4.3*).

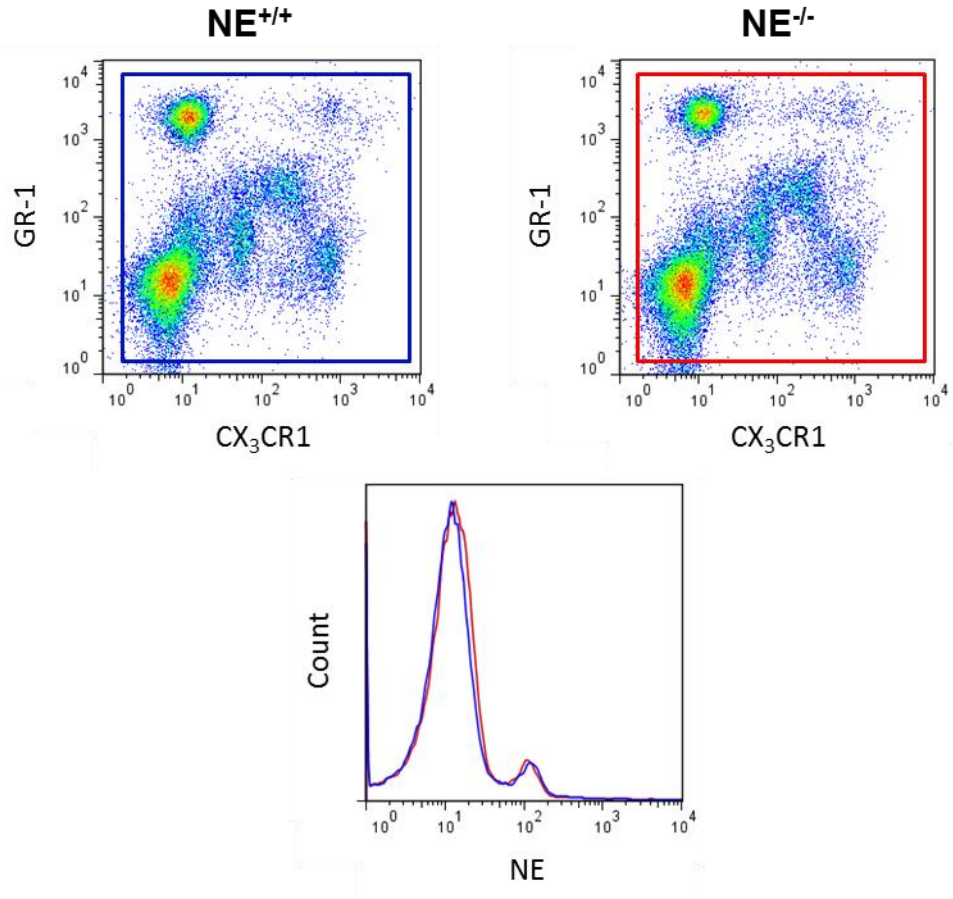


**Figure 4.10: Assaying for intracellular NE protein by flow cytometry**. Whole leukocytes harvested from the blood (shown) and BM of naïve $CX_3CR1^{+/eGFP}$ mice were ACK-lysed, fixed and permeabilised using Leucoperm reagents and immunostained for NE. $NE^{+/+}$ (blue) and $NE^{-/-}$ (red) leukocytes were directly compared.

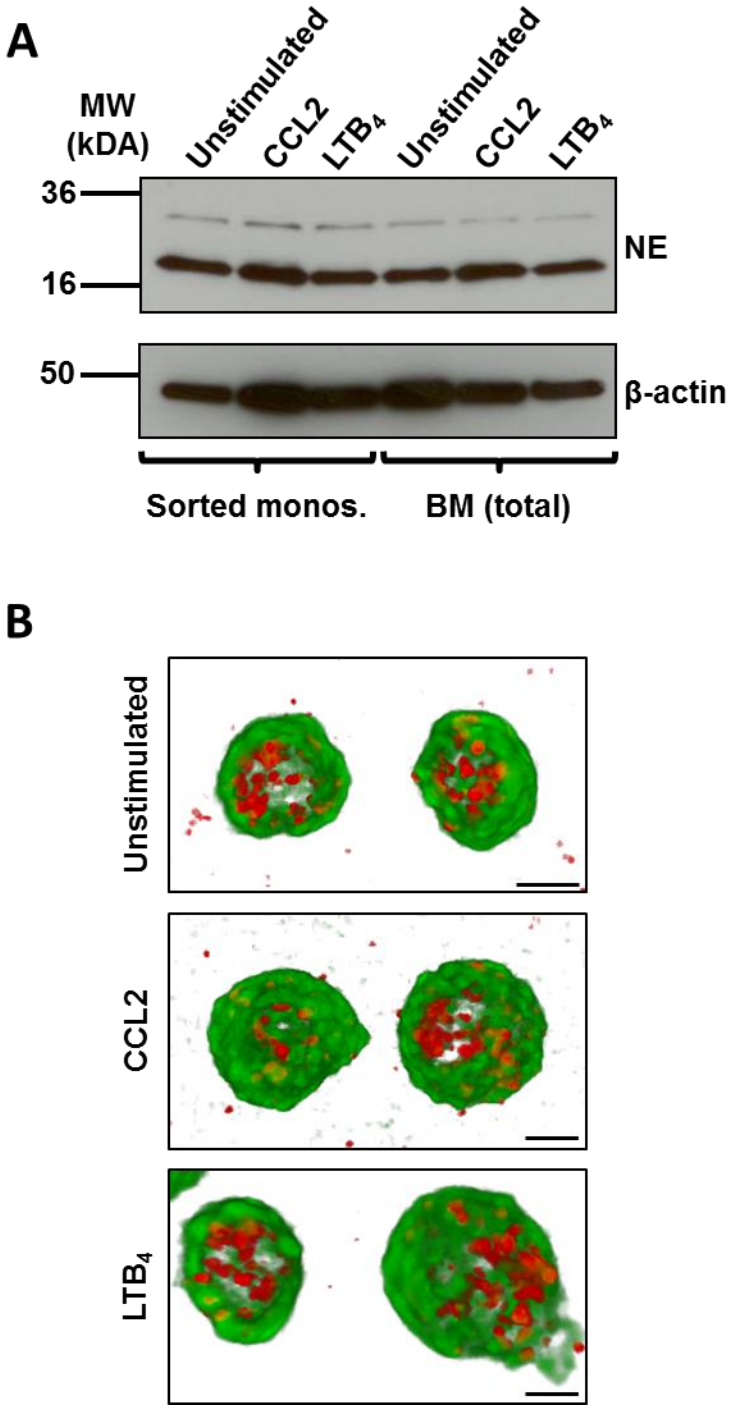


**Figure 4.11: Monocyte NE is not secreted following *in vitro* stimulation with CCL2 or $LTB_4$.** Intracellular NE expression levels were compared in naïve and stimulated leukocytes by Western blotting (A) and immunofluorescence (B). Regarding the former, $5\times10^5$ MACS-sorted monocytes and whole bone marrow (BM) leukocytes from $CX_3CR1^{+/eGFP}$ mice were cultured in 12-well plates in 500 µl RPMI-1640 media supplemented with CCL2, $LTB_4$ (each at 100 ng/ml) or vehicle (PBS). After 4 hours, cellular lysates were resolved by gel electrophoresis, transferred to a PVDF membrane and immunoprobed for NE. β-actin was used as a loading control. NE expression was also assayed for in monocytes by immunofluorescence. Cells were stimulated with CCL2, $LTB_4$ or PBS in plates as before (shown) or in suspension, though only for 45 minutes. Scale bar, 3 µm.

Reverting back to established techniques, we next endeavoured to evaluate NE release from monocytes by Western blotting. Upon MACS-sorting, monocytes were stimulated *in vitro* for 4 hours either with the monocyte-specific chemoattractant CCL2 or with $LTB_4$, a lipid mediator previously shown by our group to induce extensive NE degranulation from purified neutrophils (Young et al., 2007). Neither however triggered a tangible release of cellular NE (*Figure 4.11A*). Theorising that NE might be mobilised to the outer cell surface instead of being freely released, we next analysed the monocytes by immunofluorescence. Recognising that cell adhesion may also influence NE secretion, the cells were stimulated both in suspension and following attachment to coverslips. Irrespective of the stimulation protocol used however, monocytic NE could not be triggered for release by either CCL2 or $LTB_4$ (*Figure 4.11B*). Treatment with phorbol myristate acetate (PMA), a synthetic and general inducer of leukocyte degranulation also failed to reduce intracellular NE expression, though NE in neutrophils was shown to mobilise to the cell nucleus (*Appendix 4.4*).

***Discussion:***

It is emerging that neutrophil elastase, in spite of its name, is not exclusively found in neutrophils but rather can be expressed by several different cell types. NE expression has already been demonstrated in human macrophages and monocytes, however equivalent studies have yet to be conducted on mice. In this light, and considering our interest in exploiting mouse models to explore NE as a regulator of leukocyte migration, we sought to rigorously evaluate the expression of NE in murine monocytes in this chapter. This specifically entailed analysing levels of NE transcript and protein in the two major monocyte subsets, harvested from both the spleen and bone marrow of $CX_3CR1$-eGFP-ki mice.

As a means of isolating pure populations of classical and non-classical monocytes, whole splenocytes were originally separated by fluorescence-activated cell sorting (FACS). Both monocyte subsets are well represented in the spleen and, importantly, have been shown to share an identical morphology, transcriptome and function with their blood counterparts. Upon sorting, monocytes, as well as neutrophils and a crude population of lymphocytes, were initially assayed for NE transcript by qRT-PCR. For neutrophils, high-level transcription of NE and several other serine proteases is known to be limited to the promyelocytic stage of development. Once the mature proteins are packaged into azurophil granules gene transcription is reportedly terminated. Refuting this dogma, we were able to detect NE transcripts in mature splenic neutrophils. While NE was also expressed, albeit in lower amounts, in lymphocytes and non-classical monocytes, we were intrigued to discover a multi-fold increase in the expression of NE transcripts in classical monocytes. This is in accordance with previous reports in which mature monocytes have been shown to have a preserved capacity to increase production of granule proteins through *de novo* synthesis (Dale et al., 2008). Furthermore, NE transcripts have been directly detected in human blood monocytes (Dollery et al., 2003). This study did not however differentiate between the two monocyte subsets. In this regard, our results suggest there is a striking heterogeneity in NE expression between monocyte subsets in mice, with classical monocytes containing significantly greater quantities of the NE transcript compared to non-classical monocytes.

To determine if murine monocytes also expressed the NE protein, whole lysates of FACS-sorted classical and non-classical monocytes were analysed by Western blotting.

Neutrophil lysates were run in parallel and, as expected, were shown to contain a significant amount of NE protein. In contrast, no protein could be detected for either monocyte subset. Considering its potential role in monocyte transmigration, we initially speculated that NE was not required by monocytes under naïve conditions and only underwent translation upon stimulation. This did not seem to hold true however as incubating monocytes *in vitro* with a cocktail of inflammatory mediators did not elicit NE synthesis. Recognising the NE protein contains an N-terminal signal peptide, we considered that NE was synthesised and constitutively released by monocytes. Alternatively, it was feasible that monocytes contained NE stores but in quantities that lay below the detection limit of our Western blot assay. Neutrophils store NE in copious amounts, between 1-4 $\mu g/10^6$ cells (Edwards, 2005). It was possible that NE is packaged differently in monocytes at a lower undetectable concentration.

One final explanation we considered is that monocytes release their NE stores during cell purification. Following stimulation with the cytokine CD40 ligand, human monocytes were shown to expel almost their entire NE contents (Dollery et al., 2003). If our murine monocytes were similarly stimulated, albeit inadvertently, during FACS-sorting, this may explain the apparent absence of NE during Western blotting. To confirm if this was occurring, we incorporated a second cell purification method using MACS-technology. Whole cell suspensions from the mouse bone marrow and spleen were applied to a specific monocyte isolation kit, resulting in a pronounced enrichment of monocytes, predominantly of the classical subset. The bone marrow in particular demonstrated a high purity of classical monocytes, more than 95%, while in the spleen a purity of approximately 75% was attained. Importantly, both samples were almost completely devoid of NE-laden neutrophils. Instead, the majority of contaminating cells were GR-$1^{Int}$, Ly6G$^-$, $SSC^{hi}$ in keeping with a recent description of eosinophils (Rose et al., 2012), which, certainly in humans, do not express the NE protein (Wiedow et al., 1996).

Considering the abundance of NE transcripts detected in classical monocytes, we were particularly intrigued to re-assess their protein content by Western blotting following MACS-sorting. Due to their higher purity, bone-marrow derived monocytes were initially investigated. In stark contrast to our previous results conducted on FACS-sorted cells, upon MACS-sorting NE could be clearly detected in monocytes and at a level similar to whole bone marrow leukocytes. Moreover, the presence of multiple NE

bands on the Western blot, presumably as a result of NE autolysis, suggests NE from monocytes retains its catalytic activity. Thus, though critically dependent on the method of isolation, murine monocytes do seemingly have the capacity to store the NE protein.

This being established, we next employed immunofluorescence to explore the subcellular localisation of NE in classical monocytes MACS-sorted from the bone marrow, as well as the spleen. Though monocytes isolated from the spleen are altogether less pure, in immunofluorescence any contaminating cells can be individually identified and disregarded. Once seeded onto cover slips, we initially tried fixing and permeabilising the cells with a combination of PFA and Triton X-100. This approach however gave rise to false positive staining in $NE^{-/-}$ controls, possibly due to the incomplete quenching of free aldehyde groups in the PFA, which thereby remain susceptible to interacting non-specifically with the primary/secondary detection antibodies (Melan, 1999). We next attempted to fix and permeabilise the cells simultaneously using methanol. Although this approach bleached the endogenous eGFP fluorescence of the monocytes, it did provide specific staining for NE. In bone marrow neutrophils, NE localised to numerous intracellular stores, presumably the azurophil granules. This same granular staining was also observed in classical monocytes isolated from both the bone marrow and the spleen. This result confirms that the absence of NE protein in FACS-sorted monocytes is due not to their original source (i.e. the spleen) but to the method of cell purification.

In a study examining NE expression in human blood monocytes, approximately 60% of the monocytes analysed were unstained for NE, while the remainder varied greatly in staining intensity (Kargi et al., 1990). Within these cells, and in keeping with our findings, NE localised to intracellular granules demonstrating endogenous peroxidase activity akin to that seen in neutrophil azurophil granules. Interestingly, these granules were detected in monocytes in the same proportions as NE. While these results were attributed to different monocyte subsets, it is similarly conceivable that these cells were not heterogeneous in their ability to synthesise NE but rather had been incompletely stimulated to release their granular stores. Highly reactive, the handling and isolation of monocytes may be enough to trigger stimulation. Indeed, it is feasible that a considerable proportion of human monocytes in this study were inadvertently stimulated to undergo degranulation during centrifugation elutriation. Likewise, in our study, the process of FACS-sorting is seemingly sufficient to stimulate monocytes to

expel their entire NE contents. Interestingly, in both studies, neutrophils retain their NE stores upon isolation, implying either that they are less readily stimulated during handling or that NE is differently packaged and/or regulated in neutrophils and monocytes.

In previous studies, levels of secreted human NE have been successfully quantified by ELISA, while its enzyme activity has also been routinely assayed using the fluorogenic substrate methoxysuccinyl-Ala-Ala-Pro-Val-7-amino-4-trifluoromethyl coumarin. While this substrate is highly selective for human NE, this specificity is mostly lost in mice, as demonstrated by our group (data not shown) and others (Wiesner et al., 2005). Unfortunately, in this study we were unsuccessful in establishing an equivalent assay specific for secreted mouse NE. While NE could be accurately detected in the lysates of leukocytes, the volumes of these samples were ultimately very low, concentrating the protein content. In contrast, NE released into the media of cultured leukocytes was evidently too dilute to be detected by Western blotting. To circumvent this problem we next attempted to establish our own ELISA, a quantitative technique that accommodates high volume samples. Initially convinced we were able to detect NE in the diluted lysates of $NE^{+/+}$ leukocytes, in running equivalent controls from $NE^{-/-}$ mice it became clear that our signal read-out was not NE-specific. Though we revealed the anti-NE antibody could similarly recognise a component of foetal bovine serum, its omission in subsequent experiments was not sufficient to remove the signal generated in the knockout samples. Considering this signal weakens as the lysates are serially diluted, it is most likely caused by a separate cellular component as opposed to being an artefact of the ELISA process. Indeed, a signal could also be detected in the lysates of $NE^{-/-}$ leukocytes when processed by slot blot.

As whole cell lysates were similarly, yet successfully analysed by conventional Western blotting, one can only assume that the contaminating component in $NE^{-/-}$ leukocytes is removed during gel electrophoresis. As a result, we next tried to concentrate soluble NE by immunoprecipitation prior to conducting a Western blot, exactly as before. Regrettably, this process produced miscellaneous bands on the blot that could not be removed and, even more compounding, ran at a size similar to native NE. Interestingly, no bands were visible when fresh untouched sepharose beads were eluted suggesting they derived from the RPMI-1640 media, which was similarly used in all samples. Bypassing the need for immunoprecipitation, we also tried concentrating soluble NE by

centrifugation, however no traces of the protein could be detected upon Western blotting (data not shown).

Considering our difficulties in detecting secreted NE directly in solution, as a measure of NE degranulation we next tried to monitor the depletion of NE stores from stimulated leukocytes. For this purpose we hoped to utilise flow cytometry as this approach enables the concurrent differentiation of classical monocytes, non-classical monocytes and neutrophils. Furthermore, it would enable us to directly compare both the intracellular and surface expression of NE in naïve leukocytes harvested from the blood and leukocytes collected from inflammatory exudates. In trying to establish a working protocol, whole leukocytes from the blood and bone marrow were immunostained for NE following their fixing and permeabilisation with Leucoperm reagents. While these reagents have been successfully used to stain for azurophil granule proteins in human T-lymphocytes (Sadahira et al., 2001), we failed to detect NE stores in murine leukocytes. In researching Leucoperm, cell permeabilisation is achieved with a relatively mild set of detergents that might not sufficiently penetrate the membrane of NE-laden granules. Accordingly, we supplemented the Leucoperm kit with Triton X-100, a stronger detergent that dissolves more of the lipid membrane, as well as methanol, which previously supported NE-specific immunofluorescence, however neither provided a successful NE stain (data not shown).

This result highlights the functional limitations often exhibited by detection antibodies. Though incompatible for flow cytometry, the same rabbit anti-NE antibody was successfully applied for Western blotting and immunofluorescence. Raised against a synthetic NE peptide, it is possible that this antibody does not recognise NE in a native, folded state but rather requires it to be denatured. For Western blotting all protein samples were completely denatured by boiling in the presence of β-mercaptoethanol. Likewise, immunofluorescent staining of NE in leukocytes was best achieved using methanol, an effective protein denaturant. Even under denaturing conditions however, we were unable to specifically detect NE by ELISA or slot blot analysis and regrettably we remain without a functioning assay for secreted NE. For this purpose, we instead decided to use immunofluorescence to visualise the trafficking of NE to the cell surface upon stimulation, however this was not observed in response to CCL2, $LTB_4$ or PMA, NE instead remaining confined to intracellular granules. This conflicts with a study conducted on human monocyte-like U937 cells, which were shown to be almost

completely depleted of their intracellular stores following stimulation with PMA, albeit for over 20 hours, contrasting the much shorter stimulation period of 30 minutes used in this study (Lemansky et al., 2007). This time period was sufficient however to induce NE translocation from azurophil granules to the nucleus of neutrophils (and neutrophils only), in keeping with previous reports (Papayannopoulos et al., 2010). Furthermore, and again owing potentially to the specific set-up of our assays, we were surprised not to observe NE secretion from neutrophils stimulated with $LTB_4$, a supposedly potent inducer of azurophil degranulation (Young et al., 2007).

In conclusion, we are the first group to report NE expression in bona fide monocytes in mice. Classical monocytes in particular express relatively large quantities of NE transcript and have also been explicitly shown to store the NE protein in cytoplasmic granules. This staining was akin to that seen in neutrophils. Unlike neutrophils which display multiple types of subcellular granules, monocytes contain only one. Studies have shown that monocytic granules most closely resemble neutrophil azurophil granules: they both contain a large number of acid hydrolases and many of the same microbicidal proteins, including defensins, lysozyme, and of course NE. The manner in which NE is stored and released in these granules is however seemingly different in monocytes and neutrophils as FACS-sorting only triggered complete degranulation in monocytes. Moreover, mature classical monocytes from the spleen appear to have a greater ability to synthesise NE *de novo*. Non-classical monocytes too seem to express the NE gene though to a lesser extent, while its protein content has yet to be rigorously assessed.

# CHAPTER 5: Investigating the functional role of NE in monocyte trafficking *in vivo*.

## *5.1 Introduction*

While initial studies in NE deficient mice suggest the primary role of NE is in the intracellular killing of engulfed bacteria, it has also been implicated in numerous other physiological processes. An area of much research, several groups, including ours, have reported a functional role for NE in neutrophil transmigration, however this is a contentious issue. As touched on in the previous chapter, neutrophils have been shown to mobilise NE to the cell surface during transmigration in response to a variety of inflammatory mediators. In this state NE facilitates the migration of human neutrophils across human umbilical vein endothelial cell (HUVEC) monolayers, as treatment with an anti-NE monoclonal antibody reduces PAF-induced migration by 80% (Cepinskas et al., 1999). The use of confocal microscopy in this same study revealed migrating neutrophils localise their membrane-bound NE to the leading front. Due to its potent ability to cleave extracellular matrix proteins, it was originally postulated that surface-bound NE on invading pseudopodia mediated neutrophil migration through the dense endothelial basement membrane (EBM). In support of this, while human neutrophil chemokinesis, chemotaxis, and degranulation were unaffected in the presence of an NE-specific inhibitor, migration through Matrigel, a reconstituted EBM preparation extracted from sarcoma cells, was reduced by more than 50% (Delclaux et al., 1996). In contrast, although a loss of EBM integrity was observed following the migration of human neutrophils across a HUVEC monolayer, this was shown to be NE-independent (Huber and Weiss, 1989). Moreover, the migration of fMLP-stimulated human neutrophils across pulmonary endothelial cells and associated basal lamina was not blocked by broad-acting serine protease inhibitors (Mackarel et al., 1999).

Considering the non-specific nature of some pharmacological inhibitors and the reported resistance of surface-bound NE to endogenous inhibitors, the availability of NE-knockout mice has provided a clean and elegant tool for studying the role of NE in leukocyte migration, not only *in vitro* but *in vivo*. Nevertheless, NE's involvement in leukocyte transmigration remains unclear. Shapiro et al. report a significant defect in neutrophil infiltration in the lungs of $NE^{-/-}$ mice exposed to cigarette smoke (Shapiro et al., 2003). They also however demonstrate normal chemotaxis and Matrigel invasion of

$NE^{-/-}$ neutrophils *in vitro* and instead attribute their *in vivo* findings to an inability of $NE^{-/-}$ neutrophils to effectively penetrate the vascular endothelium. In this manner, the same group also report an impairment of $NE^{-/-}$ neutrophils to cross pulmonary vein and microvascular endothelium *in vitro* compared to WT controls (Kaynar et al., 2008). This defect was accompanied by reduced cleavage of the endothelial adhesion molecule ICAM-1. ICAM-1 has been demonstrated by other studies to be liable to NE-cleavage, as has the closely related VCAM-1 and the major selectin ligand PSGL-1. Shown to participate in leukocyte adhesion, the cleavage of these molecules by NE may regulate the sequence of attachment/detachment events that mediate leukocyte TEM (Pham, 2008).

Contradicting this notion, $NE^{-/-}$ neutrophils do not exhibit a defect in migration across cultured murine cardiac endothelial cells (Allport et al., 2002). Furthermore, NE KO mice exhibit normal profiles of neutrophil transmigration *in vivo* to the lung and peritoneum challenged with *Pseudomonas aeruginosa* or its lipopolysaccharide (Hirche et al., 2004). Similarly, $NE^{-/-}$ mice mostly display no defects in neutrophil transmigration in the cremaster muscle model, though this has been postulated to result from the occurrence of developmental compensation as significant reductions in transmigration are observed following treatment with the NE-specific small molecule inhibitor ONO-5046. Indeed, intravenous administration of ONO-5046 suppressed neutrophil migration through IL-1β- and $LTB_4$-stimulated cremasteric venules, specifically at the level of the EBM (Wang and Dangerfield, 2005) (Young et al., 2007). This is seemingly due to the ability of NE to enlarge regions of low matrix protein deposition in the EBM through which neutrophils preferably migrate (Wang et al., 2006). In keeping with this, ONO-5046 also inhibited neutrophil transmigration through laminin-1-coated filters, while a large percentage of transmigrated neutrophils in the cremaster muscle were shown to carry laminin fragments on their cell surface (Wang et al., 2006) (Voisin et al., 2009).

Leukocyte firm adhesion and transmigration was also significantly suppressed by ONO-5046 in the cremaster muscles of mice stimulated with the particulate zymosan (Young et al., 2004). Interestingly, this was also observed in $NE^{-/-}$ mice. This phenotype was attributed not to an inability to penetrate the EBM of venules but rather to impaired zymosan phagocytosis and subsequent generation and/or release of pro-inflammatory mediators. Likewise, $NE^{-/-}$ mice showed reduced levels of inflammatory cytokines and

infiltrated neutrophils in response to zymosan in an air pouch model (Adkison et al., 2002). In this same manner, NE has been shown to enhance neutrophil migration by inducing the secretion of the cytokines GM-CSF and CXCL8 from primary epithelial cells (Bédard et al., 1993) and by generating neutrophil chemotactic fragments through cleavage of various matrix proteins including laminin-332 and type XVII collagen (Mydel et al., 2008) (Lin et al., 2012).

As a whole, there is a large amount of evidence to suggest an involvement of NE in neutrophil transmigration. Indeed, in accordance with its greater potency in stimulating NE release/cell surface expression, $LTB_4$ was found to be more effective in eliciting neutrophil transmigration through mouse cremasteric venules compared to KC (CXCL1) or PAF (Young et al., 2007). The mechanism by which NE mediates neutrophil transmigration is however seemingly heterogeneous and may depend on the type/dose of stimulus or model/tissue of inflammation. In addition, NE has been implicated in the migration of other leukocyte types, largely through its ability to modify the composition of the inflammatory milieu by regulating chemokine and cytokine bioavailability and processing protein receptors. The release of NE by transmigrating neutrophils for example deactivates endothelial-bound CXCL12 attenuating subsequent T-lymphocyte migration (Rao et al., 2004). NE-cleaved matrix protein fragments also exhibit chemotactic activity for many leukocytes, for instance elastin- and fibronectin-derived peptides which have been shown to recruit monocytes (Senior et al., 1980).

In contrast to neutrophils, only a select few studies have explored a direct role for NE in the migration of other NE-expressing leukocytes, such as monocytes. In this context, ONO-5046 had no effect on CCL2-induced monocyte migration through cremasteric venules *in vivo* or across laminin/collagen IV coated filters *in vitro* (Voisin et al., 2009). In a chronic model of cigarette smoke exposure however, significantly fewer macrophages accumulated in the lungs of $NE^{-/-}$ mice compared to wild-type controls (Shapiro et al., 2003). This was attributed to a defect in the pulmonary recruitment of circulating monocytes as isolated $NE^{-/-}$ blood monocytes demonstrated impaired Matrigel penetration *in vitro*. Considering the minimal and inconsistent data collected on this matter, and in light of our recent findings confirming substantial NE expression in murine monocytes, in this chapter we aspired to rigorously and specifically investigate the function of NE in murine monocyte migration *in vivo*. We sought to

achieve this goal by directly comparing $NE^{-/-}$ and $NE^{+/+}$ mice and exploiting NE-specific inhibitors. The key objectives we wanted to address are as follows:

- Broadly assess the involvement of NE in monocyte recruitment in a peritoneal model of inflammation.
- Employ confocal microscopy to investigate the role of NE during monocyte transendothelial migration (TEM) *in vivo*.
- Assess NE activity and expression during monocyte TEM.
- Establish an *in vitro* transmigration assay to elucidate the mechanisms underpinning NE-mediated monocyte migration.

## *5.2 Results*

### *a) NE$^{-/-}$ mice exhibit a diminished accumulation of peritoneal classical monocytes in a time-and stimulus-dependent manner.*

The use of animal inflammation models has been invaluable in characterising the immune response *in vivo*. One commonly used inflammation model is the peritonitis model, which is typically performed on mice or rats. Peritonitis is described as inflammation of the peritoneal cavity, the gap that exists between the wall of the abdomen and the organs contained within. The cavity is bound by a thin serous membrane called the peritoneum. This membrane is locally breached upon an intraperitoneal (i.p.) injection, which is used to administer an inflammatory stimulus into the peritoneal cavity. This prompts a local influx of leukocytes and plasma proteins, primarily through post-capillary venules in the milky spots of the greater omentum, and synthesis of inflammatory mediators, the hallmarks of inflammation (Doherty et al., 1995). The main advantage of this model is the large volume of the peritoneal cavity, which accumulates a great amount of inflammatory exudate that can be easily collected for downstream analysis. In this context, a common use of the peritonitis model is to quantitate leukocyte recruitment by obtaining peritoneal lavage and determining the total number of infiltrated cells. Furthermore, the presence of specific cell types can be elucidated, often by flow cytometry. This approach also enables the phenotype of transmigrated leukocytes to be directly compared to their counterparts in the blood.

Exploiting the peritonitis model in this manner, we broadly investigated the functional role of NE in monocyte trafficking *in vivo*. This was specifically achieved by comparing the inflammatory profiles of NE$^{+/+}$ and NE$^{-/-}$ mice in response to acute peritonitis. As an initial inciting stimulus, we injected mice i.p. with 300 ng/ml IFN-γ for 16 hours followed by 300 ng/ml TNF-α for a further 4 hours. This reaction was used as it has been previously demonstrated by our lab to elicit a strong monocyte response in the cremaster muscle (*Appendix 5.1*). In characterising this reaction in the peritoneal cavity, leukocyte infiltrations were first evaluated by calculating the total number of peritoneal cells present in the collected lavage fluid (*Figure 5.1A*). The peritoneal cell counts of NE$^{+/+}$ and NE$^{-/-}$ mice were largely identical, suggesting NE KO mice exhibit no overwhelming defect in leukocyte recruitment. Interestingly, there were also no differences in the number of peritoneal cells when compared to PBS controls, though

this did enable the proportion of leukocyte subtypes to be directly compared across all samples during subsequent flow cytometric analysis. Specifically, relative levels of the two major monocyte subsets, neutrophils and macrophages were identified and gated, as before (*Figure 5.1B*). As in the cremaster muscle, IFN-γ/TNF-α abundantly recruited monocytes to the peritoneal cavity, specifically those of the classical subset, their relative peritoneal fraction increasing from ~1.5% in control mice to more than 10% following treatment with IFN-γ/TNF-α. Levels of non-classical monocytes appeared to be slightly down-regulated but remained at 5-10%, while macrophages seemingly vacated the cavity (explaining the comparable cell counts in PBS controls), their numbers dropping from 25% to under 10%. Of note, both monocyte subsets and macrophages were equally represented upon stimulation in $NE^{+/+}$ and $NE^{-/-}$ mice. In contrast, levels of neutrophils, though substantially up-regulated for both genotypes, were significantly less abundant in the cavities of $NE^{-/-}$ mice.

Flow cytometry was also used to analyse the proportion of leukocyte subtypes in the blood, as this represents the most immediate source of leukocytes available for transmigration (*Figure 5.1C*). Discrepancies in the blood profile of $NE^{-/-}$ mice may suggest a defect either in the migratory capacity of circulating leukocytes or in the deployment of secondary leukocyte stores, such as the bone marrow and spleen, into the blood. In accordance with the pronounced increase in peritoneal neutrophils, stimulation with IFN-γ/TNF-α also induced blood neutrophilia in both $NE^{+/+}$ and $NE^{-/-}$ mice. Levels of circulating monocytes were not however significantly different to one another or PBS controls. Thus, following IFN-γ/TNF-α–induced peritonitis no differences were observed in the proportion of either monocyte subset in the peritoneal lavage or blood of $NE^{-/-}$ mice compared to WT controls.

Stimulation with IFN-γ/TNF-α elicited a strong influx of both neutrophils and monocytes. Considering neutrophils are known to directly stimulate the mobilisation of monocytes during inflammation (Soehnlein and Lindbom, 2010) we next sought to assess monocyte recruitment to the peritoneal cavity in response to CCL2, a monocyte specific chemoattractant. Classical monocytes in particular respond to CCL2 as they abundantly express its cognate receptor CCR2 (see *Table 3.2*). To more rigorously characterise CCL2-induced peritonitis, we analysed peritoneal lavage and blood samples at both 4 and 16 hours post stimulation. No significant differences were observed in the overall number of peritoneal cells between $NE^{+/+}$ and $NE^{-/-}$ mice at

either time point (*Figure 5.2A*). Analysing the individual leukocyte subtypes, neutrophils were not recruited in response to CCL2 (*Figure 5.2B*). Levels of non-classical monocytes too were largely unchanged compared to PBS controls but the proportion of classical monocytes increased significantly at 4 hours in both genotypes from less than 1% to more than 4%. This change was however more modest in $NE^{-/-}$ mice and by 16 hours these mice contained significantly fewer classical monocytes in their cavities compared to their WT equivalents. In contrast, the proportion of peritoneal macrophages was significantly reduced in $NE^{-/-}$ mice at the earlier time point of 4 hours, but increased after 16 hours to a level comparable to that of WT mice. Importantly, this change in the proportion of macrophages does not account for the concurrent change in monocytes, and vice versa, as the same trends are observed upon plotting total cell numbers (*Figure 5.2D*). While $NE^{-/-}$ and $NE^{+/+}$ mice display different monocyte and macrophage profiles in the peritoneal lavage, relative levels of circulating monocytes were largely conserved in response to CCL2 (*Figure 5.2C*). Classical monocytosis was similarly observed 4 hours post stimulation, though returned to baseline levels after 16 hours. Surprisingly, this was also observed in PBS-treated mice. Levels of circulating non-classical monocytes and neutrophils remained largely stable throughout the reaction.

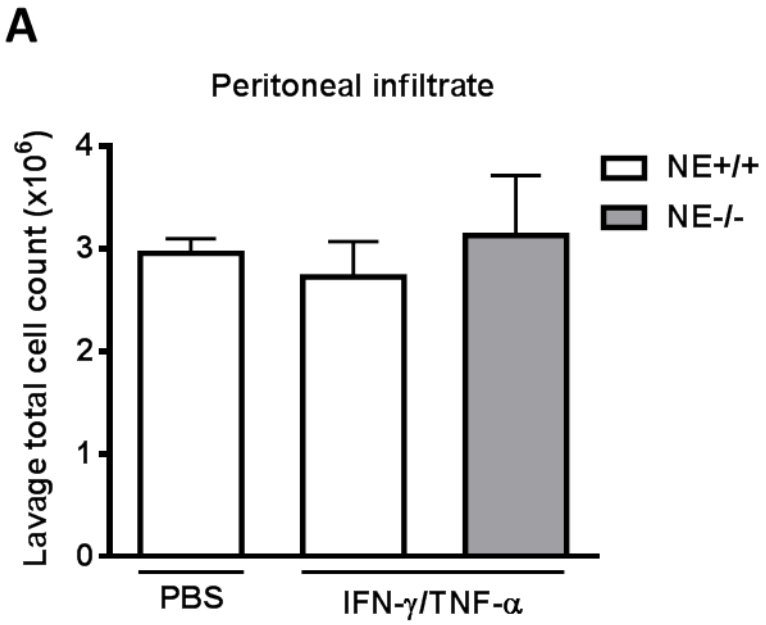

**B**

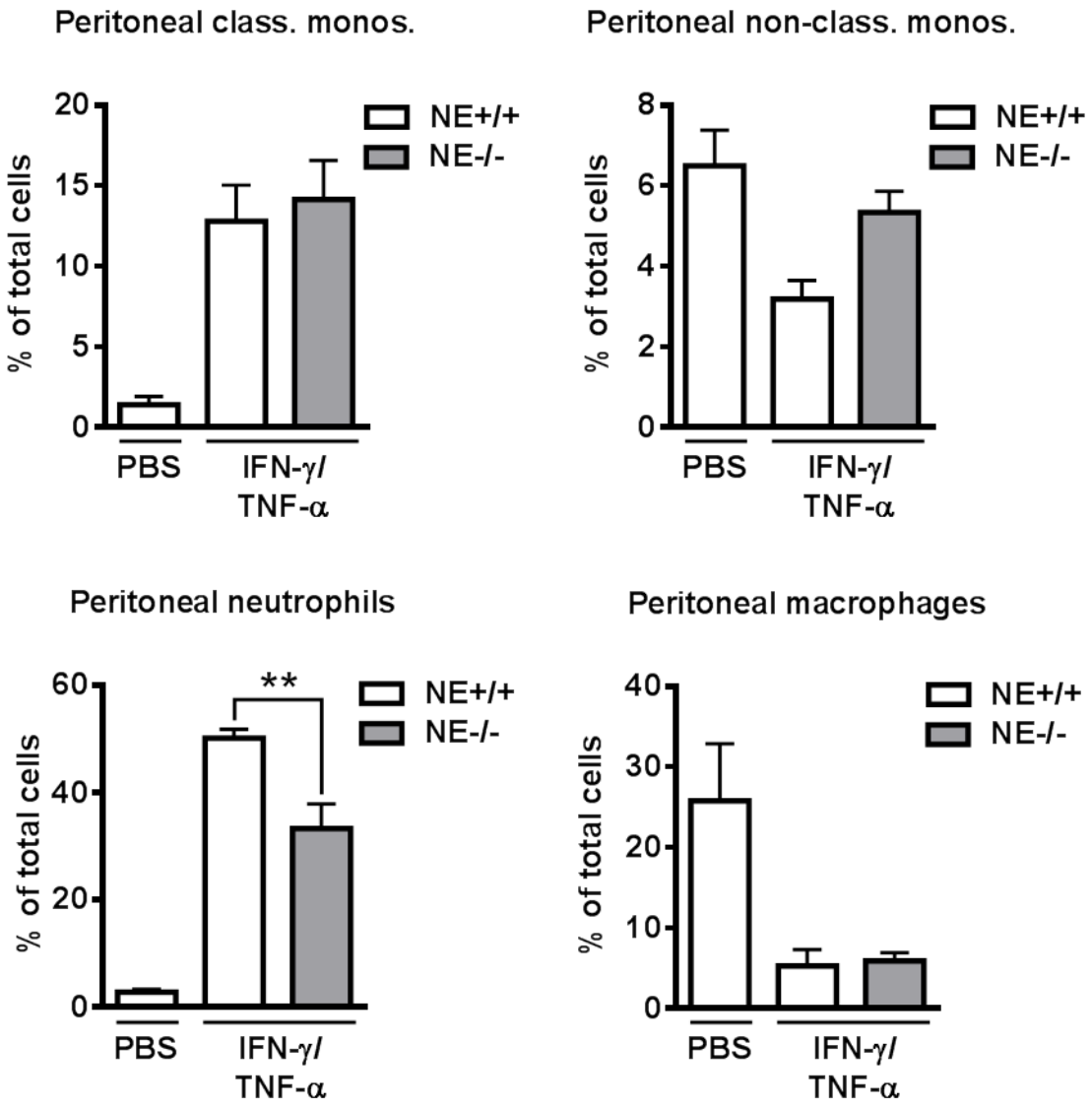
Peritoneal class. monos.
Peritoneal non-class. monos.
Peritoneal neutrophils
Peritoneal macrophages
% of total cells
NE+/+
NE-/-
PBS
IFN-γ/
TNF-α
**

**C**

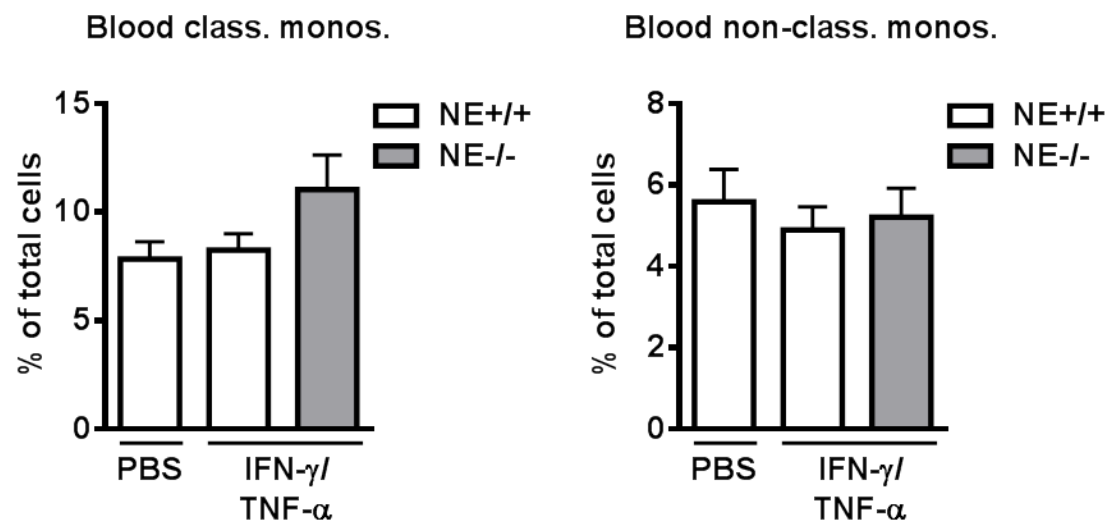
Blood class. monos.
Blood non-class. monos.
% of total cells
NE+/+
NE-/-
PBS
IFN-γ/
TNF-α

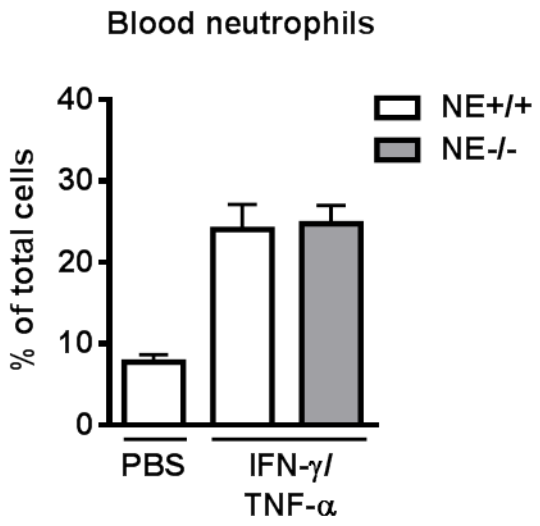


**Figure 5.1: Characterisation of peritoneal and blood leukocytes following IFN-γ/ TNF-α-induced peritonitis.** $NE^{+/+}$ and $NE^{-/-}$ $CX_3CR1^{+/eGFP}$ mice were stimulated i.p. with IFN-γ (300 ng/ml) for 16 hours and TNF-α (300 ng/ml) for a further 4 hours (total test period of 20 hours). Total leukocytes were subsequently harvested from the blood and peritoneal cavity. Peritoneal cell counts were initially calculated using a haemocytometer (A). Flow cytometry was subsequently employed to assess the relative proportion of classical monocytes ($GR\text{-}1^{+}$, $CX_3CR1^{med}$), non-classical monocytes ($GR\text{-}1^{-}$, $CX_3CR1^{hi}$), neutrophils ($GR\text{-}1^{+}$, $CX_3CR1^{-}$) and macrophages ($CX_3CR1^{low}$, $GR\text{-}1^{low}$, $SSC^{hi}$) in both the peritoneal cavity (B) and blood (C). Control mice were injected i.p. with PBS only. All data are represented as the mean ± SEM (n = 3-4 mice). FACS-data are averaged across 2-3 readings per mouse. Statistically significant differences between NE WT and KO data are indicated by asterisks (**, $p < 0.01$, Student's T-test).

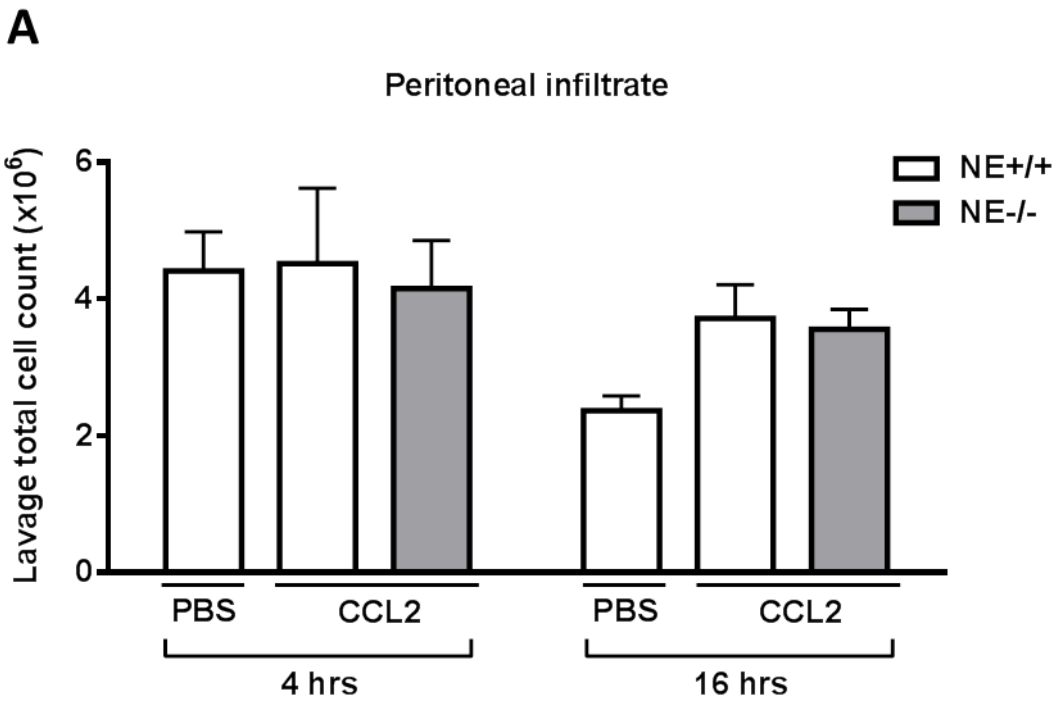

**B**

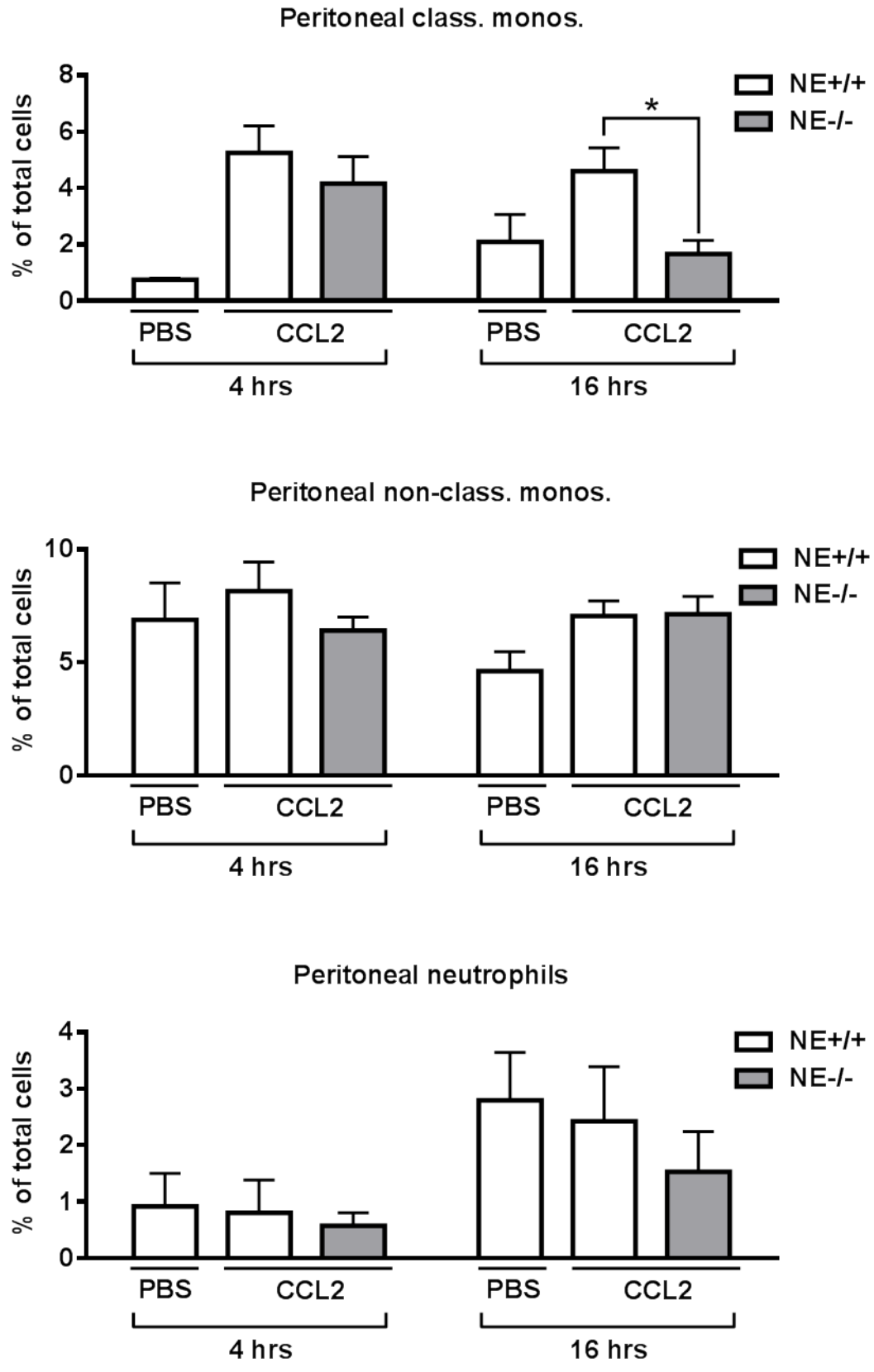
Peritoneal class. monos.
% of total cells
8
6
4
2
0
*
NE+/+
NE-/-
PBS
CCL2
PBS
CCL2
4 hrs
16 hrs
Peritoneal non-class. monos.
% of total cells
10
5
0
NE+/+
NE-/-
PBS
CCL2
PBS
CCL2
4 hrs
16 hrs
Peritoneal neutrophils
% of total cells
4
3
2
1
0
NE+/+
NE-/-
PBS
CCL2
PBS
CCL2
4 hrs
16 hrs

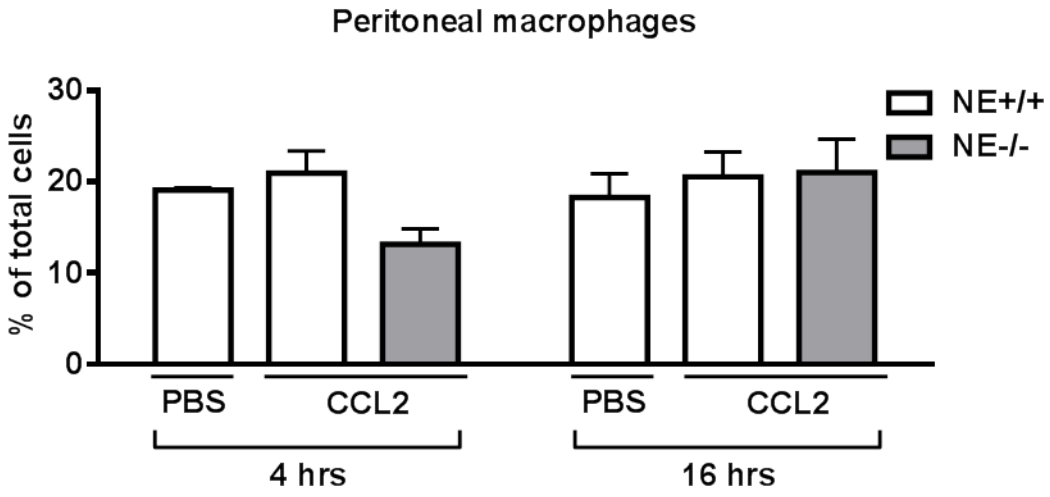
Peritoneal macrophages
% of total cells
30
20
10
0
NE+/+
NE-/-
PBS
CCL2
PBS
CCL2
4 hrs
16 hrs

C

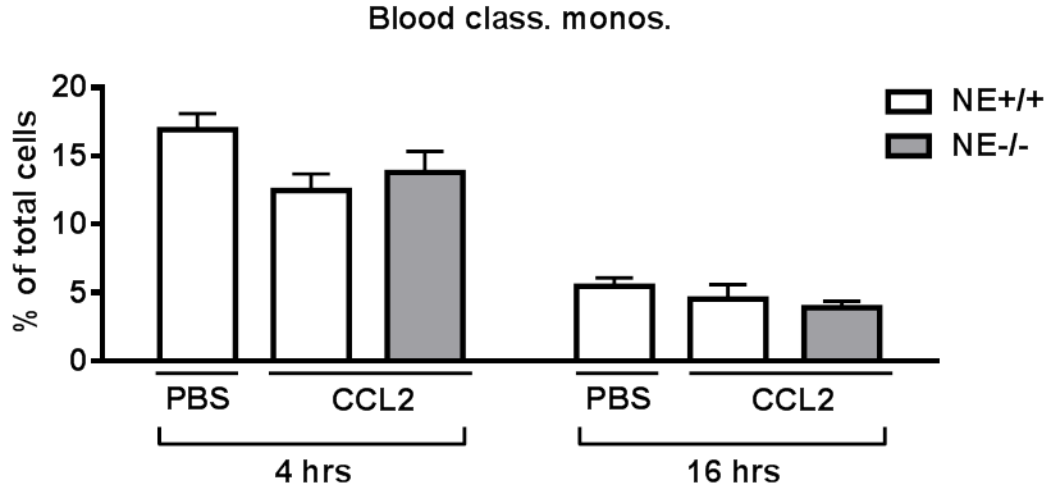
Blood class. monos.
% of total cells
20
15
10
5
0
NE+/+
NE-/-
PBS
CCL2
PBS
CCL2
4 hrs
16 hrs

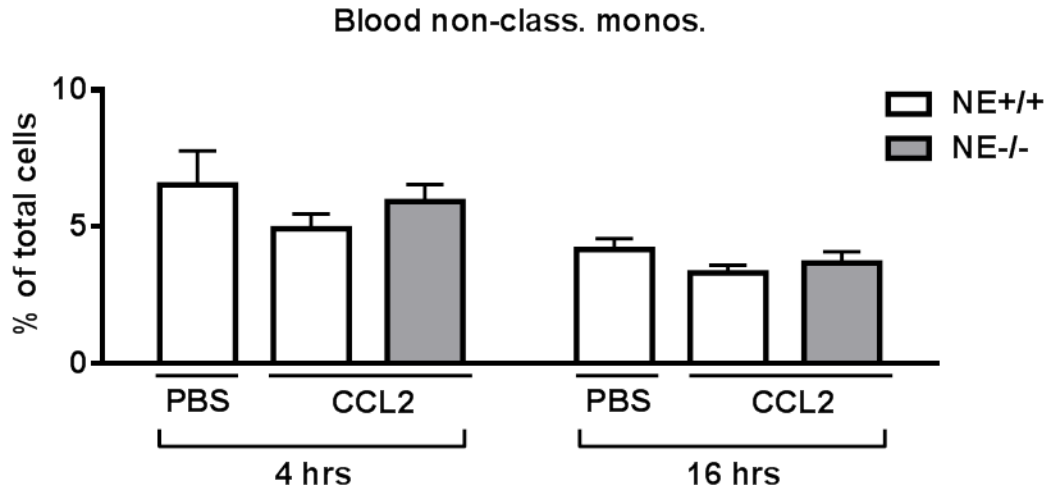
Blood non-class. monos.
% of total cells
10
5
0
NE+/+
NE-/-
PBS
CCL2
PBS
CCL2
4 hrs
16 hrs

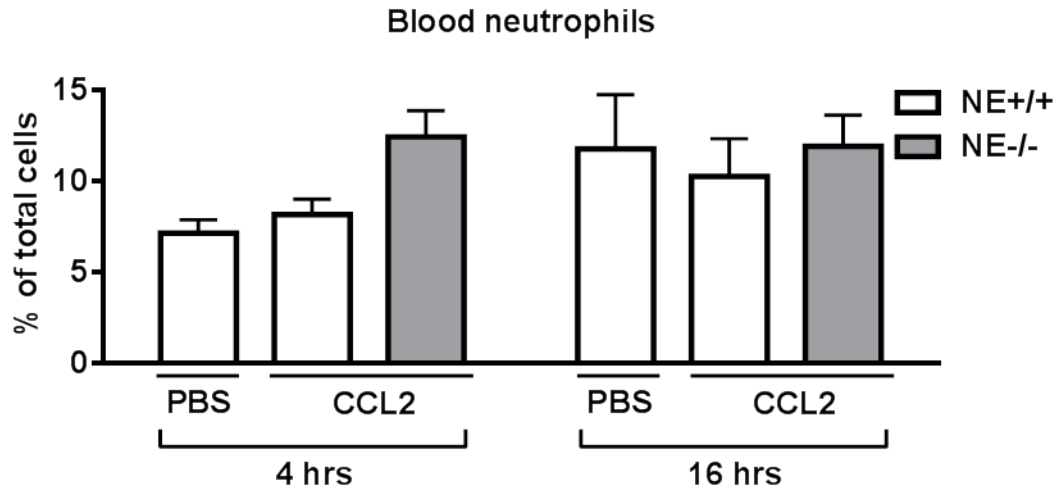
Blood neutrophils
% of total cells
15
10
5
0
NE+/+
NE-/-
PBS
CCL2
PBS
CCL2
4 hrs
16 hrs

D

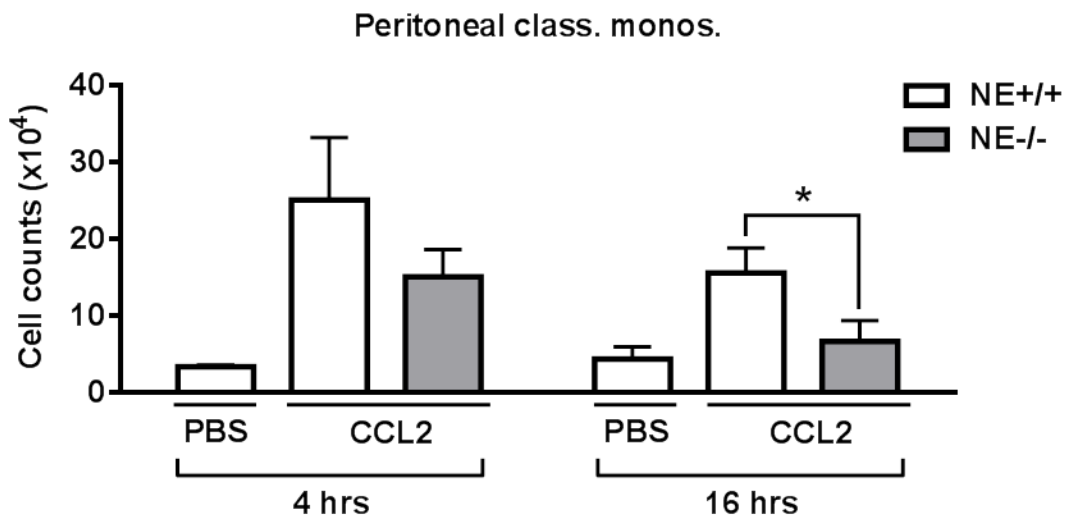
Peritoneal class. monos.
Cell counts (x10^4)
40
30
20
10
0
NE+/+
NE-/-
*
PBS
CCL2
PBS
CCL2
4 hrs
16 hrs

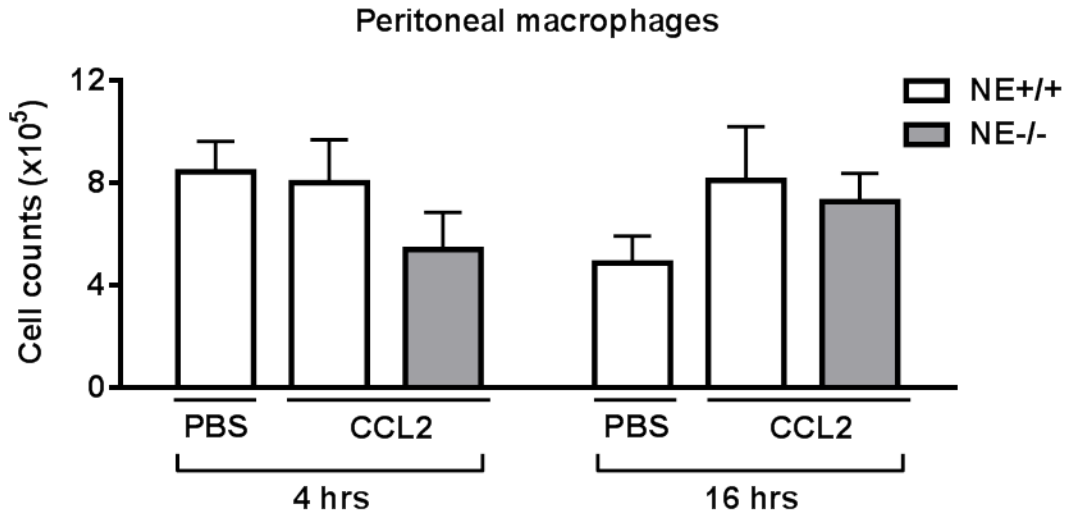
Peritoneal macrophages
Cell counts (x10^5)
12
8
4
0
NE+/+
NE-/-
PBS
CCL2
PBS
CCL2
4 hrs
16 hrs

**Figure 5.2: Characterisation of peritoneal and blood leukocytes following CCL2-induced peritonitis.** $NE^{+/+}$ and $NE^{-/-}$ $CX_3CR1^{+/eGFP}$ mice were stimulated i.p. with CCL2 (500 ng/ml) for 4 or 16 hours. Total leukocytes were subsequently harvested from the blood and peritoneal cavity. Peritoneal cell counts were initially calculated using a haemocytometer (A). Flow cytometry was subsequently employed to assess the relative proportion of classical monocytes ($GR\text{-}1^{+}$, $CX_3CR1^{med}$), non-classical monocytes ($GR\text{-}1^{-}$, $CX_3CR1^{hi}$), neutrophils ($GR\text{-}1^{+}$, $CX_3CR1^{-}$) and macrophages ($CX_3CR1^{low}$, $GR\text{-}1^{low}$, $SSC^{hi}$) in both the peritoneal cavity (B) and blood (C). Total numbers of peritoneal classical monocytes and macrophages were also calculated (D). Control mice were injected i.p. with PBS only. All data are represented as the mean ± SEM (n = 3-4 mice). FACS-data are averaged across 2-3 readings per mouse. Statistically significant differences between NE WT and KO data are indicated by asterisks (*, $p < 0.05$, Student's T-test).

### *b) $NE^{-/-}$ classical monocytes express normal levels of CD62L and CD18.*

Looking more closely at the peritoneal counts following CCL2 stimulation, total numbers of classical monocytes decreased between 4 and 16 hours in both $NE^{-/-}$ and $NE^{+/+}$ mice implying they do not simply accumulate in the cavity upon recruitment. The fate of these cells however remains currently unclear. It is possible they undergo apoptosis and hence become excluded from flow cytometric analysis. Alternatively, they may lose their typical gating phenotype by differentiating into macrophages or might even emigrate from the cavity via the draining lymphatics. Irrespective of how these cells are depleted, there remains a significant difference in the number of bona fide classical monocytes in the peritoneal cavities of $NE^{-/-}$ mice compared to WT mice at 16 hours post CCL2 stimulation. Though it is conceivable that classical monocytes are more comprehensively 'lost' from the peritoneum of $NE^{-/-}$ mice, it is equally plausible that fewer monocytes are actively recruited. Indeed, proteases have been previously implicated in influencing leukocyte dynamics during peritonitis. Upon thioglycollate stimulation for example, mice deficient for the protease ADAM-17 displayed a 2-fold increase in the number of infiltrated neutrophils at 4 hours but a reduction at 12 hours compared to WT controls, as attributed to changes in leukocyte surface expression of L-selectin (Tang et al., 2011). NE itself has also been directly proposed to regulate phasic neutrophil recruitment in response to zymosan, though in the cremaster muscle (Young et al., 2004). Although the precise involvement of NE in this reaction was not clarified, it was proposed that early recruited neutrophils induce the release of endogenous inflammatory mediators in an NE-dependent manner, initiating a secondary phase of leukocyte migration.

With these two studies in mind, we compared levels of L-selectin on classical monocytes both in the blood and lavage of $NE^{-/-}$ and $NE^{+/+}$ mice. We also looked at levels of β2 (CD18) integrins as these have been shown to mediate leukocyte migration and interact directly with NE (Cai and Wright, 1996). Neither L-selectin nor CD18 showed significantly different expression levels across the two genotypes (*Figure 5.3*). There was however a collective and well characterised decrease in CD62L levels following monocyte transmigration, as well as an increasing trend in CD18 expression over time, in keeping with previous reports (Al-Numani et al., 2003). Next, to explore NE as a potential stimulator of endogenous cytokine production, we injected catalytically active recombinant NE into the peritoneal cavity of WT mice for 4 hours. This did not however elicit an enhanced monocyte or leukocyte response when compared to PBS controls (data not shown).

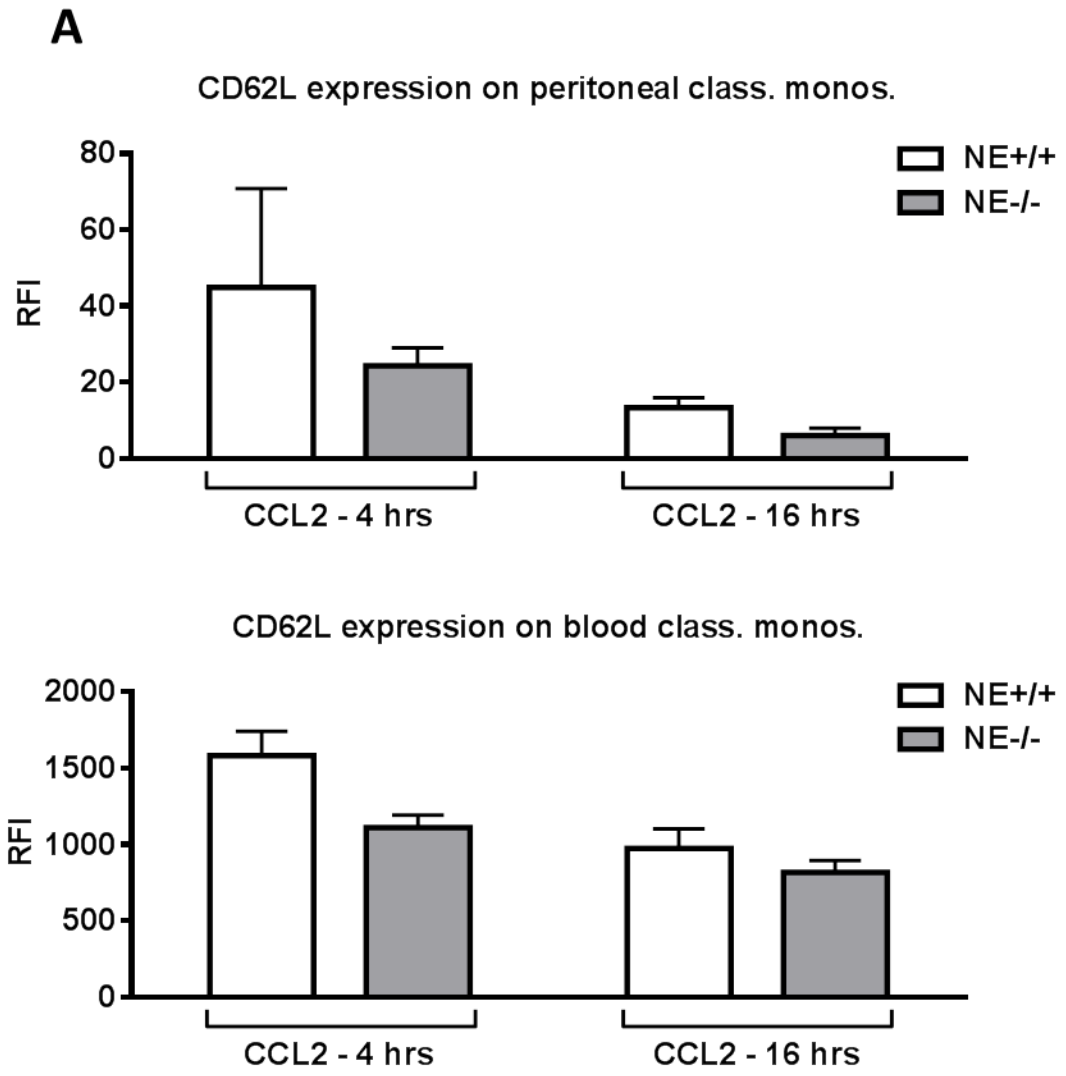

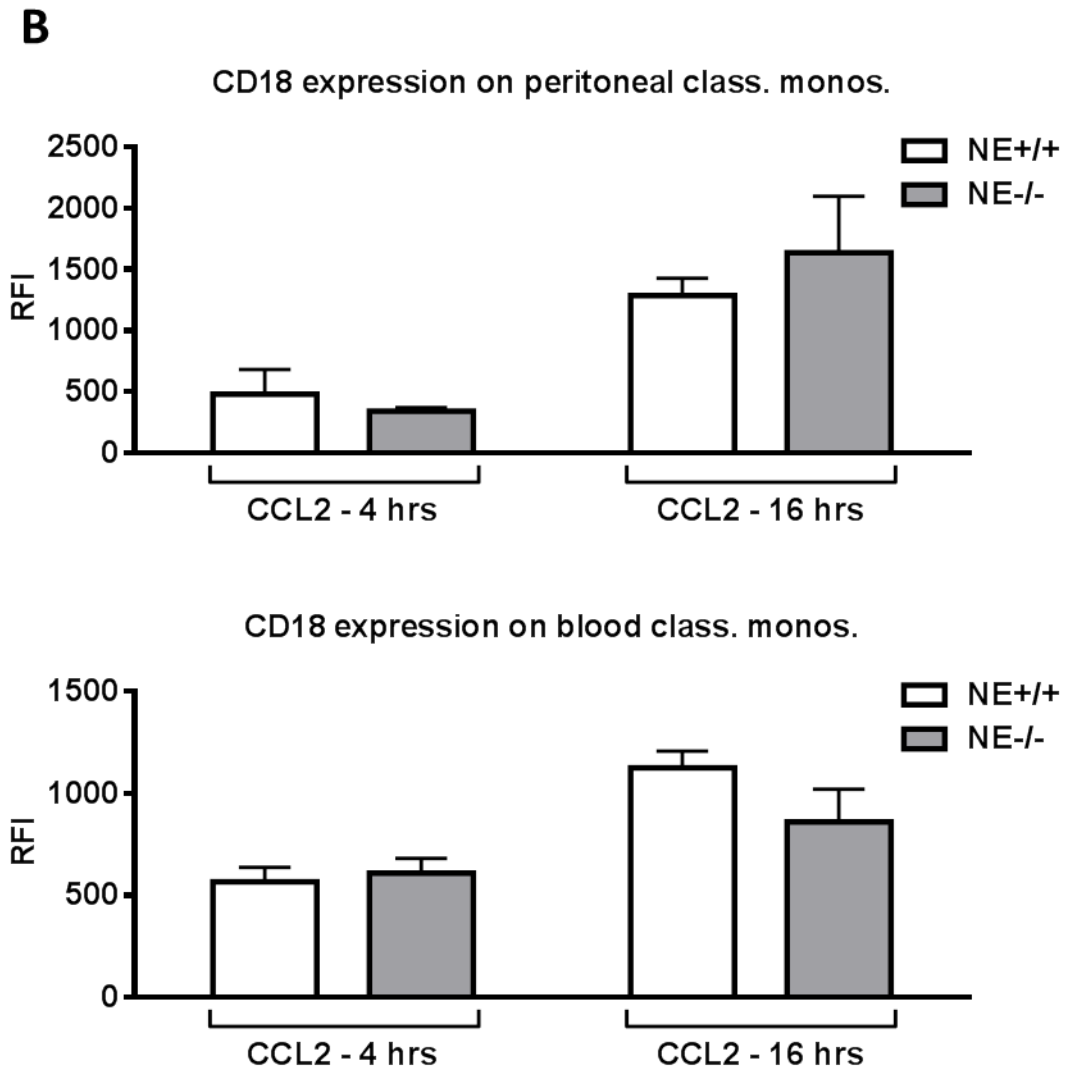


**Figure 5.3: Characterisation of CD62L and CD18 expression on classical monocytes following CCL2-induced peritonitis.** $NE^{+/+}$ and $NE^{-/-}$ $CX_3CR1^{+/eGFP}$ mice were stimulated i.p. with CCL2 (500 ng/ml) for 4 or 16 hours, after which total leukocytes were harvested from the blood and peritoneal cavity and subjected to ACK-lysis. Relative surface expression levels of L-selectin (A) and CD18 (B) were subsequently assessed on classical monocytes by flow cytometry. Data are represented as the mean ± SEM (n = 3-4 mice, one FACS reading per mouse).

### *c) $NE^{-/-}$ mice exhibit a defect in TEM in a tissue-dependent manner.*

As a means of exploring the involvement of NE in monocyte migration in greater detail, immunofluorescent labelling and confocal microscopy were subsequently employed to study monocyte infiltration in the mouse cremaster muscle. This approach enables monocyte extravasation to be directly visualised and its underlying mechanisms characterised, including how and where the monocytes interact with the vasculature. In

line with the previous peritonitis data, we initially stimulated the cremaster muscles of $NE^{-/-}$ and $NE^{+/+}$ mice with CCL2 for 16 hours, after which the tissues were collected, fixed, immunostained and imaged. At this time point however almost no eGFP+ monocytes could be seen either within the vasculature or interstitial space (data not shown). Presuming the inflammatory response had already resolved, a shorter time point of 4 hours was next explored. Indeed, monocytes were abundantly present in both $NE^{-/-}$ and $NE^{+/+}$ tissues and could be seen migrating predominantly through medium-sized post-capillary venules (20-50 μm in diameter). In contrast, and akin to CCL2-induced peritonitis, neutrophils were not actively recruited.

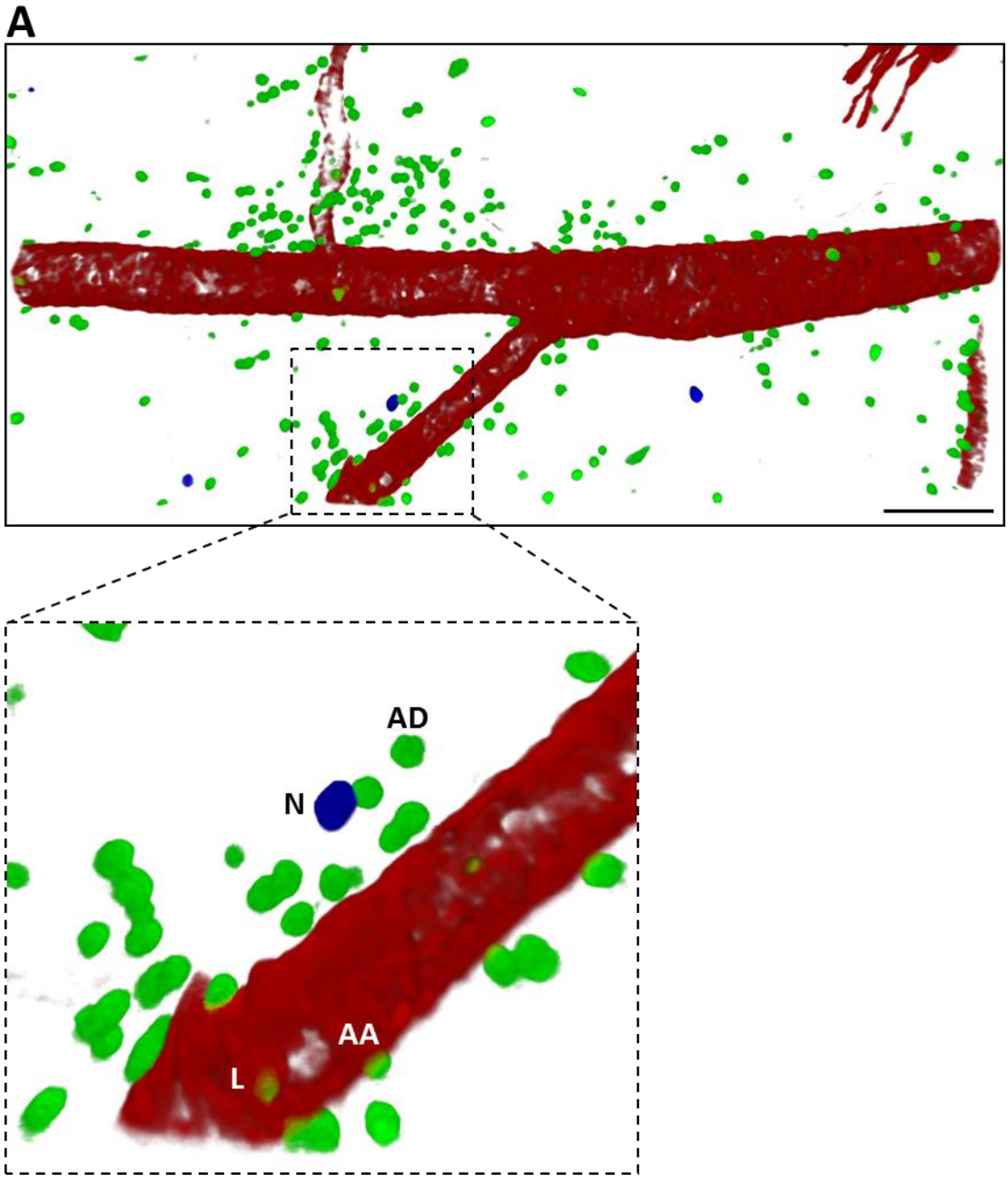

**B**

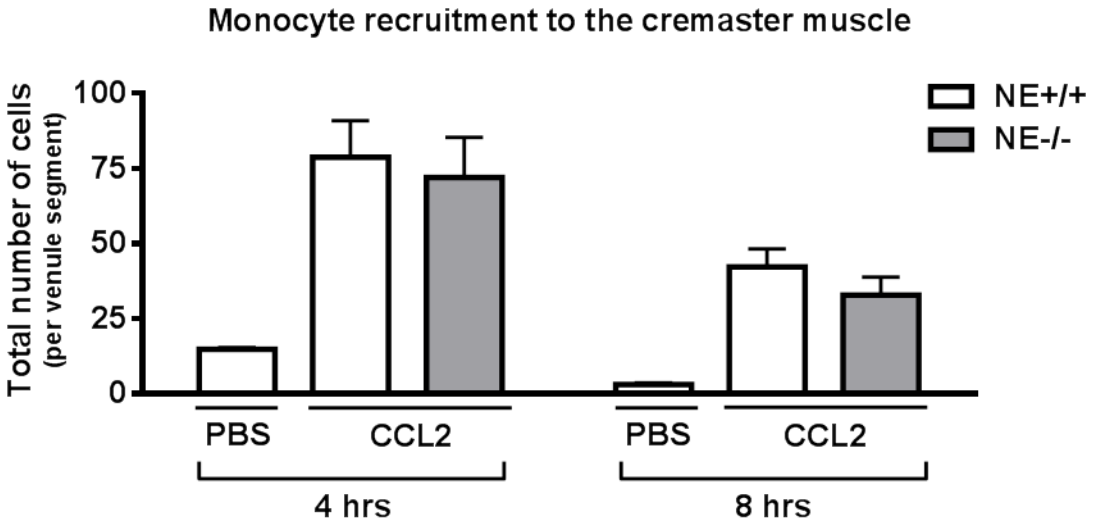
Monocyte recruitment to the cremaster muscle
Total number of cells
(per venule segment)
100
75
50
25
0
NE+/+
NE-/-
PBS
CCL2
PBS
CCL2
4 hrs
8 hrs

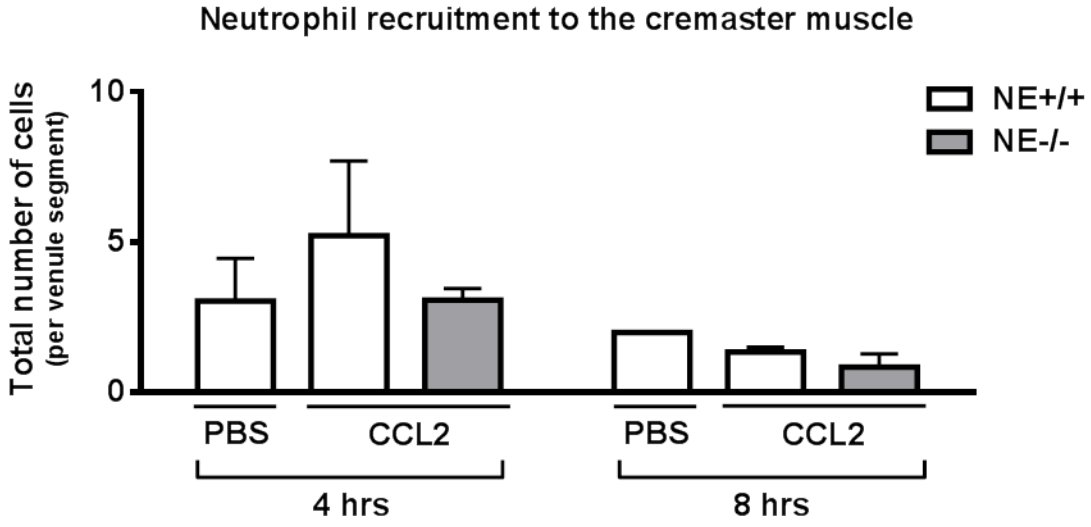
Neutrophil recruitment to the cremaster muscle
Total number of cells
(per venule segment)
10
5
0
NE+/+
NE-/-
PBS
CCL2
PBS
CCL2
4 hrs
8 hrs

**C**

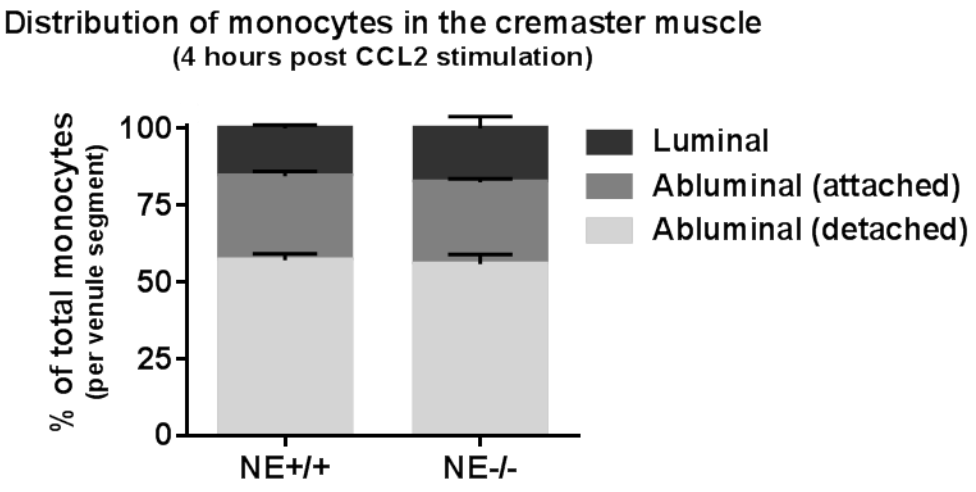
Distribution of monocytes in the cremaster muscle
(4 hours post CCL2 stimulation)
% of total monocytes
(per venule segment)
100
75
50
25
0
Luminal
Abluminal (attached)
Abluminal (detached)
NE+/+
NE-/-

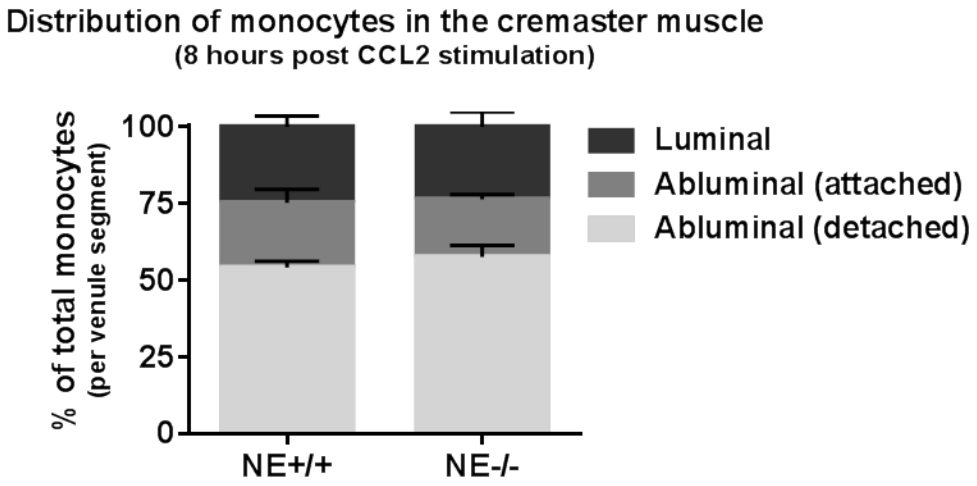


**Figure 5.4: Characterisation of CCL2-induced monocyte transmigration in the cremaster muscle.** $NE^{+/+}$ and $NE^{-/-}$ $CX_3CR1^{+/eGFP}$ mice were stimulated i.s. with CCL2 (500 ng) for 4 or 8 hours, after which the cremaster muscles were harvested, fixed in PFA and immunostained for α-SMA (red) and MRP-14 (neutrophils (N), blue). Segments of post-capillary venules were subsequently analysed by confocal microscopy and reconstructed into virtual 3D models using Imaris software (A). Total monocytes (shown in green) were counted for each venule (B) and categorised as residing within the lumen of the vessel (L) or in the abluminal space, either attached to (AA) or detached from (AD) the venular wall (C). Data are represented as the mean ± SEM (n = 2-6 mice, average of 5-6 venules per cremaster). Scale bar, 80 µm.

To generally characterise monocyte infiltration into the cremaster muscle, 5-6 distinct sections of post-capillary venules were imaged per collected tissue. Individual monocytes were subsequently counted and categorised as residing within the lumen of the vessel (luminal), attached to the outer periphery of the vessel wall (abluminal-attached), or residing in the interstitial space surrounding the vessel (abluminal-detached) (*Figure 5.4A*). After 4 hours of CCL2 stimulation, no differences were observed regarding the total numbers of monocytes or their localisation in the cremaster muscles of $NE^{-/-}$ and $NE^{+/+}$ mice. This is in correlation with the peritonitis data which also showed no significant differences at 4 hours. To investigate a later time point, the cremasters were stimulated with CCL2 for 8 hours. This too did not yield a reduced or altered monocyte response in $NE^{-/-}$ mice (*Figure 5.4B-C*). The total monocyte response was however generally reduced compared to that at 4 hours and, considering the negligible response at 16 hours, suggests CCL2-stimulated monocytes are recruited to the cremaster in one early wave after which the response begins to resolve.

As genetic compensation has been previously reported in the cremaster muscle of $NE^{-/-}$ mice, we next determined whether monocyte migration was defective in NE WT mice

treated with an NE inhibitor. GW311616A is a potent and specific intracellular NE inhibitor that is orally administered to mice and provides long-term inhibition of NE activity by covalently binding to the enzyme (Macdonald et al., 2001). This inhibitor has been previously used by our group to inhibit NE-mediated lung damage (data not published). Consistent with this study, we administered NE WT mice with the inhibitor or a vehicle control 24 hours prior to stimulating the cremaster with CCL2 for 4 hours, as before. Upon analysis, no distinct phenotype was noted for the NE-inhibited mice (*Figure 5.5*). Taken together with the data collected using the $NE^{-/-}$ mice, it appears NE is not required for the migration of monocytes through CCL2-stimulated cremasteric venules.

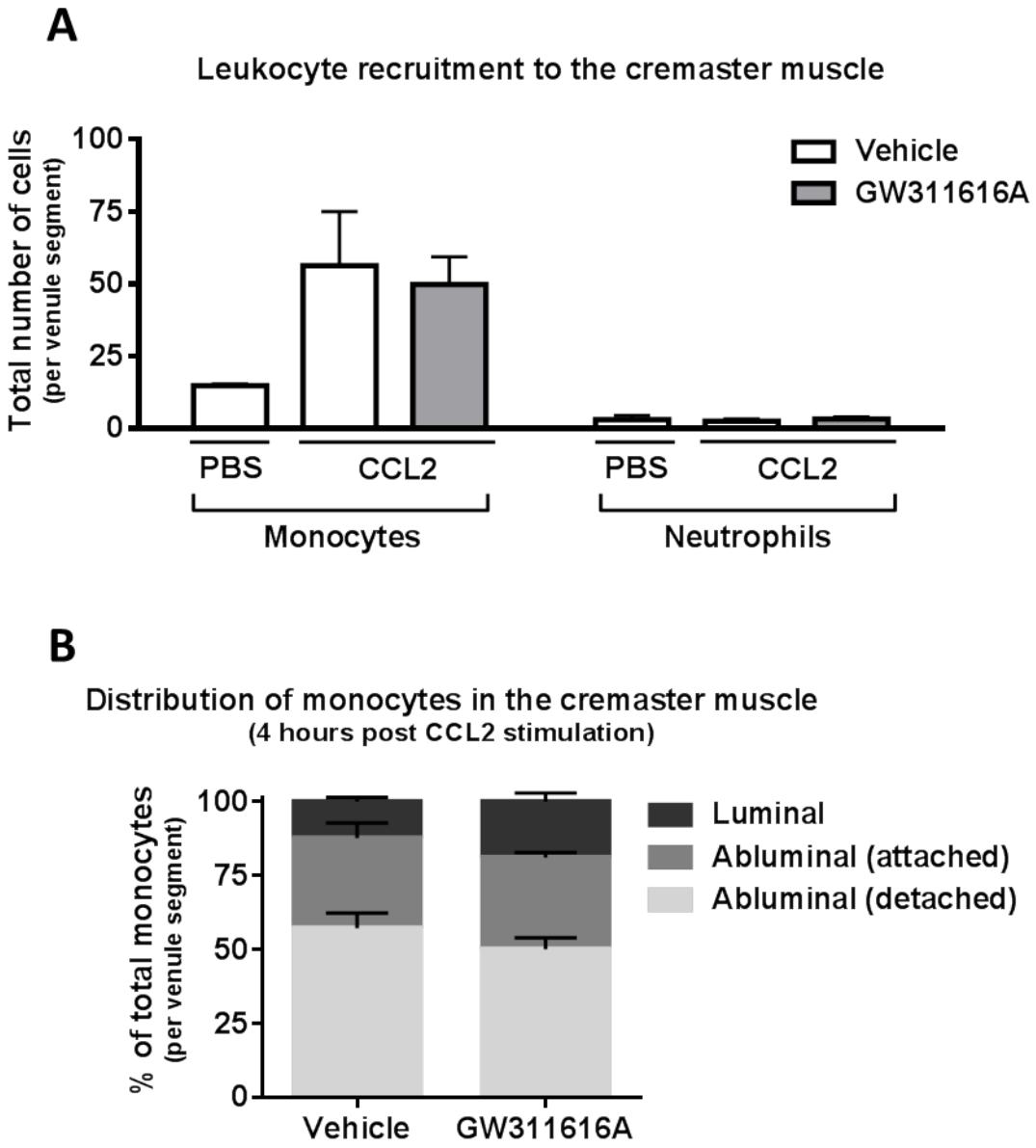

**Figure 5.5: NE blockade does not influence CCL2-induced monocyte transmigration in the cremaster muscle.** $NE^{+/+}$ $CX_3CR1^{+/eGFP}$ mice were orally administered the NE-inhibitor GW311616A (2 mg/kg) or vehicle ($H_2O$) 24 hours prior to undergoing i.s. stimulation with CCL2 (500 ng) for 4 hours. The cremaster muscles were subsequently harvested, fixed, immunostained, and analysed by confocal microscopy. Total numbers of recruited monocytes (A) and their localisation within the tissue (B) were directly compared between the two groups. Data are represented as the mean ± SEM (n = 2-3 mice, average of 5-6 venules per cremaster).

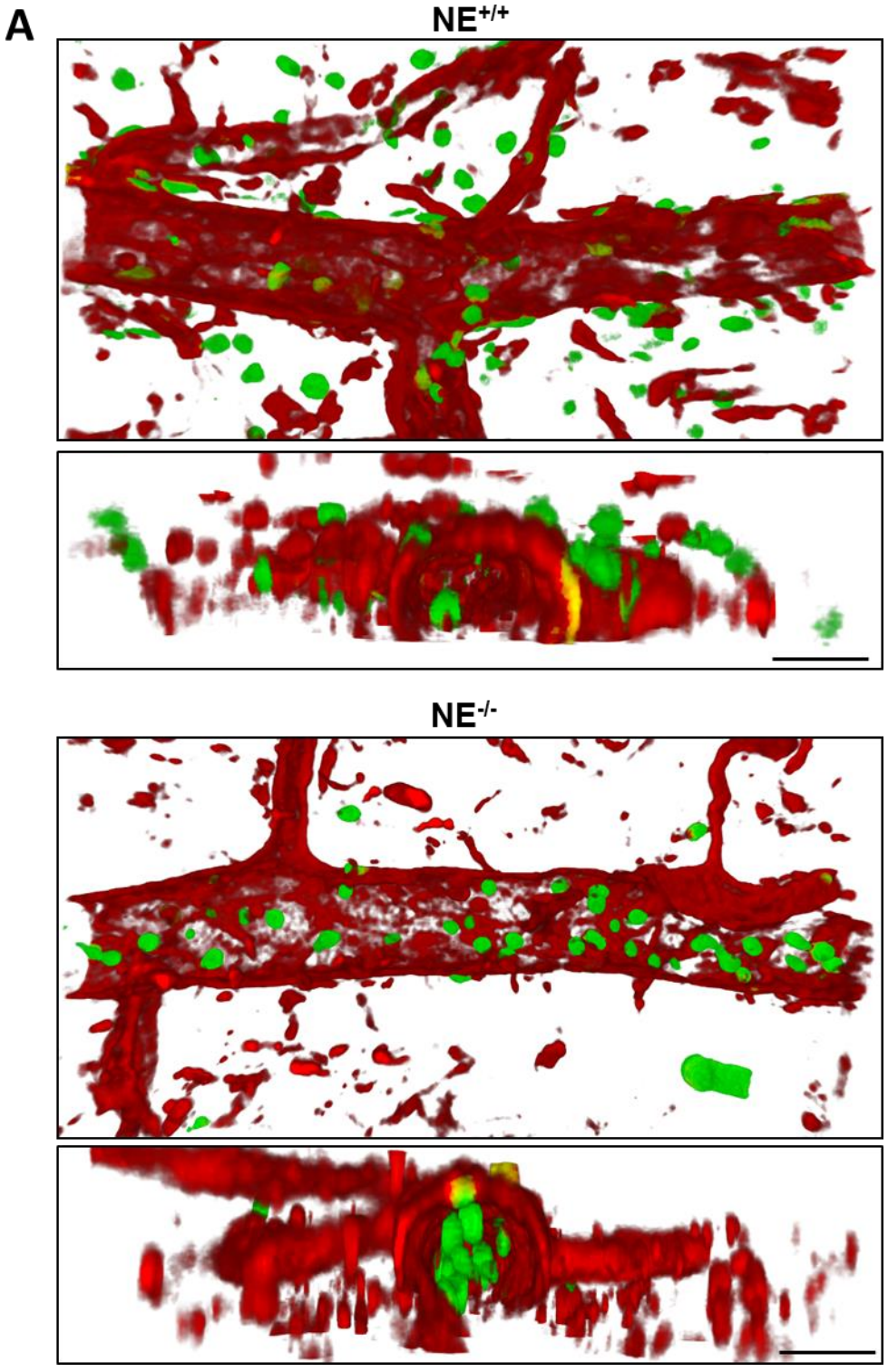

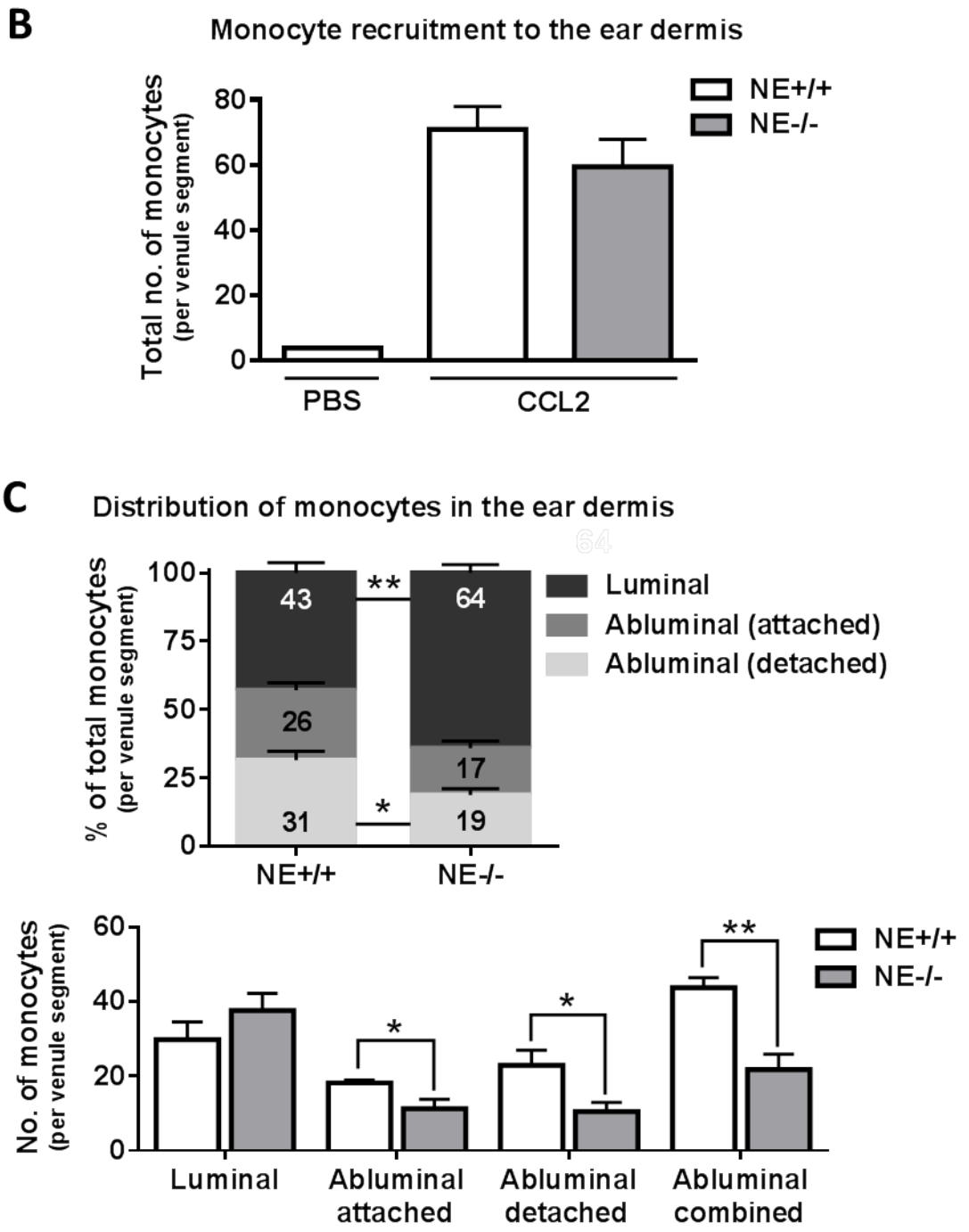


**Figure 5.6: Characterisation of CCL2-induced monocyte transmigration in the ear dermis.** $NE^{+/+}$ and $NE^{-/-}$ $CX_3CR1^{+/eGFP}$ mice were stimulated i.d. with CCL2 (1 µg, supplemented with Alexa Fluor 555–labelled mAb to PECAM-1) for 4 hours, after which the whole ears were harvested, the dorsal skin carefully separated and fixed in PFA. Segments of post-capillary venules were subsequently analysed by confocal microscopy and reconstructed into virtual 3D models using Imaris software (A). Total monocytes (shown in green) were counted for each venule (B) and categorised as residing within the lumen of the vessel or in the abluminal space, either attached to or detached from the venular wall (C). Data are represented as the mean ± SEM (n = 3-5 mice, average of 5-6 venules per ear). Scale bar, 40 µm. Statistically significant differences between NE WT and KO data are indicated by asterisks (*, $p < 0.05$, **, $p < 0.01$, Student's T-test).

Considering the inconsistent findings relating to the role of NE in the transmigration of neutrophils, specifically regarding its alleged tissue specificity, we next decided to assess monocyte TEM in $NE^{-/-}$ and $NE^{+/+}$ mice using a separate model of inflammation in the ear. CCL2 again was used as an inflammatory stimulus for 4 hours, the time-point at which we observed the greatest influx of monocytes (*Appendix 5.2*). As a means of limiting the accelerated photobleaching of eGFP observed in monocytes in the ear, a fluorescently-conjugated anti-PECAM-1 antibody was injected concurrently with the stimulus, staining the vascular endothelium *in vivo*. This enabled the ears to be immediately fixed and analysed by confocal microscopy upon harvesting. Importantly this clone of antibody does not affect leukocyte dynamics during TEM (Woodfin et al., 2011). As in the cremaster muscle, monocytes were recruited to post-capillary venules in the ear dermis to a similar extent in $NE^{-/-}$ and $NE^{+/+}$ mice (*Figure 5.6*). In contrast to before however, there was a clear difference in the localisation of monocytes within the inflamed ear, with $NE^{-/-}$ mice exhibiting significantly fewer abluminal monocytes, both attached to the outer venular wall and residing freely in the interstitial space. Instead, the majority of monocytes in these mice were confined to the venular lumen. These cells were largely spherical in morphology and appeared to have adhered to but not spread on the endothelium. Taken together, in the absence of NE it would appear that monocytes exhibit an early-stage defect in TEM through CCL2-stimulated post-capillary venules in the ear.

***d) Monocytes release NE during the early steps of TEM in vivo.***

To further understand the involvement of NE in monocyte TEM, we attempted to assay for NE activity *in vivo* using Neutrophil Elastase 680 FAST™. Comprising two fluorochromes adjoined by an NE-selective protein sequence, NE 680 FAST is optically silent in its native state but generates an intense fluorescent signal upon cleavage by NE. Assuming the catalytic activity of NE is a decisive factor, this approach should provide an indication of how NE mediates monocyte TEM, including the type and location of cells in which NE is most active. Prior to employing NE 680 FAST in this manner *in vivo*, we initially sought to verify its ability to be activated intracellularly and in an NE-specific fashion *in vitro*. This was achieved by seeding whole blood leukocytes from $NE^{-/-}$ and $NE^{+/+}$ mice onto cover slips. $CX_3CR1^{+/eGFP}$ mice were used in order to identify monocytes. The cells were subsequently fixed in PFA (half were also permeabilised

with Triton X-100) and incubated with NE 680 FAST. Upon confocal analysis, NE activity was detected irrespective of permeabilisation, though, regrettably, also irrespective of NE expression. Indeed, $NE^{-/-}$ blood leukocytes, including monocytes, produced an NE signal of equal intensity compared to WT controls (*Figure 5.7*). Recognising NE 680 FAST is designed to be used primarily *in vivo*, we next assessed its specificity in both an ear and cremaster model of inflammation. $NE^{-/-}$ and $NE^{+/+}$ mice were administered NE 680 FAST intravenously prior to inducing inflammation with either CCL2 or $LTB_4$, a potent stimulator of neutrophil chemotaxis and NE degranulation. The tissues were harvested after 4 hours, fixed in PFA and analysed by confocal microscopy. As before however, NE activity could be observed for $NE^{+/+}$ and $NE^{-/-}$ mice alike, both in the cremaster muscle and ear, and in response to CCL2 and $LTB_4$ (*Figure 5.8* and *Appendix 5.3*). This activity, while not NE-specific, did emanate from small, spherical cell-like structures. Interestingly however these cells were not monocytes nor were they neutrophils as confirmed by analysing NE 680 FAST activity in LysM-eGFP-ki mice (*Appendix 5.4*).

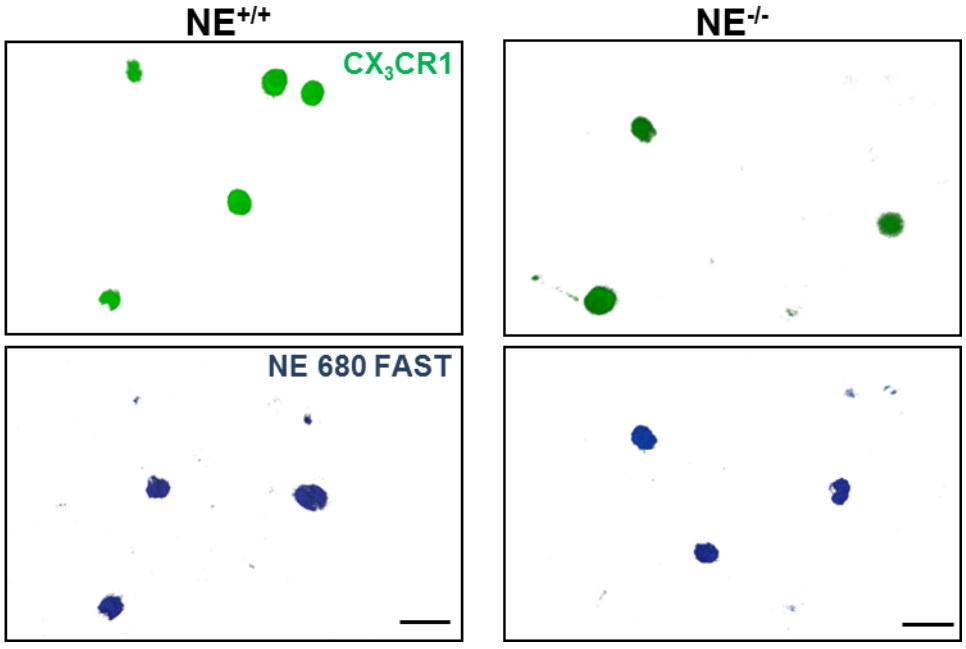


**Figure 5.7: Characterisation of NE 680 FAST activity *in vitro*.** Whole blood leukocytes harvested from $NE^{-/-}$ and $NE^{+/+}$ mice were ACK-lysed, seeded onto poly-L-lysine–coated cover slips and fixed in PFA. The cells were subsequently incubated in 250 µl PBS containing Neutrophil Elastase 680 FAST (1 µM) for 2 hours at 4°C. NE activity (blue) was determined by measuring the fluorescence intensity between 640-700 nm following excitation at 633 nm. Monocytes are shown in green. Scale bar, 15 µm.

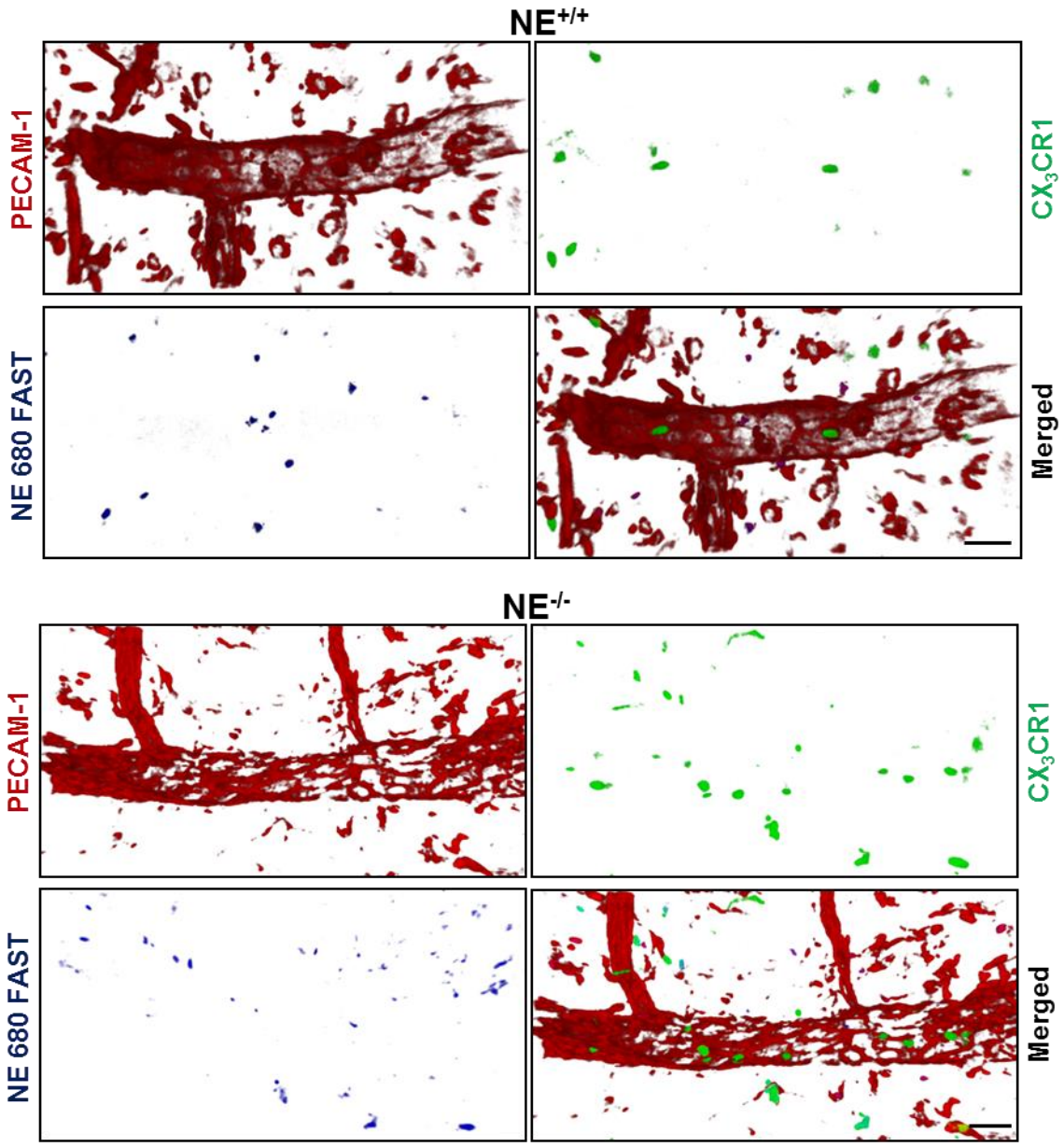


**Figure 5.8: Assaying for NE activity in $CX_3CR1$-eGFP-ki mice *in situ*.** $NE^{+/+}$ and $NE^{-/-}$ $CX_3CR1^{+/eGFP}$ mice were administered Neutrophil Elastase 680 FAST (4 nmols in 200 µl PBS) i.v. immediately prior to administering CCL2 (1 µg, supplemented with Alexa Fluor 555–labelled mAb to PECAM-1, red) i.d. for 4 hours. Whole ears were subsequently harvested, the dorsal skin carefully separated and fixed in PFA. Segments of post-capillary venules were analysed by confocal microscopy and reconstructed into virtual 3D models using Imaris software. NE activity (blue) was determined by measuring the fluorescence intensity between 640-700 nm following excitation at 633 nm. Monocytes are shown in green. Scale bar, 30 µm.

Rather than directly assaying for NE activity, as an indication of NE's involvement in monocyte TEM we next determined whether there was a depletion of intracellular NE stores in monocytes during inflammation. Though we were unable to stimulate NE release from monocytes *in vitro* in the previous chapter, in recognition of the relative

simplicity of these studies, we next endeavoured to measure NE release from monocytes undergoing extravasation *in situ* in the ear. This was achieved by immunostaining post-stimulated tissues for NE. As a means of optimising this process we initially stained for NE in $LTB_4$-stimulated ears of $NE^{+/+}$ and $NE^{-/-}$ mice. Using methanol as a joint fixative/permeabilising agent, we were unable to detect NE in WT neutrophils (data not shown). In contrast, and in reverse to staining for NE *in vitro*, the protein could be detected when using PFA as a fixative and Triton X-100 as a permeabilising agent. Indeed, intracellular NE was observed in $NE^{+/+}$ neutrophils only, located both within the vasculature and in the interstitial space, corroborating previous reports that only a small fraction of NE is freely released by neutrophils during TEM (*Figure 5.9*) (Owen et al., 1995). In contrast, the infiltrating monocytes were not strongly labelled for NE. Intrigued by this observation, we were keen to next evaluate NE expression in monocytes in response to CCL2. As an internal positive control we stained once more for neutrophils, which, while unresponsive to CCL2, are generally observed in small numbers in the lumen of post-capillary venules upon i.d. injection. As seen with $LTB_4$, upon CCL2 stimulation the majority of monocytes were depleted of their NE stores. This was seen not only for transmigrated monocytes in the interstitial space but for monocytes residing within the lumen of post-capillary venules (*Figure 5.10*). These findings are in accordance with the observed accumulation of luminal monocytes in the ears of $NE^{-/-}$ mice and strongly suggest NE is released and functionally required by monocytes early on during TEM.

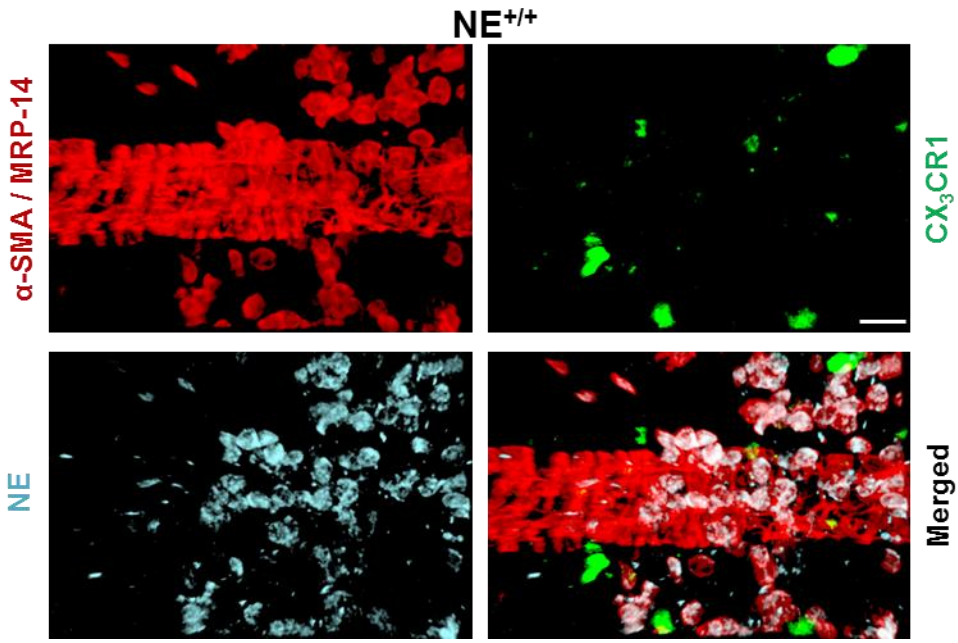

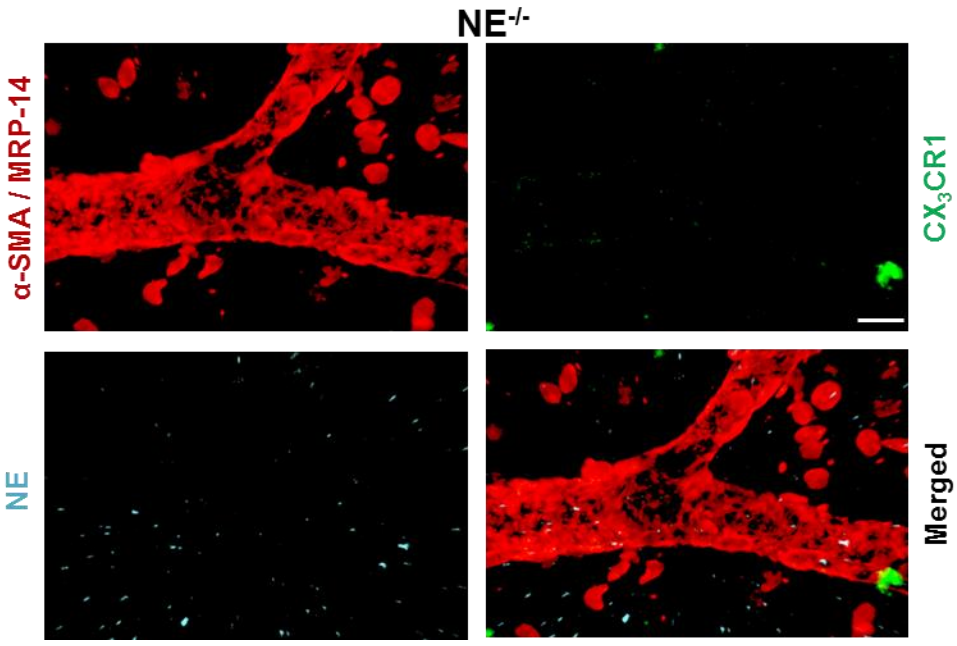


**Figure 5.9: Assaying for NE expression in $CX_3CR1$-eGFP-ki mice *in situ*.** Ears of $NE^{+/+}$ and $NE^{-/-}$ $CX_3CR1^{+/eGFP}$ mice were stimulated with $LTB_4$ (300 ng) i.d. for 4 hours. Whole ears were subsequently harvested, the dorsal skin carefully separated and fixed in PFA and immunolabelled for NE (blue), α-SMA (vasculature, red) and MRP-14 (neutrophils, red). Monocytes are shown in green. Segments of post-capillary venules were analysed by confocal microscopy and reconstructed into virtual 3D models using Imaris software. Scale bar, 20 µm.

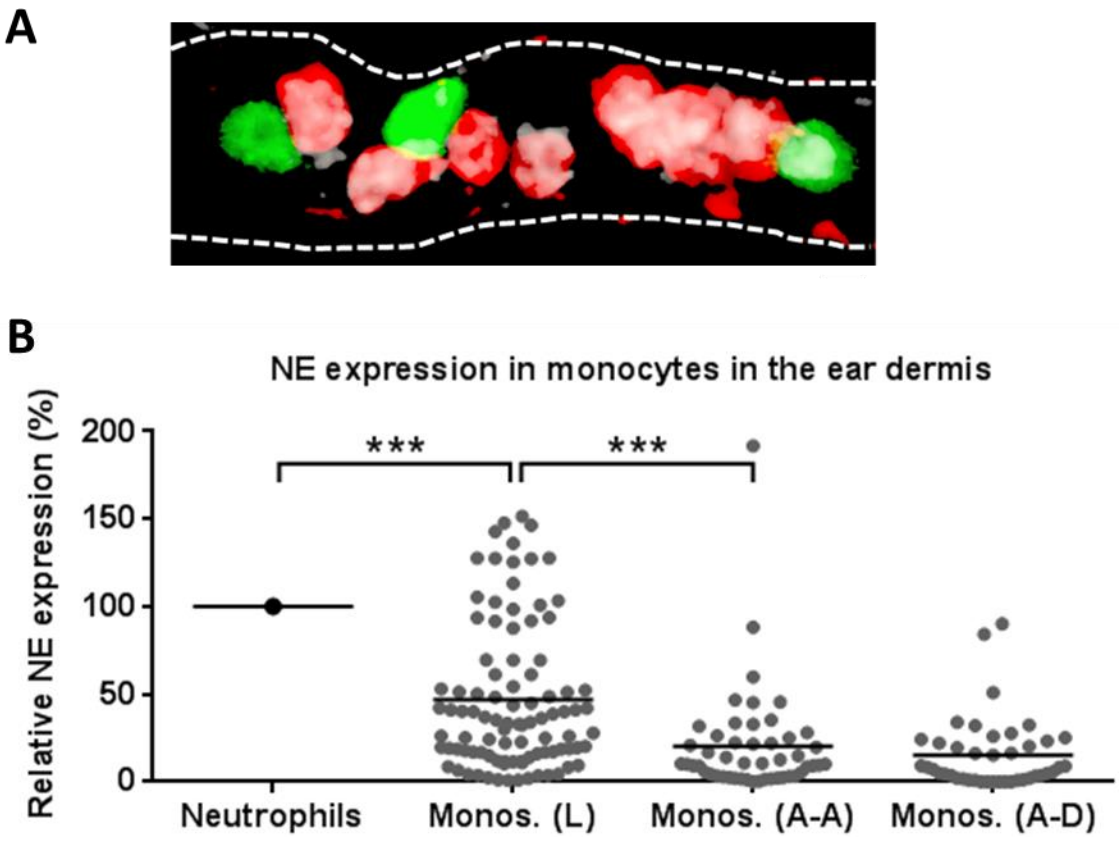

**Figure 5.10: Characterisation of NE expression during CCL2-induced monocyte transmigration in the ear dermis.** Ears of $NE^{+/+}$ $CX_3CR1^{+/eGFP}$ mice were stimulated with CCL2 (1 µg, supplemented with Alexa Fluor 555–labelled mAb to PECAM-1, dashed line) i.d. for 4 hours. Whole ears were subsequently harvested, the dorsal skin carefully separated and fixed in PFA and immunolabelled for NE (blue) and MRP-14 (neutrophils, red). Segments of post-capillary venules were analysed by confocal microscopy and reconstructed into virtual 3D models using Imaris software (A). NE expression was quantified in monocytes (green) residing within the vessel lumen (L) or in the abluminal space, either attached to (AA) or detached from (AD) the venular wall, as measured relative to the average intensity of NE expression in luminal neutrophils (set to 100%) (B). Data are pooled from 3 separate mice. Statistically significant differences are indicated by asterisks (***, $p < 0.0001$, Student's T-test). Scale bar, 5 µm.

***e) Inhibiting NE abates the transmigration of human U937 monocytes in vitro.***

Recognising that all of the preceding experiments have been conducted on constitutive KO mice for NE, to confirm monocyte TEM is mediated specifically by their own NE stores, we sought to establish an *in vitro* Transwell migration assay using pure populations of monocytes (*Figure 5.11A*). Specifically, we wanted to compare the ability of MACS-sorted $NE^{+/+}$ and $NE^{-/-}$ splenic monocytes to migrate across a confluent layer of murine skin endothelial cells (sENDs), purposely selected to more closely resemble the vasculature in the ear dermis. To optimise this assay, we initially characterised the transmigration of whole blood leukocytes towards foetal bovine serum (FBS), a rich and varied source of chemoattractants. Using this approach, after 4 hours, significant numbers of leukocytes could be seen traversing uncoated Transwell inserts with an 8 µm, but not a 3 µm, pore size. After growing a layer of sENDs on top of the membrane, transmigration was predictably delayed with significant numbers of cells accumulating at the bottom of the chamber after 16 hours (data not shown). This being established, we repeated the assay using MACS-sorted splenic classical monocytes. Considering the low number of cells yielded by this process, several spleen samples were pooled together. In keeping with our *in vivo* data, $NE^{-/-}$ monocytes demonstrated a trend towards reduced migration compared to WT controls (*Figure 5.11B*).

Though ideally wanting to replicate the Transwell assay using CCL2, as used throughout this study, the necessary expenditure with regards to both mice and reagents would have been too great. To circumvent this issue we decided to develop the Transwell assay not with primary cells but with a model cell line. Specifically, we employed the human monocyte-like U937 cell line, which is known to express NE (*Appendix 5.5*) and has been routinely studied to explore its biological properties *in*

*vitro*. For conformity, we also swapped the murine sENDs with human umbilical vein endothelial cells (HUVECs). No longer able to exploit the NE KO mice, in order to investigate the role of NE in monocyte migration we made use of the NE-specific inhibitor ONO-5046. U937 cells were pre-treated with ONO-5046 or a vehicle control before being added on top of a confluent layer of TNF-α–activated HUVECs. Using CCL2 as a chemoattractant, we observed a significant reduction in the number of infiltrating monocytes after 4 hours when NE was inhibited (*Figure 5.11C*). This strongly suggests that monocytes utilise their own NE stores during TEM.

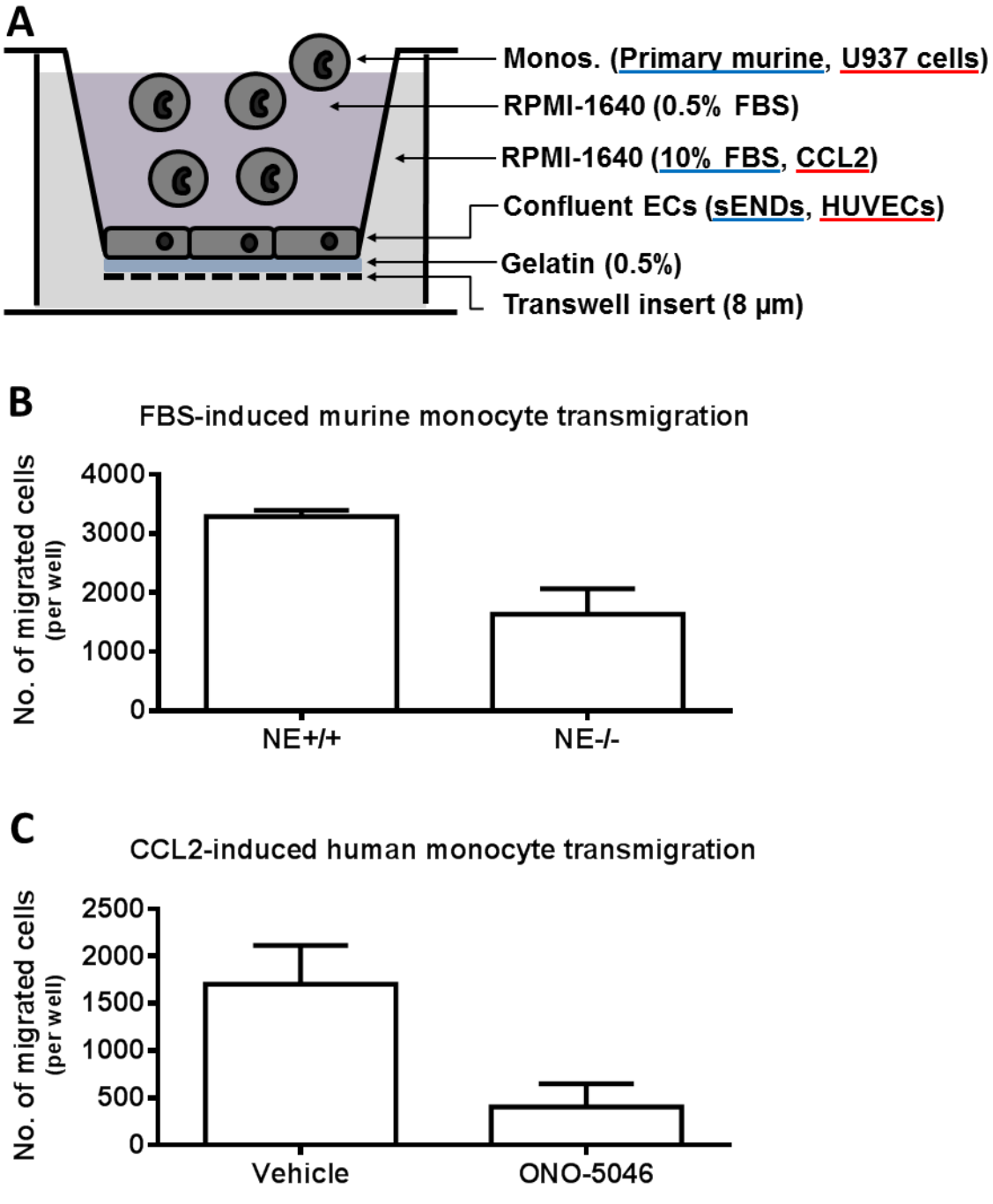

**Figure 5.11: Transwell cell migration assay.** Monocyte migration was assessed *in vitro* in 24-well plates through an endothelial cell monolayer (A). The migratory potential of $1.5\times10^5$ $NE^{+/+}$ and $NE^{-/-}$ MACS-sorted splenic monocytes through murine skin endothelial cells (sENDs) was initially compared after 16 hours in response to 10% FBS (B, blue). We subsequently compared the migratory potential of $5\times10^5$ human U937 cells pre-treated either with the NE-inhibitor ONO-5046 (50 µM) or vehicle (PBS) through human umbilical vein endothelial cells (HUVECs) after 4 hours in response to human CCL2 (10 nM) (C, red). The total number of migrated cells per well was calculated as the sum of cells counted in the lower Transwell chamber in three random fields of view (at ×4 zoom). Data are represented as the mean ± SEM (n = 1-3 mice, averaged across triplicate wells).

### *5.3 Discussion*

Having established in the previous chapter that murine monocytes express neutrophil elastase, we were keen to next describe its functional relevance. In this regard, we were specifically interested in exploring a potential role for NE in monocyte transmigration. NE has already been strongly implicated in neutrophil trafficking and while murine NE has been proposed to support pulmonary monocyte recruitment during emphysema these findings have not since been corroborated or expanded upon (Shapiro et al., 2003). In this chapter we endeavoured to comprehensively evaluate NE's involvement in monocyte migration *in vivo* by stimulating, quantifying, and directly visualising monocyte recruitment in NE deficient and WT mice.

A relatively simple model of inflammation, we initially characterised monocyte infiltration into the peritoneal cavity during peritonitis. The mice were originally stimulated with IFN-γ and TNF-α for a total of 20 hours, a reaction our group has previously used to elicit monocyte infiltration into the cremaster muscle. Indeed, the number of peritoneal monocytes significantly increased as compared to PBS controls in both $NE^{-/-}$ and $NE^{+/+}$ mice. Primarily classical monocytes were recruited, in keeping with their pro-inflammatory description. In addition, both genotypes displayed an even greater influx of neutrophils. Interestingly, while peritoneal monocytes were evenly represented, neutrophil recruitment was significantly reduced in $NE^{-/-}$ mice, which, though not unexpected, has not been previously demonstrated in response to IFN-γ and TNF-α. Under these same conditions, while NE might simply not be functionally required for infiltrating monocytes, it is also possible that any defects in monocyte recruitment in $NE^{-/-}$ mice are compensated for by the concurrent recruitment of neutrophils, albeit in an NE-independent manner and irrespective of their own reduced migration. Certainly, neutrophils are known to pave the way for classical monocytes during inflammation. The neutrophil secretion products azurocidin, LL-37, and cathepsin G for example directly promote monocyte extravasation by activating formyl peptide receptors. Moreover, neutrophil-derived cytokines promote monocyte-endothelial interactions by inducing endothelial expression of CCL2 and VCAM-1 (Soehnlein and Lindbom, 2010).

In this regard, though we could have employed neutrophil-depleting antibodies, in order to obtain a more specific model of monocyte infiltration we induced peritonitis with the

potent classical monocyte chemoattractant CCL2. While CCL2 has also been shown to mediate the migration of dendritic cells and T-lymphocytes, it does not typically attract neutrophils, as verified by our results. Using this approach, we observed a decreasing trend in the proportion and number of peritoneal classical monocytes in $NE^{-/-}$ mice at 4 hours compared to WT mice, which became significantly different by 16 hours. This reduction might be explained in several ways. It was evident in both genotypes that upon being recruited, the classical monocytes were not simply accumulating in the cavity as their total peritoneal numbers actually fell over the course of CCL2 stimulation. With this in mind, and considering the more marginal difference seen in monocyte levels at the earlier time point, it is possible that $NE^{-/-}$ monocytes undergo largely normal recruitment but are then 'lost' from the cavity at a greater rate compared to their WT equivalents. This was difficult to assess however as the mechanism by which this might occur is unclear. Highly plastic cells, it is possible that upon recruitment the monocytes quickly differentiated into macrophages. Indeed, in a model of thioglycollate-induced peritonitis, early recruited monocytes were shown to have differentiated into macrophage-like cells by 24 hours (Henderson et al., 2003). Such differentiation has been shown to be accompanied by a loss of GR-1 expression, which would explain why these cells no longer befit the $GR\text{-}1^{int}$, $CX_3CR1^{int}$ phenotype of bona fide classical monocytes (Martin et al., 2011). Though peritoneal macrophages also typically express low surface levels of $CX_3CR1$, in a previous study using $CX_3CR1$-eGFP-ki mice, monocyte-derived peritoneal macrophages were shown to retain high eGFP-fluorescence for several days (Jung et al., 2000). Taken together, freshly differentiated macrophages are likely to assume a phenotype akin to non-classical monocytes, however no obvious differences were observed in the proportion of these cells between $NE^{-/-}$ and $NE^{+/+}$ mice.

We also considered that the apparent depletion of monocytes from the peritoneum was attributable to the cells either undergoing cell death or rapidly draining from the cavity via the lymphatics. In recognition of the relatively low number of classical monocytes initially recruited to the cavity however, delineating the fate of these cells would have been extremely onerous. In this light, we focused instead on establishing whether the observed reduction in peritoneal monocytes in $NE^{-/-}$ mice in response to CCL2 was as result of a defect in monocyte recruitment. As a means of more directly investigating a potential role for NE during monocyte transendothelial migration, we employed

confocal microscopy to analyse infiltrating monocytes in the cremaster muscle. The high resolution afforded by this approach enables the interactions of monocytes and endothelial cells to be clearly visualised as the different stages of TEM are undertaken. To complement our peritonitis data, we used CCL2 as an inflammatory stimulus and compared monocyte emigration from cremasteric venules in $NE^{-/-}$ and WT mice after 4 and 16 hours. Supporting our previous results, no significant differences were seen in the number or vascular localisation of monocytes after 4 hours, with the majority of cells appearing to have successfully completed transendothelial migration. Interestingly, and in contrast to CCL2-induced peritonitis, inflammation in the cremaster muscle was seemingly already resolved by 16 hours as the tissues were almost entirely depleted of monocytes. Accordingly, a shorter time point of 8 hours was explored. Whilst monocytes were observed in the tissue, they were less plentiful than at 4 hours suggesting CCL2 recruits monocytes into the cremaster muscle in a single wave. Moreover, no differences were seen between $NE^{-/-}$ and WT mice at this time point.

It is conceivable that this lack of phenotype in $NE^{-/-}$ mice is attributed to genetic compensation, a phenomenon that has been previously described in the cremaster muscles of these mice with regards to neutrophil infiltration (Young et al., 2007). To explore this possibility we disrupted NE activity pharmacologically, rather than genetically, by administering an NE inhibitor 24 hours prior to CCL2 stimulation, however this too did not yield any differences in monocyte recruitment when compared to vehicle-treated controls. It should be noted however that in the aforementioned study NE activity was blocked by continuous intravenous infusion of the NE-inhibitor ONO-5046. Our study instead employed the distinct NE-inhibitor GW311616A, which, owing to its greater efficacy and longer half-life *in vivo*, reportedly only requires a single orally administered bolus to rapidly inhibit circulating NE activity by more than 90% and for up to 4 days (Macdonald et al., 2001). Certainly, using this approach our group has been successful in blocking NE-mediated tissue damage in the lung (data unpublished). In this light, and considering the apparent normal phenotype of $NE^{-/-}$ mice, it appears NE is not functionally required for the migration of monocytes through CCL2-stimulated cremasteric venules *in vivo*.

While the basic principles of the leukocyte adhesion cascade are thought to be largely conserved during inflammation, it is emerging that important variations exist with regards to the specific mechanisms that govern this process both in different tissues and

in response to different inflammatory stimuli. For example, it was found that mice deficient for intercellular adhesion molecule (ICAM)-2 demonstrate a defect in neutrophil recruitment to the peritoneal cavity in response to IL-1β but not TNF-α or thioglycollate (Huang et al., 2006). This same study also reports that blocking ICAM-2 in PECAM-1-deficient mice inhibits IL-1β induced neutrophil migration in the peritonitis model, but not in the cremaster muscle. Discrepancies in leukocyte transmigration into the peritoneum and cremaster muscle have been similarly observed elsewhere, for example in mice deficient for leukocyte-specific protein 1, which, while demonstrating a profound inhibition in IL-1β-induced leukocyte transmigration in the cremaster muscle actually accumulated an increased number of leukocytes in the peritoneal cavity (Liu et al., 2005).

Tissue-specificity could also be a decisive factor in this study with NE seemingly mediating monocyte migration to the peritoneum but not the cremaster muscle. As a result, we decided to continue investigating a role for NE in monocyte TEM using a separate model of inflammation in the ear dermis. Using CCL2 once more as a monocyte chemoattractant, after 4 hours we observed a significant reduction in the number of transmigrated monocytes in $NE^{-/-}$ mice. The overall number of infiltrating monocytes was however only marginally lower compared to $NE^{+/+}$ mice, accounted for by the accumulation of $NE^{-/-}$ monocytes inside the lumen of post-capillary venules. This suggests $NE^{-/-}$ monocytes exhibit normal chemotactic potential but are compromised, not in their ability to arrest on the endothelium, but in their ability to commit to transendothelial migration. In support of this, in immunostaining for NE in WT ears, almost all infiltrating monocytes, including those situated within the endothelial lining, were shown to be depleted of their intracellular NE stores. Taken together, we hypothesise that during inflammation in the ear NE is released by luminal monocytes and is functionally required to initiate monocyte TEM.

Collectively, our results implicate NE in the migration of monocytes in response to CCL2 in the peritoneum and ear but not the cremaster muscle. These discrepancies, in addition to highlighting the great diversity in leukocyte recruitment, may also provide an indication of the mechanism by which NE mediates monocyte transmigration. Ultimately the peritoneum, ear and cremaster represent three separate vascular beds with potentially characteristic protein expression patterns, signalling pathways and structural organization, which could for example respond uniquely to the inciting

injection of exogenous CCL2 or interact differently with NE and/or monocytes. Post-capillary venules in the ear for example display a larger number of gaps between adjacent subendothelial pericytes and within the basement membrane compared to those in the cremaster muscle (Voisin et al., 2010). The nature of these gaps has already been shown to regulate the extravasation of neutrophils and could potentially also influence the migration of monocytes (Wang et al., 2012). Endothelial cells too display a marked heterogeneity across different tissues with regards to their structure, protein expression, surface phenotype and secreted molecules. Furthermore, the properties of ECs are known to frequently change during inflammation, with individual steps of the same leukocyte adhesion cascade affiliated with changes in endothelial adhesion molecules and chemokines (Aird, 2012). In this regard, chemokine secretion has been stipulated to more extensively contribute to the tissue-specific patterns of leukocyte trafficking as variations in chemokine secretion are more pronounced between different endothelia than adhesion molecules (Hillyer et al., 2003).

Though we cannot be sure that monocyte TEM is governed in the same manner in the peritoneum and ear, a major difference between these two mouse models and the cremaster muscle is the prevalence of resident tissue macrophages. Whilst these cells are sparsely represented in the cremaster muscle, they constitute approximately 70% of all dermal leukocytes in the ears and 30% of all leukocytes in the peritoneal cavities of naïve mice (Dupasquier et al., 2004), (Scotland et al., 2011). Macrophages are sentinel immune cells that release inflammatory mediators in response to exogenous insults. This can lead to dramatic changes in the tissue microenvironment both directly and by shifting the expression of EC adhesion/stimulatory molecules (Zhang et al., 2011). This in turn may influence local leukocyte infiltration. In reference to our study, considering CCL2-induced monocyte migration was not significantly inhibited in the peritoneum of $NE^{-/-}$ mice at 4 hours and was seemingly unaffected altogether in the cremaster muscle, one could postulate that monocytes undergo recruitment in two distinct phases: an initial NE-independent phase and a secondary NE- and macrophage-dependent phase. In this manner, we initially hypothesised that early recruited monocytes released their NE stores, paving the way for subsequent monocyte recruitment by stimulating resident macrophages to release their own endogenous mediators. Indeed, NE has been previously shown to enhance macrophage production of various mediators *in vitro* including CCL2 (Ishihara et al., 1999). Furthermore, $NE^{-/-}$ macrophages are reputedly

impaired in their ability to generate inflammatory mediators in response to *Pseudomonas aeruginosa* infection of the lungs (Benabid et al., 2012). Injecting recombinant NE into the peritoneal cavities of naïve mice was not however sufficient to induce monocyte recruitment. The complete absence of peritoneal monocytes in this model cannot be ignored however, as these cells may be of key influence, for example by presenting NE to the macrophages or by releasing their own mediators.

Alternatively, NE may exert an effect on macrophages in an altogether different manner. Intriguingly, our peritonitis data identifies significantly fewer resident macrophages in $NE^{-/-}$ mice 4 hours, but not 16 hours after CCL2 stimulation when compared to WT mice. Such transient changes in macrophage numbers are likely to be attributed to the macrophage disappearance reaction (MDR). This occurs in response to several inflammatory stimuli, including IFN-γ/TNF-α and CCL2 as demonstrated by our own data, and is characterised by the inability to recover total macrophages from the peritoneal cavity by lavage (Barth et al., 1995). Contributing to this phenomenon is the observed increase in macrophage adhesion to the surrounding parietal peritoneum and to each other, resulting in the formation of macrophage aggregates. The reappearance of these cells in the cavity, as seen in $NE^{-/-}$ mice at 16 hours, presumably involves the breakdown of such aggregates. If the MDR is more pronounced in $NE^{-/-}$ mice, as suggested by our data, following 4 hours CCL2 stimulation, this could contribute to the observed reduction in classical monocytes in these mice at 16 hours. When aggregated, peritoneal macrophages may have a reduced capacity to become activated or secrete cytokines, potentially affecting subsequent monocyte recruitment.

Whether related to or distinct from a change in endogenous mediator generation, $NE^{-/-}$ monocytes, certainly in the ear, appear to have a reduced capacity for transendothelial migration and instead appear to accumulate inside the endothelial lining of post-capillary venules. These cells are spherical in morphology and are not seen to be extending invasive protrusions into the endothelium, an initiating step in monocyte TEM, suggesting NE exerts its function earlier on during the leukocyte adhesion cascade. Indeed, a similar phenotype has been reported for neutrophils recruited to cremasteric venules in ICAM-2 deficient mice, as attributed to a defect in post-adhesion endothelial crawling (Halai et al., 2014). Likewise, neutrophils deficient for the adhesive protein JAM-A tended to remain associated with the endothelium upon cardiac ischemia reperfusion rather than completing TEM (Corada et al., 2005). These cells

were shown to adhere more efficiently to ECs than WT neutrophils and also exhibited a defect in cell polarization, thereby limiting their motility and subsequent diapedesis across the endothelium. It is possible that $NE^{-/-}$ monocytes too exhibit increased adhesion and are limited in their ability to crawl along ECs and locate optimal sites of TEM. In this manner, NE might be required to remove existing cell-cell interactions at the trailing edge of crawling monocytes. In keeping with this notion, it has been postulated that serine proteases, including NE, are secreted by migrating monocytes to detach CD18 integrins from counter-receptors on the endothelium (Zhang et al., 2013). This however would seemingly differ from how NE and human neutrophils interact as elastase activity has actually been shown to enhance neutrophil adhesion to HUVECs (Nozawa et al., 2000).

While the precise mechanism remains to be clarified, it does appear that monocyte-derived NE specifically is involved in monocyte TEM. By establishing an *in vitro* Transwell migration assay, we were able to compare the migration of $NE^{-/-}$ and $NE^{+/+}$ monocytes directly with all other factors and potential sources of NE (e.g. ECs) remaining constant. Using this approach, we were able to demonstrate a decreasing trend in the migration of $NE^{-/-}$ monocytes across murine skin endothelial cells in response to FBS, a rich and varied source of chemoattractants. While keen to repeat these experiments using CCL2 as a stimulus, the costs and resources required to MACS-sort sufficient numbers of monocytes would have been too great. Accordingly, we conducted all subsequent assays with human-derived monocyte-like U937 cells. In evaluating their migration across human umbilical vein endothelial cells, considerably fewer cells ($P = 0.052$) accumulated in the bottom chamber in response to CCL2 when incubated with the NE-specific inhibitor ONO-5046. We are confident that significance will be reached by extending these studies.

Concomitantly, we also plan to assess levels of intracellular NE in U937 cells pre- and post-migration. If a reduction is observed, it could be suggested that NE is similarly released and generally involved in monocyte TEM in humans and mice. U937 cell transmigration assays would therefore provide an appropriate, yet simple and potentially high-throughput model system to delineate the mechanism(s) by which NE regulates monocyte TEM. In this manner, we could use phase-contrast microscopy to record videos of monocytes as they interact with the endothelium, both in the presence and absence of ONO-5046. This approach might identify the specific point at which NE-

inhibited monocytes become ‘stuck’ during TEM. Microscopy can also be used in combination with a cell adhesion assay to determine whether monocyte-EC adhesion is at all influenced when NE activity is blocked. In addition, we can monitor the expression levels of endothelial junctional molecules and secreted chemokines to determine if/how they change during normal monocyte TEM. Key molecular interactions can be similarly explored by incorporating other inhibitors or blocking antibodies, while the use of multiple chemoattractants will indicate whether NE-mediated migration is specific to CCL2. Once a mechanism has been established *in vitro*, it can be subsequently verified in mice *in vivo*, using a peritonitis and ear model of inflammation, as before.

# CHAPTER 6: Characterising the mode and dynamics of monocyte transendothelial migration *in vivo.*

## *6.1 Introduction*

Whilst our initial findings have implicated NE in monocyte transendothelial migration in mice, identifying its specific function in this process is not likely to be easy, not least considering the general lack of insight regarding the migratory behaviour of monocytes *in vivo*. Indeed, the vast majority of observations relating to the mode, dynamics, and molecular mechanisms of monocyte TEM have been made using *in vitro* models, incorporating predominantly human monocytic and endothelial cells. Though many of these studies have proven to be reproducible, reliable, and predictive of monocyte-EC interactions *in vivo* (Muller and Luscinskas, 2008), a number of inherently significant differences do ultimately exist between *in vitro* and *in vivo* models, as outlined earlier in Chapter 3. In this context, we believe there is a need to characterise the various parameters and steps of monocyte TEM as it unfolds *in vivo*.

To address this issue, our group has established a confocal intravital microscopy imaging platform to track leukocyte transmigration through murine cremasteric venules in real time. This technique offers outstanding spatial and temporal resolution, which has already been exploited by our lab to characterise transendothelial migration of neutrophils (Woodfin et al., 2011). While the initial focus of this study centred on comparing the profile, frequency, dynamics and stimulus specificity of neutrophils migrating via the paracellular and transcellular pathways, the most intriguing observation related to the 'disrupted' nature of TEM exhibited by some of the cells. This included hesitant TEM in which neutrophils, rather than passing normally through EC junctions without pause, oscillated in the junction several times before completing migration to the abluminal side, and reverse TEM in which post-migrated neutrophils moved back through EC junctions in an abluminal-to-luminal direction. These events were up-regulated in inflammation after ischemia-reperfusion injury, as attributed to reduced expression of JAM-C at EC junctions. Furthermore, and of pathophysiological relevance, it seemed that upon re-entering the circulation, reverse transmigrated neutrophils exhibited a greater propensity for ROS production, contributing to the dissemination of systemic inflammation and tissue damage in secondary organs.

The phenomenon of reverse transendothelial migration (rTEM) has also been described for monocytes. Using an *in vitro* model of a blood vessel wall consisting of human umbilical vein endothelial cells (HUVECs) grown on amniotic tissue, Randolph and Furie observed that while human monocytes incubated for 2 hours successfully transmigrated into the amniotic tissue, by 12 hours the majority of cells migrated back across the endothelium to the apical surface (Randolph and Furie, 1996). Subsequent studies demonstrated that reverse transmigrated monocytes were more inclined to differentiate into DCs as opposed to macrophages, and accordingly reverse transmigration was postulated to mediate the physiological trafficking of DCs from tissues into the lumen of lymphatic vessels (Randolph et al., 2002). A more recent study does however suggest that post-migrated monocytes employ reverse transmigration to re-enter the circulation (Bradfield et al., 2007). Though not demonstrated directly, a population of classical monocytes in the blood of thioglycollate-stimulated mice were shown to display a reverse-transmigratory phenotype, as characterised by a lack of L-selectin surface expression. Interestingly, and in accordance with neutrophil rTEM, the frequency of monocytes undergoing rTEM, both *in vitro* and *in vivo*, was enhanced upon blocking JAM-C function.

How exactly JAM-C promotes leukocyte rTEM is currently unclear. Recent findings from our group have however identified a role for the lipid mediator $LTB_4$, certainly with regards to neutrophil rTEM (data unpublished). Indeed, local administration of $LTB_4$, chosen initially due to its increased expression in the cremaster muscle upon ischemia-reperfusion injury, induced both a reduction in venular JAM-C expression and an increase in prevalence of neutrophil rTEM. In addressing the mechanism of JAM-C cleavage, as normal JAM-C expression was observed in neutrophil-depleted mice it was hypothesised that $LTB_4$ elicited both neutrophil chemotaxis and degranulation, culminating in the degradation of endothelial JAM-C by released proteases. Furthermore, and of particular relevance to our own study, it appeared that JAM-C shedding was mediated predominately by NE, as supported by the unperturbed expression pattern of JAM-C in NE KO mice.

In recognition of the exciting insights made by our group into the mechanisms and modes of neutrophil TEM, in this chapter we sought to similarly enhance our understanding of monocyte TEM by applying the same 4D intravital microscopy imaging platform to the cremaster muscles of $CX_3CR1$-eGFP-ki mice. This approach

should enable the behaviour and dynamics of transmigrating monocytes to be rigorously characterised *in vivo* over the course of an inflammatory insult. In this regard, NE will no longer constitute the primary focus of our studies, however, once the principles of monocyte migration have been established, the involvement of NE in this process can be assessed using $NE^{-/-}$ mice. The more immediate objectives of this work are as follows:

- Evaluate the frequency and dynamics of monocyte para- and transcellular TEM *in vivo*.
- Discriminate and characterise different forms of monocyte migration (e.g. hesitant and reverse TEM).
- Compare the transmigration profiles of monocytes in response to different inflammatory stimuli.
- Investigate the function of JAM-C during monocyte TEM.

### *6.2 Results*

#### *a) Monocytes primarily undergo paracellular TEM in response to CCL2 in vivo.*

Four-dimensional confocal intravital microscopy of cremasteric venules has been previously used by our group to study the mechanisms and dynamics of neutrophil TEM *in vivo* (Woodfin et al., 2011). This was performed specifically on male LysM-eGFP-ki mice, exhibiting endogenously fluorescent neutrophils. In order to visualise the vascular endothelium, mice were injected intrascrotally (i.s.) 1-4 hours prior to analysis with an Alexa Fluor 555–conjugated antibody against the EC junctional molecule PECAM-1. Importantly, the specific clone of antibody used (clone C390) was shown to neither elicit nor inhibit leukocyte transmigration. Upon exteriorising and surgically preparing one of the cremaster muscles, image stacks of half post-capillary venules were captured every minute for a period of 1 hour. These images were subsequently reconstructed *in silico*, yielding high-resolution four-dimensional videos of neutrophils interacting with the vasculature.

We used this same approach to characterise monocyte TEM in male $CX_3CR1^{+/eGFP}$ mice in this study. To elicit monocyte infiltration into the cremaster muscle we initially injected mice i.s. with CCL2, as used successfully in the previous chapter. Recognising the majority of monocytes in these studies had already completed TEM 4 hours post stimulation, we decided to exteriorise the cremaster muscle after 2 hours. Indeed, at this time point monocyte rolling and adhesion could be observed directly under the microscope. In order to study the more intricate interactions between monocytes and venular ECs, individual post-capillary venules measuring 30-50 µm in diameter were imaged for approximately an hour each. In analysing our initial videos, it was apparent that while sufficient numbers of monocytes were shown to undergo endothelial adhesion and crawling, almost no cells committed to TEM. Theorising that the CCL2 was washed away upon exteriorising the cremaster muscle, we decided to supplement the superfusion buffer, used to bathe the tissue throughout imaging, with CCL2 at a concentration of $5\times10^{-9}$ M, as used successfully previously (Voisin et al., 2009). While this did enhance the number of observed TEM events, we were unable to consistently induce the same frequency of transmigration as achieved previously for neutrophils (Woodfin et al., 2011). Furthermore, while small cell protrusions and subtle shape changes could be resolved for migrating LysM-eGFP-ki neutrophils, the relatively

weaker eGFP expression of $CX_3CR1^{+/eGFP}$ monocytes made such in-depth analysis impossible (*Figure 6.1*). Nonetheless, we were still able to visualise and analyse detailed spatiotemporal, three-dimensional dynamics of individual monocytes as they underwent TEM.

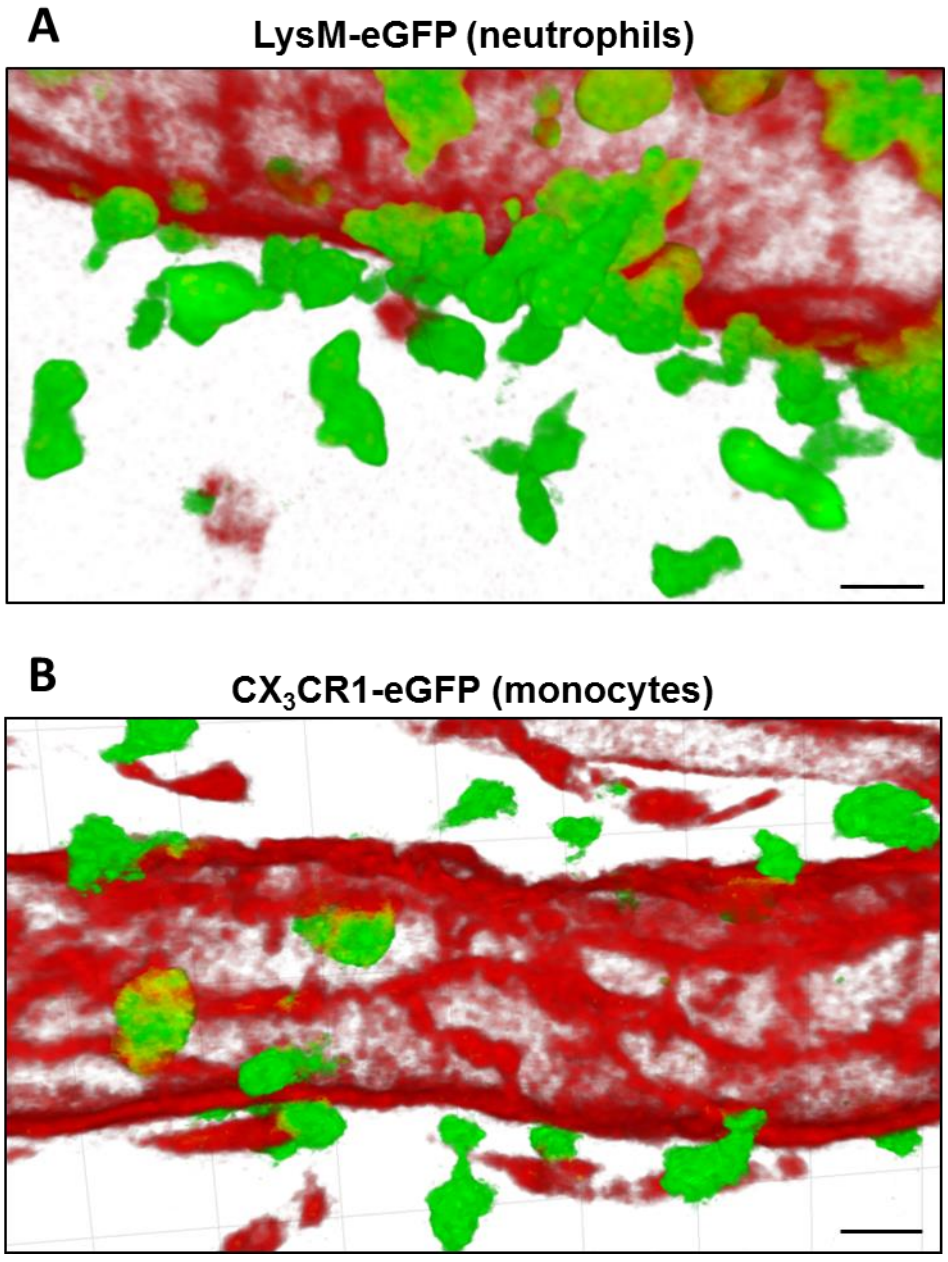


**Figure 6.1: Establishing a four-dimensional imaging platform to study leukocyte TEM in real time *in vivo*.** Confocal intravital microscopy of cremasteric venules of $LysM^{+/eGFP}$ (A) and $CX_3CR1^{+/eGFP}$ (B) mice (exhibiting green neutrophils and monocytes, respectively) administered LPS (300 ng, supplemented with Alexa Fluor 555–labelled mAb to PECAM-1, red) i.s. for 4 hours. One cremaster muscle was subsequently exteriorised and surgically prepared for 4D confocal imaging. Representative still images are shown. Original magnification, ×40. Scale bar, 10 µm.

In response to CCL2, adherent monocytes were shown to crawl across the luminal surface, principally along endothelial borders. Though the majority of cells would crawl out of sight, several could be seen undergoing TEM. This occurred almost entirely via the paracellular pathway, i.e. by squeezing through pores in endothelial cell junctions (*Figure 6.2A*). Only a select few monocytes (< 5%) could be observed crossing the endothelium in a non-junctional transcellular manner, passing instead through the body of individual ECs (*Figure 6.2B*). Multi-cellular junctions constituted more common sites of paracellular TEM compared to bi-cellular junctions (ratio of ~3:1), however the duration of TEM was largely conserved, lasting typically between 9 and 12 minutes (*Figure 6.3A*). Following transmigration, the vast majority of monocytes remained in a flattened morphology at or near the site of TEM (*Figure 6.3B* & *Video appendix 6.1A*). While some cells were shown to engage in abluminal endothelial crawling, only a select few managed to detach from the endothelium and migrate into the interstitial space.

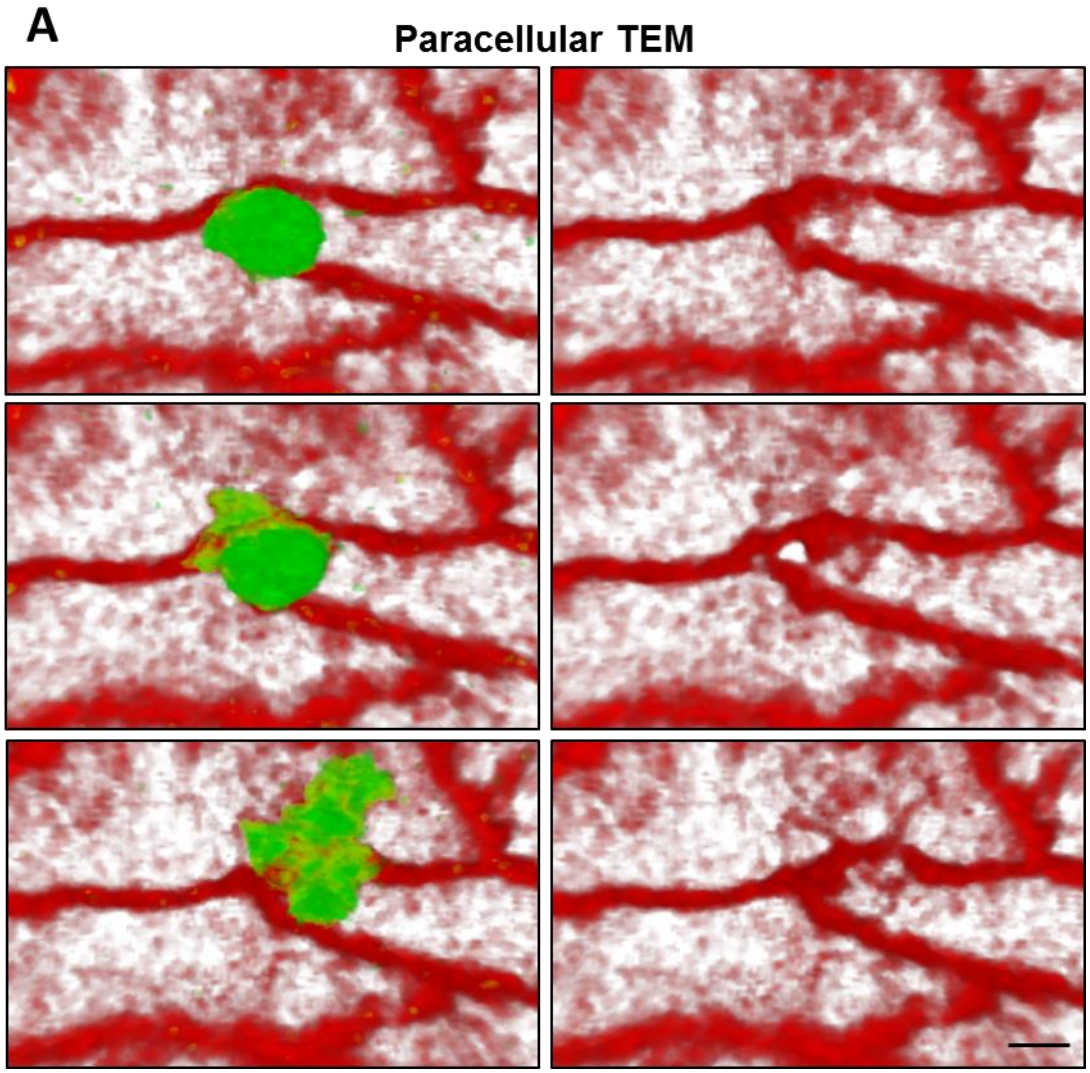

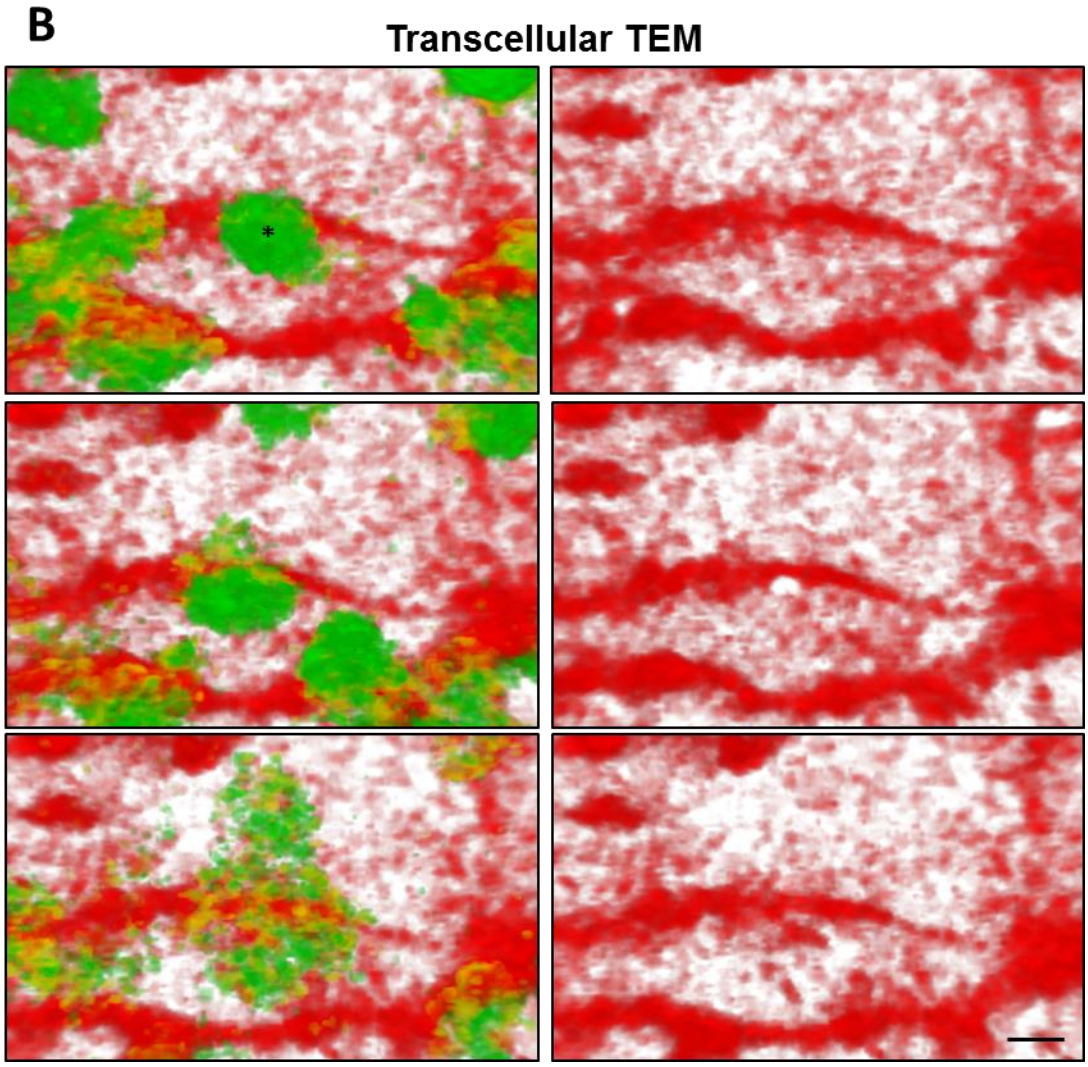


**Figure 6.2: Modes of CCL2-induced monocyte TEM.** $CX_3CR1^{+/eGFP}$ mice were administered CCL2 (500 ng, supplemented with Alexa Fluor 555–labelled mAb to PECAM-1, red) i.s. for 2 hours. One cremaster muscle was subsequently exteriorised, superfused with CCL2 ($5\times10^{-9}$ M) and imaged for 2 hours by 4D confocal microscopy. Monocytes (green (*)) were observed undergoing paracellular (A) and transcellular (B) TEM, accompanied typically by a transient pore in PECAM-1 expression (right panel) at the cell junction or in the cell body, respectively. Representative time-lapse images are shown. Original magnification, ×40. Scale bar, 5 μm.

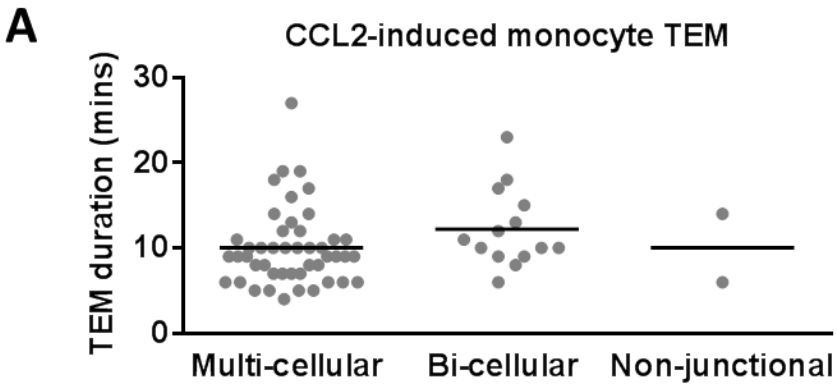

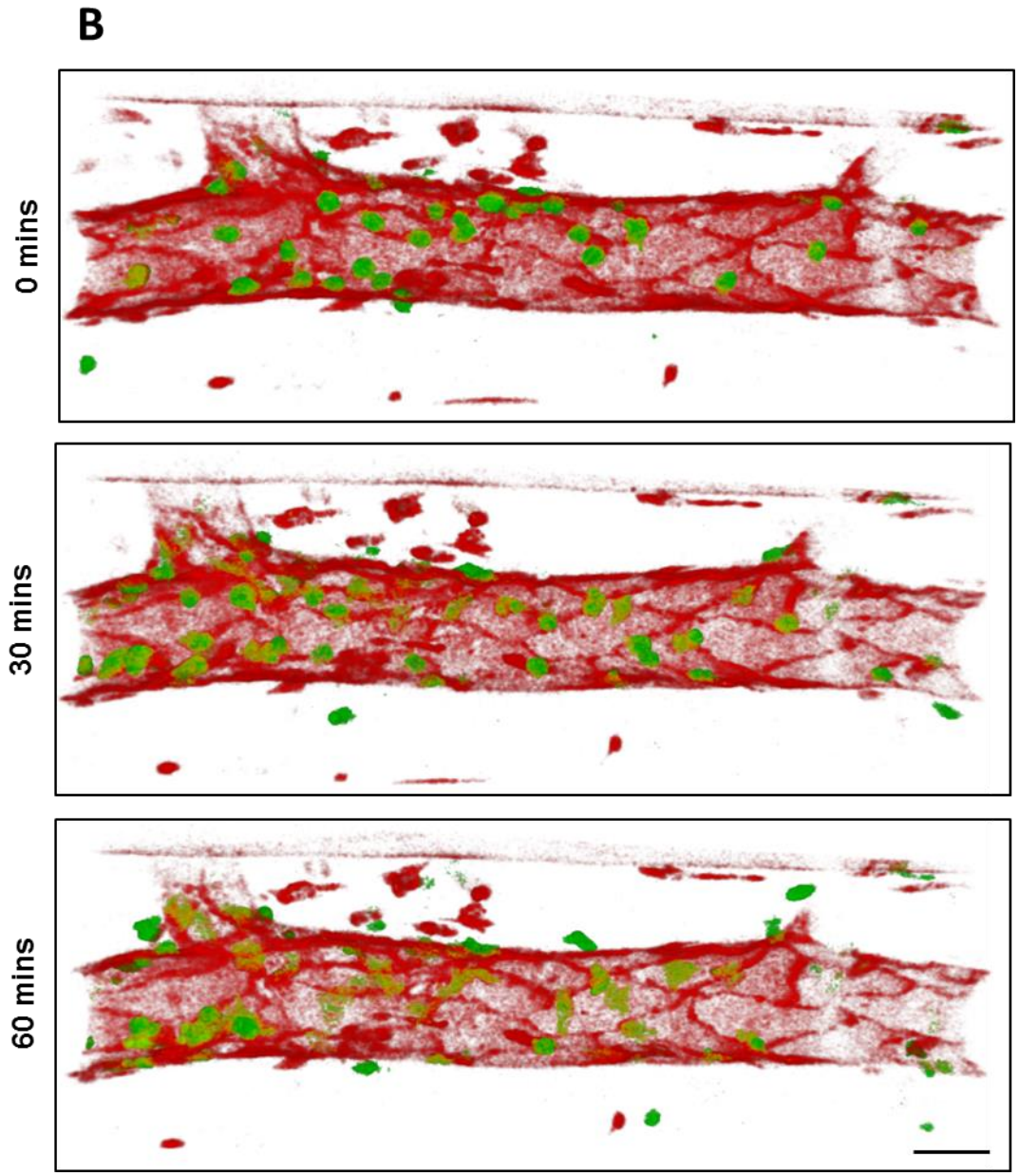


**Figure 6.3: Monocyte dynamics during CCL2-induced TEM.** In analysing CCL2-stimulated cremasteric venules, the duration of normal TEM events was recorded for monocytes undergoing paracellular (at both bi- and multi-cellular junctions) and transcellular (non-junctional) TEM (A). The duration was calculated as the time between the first frame in which a pore in PECAM-1 staining could be seen to the frame in which the monocyte had fully traversed the EC barrier. Time lapse images depict this movement of monocytes from the luminal (green, spherical) to abluminal (yellow, flat) space (B). TEM events were pooled from 6 separate venules from 4 mice. Original magnification, ×40. Scale bar, 30 μm.

***b) Monocytes exhibit disrupted forms of TEM in response to CCL2.***

In some instances, TEM was shown to take considerably longer than normal, with the cells seemingly getting stuck at the site of TEM prior to completing their passage to the

abluminal side. 'Stuck' cells did not however always complete transmigration. On the contrary, in most cases the cells remained at the site of TEM, sometimes for the duration of the entire 60-minute recording. While some cells could be seen extending protrusions into the abluminal space, either permanently or transiently, others appeared to simply sit atop the endothelial surface. On rare occasions, the cells would retract their protrusions and crawl away. Categorised collectively as an 'incomplete' TEM event, we assigned this term to any monocyte that remained stationary on the luminal surface for ≥ 25 minutes. Furthermore, we also identified and quantified crawling monocytes exhibiting a 'tailing' phenotype, characterised by the transient formation (several minutes) of a greatly elongated uropod (*Figure 6.4A*). This seemingly resulted from the monocyte extending an investigative protrusion into the endothelium whilst still crawling. Upon detaching, the tail would retract back to the cell body, returning the monocyte to a normal crawling state. Tailing events were less frequently observed than incomplete events, which in turn were less frequently observed than normal TEM events, though they all occurred predominantly at multi-cellular junctions (*Figure 6.4B*). Example videos of normal, incomplete and tailing migration events are shown in *Video appendix 6.1 and 6.2*.

***c) Monocyte TEM is not altered upon inhibiting JAM-C.***

In response to CCL2, while monocytes did exhibit incomplete and tailing phenotypes, neither reverse nor hesitant TEM was strictly observed, as has been previously described for neutrophils. These forms of disrupted neutrophil TEM were attributed to a reduction in JAM-C expression at EC junctions. Having confirmed JAM-C expression in post-capillary venules in naïve $CX_3CR1^{+/eGFP}$ mice (*Figure 6.5*), and considering CCL2 does not reportedly reduce endothelial JAM-C expression, we decided to re-characterise monocyte TEM upon disrupting JAM-C expression. This was achieved both indirectly by stimulating with the lipid mediator $LTB_4$ and directly by administering the JAM-C blocking antibody H33. $LTB_4$ is thought to promote JAM-C cleavage by inducing neutrophil degranulation (data unpublished), while H33 disrupts the retention of JAM-C at endothelial junctions by blocking interactions with its binding partner JAM-B (Lamagna et al., 2005).

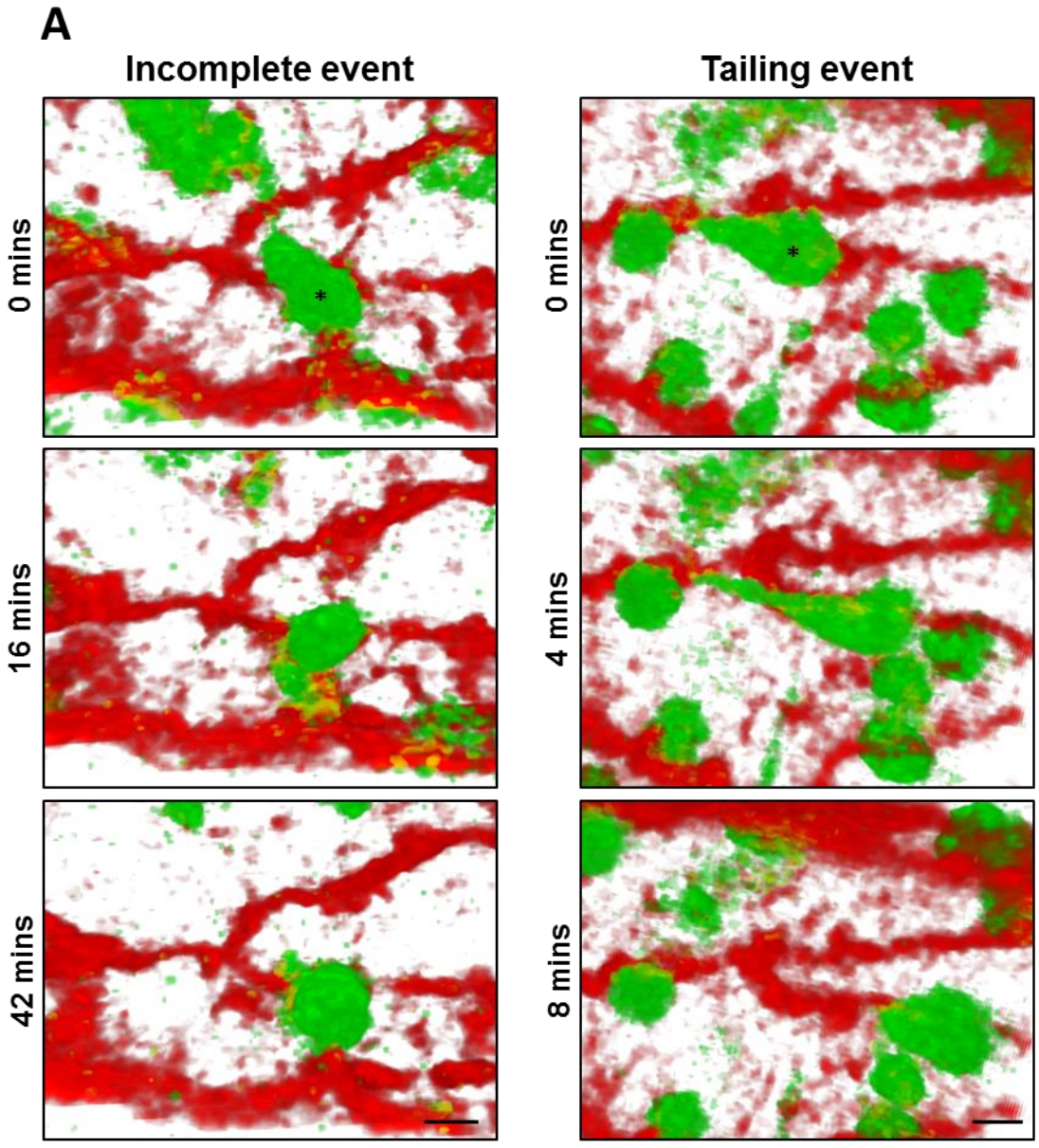
A
Incomplete event
Tailing event
0 mins
16 mins
42 mins
0 mins
4 mins
8 mins
*
*

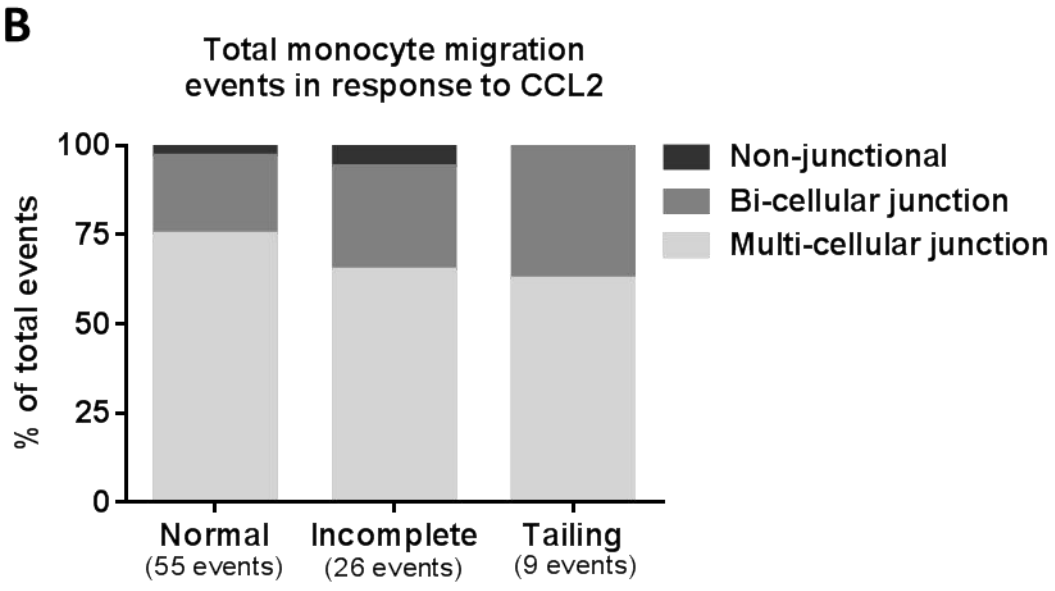
B
Total monocyte migration events in response to CCL2
% of total events
100
75
50
25
0
Normal
(55 events)
Incomplete
(26 events)
Tailing
(9 events)
Non-junctional
Bi-cellular junction
Multi-cellular junction

**Figure 6.4: Disrupted forms of monocyte migration.** In analysing CCL2-stimulared cremasteric venules, in addition to normal TEM, monocytes (*) were also observed partaking in 'incomplete' and 'tailing' events, as depicted in the above time lapse images (A). All migration events occurred predominantly at multi-cellular junctions (B). TEM events were pooled from 6 separate venules from 4 mice. Original magnification, ×40. Scale bar, 5 µm.

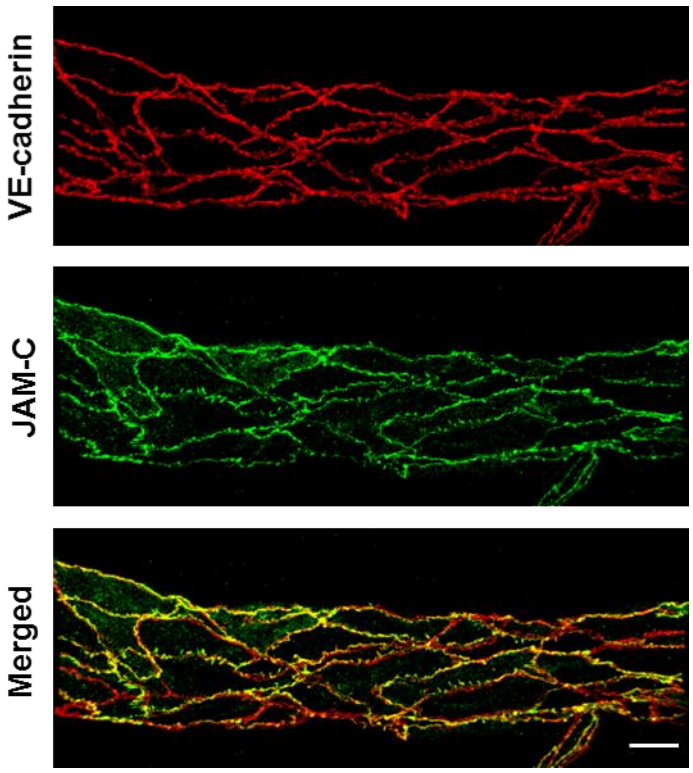


**Figure 6.5: JAM-C expression in cremasteric venules.** Cremaster muscles were harvested from naïve $CX_3CR1^{+/eGFP}$ mice, fixed in PFA and immunostained for JAM-C (green) and the endothelial junctional marker VE-cadherin (red). ECs of post-capillary venules demonstrated strong JAM-C expression along endothelial junctions and faint, diffuse expression within the cell-body. Scale bar, 10 µm.

As $LTB_4$ alone does not induce a strong monocyte response (*Appendix 6.1*), a combined stimulus of $LTB_4$ and CCL2 was injected i.s. into $CX_3CR1^{+/eGFP}$ mice for 2 hours. CCL2 alone was used in combination with the JAM-C blocking antibody H33, which was administered i.v. prior to stimulation. Under these conditions, we initially evaluated general leukocyte recruitment, in both exteriorised and intact cremasters, as compared to CCL2-only controls. After 4 hours, monocyte extravasation was largely conserved across all mice. As expected, neutrophil extravasation was amplified in the presence of $LTB_4$, a potent neutrophil chemoattractant, though interestingly only marginally in

exteriorised tissues (*Figure 6.6*). Thus, during live imaging (exteriorised tissues) the profile of infiltrating monocytes and neutrophils was comparable across all inflammatory scenarios, enabling any potential differences in the modes and dynamics of monocyte TEM to be more robustly assessed. In this regard, individual venules were recorded as before and the average number, type and duration of migration events characterised (*Figure 6.7*). Generally, normal paracellular TEM events were most frequently observed. While the duration of TEM did not significantly change, the proportion of bi-cellular junctional events was more pronounced in the presence of H33, though not $LTB_4$. This was similarly observed for incomplete migration events, which did exhibit a collective, albeit non-significant increase in frequency upon JAM-C inhibition. Importantly, monocyte reverse TEM was not observed in any of the mice analysed.

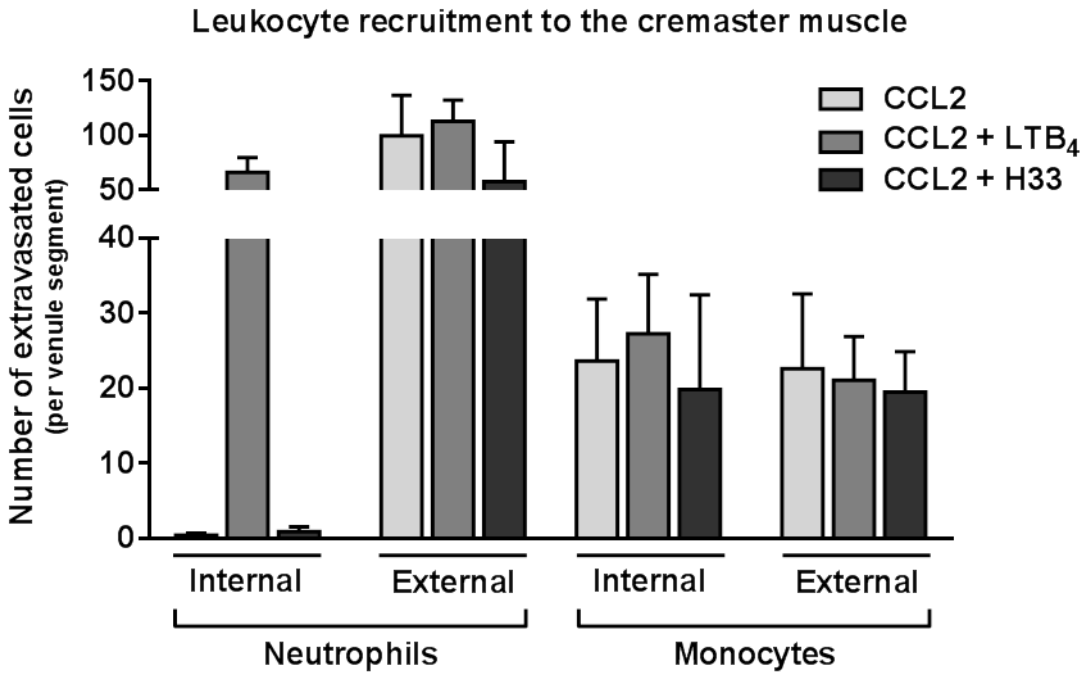


**Figure 6.6: Leukocyte infiltration is conserved during intravital microscopy.** Numbers of extravasated neutrophils and monocytes were counted in both surgically prepared (external) and intact (internal) cremasteric venules of $CX_3CR1^{+/eGFP}$ mice stimulated with CCL2 (500 ng) i.s. for a total of 4 hours. JAM-C was disrupted in some mice either by administering a JAM-C blocking mAb (H33, 3 mg/kg) immediately prior to stimulation or by supplementing the CCL2 stimulus with $LTB_4$ (300 ng). Exteriorised cremasters (2 hours post stimulation) were superfused with CCL2 ($5\times10^{-9}$ M) during 2 subsequent hours of confocal microscopy. Data are represented as the mean ± SEM (n = 3 mice, average of 5-6 venules per mouse).

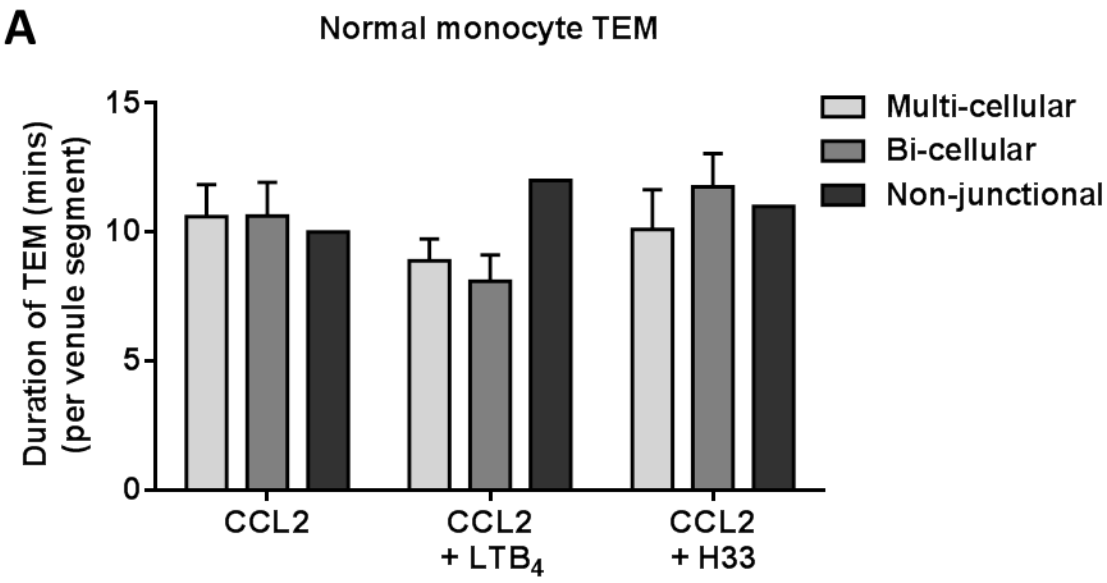
A
Normal monocyte TEM
Duration of TEM (mins)
(per venule segment)
15
10
5
0
Multi-cellular
Bi-cellular
Non-junctional
CCL2
CCL2
+ LTB4
CCL2
+ H33

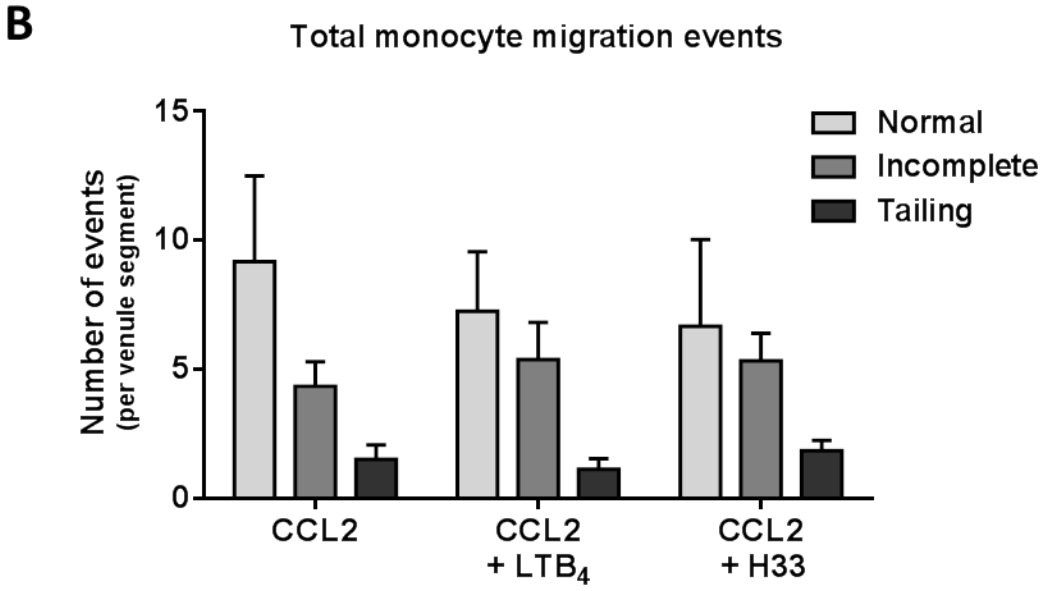
B
Total monocyte migration events
Number of events
(per venule segment)
15
10
5
0
Normal
Incomplete
Tailing
CCL2
CCL2
+ LTB4
CCL2
+ H33

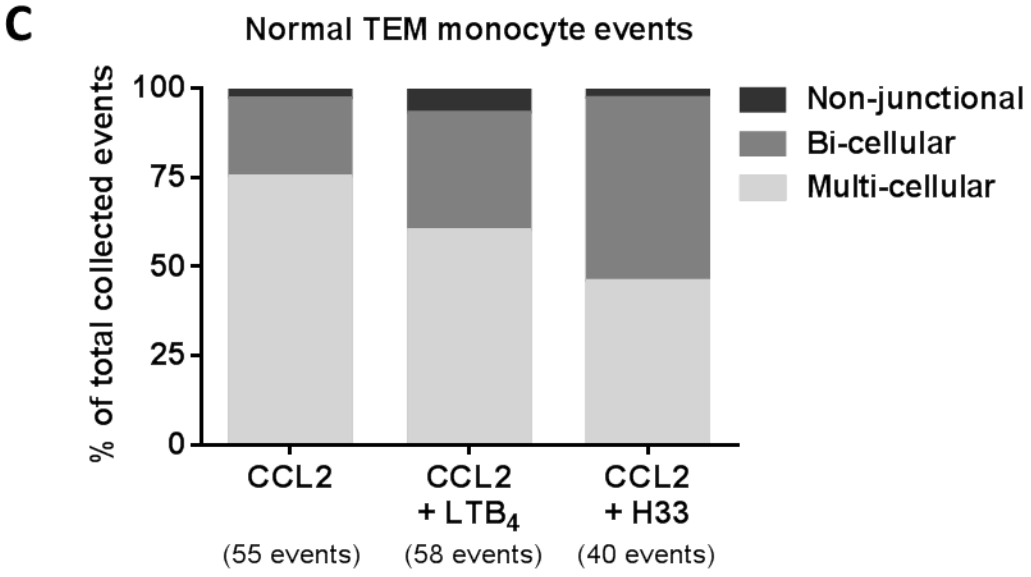
C
Normal TEM monocyte events
% of total collected events
100
75
50
25
0
Non-junctional
Bi-cellular
Multi-cellular
CCL2
(55 events)
CCL2
+ LTB4
(58 events)
CCL2
+ H33
(40 events)

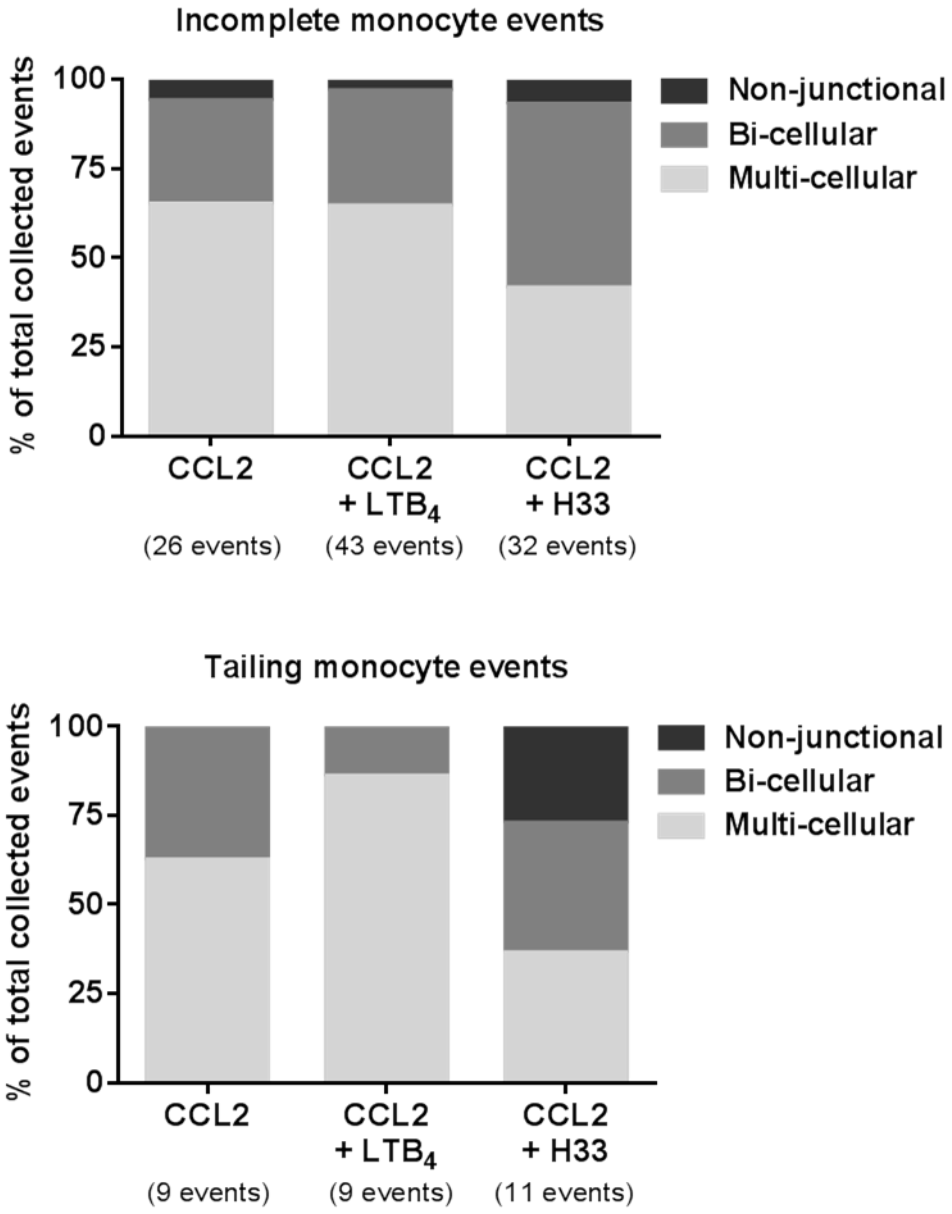


**Figure 6.7: Monocyte migration is not altered upon blocking JAM-C.** Total monocyte migration events were characterised in cremasteric venules of $CX_3CR1^{+/eGFP}$ mice stimulated with CCL2 (500 ng) i.s. for 2 hours. As before, JAM-C was disrupted in some mice either by pre-treating with the JAM-C blocking mAb H33 (3 mg/kg) or by supplementing the CCL2 stimulus with $LTB_4$ (300 ng). The average duration of normal monocyte TEM was conserved across all groups (A). The average number of normal TEM events, but also incomplete and tailing events was also largely comparable (B), as was the frequency of the different modes of migration (para- or transcellular). Data for (A) and (B) are represented as the mean ± SEM (n = 6-8 separate venules from 3-4 mice). Total migration events were pooled for (C).

### *6.3 Discussion*

While *in vitro* studies have contributed tremendously to our understanding of the mechanisms that govern leukocyte transendothelial migration, one major caveat is the general lack of supporting *in vivo* models. Due to recent advancements in intravital microscopy however, this is now beginning to be addressed. In this respect, by employing high-resolution, four-dimensional confocal imaging our group has recently provided great insight into the mode, frequency, dynamics and stimulus specificity of neutrophil transendothelial migration through inflamed venules in the cremaster muscle of LysM-eGFP-ki mice (Woodfin et al., 2011). Keen to similarly characterise the *in vivo* behaviour of migrating monocytes, in this study we exploited the same confocal imaging platform to track the movement of endogenously fluorescent monocytes in $CX_3CR1$-eGFP-ki mice.

As has been used throughout this study, as a means of stimulating monocyte migration in the cremaster muscle we administered the chemokine CCL2. In response to a single intrascrotal injection of CCL2, while monocytes were abundantly recruited to cremasteric venules and were observed adhering to and crawling along the endothelium, almost no cells commenced diapedesis. As monocytes readily completed extravasation previously in this study in surgically un-compromised tissues, we theorised that in exteriorising and flattening the cremaster muscle, as is required for confocal analysis, important CCL2 gradients were dissipated, blocking TEM. To circumvent this, we topically applied CCL2 throughout imaging. While this did enhance the frequency of monocyte TEM, we were unable to consistently induce the same number of transmigration events as achieved previously for neutrophils. While this was to be expected given the relatively lower frequency of monocytes in the blood, of particular detriment was the technical requirement to image larger ($\geq$ 40 µm diameter) post-capillary venules, which, as our previous results have already demonstrated, are less accommodating to monocyte migration compared to their smaller (25-40 µm diameter) counterparts.

Despite the various difficulties faced, we successfully managed to track monocytes as they underwent TEM. This occurred almost entirely via the paracellular pathway, predominantly at multi-cellular endothelial junctions. This is in keeping with the vast majority of *in vitro* studies, in which transcellular migration, even under the most

conducive circumstances, only represents the route of emigration for approximately 10% of monocytes (Muller, 2014). What has also been reported however, and which we have recognised directly in this study, is that para- and transcellular migration cannot always be distinguished, primarily because transcellular events seem to occur most commonly at sites directly proximal to EC junctions. Irrespective of the specific mode of TEM used, prior to initiating diapedesis, monocytes were ubiquitously observed crawling along the endothelium, most commonly along the junctional borders. Upon arresting at a chosen site of transmigration, the monocytes extended a protrusion into the endothelium forming a pore, as visualised by a gap in PECAM-1 staining, through which they would subsequently squeeze their bodies. This process took on average 10 minutes to complete, exceeding the 6 minutes recorded by our group for neutrophils. Relatively longer transmigration times have similarly been reported for monocytes *in vitro* (Chen et al., 2006). Upon completing TEM, rather than readily detaching from the venular wall and entering the interstitium, the vast majority of monocytes remained stationary at the site of migration in a flattened morphology. Interestingly, this was not routinely observed previously in intact cremaster muscles, suggesting again that exteriorising the cremaster muscle may influence monocyte behaviour.

Sticking with this point, while CCL2-induced monocyte infiltration did not differ between intact and exteriorised tissues, the latter did demonstrate significantly greater levels of neutrophil extravasation. Neutrophils have been previously shown to promote monocyte transmigration and could possibly also influence monocyte behaviour in our cremaster model. In this regard, it was clear from analysing our final reconstructed movies that many of the migration pores apparent in the inflamed endothelium were attributable not to monocytes but to other cells, most likely neutrophils, though this was not directly confirmed as neutrophils were only labelled post acquisition. Importantly, there were numerous instances in which monocytes underwent TEM through recently- or pre-existing pores (*Video appendix 6.3*). This may suggest that neutrophils can directly guide monocytes through the endothelium, a theory we hope to explore further by conducting analogous experiments in neutrophil-depleted mice.

In addition to characterising normal monocyte TEM, in this chapter we were also keen to determine whether monocytes exhibited any disrupted forms of migration *in vivo*, as we have previously described for neutrophils. Neutrophils specifically were shown to partake in hesitant TEM, in which cells oscillated in the junction prior to completing

TEM, and reverse TEM, consigned to post-migrated cells that crossed back into the endothelial lumen. With regards to CCL2-stimulated monocytes, while some transmigration events did take considerably longer than the collective average, these cells were not seen to oscillate akin to hesitant migration but rather remained stationary, presumably stuck in the junction. Monocytes remained in this 'incomplete' state for varying periods of time, sometimes for the duration of an entire recording. They also became stuck at varying stages of migration, with some cells extending considerable protrusions into the abluminal space, while others appeared simply to rest atop the junction. On rare occasions, stuck cells detached themselves entirely from the junction and re-engaged in luminal crawling. In addition to incomplete migration events, we also described a monocyte 'tailing' phenotype in which monocytes transiently displayed an elongated uropod, seemingly as a result from engaging with the endothelium in a tight yet localised manner whilst still crawling. As with normal monocyte TEM, both incomplete and tailing events occurred predominantly at EC junctions, and most likely reflect failed attempts to undergo transmigration at sub-optimal sites of the endothelium.

In response to CCL2, on no occasion did monocytes complete TEM and reverse migrate back into the vascular lumen. This is in keeping with our previous peritonitis results, in which CCL2 stimulation did not increase the proportion of circulating classical monocytes with a CD62L-negative phenotype (see *Figure 5.3*), considered to be a hallmark of reverse transmigrated cells. This may not be surprising however as CCL2 has never been implicated in reducing JAM-C expression (rather it might increase its expression (Keiper et al., 2005)), a phenomenon our group has already shown to mediate rTEM of neutrophils *in vivo* and others have shown to mediate rTEM of monocytes *in vitro* (Bradfield et al., 2007). To determine whether blocking junctional JAM-C expression in post-capillary venules can similarly induce monocyte rTEM *in vivo*, we stimulated the mouse cremaster muscle with CCL2 as before, however together with pre-treating the mice with the JAM-C blocking antibody H33 or supplementing the CCL2 with $LTB_4$, a lipid mediator previously demonstrated by our group to induce JAM-C proteolysis. Neither scenario however yielded any monocyte rTEM events. The migration profile of monocytes more generally did not dramatically change, though the relative frequency of incomplete and tailing events was marginally greater. While JAM-C expression was not directly assessed in our experiments, a reduction in junctional

JAM-C was confirmed in parallel studies using the same batch of reagents and experimental parameters (data not shown).

In this study, we have successfully utilised high-resolution confocal imaging to characterise in detail the behaviour of monocytes as they undergo transendothelial migration *in vivo* for the first time. Using the mouse cremaster muscle as a model, in response to CCL2 stimulation monocytes were shown to engage in all steps of the leukocyte adhesion cascade, including rolling and arresting on the endothelial lining, crawling intraluminally along EC borders, and eventually committing to and completing TEM, most typically at multi-cellular junctions. In addition to normal TEM, monocytes also displayed disrupted forms of migration, in which TEM was seemingly initiated but not completed. At no point however was reverse TEM strictly observed, even upon disrupting JAM-C expression. That is not to say that monocytes do not undergo rTEM *in vivo*, as it may simply be governed in a different manner to neutrophils. With regards to exploring alternative monocyte-specific mechanisms, as it relates to rTEM or otherwise, a major limitation of the current experimental set-up is the relatively small number of elicited monocyte TEM events. Thus far monocyte recruitment has been induced almost entirely with CCL2. Previously in this study, CCL2 was also used in peritonitis experiments, though demonstrated a much weaker (albeit more specific) monocyte response as compared to a joint stimulus of IFN-γ and TNF-α. In this light, we believe a greater frequency of monocyte TEM may be achieved by incorporating different inflammatory mediators and/or optimising other experimental parameters. Acquiring a greater and more consistent frequency of monocyte TEM will undoubtedly facilitate in any subsequent comparative studies and thereby provide a more suitable model in which to study monocyte behaviour *in vivo*.

# CHAPTER 7: General discussion

## *7.1 Project overview*

Whilst monocytes represent key cells of the innate immune system, their inflammatory activities following inappropriate or excessive recruitment may cause unwanted tissue injury and critically contribute to the pathogenesis of a number of major diseases. Some anti-inflammatory therapeutics do exist for such monocyte-driven pathologies, however their utility is often limited by adverse side effects, often generated through non-specific toxicity of cells uninvolved in the disease process. As such, there is an emphasis on identifying novel drug targets specific to causative cell types or subsets. The classical subset of monocytes has been most closely associated with promoting inflammatory disease activity by infiltrating sites of inflammation and differentiating into pro-inflammatory macrophages and DCs. The adhesion molecules that regulate classical monocyte trafficking are beginning to be described, however the potential role of proteases in this process remain largely unexplored. The serine protease neutrophil elastase has already been broadly implicated in neutrophil migration. Furthermore, NE is reported to play a role in the recruitment of monocytes to the lungs of mice exposed to cigarette smoke, as indicated by reduced numbers of pulmonary macrophages in $NE^{-/-}$ mice as compared to wild-type controls (Shapiro et al., 2003). We sought to build upon these previous findings in this study, focussing more directly on the expression patterns and functional properties of NE in bona fide monocytes.

### *a) Transgenic mouse models enabled the robust and concurrent study of monocyte and NE biology in vivo.*

Although many of the molecular interactions that underpin monocyte migration were originally elucidated *in vitro,* the relative simplicity of these models can make extrapolating results to a whole, living organism unreliable. Accordingly, in this study we sought to investigate monocyte migration directly *in vivo*. Naturally as this cannot be easily achieved in humans we exploited mice, which possess largely homologous classical and non-classical monocyte subsets. More specifically, we used $CX_3CR1$-eGFP-knock-in mice in which the endogenous $CX_3CR1$ gene has been replaced by the fluorescent reporter gene eGFP. $CX_3CR1$ is the cognate receptor for the chemokine

CX3CL1 and is reputedly expressed by the brain microglia and subsets of natural killer and dendritic cells, as well as all monocytes (Imai et al., 1997). Flow cytometric analysis of the blood of $CX_3CR1^{+/eGFP}$ mice however demonstrated that only monocytes exhibited high eGFP fluorescence. Classical and non-classical monocytes could be easily sub-categorised according to GR-1 expression. Employing flow cytometry in this manner, monocytes were accurately identified and quantified in biological samples prepared from the blood, but also the spleen, bone marrow and peritoneal cavity of $CX_3CR1^{+/eGFP}$ mice. Furthermore, by combining confocal microscopy and computer-assisted image processing, $eGFP^+$ monocytes could be directly visualised undergoing transendothelial migration *in situ* in the cremaster muscle and ear, providing a platform to study in great detail interactions made between individual monocytes and endothelial cells. Such analyses were conducted not only on fixed, pre-collected tissue samples, but on live cremaster tissue in anaesthetised mice. This enabled us to track monocytes in the vasculature in real time and thereby gain valuable insight into the dynamics and mechanisms of monocyte extravasation *in vivo*.

Having established selective monocyte labelling in $CX_3CR1$-eGFP-ki mice, in order to rigorously, specifically and concurrently characterise the biological properties of murine NE, $CX_3CR1$-eGFP-ki mice were crossed with NE knock-out mice. More specifically, we generated, and subsequently compared, $CX_3CR1^{+/eGFP}$ mice carrying either double mutant ($NE^{-/-}$) or wild-type ($NE^{+/+}$) copies of the NE gene. We purposely retained one functional copy of the $CX_3CR1$ gene so as to avoid any significant defects in monocyte survival and migration, as previously reported for homozygous knock-in mice. That is not to say however that $CX_3CR1^{+/eGFP}$ mice display entirely representative monocyte behaviour. The absence of one copy of *$CX_3CR1$* for instance has been shown to sufficiently impair monocyte recruitment to atherosclerotic plaques (Combadière et al., 2003). In this light and to maintain consistency, heterozygous $CX_3CR1$-eGFP-ki mice were used exclusively for all comparative NE functional and expression analyses.

***b) Murine classical monocytes express abundant NE transcript and protein.***

To date, NE expression has been definitively demonstrated in human but not murine monocytes. To address this, we initially employed qRT-PCR to assay for NE transcripts in classical and non-classical monocytes FACS-sorted from the spleens of naïve $CX_3CR1^{+/eGFP}$ mice. Both monocyte subsets are well represented in the spleen and,

importantly, have been shown to share an identical morphology, transcriptome and function with their blood counterparts. Though NE transcripts were accurately detected in both subsets, as validated by $NE^{-/-}$ negative controls, expression levels were significantly more abundant in the classical subset, exceeding even those of neutrophils. To determine whether NE was similarly expressed at the protein level, monocytes were sorted as before and analysed by Western blotting. Intriguingly, NE protein was expressed in neutrophils only, even upon extensive cytokine stimulation. To validate this result, NE expression was re-evaluated in classical monocytes purified using MACS- instead of FACS-technology. In marked contrast to before, these cells were shown to contain abundant NE protein stores. Follow-on confocal analyses revealed NE localised to small cytoplasmic granules, akin to the azurophil granules of neutrophils. This was ubiquitously observed for classical monocytes harvested from the spleen but also the bone marrow, suggesting NE is synthesised and packaged early on during monocyte development.

As a means of characterising monocyte NE secretion, prior to being subjected to Western blot or confocal analysis, MACS-sorted monocytes were stimulated *in vitro* with a range of mediators, namely CCL2, a classical monocyte chemoattractant and activator; $LTB_4$, a potent inducer of NE release, certainly from neutrophils; and PMA, a general, synthetic stimulator of cell degranulation. Monocytes did not however display depleted NE stores under any condition. Unexpectedly, neutrophils too were unresponsive to $LTB_4$, though they were shown to mobilise NE to the cell nucleus in response to PMA, in keeping with previous studies (Papayannopoulos et al., 2010). This result demonstrates not only that the cells were generally susceptible to *in vitro* stimulation, but also that NE trafficking is distinctly regulated in monocytes and neutrophils.

Interestingly, in response to CCL2 NE was shown to be depleted from monocytes recruited to post-capillary venules in the mouse ear *in vivo*. This was ubiquitously observed in post-migrated monocytes residing in the interstitial space but also in a high proportion of luminally adherent monocytes, suggesting NE is triggered for release prior to transmigration. By way of explaining the seemingly conflicting expression data generated *in vitro* and *in vivo*, it is possible that upon being administered intradermally, CCL2 induces the local production of other inflammatory mediators that harbour an independent or collective ability to stimulate NE monocyte degranulation. The TNF-like

molecule CD40L for example is expressed by endothelial cells under certain inflammatory conditions and has also been shown to trigger mass NE release from human monocytes *in vitro* (Dollery et al., 2003). Alternatively, the shear stress exerted by the circulating blood may be a decisive factor. Indeed, a number of processes during leukocyte extravasation have been shown to be shear-dependent, such as integrin adhesion and activation and pseudopod formation and retraction (Mitchell and King, 2012). Furthermore, shear stress has been directly implicated in enhancing the secretory capacity of classical monocytes during inflammation (Evani et al., 2013). In this manner, NE has been explicitly postulated to be triggered for release by monocytes upon shear exposure as a means of regulating their passage through the microcirculation (Zhang et al., 2013). Certainly, if NE degranulation is sensitive to shear stress, this may explain the complete absence of NE protein from monocytes purified via FACS-sorting, a process in which cells experience strong hydrodynamic shear forces.

***c) $NE^{-/-}$ mice exhibit defective monocyte transmigration.***

Under naïve conditions, $NE^{+/+}$ and $NE^{-/-}$ mice displayed comparable monocyte profiles, not only in the bone marrow where they are produced, but in the blood, spleen and peritoneal cavity, suggesting NE does not play a pivotal role in homeostatic monocyte trafficking *in vivo*. In order to assess its potential involvement in inflammatory trafficking, monocyte profiles were re-evaluated in response to several mouse models of acute inflammation. In this regard, we initially assessed monocyte infiltration into the peritoneal cavity during peritonitis. While no differences were observed between $NE^{+/+}$ and $NE^{-/-}$ mice in response to IFN-γ and TNF-α, upon stimulation with CCL2 significantly fewer classical monocytes were retrieved from the cavity of $NE^{-/-}$ mice. To determine if this might be attributable to a defect in monocyte transendothelial migration, we next employed confocal fluorescence microscopy to directly visualise monocytes as they migrated through CCL2-stimulated post-capillary venules in the cremaster muscle and ear dermis. While the monocyte profiles of the two genotypes were largely conserved in the cremaster muscle, in the ear a significantly smaller number of post-migrated monocytes were observed in the abluminal space of $NE^{-/-}$ mice. Total monocyte recruitment was not however reduced, rather the majority of monocytes were shown to orient along the venular lumen, seemingly incapable of breaching the endothelial wall.

Collectively, our results from the peritonitis and ear inflammation models strongly suggest a defect in CCL2-induced monocyte migration in $NE^{-/-}$ mice *in vivo*. Although we have unequivocally demonstrated NE is expressed by monocytes, we do appreciate that $NE^{-/-}$ mice are constitutive knock-outs, deficient for NE in all of their cells. As such, it is possible NE derived from non-monocytes could somehow contribute to monocyte TEM. In this regard, whilst neutrophils are reported to store NE at millimolar concentrations, they were scarcely recruited in response to CCL2 and moreover appeared to retain their NE stores intracellularly. NE might be released however by other cells, such as vascular endothelial cells, which have not been directly explored in this study but have been proposed to express NE in humans (Dollery et al., 2003). As monocyte- or even myeloid-specific conditional NE KO mice do not exist, in order to investigate the role of monocyte-derived NE more specifically, we applied monocytes to *in vitro* Transwell migration assays. Unfortunately, as primary $NE^{+/+}$ and $NE^{-/-}$ monocytes could not be purified in sufficient numbers, we instead exploited the human monocyte-like U937 cell line, routinely used to study NE biology. Interestingly, when incubated with the NE-specific inhibitor ONO-5046, considerably fewer U937 cells successfully transmigrated across an endothelial monolayer in response to CCL2, in keeping with the data generated in $NE^{-/-}$ mice. In this light, and considering NE is seemingly depleted from a subpopulation of luminal monocytes in $NE^{+/+}$ mice in the ear, we hypothesise that following their arrest on the endothelium, NE is released by monocytes where after it helps to initiate TEM.

### *7.2 Future directions*

In this study, whilst we have identified the protease neutrophil elastase as a novel mediator of inflammatory monocyte trafficking *in vivo*, its precise mode of action is currently unclear and will constitute the major focus of our future works. We assume its proteolytic activity is a central factor and that it functions at the level of the endothelium, however, being highly promiscuous, identifying its principal substrate(s) may not be straightforward. To facilitate this, we initially plan to develop the U937-HUVEC transmigration assay as it offers simple and potentially high-throughput analysis. In this manner, we are keen to first determine whether migrating U937 cells actively release their NE stores, as observed for monocytes in the mouse ear, by subjecting pre- and post-migrated cells to Western blot and immunofluorescence

analysis. Thereafter, we can use phase-contrast microscopy to record videos of U937 monocytes as they interact with the endothelium, both in the presence and absence of the NE inhibitor ONO-5046. This approach should identify the specific point at which NE-inhibited monocytes become 'stuck' during TEM and hence where NE is likely to exert its function. Microscopy can also be used in combination with a cell adhesion assay to determine whether monocyte-EC adhesion is at all influenced when NE activity is blocked. In addition, we can monitor the expression levels of endothelial junctional molecules and secreted chemokines to determine if/how they change during normal monocyte TEM. Key molecular interactions can also be explored by incorporating other inhibitors or blocking antibodies, while the use of multiple chemoattractants will indicate whether NE-mediated migration is CCL2-specific.

Once a candidate substrate or mechanism has been established *in vitro*, its physiological relevance *in vivo* can be subsequently validated in murine models of inflammation by incorporating appropriate pharmacological or genetic interventions. Representing a more direct and potentially immediate approach, the mechanisms of NE-mediated monocyte migration *in vivo* will also be explored by performing secondary comparative experiments on $NE^{-/-}$ and $NE^{+/+}$ mice. We are particularly keen to apply a 4D imaging platform to the ears of these mice, as we did for the cremaster muscle. Granted monocyte TEM is still defective in the ears of $NE^{-/-}$ mice under these conditions, we should be able to visualise, in real time, how and where migrating monocytes are being inhibited. Though our lab has no direct expertise in conducting live imaging in the ear, we have held preliminary collaborative talks with Dr. Lai Guan Ng, a principal investigator at the Singapore Immunology Network who routinely conducts high-resolution intravital multiphoton imaging of immune responses in the ear skin of multiple transgenic mice, including $CX_3CR1$-eGFP-ki mice (Li et al., 2012).

To date, in this study we have only subjected mice to acute models of inflammation. Though such studies have provided valuable insight into the role of NE during monocyte migration, we are keen to determine whether our preliminary observations extend to murine disease models, which more closely reproduce the complex and integrated physiological and pathological responses of human diseases. In this regard, we have already initiated a collaboration with Dr. Qingzhong Xiao, also located at the William Harvey Research Institute and whose research centres on atherosclerosis. Specifically, Dr. Xiao breeds and experiments on Apolipoprotein E knockout ($ApoE^{-/-}$)

mice, which spontaneously develop atherosclerotic lesions resembling those in humans evolving over time from initial fatty streaks. To explore the role of NE in this process we crossed $ApoE^{-/-}$ mice with $NE^{-/-}$ mice. Though the data we have collected from these studies is only preliminary, it would appear that $ApoE^{-/-}$ mice develop considerably smaller atherosclerotic plaques in the aortic root in the absence of NE (data unpublished). This is consistent with a reduced accumulation of lesional monocytes, to be verified in subsequent histological analyses, and supports our hypothesis that NE facilitates monocyte transendothelial migration, certainly in response to CCL2 whose expression is pronounced in atherosclerotic lesions (Barlic and Murphy, 2007).

Though we are keen to further evaluate the pathophysiology of ApoE/NE double knock-out mice, we similarly recognise the need to conduct additional studies with pharmacological NE inhibitors. To date, almost all of our functional data relating to NE has been generated using NE KO mice, which ultimately offer limited clinical relevance. Furthermore, and as regularly reported in the literature, genetic and pharmacological means of intervention do not always yield similar results. For example, atherosclerotic lesions are reduced in CCL2- and CCR2-deficient mice, however are unaffected upon treatment with a small molecule CCR2 antagonist, despite it demonstrating efficacy in several models of inflammation (Aiello et al., 2010). In the context of NE, a number of specific inhibitors exist, some of which have already been experimented with in this study, though only fleetingly. Additional studies will have to be conducted to determine more conclusively whether these inhibitors can abate monocyte transmigration in mice. In this regard, we initially plan to administer an NE inhibitor in combination with CCL2 into the ears of WT mice. It will be interesting to determine if the majority of monocytes become stuck in the vasculature, as observed in NE KO mice. Thereafter, we may also determine whether blocking NE activity has a significant effect on advanced atherosclerotic lesions or the progression of fatty streaks in ApoE KO mice.

### *7.3 Wider implications*

In deepening our understanding of monocyte trafficking in experimental mouse models, we ultimately hope to inspire innovative new ways to manipulate monocyte trafficking in humans. In this context, while enhancing targeted monocyte migration may be useful for the treatment of various cancers and infectious diseases, the ability to selectively

inhibit monocyte recruitment could revolutionise the treatment of monocyte-driven inflammatory disorders, such as chronic liver disease, rheumatoid arthritis, HIV encephalitis, atherosclerosis, and cardiac infarction. Monocytes, and particularly classical monocytes, potentiate the immunopathology of these diseases by infiltrating inflamed tissues and secreting pro-inflammatory cytokines, proteases and other mediators, culminating in tissue damage, scarring, and in some instances even death. Current treatment programs are largely limited to broad-acting anti-inflammatory agents, many of which are associated with serious side effects arising as a result of their non-selective nature. While several existing therapies do target classical monocytes more specifically, their clinical potential has been limited by safety and efficacy concerns (Leuschner et al., 2011). A number of antagonists and inhibitors have for example been designed to disrupt CCR2/CCL2 signalling, the principal axis regulating classical monocyte trafficking, however the clinical application of these agents has been hampered by compensatory monocyte recruitment mechanisms (Zhao, 2010). In this light, while new therapeutic targets are clearly needed, we maintain belief that targeting monocyte recruitment directly represents a promising therapeutic avenue, not least because pharmacological inhibition of leukocyte migration has been previously demonstrated to be highly effective under a number of clinical disease conditions (Mackay, 2008). Moreover, by targeting cell recruitment, sessile monocytes/macrophages should remain largely unaffected.

In addition to the major monocyte-driven pathologies outlined above, targeting monocyte migration may also be therapeutically beneficial for those pathologies characterised by high NE activity. Elevated levels of secreted NE in the lungs for example is one of the hallmarks of chronic obstructive pulmonary disease. Naturally, the source of this NE has always been attributed to infiltrating neutrophils. COPD is however also associated with an increased pulmonary influx of monocytes, which we have robustly demonstrated to express the NE protein and which seemingly release it in great quantities during transmigration. In this light, inhibiting monocyte infiltration into the lungs might dramatically reduce quantities of secreted NE, which is considered to be one of the predominant causes of alveolar destruction in COPD (Ohbayashi, 2002).

Whether secreted NE contributes to disease progression or not, we believe abating monocyte recruitment by disrupting NE activity represents an exciting and novel therapeutic approach for monocyte-mediated pathologies. In this context, while several

small molecule NE-inhibitors have been clinically developed, predominantly for respiratory diseases such as COPD, the majority have failed in early clinical trials because of poor pharmacokinetics and a low therapeutic index. Even Sivelestat (ONO-5046), which is widely used in Japan for the treatment of acute lung injury, has never been convincingly demonstrated to possess high clinical efficacy (Iwata et al., 2010). Though we are keen to re-evalaute the effectiveness of some of these existing compounds directly as monocyte inhibitors, as an alternative approach we also recognise the potential of targeting NE at the transcript level using siRNA. Certainly, this may be preferable as many protein inhibitors are reportedly ineffective against NE sequestered on the cell surface. In addition, considering we detected significantly greater quantitites of NE transcript in monocytes, it is conceivable that using siRNA will affect these cells more specifically while leaving the anti-microbial functions of neutrophils, which turn off NE transcription upon maturation, largely uncompromised. Off-target effects could be minimised furtherstill by incorporating monocyte-optimised siRNA delivery technologies, which have recently been demonstrated to silence CCR2 expression in classical monocytes in a number of mouse disease models (Leuschner et al., 2011).

In theory, interrupting classical monocyte migration represents a particularly efficient therapeutic strategy because it removes this destructive cell population from the inflammatory site rather than neutralising a single causative gene product. One potential caveat to this approach however is that upon inhibition the monocytes would presumably accumulate in the vasculature. Certainly, this was observed for $NE^{-/-}$ monocytes in our ear inflammation model, and was similarly observed for $NE^{-/-}$ neutrophils in a murine model of ventilator-induced lung injury (Kaynar et al., 2008). Importantly, this study showed that in the absence of NE whilst significantly fewer neutrophils were successfully recruited to the alveolar space, rather than confering protection, these mice actually developed worse parameters of acute lung injury than WT controls. This was attributed to a prolonged interaction between neutrophils, with their arsenal of proteases and reactive oxygen species, and the vasscular endothelium leading to local endothelial injury and increased permeabilty. In this light, we are keen to determine whether the retention of monocytes within the vasculature also induces an acute injurious effect. Certainly, this would be of considerable clinical relevance for

atherosclerosis, in which endothelial dysfunction contributes significantly to the initiation and progression of disease.

Whilst developing new potential therapeutics constitutes the overriding motivation for our ongoing research, considering our work on NE is still very much in its infancy we recognise that this is not likely to be realised soon, if at all. Currently our data are limited to acute models of inflammation, which have already demonstrated tissue specificty and have yet to be corroborated in more complex disease models. Even so, induced models of animal disease are usually not wholly representative of human patients. Atherosclerotic plaques in ApoE KO mice for example do not typically rupture and thus develop the thrombo-embolisms characteristic of human cardiovascular disease (Ohayon et al., 2012). Indeed, despite being the most commonly used animal model in research, many questions have been raised about the reliability of mice as models for human diseases, not least because of the long list of prospective drugs that worked well in mice but turned out to be ineffective in patient trials (Seok et al., 2013). Regarding this study more specifically, we firmly acknowledge that the monocyte profiles of mice and humans differ in several aspects. Monocytes constitute approximately 10% of total blood leukocytes in humans but only 4% in mice. Of these, 90% belong to the classical subset in humans while classical and non-classical monocytes are roughly evenly represented in mice. Discrepencies have also been reported in gene expression patterns and effector functions. For example, whereas human classical monocytes produce the immunoregulatory cytokine IL-10 in response to LPS *in vitro*, the equivalent cells from mice produce pro-inflammatory cytokines, including TNF-α and IL-1 (Soehnlein and Lindbom, 2010). Regarding monocyte behaviour *in vivo*, due to restrictions on experimentation considerably less is known for humans making it onerous to interpret, and ultimately translate, results from mouse or indeed other animal models. In this light, while we are committed to further characterising the mechanisms of monocyte migration in mice, we hope and urge for complementary studies to be conducted in patients and human tissue samples.

### *7.4 Conclusion*

In conclusion, our study is the first to characterise NE expression in murine classical monocytes. Furthermore, we have implicated NE as a regulator of classical monocyte recruitment in response to CCL2 in peritonitis and ear models of acute inflammation.

More specifically, NE appears to facilitate the initiating stages of monocyte transendothelial migration, seemingly by being released extracellularly, though its precise mode of action is still to be clarified. These results, whilst requiring further validation in murine disease models and ultimately patient samples, implicate NE as a novel and inclusive therapeutic target for monocyte-driven pathologies.

# References


Adkison, A.M., Raptis, S.Z., Kelley, D.G., Pham, C.T.N., 2002. Dipeptidyl peptidase I activates neutrophil-derived serine proteases and regulates the development of acute experimental arthritis. J. Clin. Invest. 109, 363–71.

Aiello, R.J., Perry, B.D., Bourassa, P.-A., Robertson, A., Weng, W., Knight, D.R., Smith, A.H., Frederick, K.S., Kalgutkar, A., Gladue, R.P., 2010. CCR2 receptor blockade alters blood monocyte subpopulations but does not affect atherosclerotic lesions in apoE(-/-) mice. Atherosclerosis 208, 370–5.

Aird, W.C., 2012. Endothelial cell heterogeneity. Cold Spring Harb. Perspect. Med. 2, a006429.

Akira, S., Uematsu, S., Takeuchi, O., 2006. Pathogen recognition and innate immunity. Cell 124, 783–801.

Allport, J.R., Lim, Y.-C., Shipley, J.M., Senior, R.M., Shapiro, S.D., Matsuyoshi, N., Vestweber, D., Luscinskas, F.W., 2002. Neutrophils from MMP-9- or neutrophil elastase-deficient mice show no defect in transendothelial migration under flow in vitro. J. Leukoc. Biol. 71, 821–8.

Al-Numani, D., Segura, M., Doré, M., Gottschalk, M., 2003. Up-regulation of ICAM-1, CD11a/CD18 and CD11c/CD18 on human THP-1 monocytes stimulated by Streptococcus suis serotype 2. Clin. Exp. Immunol. 133, 67–77.

Alon, R., Hammer, D.A., Springer, T.A., 1995. Lifetime of the P-selectin-carbohydrate bond and its response to tensile force in hydrodynamic flow. Nature 374, 539–42.

Arnold, L., Henry, A., Poron, F., Baba-Amer, Y., van Rooijen, N., Plonquet, A., Gherardi, R.K., Chazaud, B., 2007. Inflammatory monocytes recruited after skeletal muscle injury switch into antiinflammatory macrophages to support myogenesis. J. Exp. Med. 204, 1057–69.

Auffray, C., Fogg, D., Garfa, M., Elain, G., Join-Lambert, O., Kayal, S., Sarnacki, S., Cumano, A., Lauvau, G., Geissmann, F., 2007. Monitoring of blood vessels and tissues by a population of monocytes with patrolling behavior. Science 317, 666–70.

Auffray, C., Sieweke, M.H., Geissmann, F., 2009. Blood monocytes: development, heterogeneity, and relationship with dendritic cells. Annu. Rev. Immunol. 27, 669–92.

Bachelerie F., Ben-Baruch A., Burkhardt A.M., Combadiere C., Farber J.M., Graham G.J., Horuk R., Sparre-Ulrich A.H., Locati M., Luster A.D., Mantovani A., Matsushima K., Murphy P.M., Nibbs R., Nomiyama H., Power C.A., Proudfoot A.E., Rosenkilde M.M., Rot A., Sozzani S., Thelen M., Yoshie O., Zlotnik A., 2013. Update on the extended family of chemokine receptors and introducing a new nomenclature for atypical chemokine receptors. Pharmacol Rev. 66. 1–79.

Barlic, J., Murphy, P.M., 2007. Chemokine regulation of atherosclerosis. J. Leukoc. Biol. 82, 226–36.

Barrick, B., Campbell, E., 1999. Leukocyte proteinases in wound healing: roles in physiologic and pathologic processes. Wound Repair and 410–422.

Barth, M.W., Hendrzak, J.A., Melnicoff, M.J., Morahan, P.S., 1995. Review of the macrophage disappearance reaction. J. Leukoc. Biol. 57, 361–7.

Bédard, M., McClure, C.D., Schiller, N.L., Francoeur, C., Cantin, A., Denis, M., 1993. Release of interleukin-8, interleukin-6, and colony-stimulating factors by upper airway epithelial cells: implications for cystic fibrosis. Am. J. Respir. Cell Mol. Biol. 9, 455–62.

Belaaouaj, A., McCarthy, R., Baumann, M., Gao, Z., 1998. Mice lacking neutrophil elastase reveal impaired host defense against gram negative bacterial sepsis. Nat. Med.

Benabid, R., Wartelle, J., Malleret, L., Guyot, N., Gangloff, S., Lebargy, F., Belaaouaj, A., 2012. Neutrophil Elastase Modulates Cytokine Expression: CONTRIBUTION TO HOST DEFENSE AGAINST PSEUDOMONAS AERUGINOSA-INDUCED PNEUMONIA. J. Biol. Chem. 287, 34883–94.

Bradfield, P.F., Scheiermann, C., Nourshargh, S., Ody, C., Luscinskas, F.W., Rainger, G.E., Nash, G.B., Miljkovic-Licina, M., Aurrand-Lions, M., Imhof, B. a, 2007. JAM-C regulates unidirectional monocyte transendothelial migration in inflammation. Blood 110, 2545–55.

Cai, T.Q., Wright, S.D., 1996. Human leukocyte elastase is an endogenous ligand for the integrin CR3 (CD11b/CD18, Mac-1, alpha M beta 2) and modulates polymorphonuclear leukocyte adhesion. J. Exp. Med. 184, 1213–23.

Calderwood, D.A., 2004. Integrin activation. J. Cell Sci. 117, 657–66.

Campbell, E.J., Owen, C.A., 2007. The sulfate groups of chondroitin sulfate- and heparan sulfate-containing proteoglycans in neutrophil plasma membranes are novel binding sites for human leukocyte elastase and cathepsin G. J. Biol. Chem. 282, 14645–54.

Carlin, L.M., Stamatiades, E.G., Auffray, C., Hanna, R.N., Glover, L., Vizcay-Barrena, G., Hedrick, C.C., Cook, H.T., Diebold, S., Geissmann, F., 2013. Nr4a1-dependent Ly6C(low) monocytes monitor endothelial cells and orchestrate their disposal. Cell 153, 362–75.

Carman, C. V, Springer, T.A., 2004. A transmigratory cup in leukocyte diapedesis both through individual vascular endothelial cells and between them. J. Cell Biol. 167, 377–88.

Cepinskas, G., Sandig, M., Kvietys, P.R., 1999. PAF-induced elastase-dependent neutrophil transendothelial migration is associated with the mobilization of elastase

to the neutrophil surface and localization to the migrating front. J. Cell Sci. 112 Pt 1, 1937–45.

Charo, I.F., Taub, R., 2011. Anti-inflammatory therapeutics for the treatment of atherosclerosis. Nat. Rev. Drug Discov. 10, 365–76.

Chen, C.-N., Chang, S.-F., Lee, P.-L., Chang, K., Chen, L.-J., Usami, S., Chien, S., Chiu, J.-J., 2006. Neutrophils, lymphocytes, and monocytes exhibit diverse behaviors in transendothelial and subendothelial migrations under coculture with smooth muscle cells in disturbed flow. Blood 107, 1933–42.

Chua, F., Laurent, G.J., 2006. Neutrophil elastase: mediator of extracellular matrix destruction and accumulation. Proc. Am. Thorac. Soc. 3, 424–7.

Combadière, C., Potteaux, S., Gao, J.-L., Esposito, B., Casanova, S., Lee, E.J., Debré, P., Tedgui, A., Murphy, P.M., Mallat, Z., 2003. Decreased atherosclerotic lesion formation in CX3CR1/apolipoprotein E double knockout mice. Circulation 107, 1009–16.

Combadière, C., Potteaux, S., Rodero, M., Simon, T., Pezard, A., Esposito, B., Merval, R., Proudfoot, A., Tedgui, A., Mallat, Z., 2008. Combined inhibition of CCL2, CX3CR1, and CCR5 abrogates Ly6C(hi) and Ly6C(lo) monocytosis and almost abolishes atherosclerosis in hypercholesterolemic mice. Circulation 117, 1649–57.

Corada, M., Chimenti, S., Cera, M.R., Vinci, M., Salio, M., Fiordaliso, F., De Angelis, N., Villa, A., Bossi, M., Staszewsky, L.I., Vecchi, A., Parazzoli, D., Motoike, T., Latini, R., Dejana, E., 2005. Junctional adhesion molecule-A-deficient polymorphonuclear cells show reduced diapedesis in peritonitis and heart ischemia-reperfusion injury. Proc. Natl. Acad. Sci. U. S. A. 102, 10634–9.

Cybulsky, M.I., Iiyama, K., Li, H., Zhu, S., Chen, M., Iiyama, M., Davis, V., Gutierrez-Ramos, J.C., Connelly, P.W., Milstone, D.S., 2001. A major role for VCAM-1, but not ICAM-1, in early atherosclerosis. J. Clin. Invest. 107, 1255–62.

Dale, D.C., Boxer, L., Liles, W.C., 2008. The phagocytes: neutrophils and monocytes. Blood 112, 935–45.

Dangerfield, J., Larbi, K.Y., Huang, M.-T., Dewar, A., Nourshargh, S., 2002. PECAM-1 (CD31) homophilic interaction up-regulates alpha6beta1 on transmigrated neutrophils in vivo and plays a functional role in the ability of alpha6 integrins to mediate leukocyte migration through the perivascular basement membrane. J. Exp. Med. 196, 1201–11.

Delacourt, C., Hérigault, S., Delclaux, C., Poncin, A., Levame, M., Harf, A., Saudubray, F., Lafuma, C., 2002. Protection against acute lung injury by intravenous or intratracheal pretreatment with EPI-HNE-4, a new potent neutrophil elastase inhibitor. Am. J. Respir. Cell Mol. Biol. 26, 290–7.

Delclaux, C., Delacourt, C., D'Ortho, M.P., Boyer, V., Lafuma, C., Harf, A., 1996. Role of gelatinase B and elastase in human polymorphonuclear neutrophil migration across basement membrane. Am. J. Respir. Cell Mol. Biol. 14, 288–95.

DeVol, R., Bedroussian, A., 2007. An unhealthy America: The economic burden of chronic disease. Santa Monica, CA. Milken Institute. Available at: http://www.milkeninstitute.org/

Doherty, N.S., Griffiths, R.J., Hakkinen, J.P., Scampoli, D.N., Milici, A.J., 1995. Post-capillary venules in the "milky spots" of the greater omentum are the major site of plasma protein and leukocyte extravasation in rodent models of peritonitis. Inflamm. Res. 44, 169–77.

Dollery, C.M., Owen, C. a, Sukhova, G.K., Krettek, A., Shapiro, S.D., Libby, P., 2003. Neutrophil elastase in human atherosclerotic plaques: production by macrophages. Circulation 107, 2829–36.

Domínguez, P.M., Ardavín, C., 2010. Differentiation and function of mouse monocyte-derived dendritic cells in steady state and inflammation. Immunol. Rev. 234, 90–104.

Dong, Z.M., Brown, A.A., Wagner, D.D., 2000. Prominent role of P-selectin in the development of advanced atherosclerosis in ApoE-deficient mice. Circulation 101, 2290–5.

Dunne, J.L., Ballantyne, C.M., Beaudet, A.L., Ley, K., 2002. Control of leukocyte rolling velocity in TNF-alpha-induced inflammation by LFA-1 and Mac-1. Blood 99, 336–41.

Dupasquier, M., Stoitzner, P., van Oudenaren, A., Romani, N., Leenen, P.J.M., 2004. Macrophages and dendritic cells constitute a major subpopulation of cells in the mouse dermis. J. Invest. Dermatol. 123, 876–9.

Edwards, S.W., 2005. Biochemistry and Physiology of the Neutrophil. Cambridge University Press.

Elsaid, K.A., Jay, G.D., Chichester, C.O., 2003. Detection of collagen type II and proteoglycans in the synovial fluids of patients diagnosed with non-infectious knee joint synovitis indicates early damage to the articular cartilage matrix. Osteoarthritis Cartilage 11, 673–80.

Evani, S.J., Dallo, S.F., Murthy, A.K., Ramasubramanian, A.K., 2013. Shear Stress Enhances Chemokine Secretion from Chlamydia pneumoniae-infected Monocytes. Cell. Mol. Bioeng. 6, 326–334.

Faust, N., Varas, F., Kelly, L.M., Heck, S., Graf, T., 2000. Insertion of enhanced green fluorescent protein into the lysozyme gene creates mice with green fluorescent granulocytes and macrophages. Blood 96, 719–26.

Fitzpatrick, F.A., 2001. Inflammation, carcinogenesis and cancer. Int. Immunopharmacol. 1, 1651–67.

Garcia, R., Gusmani, L., Murgia, R., Guarnaccia, C., Cinco, M., Rottini, G., 1998. Elastase is the only human neutrophil granule protein that alone is responsible for in vitro killing of Borrelia burgdorferi. Infect. Immun. 66, 1408–12.

Gautier, E.L., Jakubzick, C., Randolph, G.J., 2009. Regulation of the migration and survival of monocyte subsets by chemokine receptors and its relevance to atherosclerosis. Arterioscler. Thromb. Vasc. Biol. 29, 1412–8.

Geissmann, F., Jung, S., Littman, D.R., 2003. Blood monocytes consist of two principal subsets with distinct migratory properties. Immunity 19, 71–82.

Gerszten, R.E., Lim, Y.C., Ding, H.T., Snapp, K., Kansas, G., Dichek, D.A., Cabañas, C., Sánchez-Madrid, F., Gimbrone, M.A., Rosenzweig, A., Luscinskas, F.W., 1998. Adhesion of monocytes to vascular cell adhesion molecule-1-transduced human endothelial cells: implications for atherogenesis. Circ. Res. 82, 871–8.

Grage-Griebenow, E., Flad, H.-D., Ernst, M., 2001. Heterogeneity of human peripheral blood monocyte subsets. J. Leukoc. Biol. 69, 11–20.

Halai, K., Whiteford, J., Ma, B., Nourshargh, S., Woodfin, A., 2014. ICAM-2 facilitates luminal interactions between neutrophils and endothelial cells in vivo. J. Cell Sci. 127, 620–9.

Heck, L.W., Blackburn, W.D., Irwin, M.H., Abrahamson, D.R., 1990. Degradation of basement membrane laminin by human neutrophil elastase and cathepsin G. Am. J. Pathol. 136, 1267–74.

Henderson, R.B., Hobbs, J. a R., Mathies, M., Hogg, N., 2003. Rapid recruitment of inflammatory monocytes is independent of neutrophil migration. Blood 102, 328–35.

Henriksen, P. a, Sallenave, J.-M., 2008. Human neutrophil elastase: mediator and therapeutic target in atherosclerosis. Int. J. Biochem. Cell Biol. 40, 1095–100.

Hillyer, P., Mordelet, E., Flynn, G., Male, D., 2003. Chemokines, chemokine receptors and adhesion molecules on different human endothelia: discriminating the tissue-specific functions that affect leucocyte migration. Clin. Exp. Immunol. 134, 431–441.

Hirche, T.O., Atkinson, J.J., Bahr, S., Belaaouaj, A., 2004. Deficiency in neutrophil elastase does not impair neutrophil recruitment to inflamed sites. Am. J. Respir. Cell Mol. Biol. 30, 576–84.

Horwitz, M., Benson, K.F., Duan, Z., Li, F.-Q., Person, R.E., 2004. Hereditary neutropenia: dogs explain human neutrophil elastase mutations. Trends Mol. Med. 10, 163–70.

Horwitz, M., Duan, Z., Korkmaz, B., Lee, H.-H., Mealiffe, M.E., Salipante, S.J., 2007. Neutrophil elastase in cyclic and severe congenital neutropenia. Blood 109, 1817–24.

Huang, M.-T., Larbi, K.Y., Scheiermann, C., Woodfin, A., Gerwin, N., Haskard, D.O., Nourshargh, S., 2006. ICAM-2 mediates neutrophil transmigration in vivo: evidence for stimulus specificity and a role in PECAM-1-independent transmigration. Blood 107, 4721–7.

Huber, A.R., Weiss, S.J., 1989. Disruption of the subendothelial basement membrane during neutrophil diapedesis in an in vitro construct of a blood vessel wall. J. Clin. Invest. 83, 1122–36.

Imai, T., Hieshima, K., Haskell, C., Baba, M., Nagira, M., Nishimura, M., Kakizaki, M., Takagi, S., Nomiyama, H., Schall, T.J., Yoshie, O., 1997. Identification and Molecular Characterization of Fractalkine Receptor CX3CR1, which Mediates Both Leukocyte Migration and Adhesion. Cell 91, 521–530.

Ingersoll, M., Platt, A.M., Potteaux, S., Randolph, G.J., 2011. Monocyte trafficking in acute and chronic inflammation. Trends Immunol. 32, 470–7.

Ingersoll, M., Spanbroek, R., Lottaz, C., Gautier, E.L., Frankenberger, M., Hoffmann, R., Lang, R., Haniffa, M., Collin, M., Tacke, F., Habenicht, A.J.R., Ziegler-Heitbrock, L., Randolph, G.J., 2010. Comparison of gene expression profiles between human and mouse monocyte subsets. Blood 115, e10–9.

Ishihara, K., Yamaguchi, Y., Okabe, K., Ogawa, M., 1999. Neutrophil elastase enhances macrophage production of chemokines in receptor-mediated reaction. Res. Commun. Mol. Pathol. Pharmacol. 103, 139–47.

Iwata, K., Doi, A., Ohji, G., Oka, H., Oba, Y., Takimoto, K., Igarashi, W., Gremillion, D.H., Shimada, T., 2010. Effect of neutrophil elastase inhibitor (sivelestat sodium) in the treatment of acute lung injury (ALI) and acute respiratory distress syndrome (ARDS): a systematic review and meta-analysis. Intern. Med. 49, 2423–32.

Jakubzick, C., Tacke, F., Ginhoux, F., Wagers, A.J., van Rooijen, N., Mack, M., Merad, M., Randolph, G.J., 2008. Blood monocyte subsets differentially give rise to CD103+ and CD103- pulmonary dendritic cell populations. J. Immunol. 180, 3019–27.

Janoff, A., Scherer, J., 1968. Mediators of inflammation in leukocyte lysosomes. IX. Elastinolytic activity in granules of human polymorphonuclear leukocytes. J. Exp. Med. 128, 1137–55.

Jung, S., Aliberti, J., Graemmel, P., 2000. Analysis of fractalkine receptor CX3CR1 function by targeted deletion and green fluorescent protein reporter gene insertion. Mol. Cell. Biol. 20, 4106–4114.

Jung, U., Ley, K., 1999. Mice lacking two or all three selectins demonstrate overlapping and distinct functions for each selectin. J. Immunol. 162, 6755–62.

Kargi, H.A., Campbell, E.J., Kuhn, C., 1990. Elastase and cathepsin G of human monocytes: heterogeneity and subcellular localization to peroxidase-positive granules. J. Histochem. Cytochem. 38, 1179–86.

Kawanaka, N., Yamamura, M., Aita, T., Morita, Y., Okamoto, A., Kawashima, M., Iwahashi, M., Ueno, A., Ohmoto, Y., Makino, H., 2002. CD14+,CD16+ blood monocytes and joint inflammation in rheumatoid arthritis. Arthritis Rheum. 46, 2578–86.

Kaynar, A.M., Houghton, A.M., Lum, E.H., Pitt, B.R., Shapiro, S.D., 2008. Neutrophil elastase is needed for neutrophil emigration into lungs in ventilator-induced lung injury. Am. J. Respir. Cell Mol. Biol. 39, 53–60.

Keiper, T., Al-Fakhri, N., Chavakis, E., Athanasopoulos, A.N., Isermann, B., Herzog, S., Saffrich, R., Hersemeyer, K., Bohle, R.M., Haendeler, J., Preissner, K.T., Santoso, S., Chavakis, T., 2005. The role of junctional adhesion molecule-C (JAM-C) in oxidized LDL-mediated leukocyte recruitment. FASEB J. 19, 2078–80.

Kolaczkowska, E., Grzybek, W., van Rooijen, N., Piccard, H., Plytycz, B., Arnold, B., Opdenakker, G., 2009. Neutrophil elastase activity compensates for a genetic lack of matrix metalloproteinase-9 (MMP-9) in leukocyte infiltration in a model of experimental peritonitis. J. Leukoc. Biol. 85, 374–81.

Korkmaz, B., Horwitz, M., Jenne, D., Gauthier, F., 2010. Neutrophil elastase, proteinase 3, and cathepsin G as therapeutic targets in human diseases. Pharmacol. Rev. 62, 726–759.

Kumar, V., Abbas, A.K., Fausto, N., Aster, J.C., 2010. Robbins and Cotran: Pathologic Basis of Disease., Eighth edi. ed. Elsevier Inc., Philadelphia.

Lamagna, C., Meda, P., Mandicourt, G., Brown, J., Gilbert, R.J.C., Jones, E.Y., Kiefer, F., Ruga, P., Imhof, B.A., Aurrand-Lions, M., 2005. Dual interaction of JAM-C with JAM-B and alpha(M)beta2 integrin: function in junctional complexes and leukocyte adhesion. Mol. Biol. Cell 16, 4992–5003.

Laszik, Z., Jansen, P.J., Cummings, R.D., Tedder, T.F., McEver, R.P., Moore, K.L., 1996. P-selectin glycoprotein ligand-1 is broadly expressed in cells of myeloid, lymphoid, and dendritic lineage and in some nonhematopoietic cells. Blood 88, 3010–21.

Lemansky, P., Smolenova, E., Wrocklage, C., Hasilik, A., 2007. Neutrophil elastase is associated with serglycin on its way to lysosomes in U937 cells. Cell. Immunol. 246, 1–7.

Leuschner, F., Dutta, P., Gorbatov, R., Novobrantseva, T.I., Donahoe, J.S., Courties, G., Lee, K.M., Kim, J.I., Markmann, J.F., Marinelli, B., Panizzi, P., Lee, W.W., Iwamoto, Y., Milstein, S., Epstein-Barash, H., Cantley, W., Wong, J., Cortez-Retamozo, V., Newton, A., Love, K., Libby, P., Pittet, M.J., Swirski, F.K., Koteliansky, V., Langer, R., Weissleder, R., Anderson, D.G., Nahrendorf, M.,

2011. Therapeutic siRNA silencing in inflammatory monocytes in mice. Nat. Biotechnol. 29, 1005–10.

Ley, K., Laudanna, C., Cybulsky, M.I., Nourshargh, S., 2007. Getting to the site of inflammation: the leukocyte adhesion cascade updated. Nat. Rev. Immunol. 7, 678–89.

Li, J.L., Goh, C.C., Keeble, J.L., Qin, J.S., Roediger, B., Jain, R., Wang, Y., Chew, W.K., Weninger, W., Ng, L.G., 2012. Intravital multiphoton imaging of immune responses in the mouse ear skin. Nat. Protoc. 7, 221–34.

Li, L., Huang, L., Sung, S., Vergis, A., 2008. The chemokine receptors CCR2 and CX3CR1 mediate monocyte/macrophage trafficking in kidney ischemia–reperfusion injury. Kidney Int. 74, 1526–1537.

Liau, D.F., Yin, N.X., Ryan, S.F., 1993. Isolation of human polymorphonuclear leukocyte elastase by chromatography on immobilized benzamidine. Prep. Biochem. 23, 439–47.

Lin, L., Betsuyaku, T., Heimbach, L., Li, N., Rubenstein, D., Shapiro, S.D., An, L., Giudice, G.J., Diaz, L.A., Senior, R.M., Liu, Z., 2012. Neutrophil elastase cleaves the murine hemidesmosomal protein BP180/type XVII collagen and generates degradation products that modulate experimental bullous pemphigoid. Matrix Biol. 31, 38–44.

Liu, L., Cara, D.C., Kaur, J., Raharjo, E., Mullaly, S.C., Jongstra-Bilen, J., Jongstra, J., Kubes, P., 2005. LSP1 is an endothelial gatekeeper of leukocyte transendothelial migration. J. Exp. Med. 201, 409–18.

Lloyd-Jones, D., Adams, R.J., Brown, T.M., Carnethon, M., Dai, S., De Simone, G., Ferguson, T.B., Ford, E., Furie, K., Gillespie, C., Go, A., Greenlund, K., Haase, N., Hailpern, S., Ho, P.M., Howard, V., Kissela, B., Kittner, S., Lackland, D., Lisabeth, L., Marelli, A., McDermott, M.M., Meigs, J., Mozaffarian, D., Mussolino, M., Nichol, G., Roger, V.L., Rosamond, W., Sacco, R., Sorlie, P., Stafford, R., Thom, T., Wasserthiel-Smoller, S., Wong, N.D., Wylie-Rosett, J., 2010. Executive summary: heart disease and stroke statistics--2010 update: a report from the American Heart Association. Circulation 121, 948–54.

López-Boado, Y.S., Espinola, M., Bahr, S., Belaaouaj, A., 2004. Neutrophil serine proteinases cleave bacterial flagellin, abrogating its host response-inducing activity. J. Immunol. 172, 509–15.

Lucas, S.D., Costa, E., Guedes, R.C., Moreira, R., 2013. Targeting COPD: advances on low-molecular-weight inhibitors of human neutrophil elastase. Med. Res. Rev. 33 Suppl 1, E73–101.

Macdonald, S.J.., Dowle, M.D., Harrison, L.A., Shah, P., Johnson, M.R., Inglis, G.G.., Clarke, G.D.., Smith, R.A., Humphreys, D., Molloy, C.R., Amour, A., Dixon, M., Murkitt, G., Godward, R.E., Padfield, T., Skarzynski, T., Singh, O.M.., Kumar, K.A., Fleetwood, G., Hodgson, S.T., Hardy, G.W., Finch, H., 2001. The discovery

of a potent, intracellular, orally bioavailable, long duration inhibitor of human neutrophil elastase—GW311616A a development candidate. Bioorg. Med. Chem. Lett. 11, 895–898.

Mackarel, A.J., Cottell, D.C., Russell, K.J., FitzGerald, M.X., O'Connor, C.M., 1999. Migration of neutrophils across human pulmonary endothelial cells is not blocked by matrix metalloproteinase or serine protease inhibitors. Am. J. Respir. Cell Mol. Biol. 20, 1209–19.

Mackay, C.R., 2008. Moving targets: cell migration inhibitors as new anti-inflammatory therapies. Nat. Immunol. 9, 988–98.

Martin, W.J., Shaw, O., Liu, X., Steiger, S., Harper, J.L., 2011. Monosodium urate monohydrate crystal-recruited noninflammatory monocytes differentiate into M1-like proinflammatory macrophages in a peritoneal murine model of gout. Arthritis Rheum. 63, 1322–32.

Massena, S., Christoffersson, G., Hjertström, E., Zcharia, E., Vlodavsky, I., Ausmees, N., Rolny, C., Li, J.-P., Phillipson, M., 2010. A chemotactic gradient sequestered on endothelial heparan sulfate induces directional intraluminal crawling of neutrophils. Blood 116, 1924–31.

Medzhitov, R., 2008. Origin and physiological roles of inflammation. Nature 454, 428–35.

Melan, M.A., 1999. Overview of cell fixatives and cell membrane permeants. Methods Mol. Biol. 115, 45–55.

Metzler, K.D., Goosmann, C., Lubojemska, A., Zychlinsky, A., Papayannopoulos, V., 2014. A Myeloperoxidase-Containing Complex Regulates Neutrophil Elastase Release and Actin Dynamics during NETosis. Cell Rep. 8, 883–896.

Mihara, K., Ramachandran, R., Renaux, B., Saifeddine, M., Hollenberg, M.D., 2013. Neutrophil elastase and proteinase-3 trigger G protein-biased signaling through proteinase-activated receptor-1 (PAR1). J. Biol. Chem. 288, 32979–90.

Mitchell, M.J., King, M.R., 2012. Shear-induced resistance to neutrophil activation via the formyl peptide receptor. Biophys. J. 102, 1804–14.

Mogensen, T.H., 2009. Pathogen recognition and inflammatory signaling in innate immune defenses. Clin. Microbiol. Rev. 22, 240–73, Table of Contents.

Mouse Mutant Resource, The Jackson Laboratory, Bar Harbor, Maine. World Wide Web (http://mousemutant.jax.org/). Strain no. 006112, B6;129X1-Elanetm1Sds /J. (Oct, 2012).

Muller, W.A, 2013. Getting leukocytes to the site of inflammation. Vet. Pathol. Online 50, 7–22.

Muller, W.A, 2011. Mechanisms of leukocyte transendothelial migration. Annu. Rev. Pathol. 6, 323–44.

Muller, W.A., 2001. Migration of leukocytes across endothelial junctions: some concepts and controversies. Microcirculation 8, 181–93.

Muller, W.A., 2014. How endothelial cells regulate transmigration of leukocytes in the inflammatory response. Am. J. Pathol. 184, 886–96.

Muller, W.A., Luscinskas, F.W., 2008. Assays of transendothelial migration in vitro. Methods Enzymol. 443, 155–76.

Muller, W.A., Weigl, S.A., Deng, X., Phillips, D.M., 1993. PECAM-1 is required for transendothelial migration of leukocytes. J. Exp. Med. 178, 449–60.

Mydel, P., Shipley, J.M., Adair-Kirk, T.L., Kelley, D.G., Broekelmann, T.J., Mecham, R.P., Senior, R.M., 2008. Neutrophil elastase cleaves laminin-332 (laminin-5) generating peptides that are chemotactic for neutrophils. J. Biol. Chem. 283, 9513–22.

Nahrendorf, M., Swirski, F.K., Aikawa, E., Stangenberg, L., Wurdinger, T., Figueiredo, J.-L., Libby, P., Weissleder, R., Pittet, M.J., 2007. The healing myocardium sequentially mobilizes two monocyte subsets with divergent and complementary functions. J. Exp. Med. 204, 3037–47.

Newton, K., Dixit, V.M., 2012. Signaling in innate immunity and inflammation. Cold Spring Harb. Perspect. Biol. 4.

Newton, R.A., Hogg, N., 1998. The human S100 protein MRP-14 is a novel activator of the beta 2 integrin Mac-1 on neutrophils. J. Immunol. 160, 1427–35.

Nourshargh, S., Hordijk, P.L., Sixt, M., 2010. Breaching multiple barriers: leukocyte motility through venular walls and the interstitium. Nat. Rev. Mol. Cell Biol. 11, 366–78.

Nozawa, F., Hirota, M., Okabe, A., Shibata, M., Iwamura, T., Haga, Y., Ogawa, M., 2000. Elastase activity enhances the adhesion of neutrophil and cancer cells to vascular endothelial cells. J. Surg. Res. 94, 153–8.

Ohayon, J., Mesnier, N., Broisat, A., Toczek, J., Riou, L., Tracqui, P., 2012. Elucidating atherosclerotic vulnerable plaque rupture by modeling cross substitution of ApoE-/- mouse and human plaque components stiffnesses. Biomech. Model. Mechanobiol. 11, 801–13.

Ohbayashi, H., 2002. Neutrophil elastase inhibitors as treatment for COPD. Expert Opin. Investig. Drugs 11, 965–80.

Owen, C.A., Campbell, M.A., Boukedes, S.S., Campbell, E.J., 1997. Cytokines regulate membrane-bound leukocyte elastase on neutrophils: a novel mechanism for effector activity. Am. J. Physiol. 272, L385–93.

Owen, C.A., Campbell, M.A., Boukedes, S.S., Stockley, R.A., Campbell, E.J., 1994. A discrete subpopulation of human monocytes expresses a neutrophil-like proinflammatory (P) phenotype. Am. J. Physiol. 267, L775–85.

Owen, C.A., Campbell, M.A., Sannes, P.L., Boukedes, S.S., Campbell, E.J., 1995. Cell surface-bound elastase and cathepsin G on human neutrophils: a novel, non-oxidative mechanism by which neutrophils focus and preserve catalytic activity of serine proteinases. J. Cell Biol. 131, 775–89.

Papayannopoulos, V., Metzler, K.D., Hakkim, A., Zychlinsky, A., 2010. Neutrophil elastase and myeloperoxidase regulate the formation of neutrophil extracellular traps. J. Cell Biol. 191, 677–91.

Pham, C.T.N., 2006. Neutrophil serine proteases: specific regulators of inflammation. Nat. Rev. Immunol. 6, 541–50.

Phillipson, M., Heit, B., Colarusso, P., Liu, L., Ballantyne, C.M., Kubes, P., 2006. Intraluminal crawling of neutrophils to emigration sites: a molecularly distinct process from adhesion in the recruitment cascade. J. Exp. Med. 203, 2569–75.

Proebstl, D., Voisin, M.-B., Woodfin, A., Whiteford, J., D'Acquisto, F., Jones, G.E., Rowe, D., Nourshargh, S., 2012. Pericytes support neutrophil subendothelial cell crawling and breaching of venular walls in vivo. J. Exp. Med. 209, 1219–34.

Proudfoot, A.E.I., Handel, T.M., Johnson, Z., Lau, E.K., LiWang, P., Clark-Lewis, I., Borlat, F., Wells, T.N.C., Kosco-Vilbois, M.H., 2003. Glycosaminoglycan binding and oligomerization are essential for the in vivo activity of certain chemokines. Proc. Natl. Acad. Sci. U. S. A. 100, 1885–90.

Rainger, G.E., Rowley, A.F., Nash, G.B., 1998. Adhesion-dependent release of elastase from human neutrophils in a novel, flow-based model: specificity of different chemotactic agents. Blood 92, 4819–27.

Randolph, G.J., Furie, M.B., 1996. Mononuclear phagocytes egress from an in vitro model of the vascular wall by migrating across endothelium in the basal to apical direction: role of intercellular adhesion molecule 1 and the CD11/CD18 integrins. J. Exp. Med. 183, 451–462.

Randolph, G.J., Sanchez-Schmitz, G., Liebman, R.M., Schakel, K., 2002. The CD16+ (Fc RIII+) Subset of Human Monocytes Preferentially Becomes Migratory Dendritic Cells in a Model Tissue Setting. J. Exp. Med. 196, 517–527.

Rao, R.M., Betz, T. V, Lamont, D.J., Kim, M.B., Shaw, S.K., Froio, R.M., Baleux, F., Arenzana-Seisdedos, F., Alon, R., Luscinskas, F.W., 2004. Elastase release by transmigrating neutrophils deactivates endothelial-bound SDF-1alpha and attenuates subsequent T lymphocyte transendothelial migration. J. Exp. Med. 200, 713–24.

Rivier, A., Pène, J., Rabesandratana, H., Chanez, P., Bousquet, J., Campbell, A.M., 1995. Blood monocytes of untreated asthmatics exhibit some features of tissue macrophages. Clin. Exp. Immunol. 100, 314–8.

Robbins, C.S., Chudnovskiy, A., Rauch, P.J., Figueiredo, J.-L., Iwamoto, Y., Gorbatov, R., Etzrodt, M., Weber, G.F., Ueno, T., van Rooijen, N., Mulligan-Kehoe, M.J., Libby, P., Nahrendorf, M., Pittet, M.J., Weissleder, R., Swirski, F.K., 2012. Extramedullary hematopoiesis generates Ly-6C(high) monocytes that infiltrate atherosclerotic lesions. Circulation 125, 364–74.

Robbins, C.S., Swirski, F.K., 2010. The multiple roles of monocyte subsets in steady state and inflammation. Cell. Mol. Life Sci. 67, 2685–93.

Rose, S., Misharin, A., Perlman, H., 2012. A novel Ly6C/Ly6G-based strategy to analyze the mouse splenic myeloid compartment. Cytometry. A 81, 343–50.

Sadahira, Y., Akisada, K., Sugihara, T., Hata, S., Uehira, K., Muraki, N., Manabe, T., 2001. Comparative ultrastructural study of cytotoxic granules in nasal natural killer cell lymphoma, intestinal T-cell lymphoma, and anaplastic large cell lymphoma. Virchows Arch. 438, 280–8.

Sadallah, S., Hess, C., Miot, S., Spertini, O., Lutz, H., Schifferli, J.A., 1999. Elastase and metalloproteinase activities regulate soluble complement receptor 1 release. Eur. J. Immunol. 29, 3754–61.

Sasmono, R.T., Oceandy, D., Pollard, J.W., Tong, W., Pavli, P., Wainwright, B.J., Ostrowski, M.C., Himes, S.R., Hume, D.A., 2003. A macrophage colony-stimulating factor receptor-green fluorescent protein transgene is expressed throughout the mononuclear phagocyte system of the mouse. Blood 101, 1155–63.

Sato, T., Takahashi, S., Mizumoto, T., Harao, M., Akizuki, M., Takasugi, M., Fukutomi, T., Yamashita, J., 2006. Neutrophil elastase and cancer. Surg. Oncol. 15, 217–22.

Schenkel, A.R., Mamdouh, Z., Chen, X., Liebman, R.M., Muller, W.A., 2002. CD99 plays a major role in the migration of monocytes through endothelial junctions. Nat. Immunol. 3, 143–50.

Schenkel, A.R., Mamdouh, Z., Muller, W. a, 2004. Locomotion of monocytes on endothelium is a critical step during extravasation. Nat. Immunol. 5, 393–400.

Scotland, R.S., Stables, M.J., Madalli, S., Watson, P., Gilroy, D.W., 2011. Sex differences in resident immune cell phenotype underlie more efficient acute inflammatory responses in female mice. Blood 118, 5918–27.

Senior, R.M., Griffin, G.L., Mecham, R.P., 1980. Chemotactic activity of elastin-derived peptides. J. Clin. Invest. 66, 859–62.

Seok, J., Warren, H.S., Cuenca, A.G., Mindrinos, M.N., Baker, H. V, Xu, W., Richards, D.R., McDonald-Smith, G.P., Gao, H., Hennessy, L., Finnerty, C.C., López, C.M.,

Honari, S., Moore, E.E., Minei, J.P., Cuschieri, J., Bankey, P.E., Johnson, J.L., Sperry, J., Nathens, A.B., Billiar, T.R., West, M.A., Jeschke, M.G., Klein, M.B., Gamelli, R.L., Gibran, N.S., Brownstein, B.H., Miller-Graziano, C., Calvano, S.E., Mason, P.H., Cobb, J.P., Rahme, L.G., Lowry, S.F., Maier, R. V, Moldawer, L.L., Herndon, D.N., Davis, R.W., Xiao, W., Tompkins, R.G., 2013. Genomic responses in mouse models poorly mimic human inflammatory diseases. Proc. Natl. Acad. Sci. U. S. A. 110, 3507–12.

Serbina, N.V, Jia, T., Hohl, T.M., Pamer, E.G., 2008. Monocyte-mediated defense against microbial pathogens. Annu. Rev. Immunol. 26, 421–52.

Serbina, N.V, Pamer, E.G., 2006. Monocyte emigration from bone marrow during bacterial infection requires signals mediated by chemokine receptor CCR2. Nat. Immunol. 7, 311–7.

Serhan, C.N., Chiang, N., Van Dyke, T.E., 2008. Resolving inflammation: dual anti-inflammatory and pro-resolution lipid mediators. Nat. Rev. Immunol. 8, 349–61.

Serhan, C.N., Savill, J., 2005. Resolution of inflammation: the beginning programs the end. Nat. Immunol. 6, 1191–7.

Shapiro, S.D., Goldstein, N.M., Houghton, a M., Kobayashi, D.K., Kelley, D., Belaaouaj, A., 2003. Neutrophil elastase contributes to cigarette smoke-induced emphysema in mice. Am. J. Pathol. 163, 2329–35.

Shi, C., Pamer, E.G., 2011. Monocyte recruitment during infection and inflammation. Nat. Rev. Immunol. 11, 762–74.

Si-Tahar, M., Pidard, D., Balloy, V., Moniatte, M., Kieffer, N., Van Dorsselaer, A., Chignard, M., 1997. Human neutrophil elastase proteolytically activates the platelet integrin alphaIIbbeta3 through cleavage of the carboxyl terminus of the alphaIIb subunit heavy chain. Involvement in the potentiation of platelet aggregation. J. Biol. Chem. 272, 11636–47.

Soehnlein, O., Lindbom, L., 2010. Phagocyte partnership during the onset and resolution of inflammation. Nat. Rev. Immunol. 10, 427–39.

Soehnlein, O., Zernecke, A., Eriksson, E.E., Rothfuchs, A.G., Pham, C.T., Herwald, H., Bidzhekov, K., Rottenberg, M.E., Weber, C., Lindbom, L., 2008. Neutrophil secretion products pave the way for inflammatory monocytes. Blood 112, 1461–71.

Springer, T.A., 1994. Traffic signals for lymphocyte recirculation and leukocyte emigration: the multistep paradigm. Cell 76, 301–14.

Sunderkötter, C., Nikolic, T., Dillon, M.J., Van Rooijen, N., Stehling, M., Drevets, D. a, Leenen, P.J.M., 2004. Subpopulations of mouse blood monocytes differ in maturation stage and inflammatory response. J. Immunol. 172, 4410–7.

Swirski, F.K., Libby, P., Aikawa, E., Alcaide, P., Luscinskas, F.W., Weissleder, R., Pittet, M.J., 2007. Ly-6Chi monocytes dominate hypercholesterolemia-associated monocytosis and give rise to macrophages in atheromata. J. Clin. Invest. 117, 195–205.

Swirski, F.K., Nahrendorf, M., Etzrodt, M., Wildgruber, M., Cortez-Retamozo, V., Panizzi, P., Figueiredo, J.-L., Kohler, R.H., Chudnovskiy, A., Waterman, P., Aikawa, E., Mempel, T.R., Libby, P., Weissleder, R., Pittet, M.J., 2009a. Identification of splenic reservoir monocytes and their deployment to inflammatory sites. Science 325, 612–6.

Swirski, F.K., Weissleder, R., Pittet, M.J., 2009b. Heterogeneous in vivo behavior of monocyte subsets in atherosclerosis. Arterioscler. Thromb. Vasc. Biol. 29, 1424–32.

Tacke, F., Alvarez, D., Kaplan, T., 2007. Monocyte subsets differentially employ CCR2, CCR5, and CX3CR1 to accumulate within atherosclerotic plaques. J. Clin. Invest. 117.

Tang, J., Zarbock, A., Gomez, I., Wilson, C.L., Lefort, C.T., Stadtmann, A., Bell, B., Huang, L.-C., Ley, K., Raines, E.W., 2011. Adam17-dependent shedding limits early neutrophil influx but does not alter early monocyte recruitment to inflammatory sites. Blood 118, 786–94.

Tedder, T.F., Steeber, D.A., Pizcueta, P., 1995. L-selectin-deficient mice have impaired leukocyte recruitment into inflammatory sites. J. Exp. Med. 181, 2259–64.

Tkalcevic, J., Novelli, M., Phylactides, M., Iredale, J.P., Segal, A.W., Roes, J., 2000. Impaired Immunity and Enhanced Resistance to Endotoxin in the Absence of Neutrophil Elastase and Cathepsin G. Immunity 12, 201–210.

Tsou, C.-L., Peters, W., Si, Y., Slaymaker, S., Aslanian, A.M., Weisberg, S.P., Mack, M., Charo, I.F., 2007. Critical roles for CCR2 and MCP-3 in monocyte mobilization from bone marrow and recruitment to inflammatory sites. J. Clin. Invest. 117, 902–9.

Valledor, A.F., Borràs, F.E., Cullell-Young, M., Celada, A., 1998. Transcription factors that regulate monocyte/macrophage differentiation. J. Leukoc. Biol. 63, 405–17.

Van der Laan, A.M., Ter Horst, E.N., Delewi, R., Begieneman, M.P. V, Krijnen, P.A.J., Hirsch, A., Lavaei, M., Nahrendorf, M., Horrevoets, A.J., Niessen, H.W.M., Piek, J.J., 2014. Monocyte subset accumulation in the human heart following acute myocardial infarction and the role of the spleen as monocyte reservoir. Eur. Heart J. 35, 376–85.

Voisin, M.-B., Pröbstl, D., Nourshargh, S., 2010. Venular basement membranes ubiquitously express matrix protein low-expression regions: characterization in multiple tissues and remodeling during inflammation. Am. J. Pathol. 176, 482–95.

Voisin, M.-B., Woodfin, A., Nourshargh, S., 2009. Monocytes and neutrophils exhibit both distinct and common mechanisms in penetrating the vascular basement membrane in vivo. Arterioscler. Thromb. Vasc. Biol. 29, 1193–9.

Wang, S., Cao, C., Chen, Z., Bankaitis, V., Tzima, E., Sheibani, N., Burridge, K., 2012. Pericytes regulate vascular basement membrane remodeling and govern neutrophil extravasation during inflammation. PLoS One 7, e45499.

Wang, S., Dangerfield, J., 2005. PECAM-1, alpha6 integrins and neutrophil elastase cooperate in mediating neutrophil transmigration. J. Cell Sci. 118, 2067–76.

Wang, S., Voisin, M.-B., Larbi, K.Y., Dangerfield, J., Scheiermann, C., Tran, M., Maxwell, P.H., Sorokin, L., Nourshargh, S., 2006. Venular basement membranes contain specific matrix protein low expression regions that act as exit points for emigrating neutrophils. J. Exp. Med. 203, 1519–32.

Weber, C., Noels, H., 2011. Atherosclerosis: current pathogenesis and therapeutic options. Nat. Med. 17, 1410–22.

Weinrauch, Y., Drujan, D., Shapiro, S.D., Weiss, J., Zychlinsky, A., 2002. Neutrophil elastase targets virulence factors of enterobacteria. Nature 417, 91–4.

Weninger, W., Biro, M., Jain, R., 2014. Leukocyte migration in the interstitial space of non-lymphoid organs. Nat. Rev. Immunol. 14, 232–46.

Wiedow, O., Muhle, K., Streit, V., Kameyoshi, Y., 1996. Human eosinophils lack human leukocyte elastase. Biochim. Biophys. Acta 1315, 185–7.

Wiesner, O., Litwiller, R.D., Hummel, A.M., Viss, M.A., McDonald, C.J., Jenne, D.E., Fass, D.N., Specks, U., 2005. Differences between human proteinase 3 and neutrophil elastase and their murine homologues are relevant for murine model experiments. FEBS Lett. 579, 5305–12.

Wittamer, V., Bondue, B., Guillabert, A., Vassart, G., Parmentier, M., Communi, D., 2005. Neutrophil-mediated maturation of chemerin: a link between innate and adaptive immunity. J. Immunol. 175, 487–93.

Wong, K.L., Tai, J.J.-Y., Wong, W.-C., Han, H., Sem, X., Yeap, W.-H., Kourilsky, P., Wong, S.-C., 2011. Gene expression profiling reveals the defining features of the classical, intermediate, and nonclassical human monocyte subsets. Blood 118, e16–31.

Woodfin, A., Voisin, M.-B., Beyrau, M., Colom, B., Caille, D., Diapouli, F.-M., Nash, G.B., Chavakis, T., Albelda, S.M., Rainger, G.E., Meda, P., Imhof, B. a, Nourshargh, S., 2011. The junctional adhesion molecule JAM-C regulates polarized transendothelial migration of neutrophils in vivo. Nat. Immunol. 12, 761–9.

Woodfin, A., Voisin, M.-B., Imhof, B.A., Dejana, E., Engelhardt, B., Nourshargh, S., 2009. Endothelial cell activation leads to neutrophil transmigration as supported by the sequential roles of ICAM-2, JAM-A, and PECAM-1. Blood 113, 6246–57.

Yang, J., Zhang, L., Yu, C., Yang, X.-F., Wang, H., 2014. Monocyte and macrophage differentiation: circulation inflammatory monocyte as biomarker for inflammatory diseases. Biomark. Res. 2, 1.

Young, R., Thompson, R., Larbi, K., 2004. Neutrophil elastase (NE)-deficient mice demonstrate a nonredundant role for NE in neutrophil migration, generation of proinflammatory mediators, and phagocytosis. J. Immunol. 172, 4493–502.

Young, R., Voisin, M.-B., Wang, S., Dangerfield, J., Nourshargh, S., 2007. Role of neutrophil elastase in LTB4-induced neutrophil transmigration in vivo assessed with a specific inhibitor and neutrophil elastase deficient mice. Br. J. Pharmacol. 151, 628–37.

Zhang, J., Alcaide, P., Liu, L., Sun, J., He, A., Luscinskas, F.W., Shi, G.-P., 2011. Regulation of endothelial cell adhesion molecule expression by mast cells, macrophages, and neutrophils. PLoS One 6, e14525.

Zhang, X., Zhan, D., Shin, H.Y., 2013. Integrin subtype-dependent CD18 cleavage under shear and its influence on leukocyte-platelet binding. J. Leukoc. Biol. 93, 251–8.

Zhao, Q., 2010. Dual targeting of CCR2 and CCR5: therapeutic potential for immunologic and cardiovascular diseases. J. Leukoc. Biol. 88, 41–55.

# Appendix

## CHAPTER 3:

**Appendix 3.1: Fluorophore selection guide for four-colour flow cytometry.**

| Channel | Excitation laser | Filter range (nm) | Fluorophores |
|---|---|---|---|
| FL1 (green) | Argon 488 | 515–545 | GFP/eGFP<br>Alexa Fluor® 488<br>Fluorescein (FITC) |
| FL2 (yellow) | Argon 488 | 564–606 | R-phycoerythrin (PE)<br>Alexa Fluor® 546/555<br>Cy3 |
| FL3 (red) | Argon 488 | ≥ 670 | 7-AAD<br>PE-Cy5<br>PE-Cy7 |
| FL4 (far-red) | He-Ne 635 | 656–667 | Alexa Fluor® 647<br>Allophycocyanin (APC) |

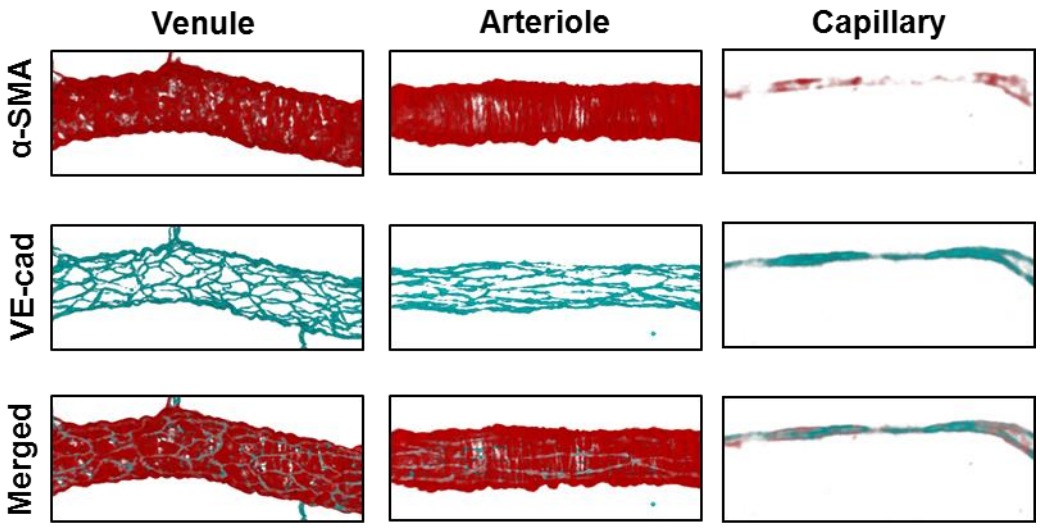


**Appendix 3.2: Morphological characteristics of blood vessels.** Representative confocal images of cremasteric venules, arterioles and capillaries, illustrating morphological differences in their endothelial junctions (VE-cadherin) and associated pericytes (α-SMA).

A) Murine NE:

ATGGCCCTTGGCAGACTATCCAGCCGGACTCTGGCTGCCATGCTACTGGCATTGTTCCTGGGTGGCCCAG
CACTGGCCTCAGAGATTGTTGGTGGCCGGCCGGCCCGGCCCCATGCTTGGCCCTTCATGGCATCCCTGCA
GAGGCGTGGAGGTCATTTCTGTGGTGCCACCCTCATTGCCAGGAACTTCGTCATGTCAGCAGCCCACTGT
GTGAACGGCCTAAATTTCCGGTCAGTGCAGGTAGTGCTGGGAGCCCATGACCTGCGGCGACAGGAGCGCA
CTCGACAGACCTTCTCTGTGCAGCGGATCTTCGAGAATGGCTTTGACCCATCACAACTGCTGAACGACAT
TGTGATTATCCAGCTCAATGGCTCCGCTACCATTAACGCCAACGTGCAGGTGGCCCAGCTGCCTGCCCAG
GGCCAGGGCGTGGGTGACAGAACTCCATGTCTGGCCATGGGCTGGGGCAGGTTGGGCACAAACAGACCAT
CACCCAGTGTGCTACAAGAGCTCAATGTGACAGTGGTGACTAACATGTGCCGCCGTCGTGTGAACGTATG
CACTCTGGTGCCACGTCGGCAGGCAGGCATCTGCTTCGGGGACTCTGGCGGACCCTTGGTCTGTAACAAC
CTTGTCCAAGGCATTGACTCCTTCATCCGAGGAGGCTGTGGATCTGGATTGTACCCAGATGCCTTCGCCC
CTGTGGCTGAGTTTGCAGATTGGATCAATTCCATTATCCGAAGCCATAATGACCACCTTCTTACCCATCC
CAAAGACCGAGAGGGCAGGACCAACTAG

B) Murine GAPDH:

ATGGTGAAGGTCGGTGTGAACGGATTTGGCCGTATTGGGCGCCTGGTCACCAGGGCTGCCATTTGCAGTGGCAAAGTG
GAGATTGTTGCCATCAACGACCCCTTCATTGACCTCAACTACATGGTCTACATGTTCCAGTATGACTCCACTCACGGCAAA
TTCAACGGCACAGTCAAGGCCGAGAATGGGAAGCTTGTCATCAACGGGAAGCCCATCACCATCTTCCAGGAGCGAGACC
CCACTAACATCAAATGGGGTGAGGCCGGTGCTGAGTATGTCGTGGAGTCTACTGGTGTCTTCACCACCATGGAGAAGGC
CGGGGCCCACTTGAAGGGTGGAGCCAAAAGGGTCATCATCTCCGCCCCTTCTGCCGATGCCCCCATGTTTGTGATGGGT
GTGAACCACGAGAAATATGACAACTCACTCAAGATTGTCAGCAATGCATCCTGCACCACCAACTGCTTAGCCCCCCTGGC
CAAGGTCATCCATGACAACTTTGGCATTGTGGAAGGGCTCATGACCACAGTCCATGCCATCACTGCCACCCAGAAGACTG
TGGATGGCCCCTCTGGAAAGCTGTGGCGTGATGGCCGTGGGGCTGCCCAGAACATCATCCCTGCATCCACTGGTGCTGC
CAAGGCTGTGGGCAAGGTCATCCCAGAGCTGAACGGGAAGCTCACTGGCATGGCCTTCCGTGTTCCTACCCCCAATGTG
TCCGTCGTGGATCTGACGTGCCGCCTGGAGAAACCTGCCAAGTATGATGACATCAAGAAGGTGGTGAAGCAGGCATCTG
AGGGCCCACTGAAGGGCATCTTGGGCTACACTGAGGACCAGGTTGTCTCCTGCGACTTCAACAGCAACTCCCACTCTTCC
ACCTTCGATGCCGGGGCTGGCATTGCTCTCAATGACAACTTTGTCAAGCTCATTTCCTGGTATGACAATGAATACGGCTAC
AGCAACAGGGTGGTGGACCTCATGGCCTACATGGCCTCCAAGGAGTAA

C) Murine cyclophilin:

ATGGTCAACCCCACCGTGTTCTTCGACATCACGGCCGATGACGAGCCCTTGGGCCGCGTCTCCTTCGAGCTGTTTGCAGA
CAAAGTTCCAAAGACAGCAGAAAACTTTCGAGCTCTGAGCACTGGAGAGAAAGGATTTGGCTATAAGGGTTCCTCCTTT
CACAGAATTATTCCAGGATTCATGTGCCAGGGTGGTGACTTTACACGCCATAATGGCACTGGCGGCAGGTCCATCTACG
GAGAGAAATTTGAGGATGAGAACTTCATCCTAAAGCATACAGGTCCTGGCATCTTGTCCATGGCAAATGCTGGACCAAA
CACAAACGGTTCCCAGTTTTTTATCTGCACTGCCAAGACTGAATGGCTGGATGGCAAGCATGTGGTCTTTGGGAAGGTGA
AAGAAGGCATGAACATTGTGGAAGCCATGGAGCGTTTTGGGTCCAGGAATGGCAAGACCAGCAAGAAGATCACCATTT
CCGACTGTGGACAGCTCTAA

**Appendix 3.3: qPCR primers used for mRNA quantification.** Coding sequences of transcripts for murine NE (access. no. NM_015779.2), GAPDH (access. no. M32599) and cyclophilin (access. no. M60456.1). Successive exons are differentiated by a change in text colour. The sequence regions used for PCR primer design are highlighted in green.

```
Mouse       malgr-lssrtlaamllalflggpalaseivggrparphawpfmaslqrrgghfcgatli
Human       mtlgrrlaclflacvlpalllggtalaseivggrrarphawpfmvslqlrgghfcgatli
            *:*** *:.  **.:* **:*** ********** *********.*** ***********

Mouse       arnfvmsaahcvnglnfrsvqvvlgahdlrrqertrqtfsvqrifengfdpsqllndivi
Human       apnfvmsaahcvanvnvravrvvlgahnlsrreptrqvfavqrifengydpvnllndivi
            * **********  :*.*:*:******:* *:* ***.*:********:** :*******

Mouse       iqlngsatinanvqvaqlpaqgqgvgdrtpclamgwgrlgtnrpspsvlqelnvtvvtnm
Human       lqlngsatinanvqvaqlpaqgrrlgngvqclamgwgllgrnrgiasvlqelnvtvvtsl
            :*********************: :*: . ******* ** **   ************.:

Mouse       crrrvnvctlvprrqagicfgdsggplvcnnlvqgidsfirggcgsglypdafapvaefa
Human       crr-snvctlvrgrqagvcfgdsgsplvcnglihgiasfvrggcasglypdafapvaqfv
            ***  ******  ****:******.***** *::** **:****.************:*.

Mouse       dwinsiirshndhllthpkdregrtn--
Human       nwidsiigrsednpcphprdpdpasrth
            :**:***:  :*.   **:* :  :.
```

**Appendix 3.4: Protein sequences for mouse and human NE.** Comparative analysis of mouse and human NE, demonstrating 73% amino acid homology. Our lab has previously raised an anti-murine NE antibody (SY0049) by immunising rabbits with a synthetic peptide analogous to residues 84-98 (highlighted in green) of the mouse NE protein. Alignment was made using Clustal Omega. (*) indicates positions which have a single, fully conserved residue. (:) indicates conservation between groups of strongly similar properties. (.) indicates conservation between groups of weakly similar properties.

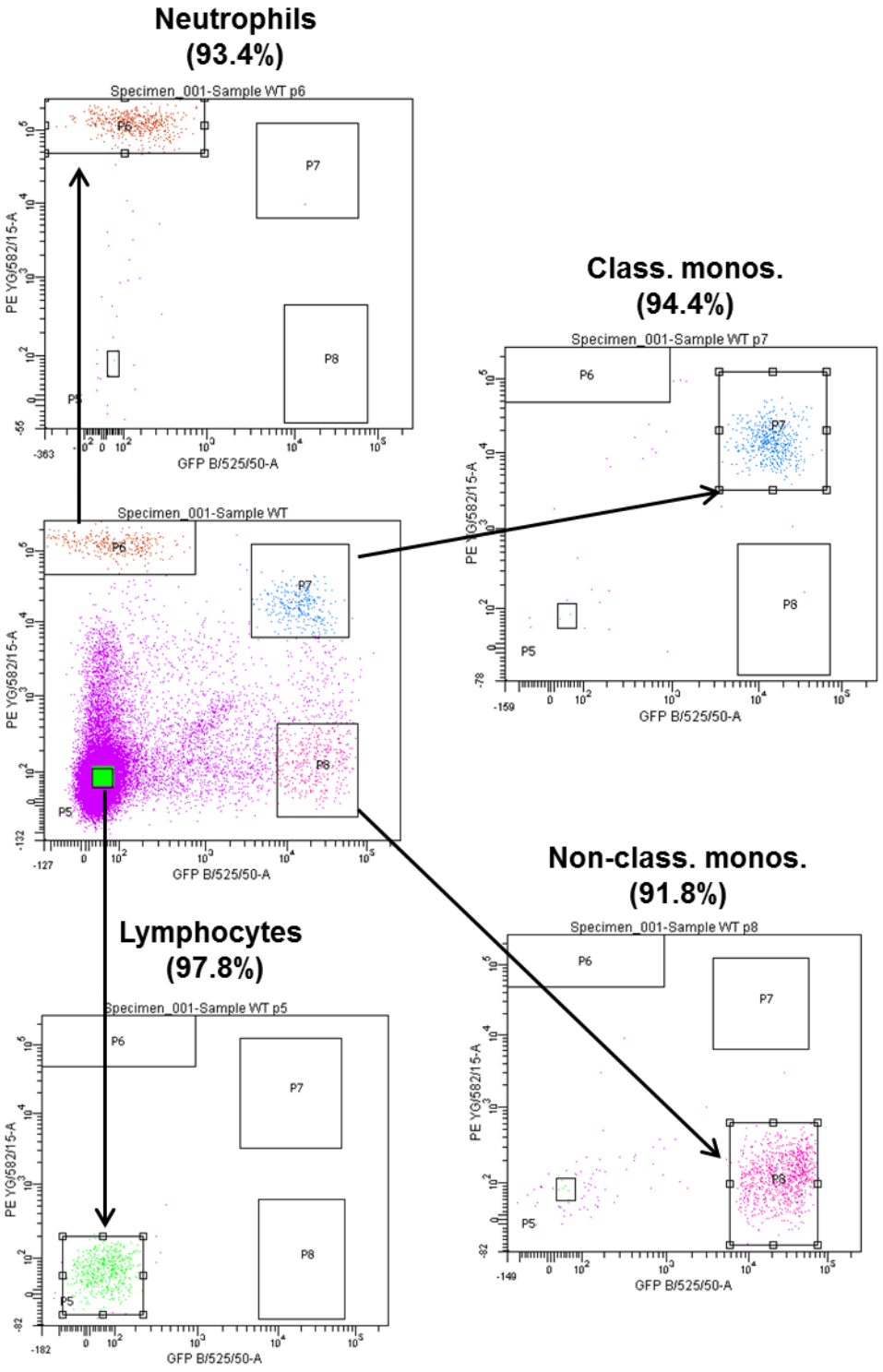


**Appendix 4.1: Enriching leukocyte populations by FACS-sorting.** Populations of classical monocytes, non-classical monocytes, neutrophils and lymphocytes were FACS-sorted from whole splenocytes according to GR-1 (y-axis) and $CX_3CR1$ (x-axis) expression. Upon completion, cell purities were established by re-running a small fraction of each sorted population through the cytometer (a representative sequence of runs is shown above). Purities are represented as the proportion of cells that fall within their original sort gates.

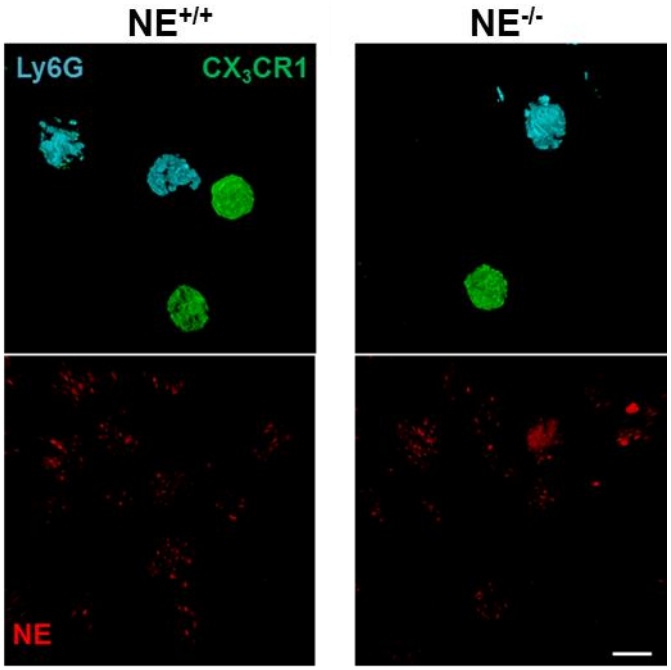


**Appendix 4.2: Non-specific labelling of NE in PFA-fixed leukocytes.** Whole BM leukocytes were harvested from $CX_3CR1^{+/eGFP}$ mice, seeded onto cover slips, fixed with 4% PFA and permeabilised with Triton X-100. The cells were subsequently immunostained for NE (red) and the neutrophil marker Ly6G (blue). $CX_3CR1\text{-}eGFP^{+}$ monocytes are shown in green. $NE^{-/-}$ leukocytes were used as a negative control but also stained 'positively' for NE. Scale bar, 5 µm.

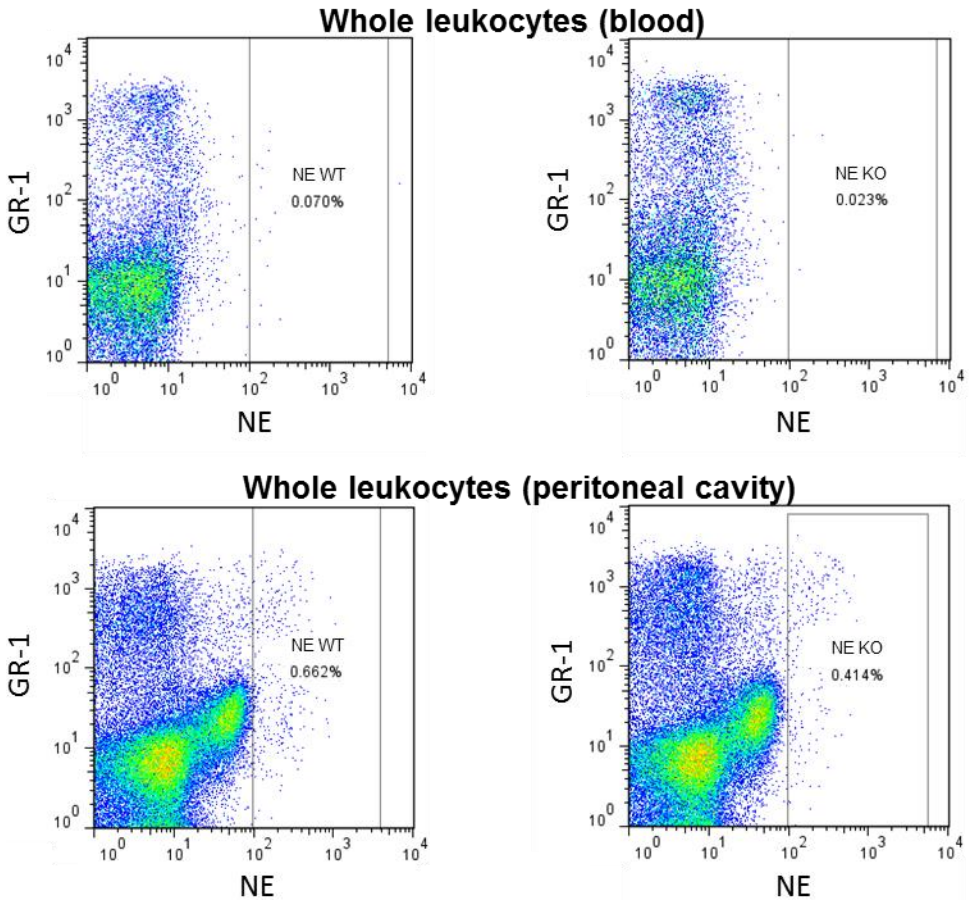

**Appendix 4.3: Assaying for NE protein expression by flow cytometry**. Whole leukocytes were harvested from the blood and peritoneal cavity of $CX_3CR1^{+/eGFP}$ mice stimulated i.p. for 4 hours with IFN-γ and TNF-α (300 ng/ml each). The cells were ACK-lysed, immunostained for NE, and analysed by flow cytometry. $NE^{+/+}$ and $NE^{-/-}$ leukocytes were directly compared.

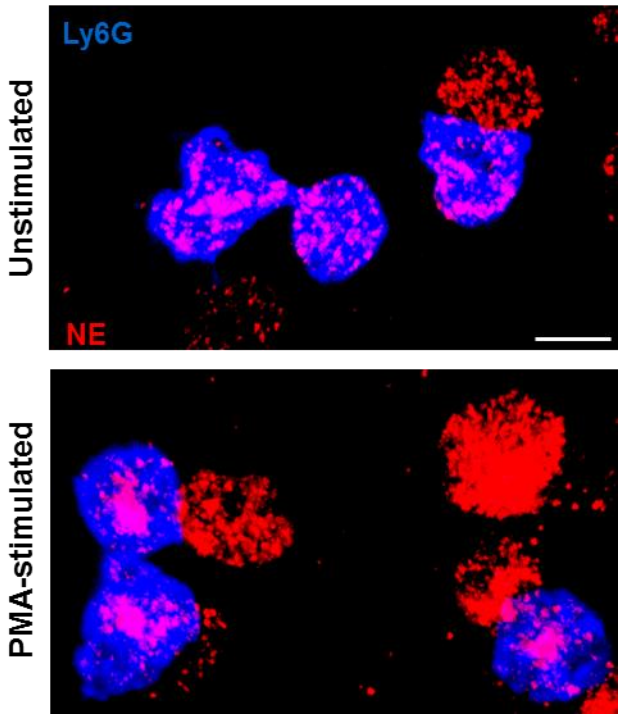


**Appendix 4.4: NE mobilises to the nucleus of neutrophils following PMA stimulation.** Whole bone marrow leukocytes harvested from $CX_3CR1^{+/eGFP}$ mice were stimulated in 12-well plates in 500 µl RPMI-1640 media supplemented with PMA (10 ng/ml) or vehicle (PBS). The cells were subsequently seeded onto coverslips, fixed/permeabilised with methanol, immunostained for NE (red) and the neutrophil marker Ly6G (blue) and analysed by confocal microscopy. Scale bar, 5 µm.

**CHAPTER 5:**

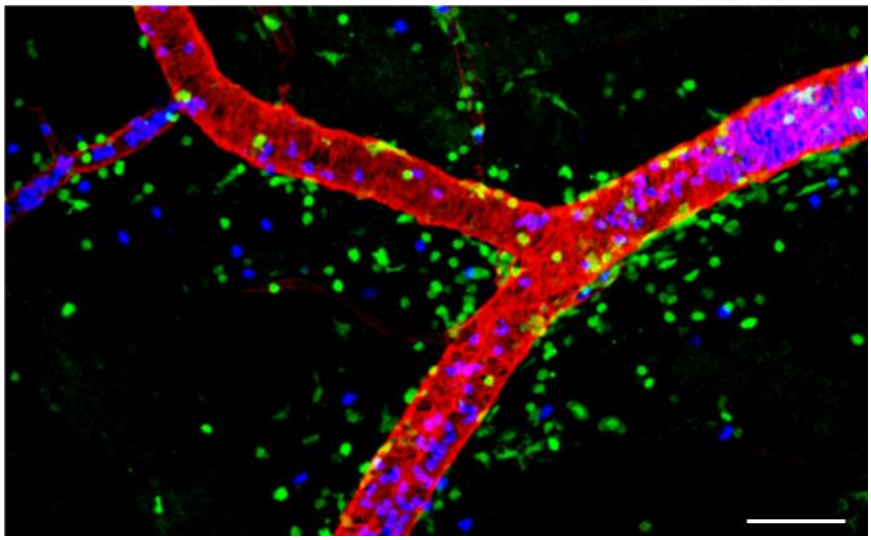

**Appendix 5.1: IFN-γ/TNF-α-induced monocyte transmigration in the cremaster muscle.** $CX_3CR1^{+/eGFP}$ mice were stimulated i.s. with IFN-γ (300 ng) for 16 hours and TNF-α (300 ng) for a further 4 hours, after which the cremaster muscles were harvested, fixed in PFA and immunostained for α-SMA (red) and MRP-14 (neutrophils, blue). Segments of post-capillary venules were subsequently analysed by confocal microscopy and reconstructed into virtual 3D models using Imaris software. Monocytes are shown in green. Scale bar, 100 μm. Image generated by Dr. Martina Beyrau.

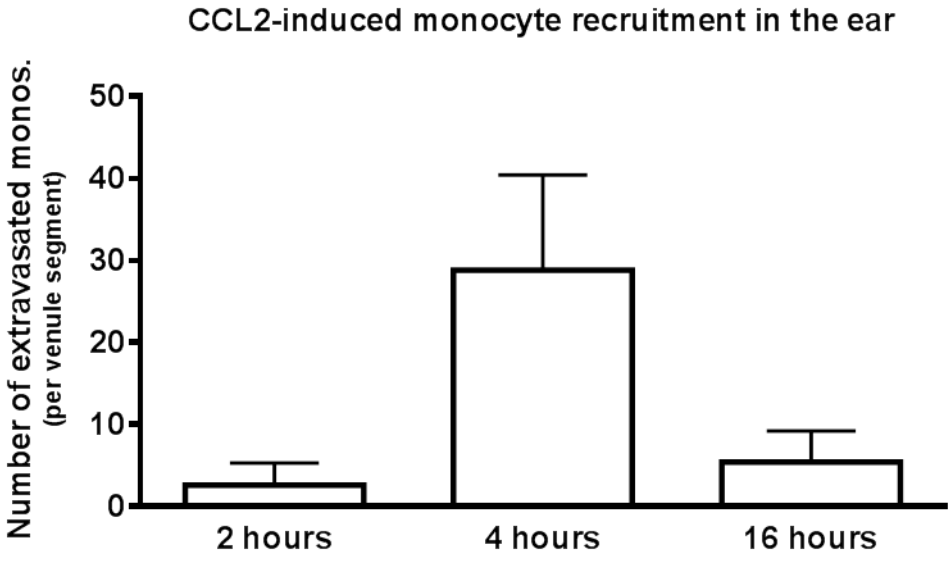


**Appendix 5.2: Time course of CCL2-induced monocyte transmigration in the ear dermis.** $NE^{+/+}$ $CX_3CR1^{+/eGFP}$ mice were stimulated i.d. with CCL2 (1 μg) for 2, 4 or 16 hours. Whole ears were subsequently harvested, the dorsal skin carefully separated and fixed in PFA, and immunostained for the EC junctional marker VE-cadherin. Segments of post-capillary venules were analysed by confocal microscopy and reconstructed into virtual 3D models using Imaris software. Total numbers of extravasated monocytes were counted for each venule. Data are represented as the mean ± SD (n = 6 separate venules from 1 mouse).

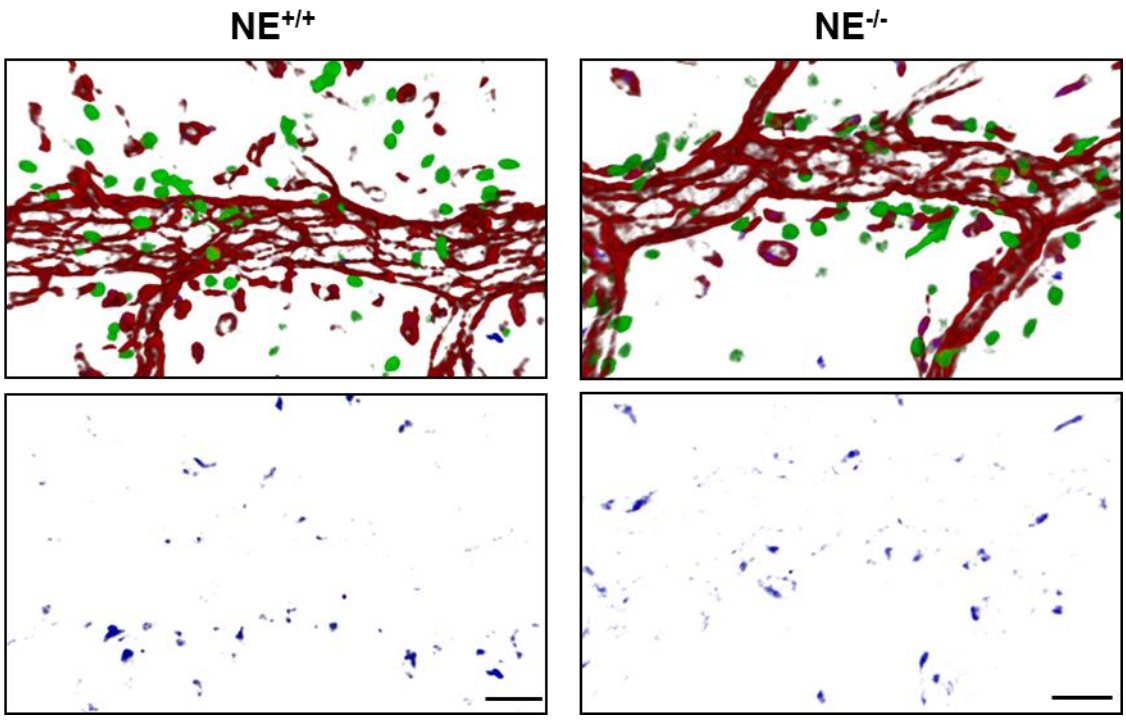


**Appendix 5.3: Assaying for NE activity in the cremaster muscle of $CX_3CR1$-eGFP-ki mice**. $NE^{+/+}$ and $NE^{-/-}$ $CX_3CR1^{+/eGFP}$ mice were administered Neutrophil Elastase 680 FAST (4 nmols in 200 µl PBS) i.v. immediately prior to administering $LTB_4$ (300 ng, supplemented with 2.5 µg Alexa Fluor 555–labelled mAb to PECAM-1, red) i.s. for 4 hours. The cremasters were harvested and fixed in PFA, after which segments of post-capillary venules were analysed by confocal microscopy and reconstructed into virtual 3D models using Imaris software. NE activity (blue) was determined by measuring the fluorescence intensity between 640-700 nm following excitation at 633 nm. Monocytes are shown in green. Scale bar, 30 µm.

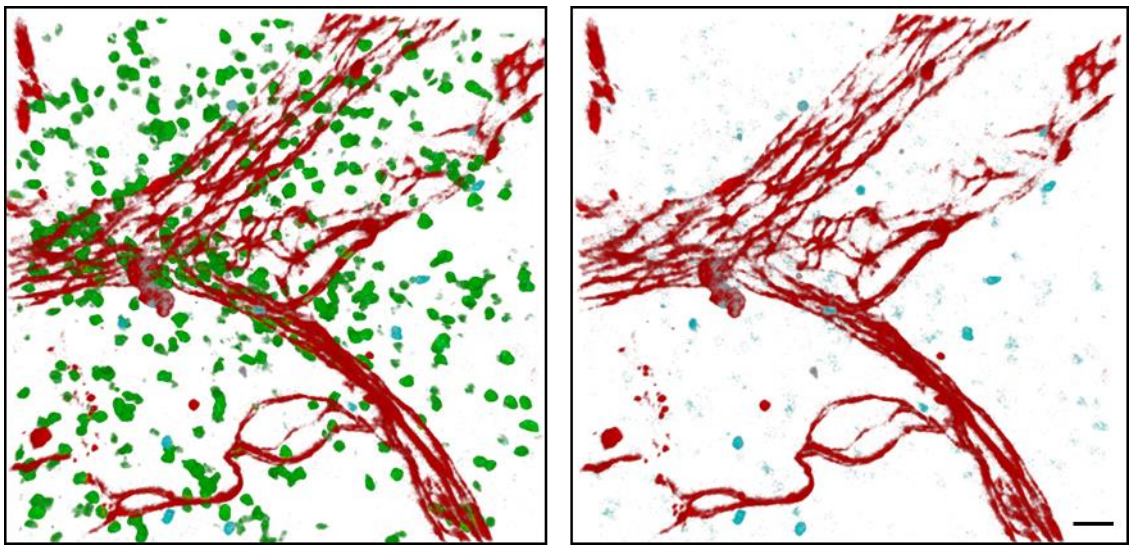

**Appendix 5.4: Assaying for NE activity in LysM-eGFP-ki mice *in situ*.** $LysM^{+/eGFP}$ mice exhibiting $eGFP^{+}$ neutrophils (green) were administered Neutrophil Elastase 680 FAST (4 nmols in 200 µl PBS) i.v. immediately prior to administering $LTB_4$ (300 ng in 30 µl PBS) i.d. for 4 hours. Whole ears were subsequently harvested, the dorsal skin carefully separated and fixed in PFA. Upon immunolabelling the vasculature (VE-cadherin, red), individual venule segments were analysed by confocal microscopy. NE activity (blue) was determined by measuring the fluorescence intensity between 640-700 nm following excitation at 633 nm. Scale bar, 30 µm.

**A**

**Summary of PCR primers used to amplify human NE.**

| Gene (reference) | Primer type | Primer name | Melting temp. | Sequence 5'→ 3' | Amplicon size (bp) |
|---|---|---|---|---|---|
| NE (Access. No. NM_001972 .2) | Forward | hNEfor | 56.1°C | CAC TGC GTG GCG AAT GTA AA | 162 |
| | Reverse | hNErev | 54.5°C | GAG CTG GAG AAT CAC GAT GT | |

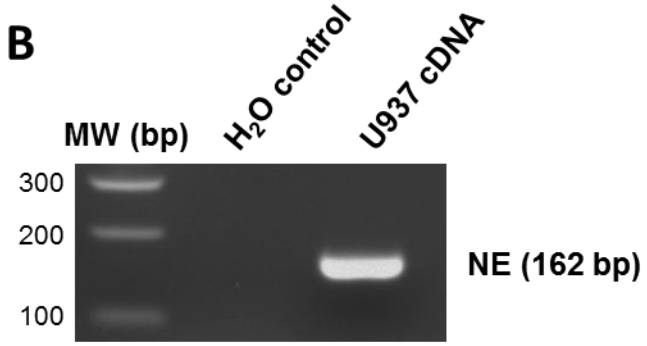


**Appendix 5.5: NE transcript is expressed in human U937 cells.** Total cellular RNA was extracted from U937 cells ($10^6$) and converted into cDNA. Conventional PCR was subsequently performed with primers specific for human NE (A). The same PCR cycling parameters and reaction mixtures were used as before for murine NE (*Tables 2.2* and *2.4*). PCR products were resolved on a 1.5% agarose gel (B). The $H_2O$ control contains no cDNA template.

**CHAPTER 6:**

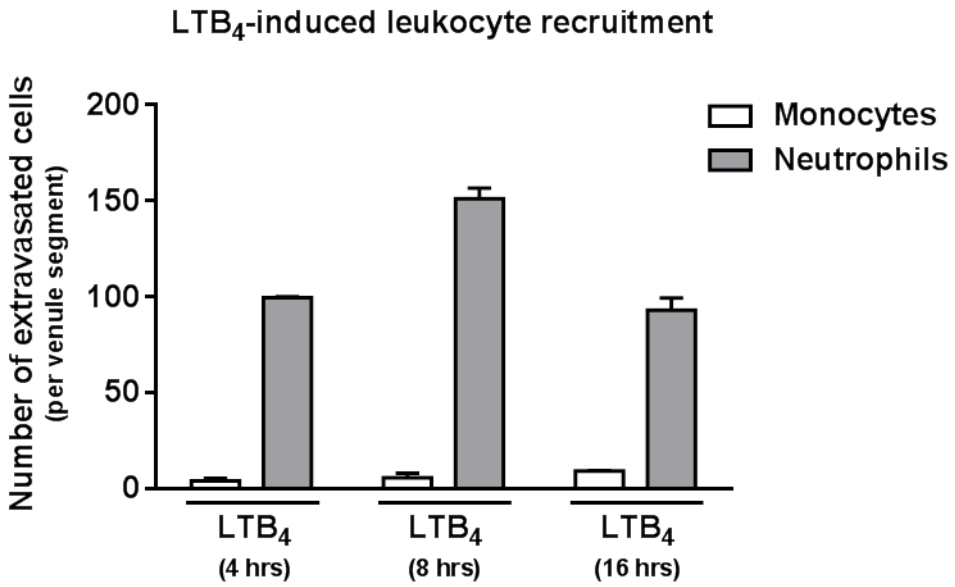


**Appendix 6.1: Characterisation of $LTB_4$-induced leukocyte transmigration in the ear dermis.** $NE^{+/+}$ $CX_3CR1^{+/eGFP}$ mice were stimulated i.d. with $LTB_4$ (300 ng) for 4, 8, or 16 hours, after which the whole ears were harvested, the dorsal skin carefully separated and fixed in PFA. Upon immunolabelling the vasculature (VE-cadherin) and neutrophils (MRP-14), total extravasated monocytes and neutrophils were counted in individual venule segments using confocal microscopy. Data are represented as the mean ± SEM (n = 2 mice, average of 5-6 venules per ear).

# Video Appendix

(N.B. videos are stored on accompanying USB stick)

**Video appendix 6.1: Normal monocyte transendothelial migration.** $CX_3CR1^{+/eGFP}$ mice were administered CCL2 (500 ng, supplemented with Alexa Fluor 555–labelled mAb to PECAM-1, red) i.s. for 2 hours. One cremaster muscle was subsequently exteriorised and superfused with CCL2 ($5\times10^{-9}$ M). Individual post-capillary venules were imaged for ~60 minutes by 4D confocal microscopy. Luminal monocytes (green, spherical) were observed crawling across the endothelium scanning for sites of transmigration. Once an optimal site was reached, the monocytes come to rest prior to squeezing their bodies through endothelial pores and into the abluminal space (yellow, flat) (A). TEM occurred principally by the paracellular pathway, i.e. by squeezing through pores in endothelial cell junctions (B). Original magnification, ×40. Cell of interest is denoted by a grey dot.

**Video appendix 6.2: Disrupted forms of monocyte migration.** In analysing CCL2-stimulated cremasteric venules, in addition to normal TEM, some monocytes could be observed undergoing disrupted forms of TEM. This included 'incomplete' events, in which monocytes (green) seemingly get stuck at the site of TEM (A) and 'tailing' events, in which monocytes display an elongated uropod, seemingly as a result from engaging tightly with the endothelium (PECAM-1, red) whilst still crawling (B). Original magnification, ×40. Cell of interest is denoted by a grey dot.

**Video appendix 6.3: Leukocyte-assisted monocyte migration.** In analysing CCL2-stimulated cremasteric venules, transmigration pores in the endothelium (PECAM-1, red) could be observed in the absence of monocytes (green). These pores, formed presumably by other leukocyte types, were shown in several instances to accommodate subsequent monocyte TEM. Original magnification, ×40. Pore of interest is denoted by a grey dot.